

UNIVERSIDADE DE SÃO PAULO  
FACULDADE DE ODONTOLOGIA DE BAURU

ALINE DIONIZIO VALLE

**Proteomic analysis of jejunum and ileum in rats exposed to  
acute or chronic fluoride dose**

BAURU

2020



ALINE DIONIZIO VALLE

**Proteomic analysis of jejunum and ileum in rats exposed to acute or chronic fluoride dose**

**Análise proteômica do jejuno e íleo em ratos expostos a dose aguda ou crônica de fluoreto**

Thesis presented to the Bauru School of Dentistry of the University of São Paulo to obtain the degree of PhD in Science in the Applied Dental Science Program, Oral Biology, Stomatology, Radiology and Imaging concentration area.

Supervisor: Prof. Dr. Marília Afonso Rabelo Buzalaf

Tese apresentada à Faculdade de Odontologia de Bauru da Universidade de São Paulo para obtenção do título de Doutor em Ciências no Programa de Ciências Odontológicas Aplicadas, área de concentração Biologia Oral, Estomatologia, Radiologia e Imaginologia.

Orientadora: Profa. Dra. Marília Afonso Rabelo Buzalaf

**Versão Corrigida**

BAURU  
2020

Valle, Aline Dionizio  
Proteomic analysis of jejunum and ileum in rats  
exposed to acute or chronic fluoride dose/ Aline  
Dionizio Valle. – Bauru, 2020.  
164p. : il. ; 31cm.

Tese (Doutorado) – Faculdade de Odontologia  
de Bauru. Universidade de São Paulo

Orientadora: Prof. Dr<sup>a</sup> Marília Afonso Rabelo Buzalaf

**Nota:** A versão original desta tese encontra-se disponível no Serviço de Biblioteca e Documentação da Faculdade de Odontologia de Bauru – FOB/USP.

Autorizo, exclusivamente para fins acadêmicos e científicos, a reprodução total ou parcial desta dissertação/tese, por processos fotocopiadores e outros meios eletrônicos.

Assinatura:

Data:

Comitê de Ética em Animais da  
FOB-USP

Protocolo nº: 014/2011 e 012/2016

Data: 28/06/2011 e 25/05/2016

**(Cole a cópia de sua folha de aprovação aqui)**



---

---

## DEDICATÓRIA

Dedico esta tese à minha família e meu marido,

Aos meus pais **Rubens** e **Lucimar**,

Minha base, meus maiores exemplos, sempre me apoiaram, me incentivaram a lutar pelos meus objetivos, sempre com muita dedicação e amor incondicional, a mim dedicado.

À minha irmã **Amanda**,

Agradeço por mesmo de longe sempre estar presente me ajudando, incentivando e me apoiando.

Ao meu marido **Cesar**,

Meu amor, meu amigo, pessoa que me acalma e me incentiva. Obrigada por sempre estar ao meu lado, me fazendo rir e me fazendo ser forte. Hoje meu incentivo é a nossa família!

---

---





---

---

## AGRADECIMENTOS

Agradeço primeiramente a **Deus e Maria**.

Eles que me concedeu o dom da vida, que estão presentes em todos os momentos me dando força e luz para trilhar meus objetivos. Levanto todas as manhãs agradecendo por mais um dia, pois me ensinam que tropeçar é um aprendizado e que são nos tropeços da vida que mais aprendemos.

Aos meus pais **Rubens e Lucimar**.

Obrigada por sermos uma família, a qual sei que posso contar a qualquer hora, para qualquer situação, por mais difícil que seja, estão ao meu lado, ou puxando a orelha ou me abraçando e me dando palavras de carinho. Obrigada por me ensinarem a nunca desistir e me dizer que não seria fácil, mas que seria possível, se me dedicasse. Neste trabalho, vocês fizeram parte a todo momento, me levando a faculdade, me incentivando, cuidando da minha saúde, me fazendo rir quando estava preocupada, enfim, obrigada por serem quem são, e serem os meus pais, amo vocês infinitamente. São meus maiores orgulhos

À minha irmã **Amanda**.

Imagino o quão difícil é você estar tão longe de nós e te admiro por isso, obrigada por mesmo de longe sempre me ajudar, obrigada por me apoiar, ser amiga e irmã. Te amo!

Ao meu marido **Cesar**.

Obrigada por ser meu acalanto e meu porto seguro em momentos de nervoso, de desespero com as análises, prazos, etc, afinal eu sou ligada no 220v e por muitas vezes preciso desacelerar. Não tenho palavras pra descrever o quão importante você é para mim, durante esses quatro anos, em meio a loucura de um doutorado nos casamos e nos tornamos uma família, a qual é por ela que me dedico e busco cada dia melhorar mais e mais. Obrigada por tudo e principalmente por me ensinar que o amor e companheirismo está acima de qualquer coisa. Te amo vida!

---

---



---

---

Ao meu **cunhado Samuel**

Obrigada por fazer parte da nossa família, e principalmente por cuidar tão bem da minha irmã. Além claro, de sempre compartilhar dos momentos do meu doutorado, se preocupando e aconselhando.

À minha **avó Zenaide**

Vó, madrinha, muito obrigada por sempre cuidar de mim e vibrar a cada conquista, me ensinar que nada é fácil, mas que um dia sempre colhemos a recompensa. A senhora é um exemplo de força e dedicação pela família, se Deus permitir seguirei seus passos!

Ao Tio **Ricardo**

O primeiro cientista da família, quem sempre me apoiou e vibrou comigo a cada passo dado no âmbito acadêmico. Obrigada por vibrar comigo cada conquista e sempre que necessário me ajudar para chegar até aqui.

Aos **“tops”** e **“jogatina”** família e amigos.

Neste percurso estiveram ao meu lado, brincando comigo, me fazendo rir para desestressar e minimizar. Obrigada pelo carinho e amizade. E por serem minha família. Aqueles que escolhi para viver lado a lado.

A família **Souza Valle**.

Sogra, sogro, cunhados e cunhadas. Obrigada por fazerem parte dos meus dias neste período, por serem minha segunda família.

À minha amiga **Isabela e Beatriz**

Esse ano além de uma tese, comemoro com vocês uma década de amizade. Quem diria, aquelas companheiras de bancada no laboratório se tornariam mais que amigas, se tornaria comadres. Agradeço por sempre me ajudarem e estarem presentes nos meus dias, seja pra eu desabafar, me ajudarem nos tropeços de uma tese, me fazerem dar risada, tomar café, passear, enfim. Nossa amizade cresceu e se fortificou, amigo é presente de Deus e devemos cuidar, com certeza cuidarei para que nunca se acabe.

---

---



---

---

**À minha amiga Heloisa.**

Helo, com você aprendi muito, da iniciação ao mestrado como minha co-orientadora. E hoje como minha amiga, além de todo aprendizado profissional, aprendi com você a compartilhar meu conhecimento, a ser humilde e pedir ajuda, e principalmente não desistir. Te admiro muito e te quero sempre perto.

**À minhas amigas Tamara, Tati e Ju Trevizol.**

Meninas, muito obrigada por sempre estarem presente e serem tão prestativas, sempre se propondo a me ajudar e aprenderem. Considero vocês muito mais que amigas de laboratório, considero amigas da vida, quero ter vocês sempre por perto.

**Aos meus colegas do laboratório de bioquímica.**

Técnicas Larissa e Thelma, e alunos amigos, obrigada por cada um me ensinar um pouquinho do tanto que sabe, e por dividirem risadas, isso contribuiu e contribuirá muito para minha formação. Obrigada pelo carinho e companhia em todos esses dias.

**Aos professores Rodrigo e Ana Carolina.**

Agradeço por todo ensinamento, nestes 10 anos aprendi muito com vocês. Saibam que farei o possível para colocar em prática cada detalhe ensinado por vocês.

**Ao professor Rafael Lima, Leo e amigas da UFPA**

Não tenho palavras pra expressar minha admiração e minha gratidão. Fazer parte do grupo de vocês me fez aprender e crescer muito profissionalmente. Vocês são demais! Parabéns por quão bem conduz seus estudos e alunos Rafa!

**Aos funcionários do Biotério**

Obrigada por me ajudarem com os cuidados dos animais, me auxiliando e me instruindo da melhor forma.

---

---



---

---

À **Faculdade de Odontologia de Bauru-USP**, na pessoa do senhor diretor **Prof. Dr. Carlos Ferreira do Santos** e da senhora presidente da **Comissão de Pós-Graduação, Profa. Dra. Izabel Regina Fischer Rubira de Bullen**, pela oportunidade em realizar pós-graduação em nível de Doutorado nesta instituição, ao qual tenho orgulho e profundo respeito. Muito obrigada.

À **Fundação de Amparo à Pesquisa do Estado de São Paulo (FAPESP)**, pelo apoio financeiro concedido durante a realização deste estudo de Doutorado.

Ao **CNPq**, pelo apoio financeiro inicial deste projeto, que foi fundamental para o desenvolvimento desse trabalho.

---

---





---

---

## AGRADECIMENTOS ESPECIAIS

À professora Marília Afonso Rabelo Buzalaf da Faculdade de Odontologia de Bauru. Esse ano completo 10 anos no laboratório de bioquímica, durante essa década foram um ano de estágio, três iniciações científicas, um estágio no exterior, dois anos de mestrado e 4 anos de doutorado, e todos orientados pela senhora. Durante esse período, incluindo o primeiro contato que tivemos, sempre se mostrou ser uma pessoa maravilhosa, que não mede esforços para compartilhar suas conquistas e conhecimentos com os alunos, que torce e vibra por nós a cada vitória e trabalho apresentado. Nestes anos também pude ver que além de nossa orientadora também é mãe, esposa, filha, empresária, professora e pesquisadora, e que mesmo com tantos afazeres, não deixa se de dedicar a eles e a nós (alunos).

Segundo o dicionário professor é “Pessoa que, por conhecimento adquirido ou experiência de vida, pode ser mentor, espelho e ou norte para outros que desconhecem fatos ou acontecimentos”. Com toda certeza a senhora faz jus a este significado. Outra frase que elucida muito bem a senhora é “Eu nunca poderia pensar em educação sem amor. É por isso que me considero um educador: acima de tudo porque sinto amor.” *Paulo Freire*. A senhora transmite no olhar o amor pelos alunos e pelo que faz, com certeza assim, tudo fica mais tranquilo e mais satisfatório. Além disso nos encoraja, nos mostra que mesmo com tantos compromissos sempre é possível encontrarmos um horário para fazermos e aprendermos coisas novas, a senhora é nosso exemplo de profissional e de pessoa.

Obrigada imensamente, por toda oportunidade que me destes, por toda confiança que depositastes em mim e ainda depositas. Através da senhora pude conhecer o lado acadêmico e da pesquisa mais de perto, participar ativamente das atividades, e descobrir a minha admiração pela pesquisa. A senhora com certeza foi peça fundamental para que eu me tornasse hoje a profissional que sou.

Que Deus e Nossa Senhora, continuem lhe abençoando e guiando, para que continue essa profissional e pessoa que é conquistando cada dia mais seus objetivos e realizações.

---

---



---

---

*“As nuvens mudam sempre de posição, mas são sempre nuvens no céu.  
Assim devemos ser todo dia, mutantes,  
porém leais com o que pensamos  
e sonhamos” (Paulo Beleki).*

---

---



---

---

## ABSTRACT

### **Proteomic analysis of jejunum and ileum in rats exposed to acute or chronic fluoride dose.**

The gastrointestinal tract (GIT) is considered the main route of exposure to fluoride (F), which is rapidly absorbed from it. Exposure to this ion can generate considerable changes in the morphology of the intestine, which can affect its functions, leading to gastrointestinal symptoms that represent the first signs of F toxicity. In previous studies performed by our research group, it was observed that exposure to F interferes significantly in the expression of several proteins in the duodenum. Due to the distinct anatomical, histological and physiological characteristics found among the different distinct segments of the small intestine, the present study aimed to evaluate the effect of acute or chronic exposure to F on the proteomic profile of the jejunum and the ileum of rats. Male 60-day-old *Wistar* rats were treated for 30 days with chronic doses of 0 mgF/L, 10 mgF/L or 50 mgF/L. The acute dose of F (25 mg/Kg body weight) or deionized water (control) was administered once by gastric gavage. After the experimental periods, the jejunum and the ileum were collected. Proteomic analysis of both segments was performed using the nanoACQUITY UPLC-Xevo QTof MS system (Waters, Manchester, UK), in order to better understand the mechanisms involved in acute or chronic F toxicity, which led to the morphological changes observed in our previous studies. The difference in expression between the groups was obtained using the PLGS software, considering  $p < 0.05$  and  $1 - p > 0.95$  for the down and upregulated proteins, respectively. Under acute exposure to F, most of the proteins with altered expression were upregulated in the group 25 mg/Kg F vs. Control. Our results, when analyzed together (jejunum and ileum), suggest that the gastrointestinal symptoms found in these cases may be related to inhibition of protein synthesis by exposure to a high dose of F, such as changes in proteins that regulate the cytoskeleton and energy metabolism, mainly in carbohydrate metabolism. Under chronic exposure to F, most of the proteins with altered expression were upregulated in the group 10 mgF/L vs. control and in the comparison 50 mgF/L vs. control. In the jejunum, there were changes in the abundance of several proteins correlated with

---

---



---

---

protein synthesis, glucose homeostasis, energy metabolism and neural functions. Moreover, in the ileum, a decrease in gastrotropin was found, which may be associated with diarrhea, a common symptom found in cases of F toxicity. In addition, changes in different myosin isoforms were observed, which might have contributed to the structural alterations found in the histological analysis previously performed. In conclusion, acute exposure to F mostly downregulates several proteins, with emphasis on partners involved in protein synthesis, cytoskeleton and energy metabolism, which might help explain the gastrointestinal symptoms found in cases of acute exposure to this ion. Distinctly from which was observed for the acute treatment, under chronic treatment with both F concentrations an increase in the expression of proteins was observed, which might indicate an adaptation of the body, in attempt to fight the deleterious effects of this ion.

**Key-words:** Fluoride. Ileum. Jejunum. Proteomic analysis. Chronic exposure. Acute exposure.

---

---





---

---

## RESUMO

### **Análise proteômica do jejuno e íleo em ratos expostos a dose aguda ou crônica de fluoreto.**

O trato gastrointestinal (TGI) é considerado a principal via de exposição ao fluoreto (F), que é rapidamente absorvido por ele. A exposição a esse íon pode gerar alterações consideráveis na morfologia do intestino, o que pode afetar suas funções, levando a sintomas gastrointestinais que representam os primeiros sinais de toxicidade do F. Em estudos anteriores realizados pelo nosso grupo de pesquisa, observou-se que a exposição ao F interfere significativamente na expressão de várias proteínas no duodeno. Devido às distintas características anatômicas, histológicas e fisiológicas encontradas entre os diferentes segmentos do intestino delgado, o presente estudo teve como objetivo avaliar o efeito da exposição aguda ou crônica a F no perfil proteômico do jejuno e íleo de ratos. Ratos Wistar machos de 60 dias de idade foram tratados por 30 dias com doses crônicas de 0 mgF/L, 10 mgF/L ou 50 mgF/L. A dose aguda de F (25 mg/kg de peso corporal) ou água deionizada (controle), foram administradas uma única vez, por gavagem gástrica. Após os períodos experimentais, o jejuno e o íleo foram coletados. A análise proteômica de ambos os segmentos foi realizada com o sistema nanoACQUITY UPLC-Xevo QTof MS (Waters, Manchester, Reino Unido), a fim de melhor compreender os mecanismos envolvidos na toxicidade aguda ou crônica da F, o que levou às alterações morfológicas observadas em nossos estudos anteriores. A diferença de expressão entre os grupos foi obtida no software PLGS, considerando  $p < 0.05$  e  $1-p > 0.95$  para as proteínas sub e supregulada, respectivamente. Sob exposição aguda a F, a maioria das proteínas com expressão alterada foi aumentada no grupo 25 mg/Kg F vs. Controle. Nossos resultados, quando analisados em conjunto (jejuno e íleo), sugerem que os sintomas gastrointestinais encontrados nesses casos podem estar relacionados à inibição da síntese de proteínas pela exposição a uma alta dose de F, como alterações nas proteínas que regulam o citoesqueleto e o metabolismo energético, principalmente no metabolismo de carboidratos. Sob exposição crônica a F, a maioria das proteínas com expressão alterada foi aumentada no grupo 10 mgF/L vs. controle e na comparação 50 mgF/L vs. controle. No jejuno, houve alterações na abundância de várias proteínas correlacionadas com a síntese de proteínas, homeostase da glicose, metabolismo

---

---



---

---

energético e funções neurais. Além disso, no íleo, foi encontrada uma diminuição da gastrotropina, que pode estar associada à diarreia, sintoma comum encontrado nos casos de toxicidade por F. Em adição, foram observadas alterações nas diferentes isoformas da miosina, o que pode ter contribuído para as alterações estruturais encontradas na análise histológica realizada anteriormente. Em conclusão, a exposição aguda ao F na maioria das vezes regula negativamente várias proteínas, com ênfase nos parceiros envolvidos na síntese de proteínas, no citoesqueleto e no metabolismo energético, o que pode ajudar a explicar os sintomas gastrointestinais encontrados nos casos de exposição aguda a esse íon. Distintamente do que foi observado no tratamento agudo, no tratamento crônico com ambas as concentrações de F foi observado um aumento na expressão de proteínas, o que pode indicar uma adaptação do corpo, na tentativa de combater os efeitos deletérios desse íon.

**Palavras-chave:** Fluoreto. Íleo. Jejuno. Análise proteômica. Exposição crônica. Exposição aguda.

---

---



---

---

## SUMÁRIO

<b>1</b>	<b>INTRODUCTION .....</b>	<b>17</b>
<b>1.1</b>	<b>Objectives.....</b>	<b>20</b>
<b>2</b>	<b>ARTICLES .....</b>	<b>23</b>
<b>2.1</b>	<b>Article 1: Effects of chronic fluoride exposure on the jejunum of rats: insights from proteomics and enteric innervation analysis .....</b>	<b>23</b>
<b>2.2</b>	<b>Article 2: Intestinal changes associated to fluoride exposure: new insights from ileum analysis .....</b>	<b>59</b>
<b>2.3</b>	<b>Article 3: Effects of acute fluoride exposure on the jejunum and ileum of rats.....</b>	<b>83</b>
<b>3</b>	<b>DISCUSSION.....</b>	<b>119</b>
	<b>REFERENCES .....</b>	<b>131</b>
	<b>ANNEX .....</b>	<b>143</b>

---

---



# **1 INTRODUCTION**

---

---





## 1 INTRODUCTION

Fluorine is the thirteenth most abundant element in the earth's crust (SHANTHAKUMARI; SRINIVASALU; SUBRAMANIAN, 2004). In the form of its negatively charged ion, called fluoride (F<sup>-</sup>), it is important for many physiological cellular processes in the organism (YAN *et al.*, 2011). F is present in biological fluids and tissues as a trace element and 99% of the F in the organism is accumulated in the hard tissues. F can also be artificially added to the drinking water and fluoridated dental products, which together are the main source of F for human consumption (BUZALAF, 2018; BUZALAF; WHITFORD, 2011).

Because of its widely known ability to control dental caries, since the 1940's many cities worldwide have adopted artificial fluoridation of drinking water as a standard public health policy (IHEOZOR-EJIOFOR *et al.*, 2015). In Brazil, since 1974, artificial fluoridation of water from public supply is mandatory in cities where there is a water treatment station and this is regulated by law (Brazil, Ministry of Health, Decree n°76872, 1975; Brazil, Ministry of Health, Federal Law N°. 6050.1974)(BRASIL, 1974; 1976). However, since F is an element naturally found in water, in some cities the concentration naturally found is above the recommended limits (0.7 – 1.2 mgF/L), which can cause deleterious effects (WHITFORD, 1996). Among these effects, the most known is fluorosis, which can be dental (DENBESTEN; LI, 2011) or skeletal (KRISHNAMACHARI, 1986). A plethora of experimental studies attest that, when F is administered to animals in high doses, distinct alterations in different tissues affecting diverse proteins and enzymes are found (ARAUJO *et al.*, 2019; BARBIER; ARREOLA-MENDOZA; DEL RAZO, 2010; CARVALHO *et al.*, 2013; KOBAYASHI *et al.*, 2014; KOBAYASHI *et al.*, 2009; LIMA LEITE *et al.*, 2014; LOBO *et al.*, 2015; PEREIRA *et al.*, 2018; PEREIRA *et al.*, 2016; PEREIRA *et al.*, 2013; STRUNECKA *et al.*, 2007). Among these tissues, morphological and proteomic changes were found in the jejunum (DIONIZIO *et al.*, 2018) and duodenum (MELO *et al.*, 2017) of rats. This is expected, since most of the F is absorbed from the small intestine (NOPAKUN; MESSER, 1990; NOPAKUN; MESSER; VOLLER, 1989).

Several researches with different designs (in vitro laboratory studies and in vivo animal and human studies) have shown that F has a toxic effect, which is related to the amount and timing of exposure (BARBIER; ARREOLA-MENDOZA; DEL RAZO,

---

2010; PEREIRA *et al.*, 2018). This effect can be classified as acute or chronic (for review see (DENBESTEN; LI, 2011; WHITFORD, 1992; 2011).

Acute toxicity occurs by ingesting a large amount of F at a single time. The signs and symptoms related to this type of intoxication are vomiting with blood, diarrhea, bronchospasm, ventricular fibrillation, dilated pupils, hemoptysis, cramps, cardiac collapse, hypercalcemia, hypocalcemia and impaired renal function. In the literature, we found both accidental and intentional cases of acute F toxicity (WHITFORD, 1992; 2011).

Chronic toxicity occurs when above-the-optimal F concentrations are ingested over a certain period of time (DENBESTEN; LI, 2011). The main sources of chronic F intake are water and dentifrice. Despite daily ingestion of F in the range between 0.05 and 0.07 mg/kg body weight/ day is still recognized as the optimal level of F intake, the precise level of daily F intake able to control caries and that is not associated with increased risk of dental fluorosis is not known so far (BUZALAF, 2018).

After ingestion, F can cross the cell membranes mainly by diffusion of its weak acid (HF) (BUZALAF; WHITFORD, 2011), causing adverse effects by invading soft tissues such as brain, liver, intestine, heart and lung, with several structural and metabolic changes being observed after its excessive administration (BARBIER; ARREOLA-MENDOZA; DEL RAZO, 2010; CHOUHAN; FLORA, 2008) (INKIELEWICZ-STEPNIAK; CZARNOWSKI, 2010). In general, it is recognized that the toxic effects of F are due mainly to enzymatic inhibition, destruction of collagen, paralysis of activities of the immune system and damage to the gastrointestinal tract (GIT) (CHOUHAN; FLORA, 2008).

Being the main route of F absorption, the GIT can be exposed to high concentrations of F daily (BUZALAF; WHITFORD, 2011), which and can lead to considerable changes in the morphology of the intestine, which in turn affects its functions (CHAUHAN; OJHA; MAHMOOD, 2011; DIONIZIO *et al.*, 2018; MELO *et al.*, 2017). Moreover, the complex functions of the GIT, which include mixing and spreading food, providing digestive enzymes, reabsorption and secretion, as well as maintaining adequate blood flow levels, depend on intense coordination of autonomic neuronal networks (COOKE, 2000; FURNESS *et al.*, 1995). These networks are embedded in the walls of the intestine and are formed by the interconnection of ganglionic and aganglionic plexuses and also over a highly sophisticated network of

---

---

polysynaptic circuits (FURNESS *et al.*, 2004), this large set being called Enteric Nervous System (ENS) (SCHAFER; VAN GINNEKEN; COPRAY, 2009).

In a recent study, our research group evaluated the effect of acute or chronic exposure to F, on the general population of enteric neurons and on the subpopulations that express the main enteric neurotransmitters in the duodenum, jejunum and ileum. Relevant changes were found (MELO, 2015; MELO *et al.*, 2017). This study also reported important proteomic alterations in the duodenum of rats treated with F. Among them are: 1) F, when chronically administered in the dose of 10 mg/L through the drinking water, altered the expression of 229 proteins, among which most were upregulated when compared to the control group (deionized water), being the “pyridine metabolism” the most affected biological process (MELO *et al.*, 2017); 2) F altered the expression of 284 proteins after chronic exposure to water containing 50 mgF/L when compared with control, being “protein polymerization” the mostly affected biological process (MELO *et al.*, 2017); 3) After acute administration of F in the dose of 25 mg/kg (gastric gavage), F altered the expression of 356 proteins with the vast majority of these proteins having their expression downregulated and the mostly affected biological process was “generation of precursors and energy” (MELO, 2015). It is important to highlight that both under acute and chronic F exposure, the effect of F in the duodenum was much more pronounced than that observed in proteomic studies conducted with other organs, such as kidneys (DE CARVALHO *et al.*, 2013; KOBAYASHI *et al.*, 2009; XU *et al.*, 2005), brain (GE *et al.*, 2011; NIU *et al.*, 2014) and liver (ARAUJO *et al.*, 2019; DIONIZIO *et al.*, 2019; KHAN *et al.*, 2019; PEREIRA *et al.*, 2018; PEREIRA *et al.*, 2013), even with similar doses of F. The most probable reason for the higher susceptibility of the duodenum to the effects of F, when compared to the other organs, lies on the fact that 70-75% of the absorption of F occurs in the small intestine (NOPAKUN; MESSER, 1990; NOPAKUN; MESSER; VOLLER, 1989). Consequently, when a certain dose of F is ingested, the cells in the intestinal wall are exposed to a higher concentration of F than the cells of the other organs, which will come into contact only with the F that is absorbed (BUZALAF; WHITFORD, 2011).

Due to the distinct anatomical, histological and physiological characteristics found among the different distinct segments of the small intestine (GUYTON; HALL, 2015) and considering the important changes observed in the general population of neurons in the jejunum and ileum and in subpopulations that express the main enteric neurotransmitters in our previous study (MELO, 2015), it is extremely important to

---

perform proteomic analysis of these two intestinal segments, in order to obtain information about the possible mechanisms involved in the alteration of the ENS by exposure to F, which may explain the gastrointestinal symptoms caused by this exposure.

### **1.1 OBJECTIVES**

The general aim of this study was to investigate the effect of acute or chronic exposure to F on the protein expression profile of the jejunum and ileum of rats, using proteomic analyses. Moreover, proteomics findings were associated with the morphological alterations in the SNE performed in a previous study (Melo et al. 2015), in order to provide mechanistic rationale to explain the gastrointestinal symptoms caused by F.

**2 ARTICLES**

---

---



## 2 ARTICLES

### 2.1 Article 1

Article formatted according to **Scientific Reports** Guidelines.

**Published on 16.02.2018** (Dionizio, Aline Salgado; Melo, Carina Guimarães Souza; Sabino-Arias, Isabela Tomazini; Ventura, Talita Mendes Silva; Leite, Aline Lima; Souza, Sara Raquel Garcia; Santos, Erika Xavier; Heubel, Alessandro Domingues; Souza, Juliana Gadelha; Perles, Juliana Vanessa Colombo Martins; Zaroni, Jacqueline Nelisis; Buzalaf, Marília Afonso Rabelo. Chronic treatment with fluoride affects the jejunum: insights from proteomics and enteric innervation analysis. *Scientific Reports*, v. 8, e. 3180, 2018.). License by Creative Commons license <http://creativecommons.org/licenses/by/4.0/>.

**Effects of chronic fluoride exposure on the jejunum of rats: insights from proteomics and enteric innervation analysis.**

Aline Salgado Dionizio<sup>1</sup>, Carina Guimarães Souza Melo<sup>1</sup>, Isabela Tomazini Sabino-Arias<sup>1</sup>, Talita Mendes Silva Ventura<sup>1</sup>, Aline Lima Leite<sup>1</sup>, Sara Raquel Garcia Souza<sup>2</sup>, Erika Xavier Santos<sup>2</sup>, Alessandro Domingues Heubel<sup>1</sup>, Juliana Gadelha Souza<sup>1</sup>, Juliana Vanessa Colombo Martins Perles<sup>2</sup>, Jacqueline Nelisis Zaroni<sup>2</sup> & Marília Afonso Rabelo Buzalaf<sup>1</sup>

1 Department of Biological Sciences, Bauru School of Dentistry, University of São Paulo, Bauru, Brazil.

2 Department of Morphophysiological Sciences, State University of Maringá, Maringá, Brazil.

Corresponding author

Marília Afonso Rabelo Buzalaf

Alameda Octávio Pinheiro Brisolla, 9-75

Bauru-SP, Brazil, 17012-901

Phone: # 55 14 3235-8346      Email: [mbuzalaf@fob.usp.br](mailto:mbuzalaf@fob.usp.br)

---

## Abstract

Gastrointestinal symptoms are the first signs of fluoride (F) toxicity. In the present study, the jejunum of rats chronically exposed to F was evaluated by proteomics, as well as by morphological analysis. Wistar rats received water containing 0, 10 or 50 mgF/L during 30 days. HuC/D, neuronal Nitric Oxide (nNOS), Vasoactive Intestinal Peptide (VIP), Calcitonin Gene Related Peptide (CGRP), and Substance P (SP) were detected in the myenteric plexus of the jejunum by immunofluorescence. The density of nNOS-IR neurons was significantly decreased (compared to both control and 10 mgF/L groups), while the VIP-IR varicosities were significantly increased (compared to control) in the group treated with the highest F concentration. Significant morphological changes were seen observed in the density of HUC/D-IR neurons and in the area of SP-IR varicosities for F-treated groups compared to control. Changes in the abundance of various proteins correlated with relevant biological processes, such as protein synthesis, glucose homeostasis and energy metabolism were revealed by proteomics.

## Introduction

Fluoride (F) is considered one of the essential elements for the maintenance of the normal cellular processes in the organism<sup>1</sup> and is largely employed in dentistry to control dental caries<sup>2</sup>. However, when excessive amounts are ingested, F can induce oxidative stress and lipid peroxidation, alter intracellular homeostasis and cell cycle, disrupt communication between cells and signal transduction and induce apoptosis<sup>3</sup>.

Nearly 25% of ingested F is absorbed from the stomach as an undissociated molecule (HF) in a process that is inversely related to pH<sup>4</sup>, while the remainder is absorbed in the ionic form (F<sup>-</sup>) from the small intestine, in a pH-independent manner<sup>5</sup>. Due to its major role in F absorption, the gastrointestinal tract (GIT) is considered the main route of exposure to F<sup>6</sup>. Thus, gastrointestinal symptoms, including nausea, vomiting, diarrhea and abdominal pain are the first signs of F toxicity<sup>7-10</sup>.

The Enteric Nervous System (ENS) is an interconnected network of neurons disposed in the walls of the intestine that controls the function of the GIT<sup>11</sup>. Due to its control function, changes in ENS affect the absorption, secretion, permeability and motility of the GIT<sup>12</sup>. Recently, immunofluorescence techniques revealed important

---



alterations in the morphology of different types of enteric neurons and proteomic analysis demonstrated changes in the expression of several proteins of the duodenum of rats<sup>13</sup> after chronic exposure to F, providing the first insights for the comprehension of the mechanisms involved in the effects of F on the intestine. However, the effect of F on the ENS and proteomic profile of the jejunum has never been reported. Considering that each segment of the small intestine has distinct anatomical, histological and physiological characteristics with functional implications<sup>14</sup>, this study evaluated the morphology of distinct subtypes of enteric neurons of the jejunum after chronic exposure to F. Quantitative label-free proteomics tools were employed to evaluate the changes on the pattern of protein profile of the jejunum, after exposure to F, in attempt to provide mechanistic explanations for the effects of this ion in the intestine.

## **Material and Methods**

**Animals and treatment.** The Ethics Committee for Animal Experiments of Bauru Dental School, University of São Paulo approved all experimental protocols (#014/2011 and #012/2016). All experimental protocols were approved by. The assays conformed with the guidelines of the National Research Council. Eighteen adult male rats (60 days of life - *Rattus norvegicus*, Wistar type) were randomly assigned to 3 groups (n = 6/group). They remained one by one in metabolic cages, having access to water and food ad libitum under standard conditions of light and temperature. The animals received deionized water (0 mgF/L), 10 mgF/L and 50 mgF/L for 30 days as sodium fluoride (NaF) dissolved in deionized water, in order to simulate chronic intoxication with F. Since rodents metabolize F 5 times faster than humans, these F concentrations correspond to ~2 and 10 mg/L in the drinking water of humans<sup>15</sup>. After the experimental period, the animals received an intramuscular injection of anesthetic and muscle relaxant (ketamine chlorhydrate and xylazine chlorhydrate, respectively). While the rats were anesthetized, the peritoneal and thoracic cavities were exposed, and the heart was punctured for blood collection, using a heparinized syringe. Plasma was obtained by centrifugation at 800 g for 5 minutes for quantification of F, described in a previous publication<sup>13</sup>. After blood collection, the jejunum was collected for histological, immunofluorescence and proteomic analysis. For the collection of the jejunum, animal chow was removed from the animals 18 hours prior the euthanasia to

---

decrease the volume of fecal material inside the small intestine, facilitating the cleaning process for posterior processing. After laparotomy, to remove the jejunum, initially the small intestine was localized, and the jejunum proximal limit was identified by the portion after the duodenojejunal flexure that is attached to the posterior abdominal wall by the ligament of Treitz. After incisions in the flexure and ligament, 20 centimeters distally to the incision were despised and then 15 centimeters of the jejunum were harvested for processing. After harvesting, the jejunum was washed with PBS solution applied several times with a syringe in the lumen to remove completely any residue of fecal material.

**Histological analysis.** This analysis was performed exactly as described by Melo, et al.<sup>13</sup>.

**Myenteric plexus immunofluorescence, morphometric and quantitative analysis.** These analyses were performed exactly as described by Melo, et al.<sup>13</sup>.

**Proteomic analysis.** The frozen jejunum was homogenized in a cryogenic mill (model 6770, SPEX, Metuchen, NJ, EUA). Samples from 2 animals were pooled and analyses were carried out in triplicates. Protein extraction was performed by incubation in lysis buffer (7 M urea, 2 M thiourea, 40 mM DTT, all diluted in AMBIC solution) under constant stirring at 4 °C. Samples were centrifuged at 14000 rpm for 30 min at 4 °C and the supernatant was collected. Protein quantification was performed<sup>16</sup>. To 50 µL of each sample (containing 50 µg protein) 25 µL of 0.2% Rapigest (WATERS cat#186001861) was added, followed by agitation and then 10 µL 50 mM AMBIC were added. Samples were incubated for 30 min at 37 °C. Samples were reduced (2.5 µL 100 mM DTT; BIORAD, cat# 161-0611) and alkylated (2.5 µL 300 mM IAA; GE, cat# RPN 6302 V) under dark at room temperature for 30 min. Digestion was performed at 37 °C overnight by adding 100 ng trypsin (PROMEGA, cat #V5280). After digestion, 10 µL of 5% TFA were added, incubated for 90 min at 37 °C and sample was centrifuged (14000 rpm at 6 °C for 30 min). Supernatant was purified using C 18 Spin columns (PIERCE, cat #89870). Samples were resuspended in 200 µL 3% acetonitrile.

**LC-MS/MS and bioinformatics analyses.** The peptides identification was done on a nanoAcquity UPLC-Xevo QToF MS system (WATERS, Manchester, UK), using the PLGS software, as previously described<sup>17</sup>. Difference in abundance among the groups

---

was obtained using the Monte-Carlo algorithm in the ProteinLynx Global Server (PLGS) software and displayed as  $p < 0.05$  for down-regulated proteins and  $1 - p > 0.95$  for up-regulated proteins. Bioinformatics analysis was done to compare the treated groups with the control group (Tables S1–S5), as previously reported<sup>17–20</sup>. The software CYTOSCAPE 3.0.4 (JAVA) was used to build networks of molecular interaction between the identified proteins, with the aid of ClueGo and ClusterMarker applications.

## Results

**Morphological analysis of the jejunum wall thickness.** The mean ( $\pm$ SD) thickness of the jejunum tunica muscularis was significantly higher in the 50 mgF/L ( $93.0 \pm 1.4 \mu\text{m}^2$ ) when compared to control ( $81.5 \pm 1.1 \mu\text{m}^2$ ) and 10 mgF/L ( $84.2 \pm 2.5 \mu\text{m}^2$ ) groups (Bonferroni's test,  $p < 0.05$ ). The total thickness of the jejunum wall was significantly lower in the 50 mgF/L ( $742.25 \pm 7.8 \mu\text{m}^2$ ) and 10 mgF/L ( $734.4 \pm 11.8 \mu\text{m}^2$ ) when compared to control ( $783.15 \pm 5.8 \mu\text{m}^2$ ) (Bonferroni's test,  $p < 0.05$ ).

**Myenteric HuC/D – IR neurons analysis.** When the general population of neuron was morphometrically analyzed, the cell bodies areas ( $\mu\text{m}^2$ ) of the HuC/D–IR neurons were not significantly different among the groups ( $p > 0.05$ ). In the semi-quantitative analyses (neurons/cm<sup>2</sup>), a significant decrease in the density was observed in the treated groups when compared with control ( $p < 0.05$ ) (Table 1).

**Myenteric nNOS –IR neurons analysis.** The cell bodies areas ( $\mu\text{m}^2$ ) of the nNOS-IR neurons did not present a significant difference among the groups ( $p > 0.05$ ) in the morphometric analysis. As for the semi-quantitative analyses, a decrease in the mean value of the density for the group treated with 50 mgF/L when compared with the other groups was observed ( $p < 0.05$ ; Table 1).

**Myenteric varicosities VIP-IR, CGRP-IR or SP-IR morphometric analysis.** A significant increase in the VIP-IR varicosity areas ( $\mu\text{m}^2$ ) was detected in the group treated with 50 mgF/L when compared with the control group ( $p < 0.05$ ). For the CGRP-IR varicosity areas, the groups did not differ significantly ( $p > 0.05$ ). However, SP-IP varicosity areas were significantly increased in the treated groups when compared with control. In addition, the group treated with 10mgF/L presented an area significantly

---

higher than the group treated with 50 mgF/L (Table 1). Typical images of the immunofluorescences are shown in Figs 1 and 2.

**Table 1.** Means and standard errors of the values of the cell bodies areas and density of HUC/D-IR and nNOS-IR neurons and VIP-IR, CGRP-IR, and SP-IR values of myenteric neurons varicosities areas of the jejunum of rats chronically exposed or not to fluoride in the drinking water.

ANALYSIS	Control	10 mgF/L	50 mgF/L
Cell bodies areas of the HuC/D-IR neurons ( $\mu\text{m}^2$ )	304.9 $\pm$ 3.5 <sup>a</sup>	310.7 $\pm$ 3.8 <sup>a</sup>	304.8 $\pm$ 3.8 <sup>a</sup>
Density HuC/D-IR neurons (neurons/cm <sup>2</sup> )	16,968 $\pm$ 350 <sup>a</sup>	15,420 $\pm$ 392 <sup>b</sup>	15,230 $\pm$ 380 <sup>b</sup>
Cell bodies areas of the nNOS-IR neurons ( $\mu\text{m}^2$ )	291.4 $\pm$ 3.2 <sup>a</sup>	296.6 $\pm$ 3.5 <sup>a</sup>	289.6 $\pm$ 2.9 <sup>a</sup>
Density nNOS-IR neurons (neurons/cm <sup>2</sup> )	5,725 $\pm$ 123 <sup>a</sup>	5,559 $\pm$ 134 <sup>a</sup>	5,176 $\pm$ 146 <sup>b</sup>
Area VIP-IR varicosities ( $\mu\text{m}^2$ )	3.08 $\pm$ 0.52 <sup>a</sup>	3.98 $\pm$ 0.03 <sup>ab</sup>	4.46 $\pm$ 0.04 <sup>b</sup>
Area CGRP-IR varicosities ( $\mu\text{m}^2$ )	3.31 $\pm$ 0.03 <sup>a</sup>	3.35 $\pm$ 0.04 <sup>a</sup>	3.38 $\pm$ 0.03 <sup>a</sup>
Area SP-IR varicosities ( $\mu\text{m}^2$ )	2.81 $\pm$ 0.01 <sup>a</sup>	4.86 $\pm$ 0.03 <sup>b</sup>	4.64 $\pm$ 0.03 <sup>c</sup>

Means followed by different letters in the same line are significantly different according to Fisher's test (density HuC/D-IR and nNOS-IR neurons) or Tukey's test (other variables).  $p < 0.05$ .  $n = 6$ .

**Proteomic analysis of the jejunum.** The total numbers of proteins identified in the control, 10 and 50 mgF/L groups were 294, 343 and 322, respectively. These proteins were present in the 3 pooled samples for each group. Among them, 81 (Table S1), 120 (Table S2) and 99 (Table S3) proteins were uniquely identified in the control, 10 mgF/L and 50 mgF/L groups, respectively. In the quantitative analysis of the 10 mgF/L vs. control group, 30 proteins with change in expression were detected (Table S4). As for the comparison 50 mgF/L vs. control group, 40 proteins with change in expression were found (Table S5). Most of the proteins with changed expression were upregulated in the groups treated with F when compared with the control group (21 and 23 proteins in the groups treated with 10 mgF/L and 50 mgF/L, Tables S4 and S5, respectively). Figures 3 and 4 show the functional classification according to the biological process with the most significant term, for the comparisons 10 mgF/L vs. control and 50 mgF/L vs. control, respectively. The group exposed to the highest F concentration had the largest alteration, with change in 15 functional categories (Fig. 4). Among them, the categories with the highest percentage of associated genes were: Cellular respiration (14.3%), NAD metabolic process (10.2%), Oxygen transport (10.2%), Chromatin silencing (8.2%) and ER-associated ubiquitin-dependent protein catabolic process

(8.2%). Exposure to the lowest F concentration influenced 12 functional categories (Fig. 3). The biological processes with the highest percentage of affected genes were: Nicotinamide nucleotide metabolic process (25%), Regulation of neuronal synaptic plasticity (11.4%), NAD metabolic process (15.9%) and Positive regulation of response to wounding (9.1%). It should be highlighted that Regulation of oxidative stress-induced intrinsic apoptotic signaling pathway was also identified, with 4.5% of affected genes (4.5%). Figures 5 and 6 show the subnetworks created by CLUSTERMARK for the comparisons 10 mgF/L vs. control and 50 mgF/L vs. control, respectively. For the 10 mgF/L group (Fig. 5), most of the proteins with change in expression interacted with *Solute carrier family 2, facilitated glucose transporter member 4* (GLUT4; P19357) and *Small ubiquitin-related modifier 3* (Q5XIF4) (Fig. 5A) or with *Polyubiquitin-C* (Q63429) and *Elongation factor 2* (P05197) (Fig. 5B). As for the group treated with 50 mgF/L, most of the proteins with change in expression interacted with GLUT4 (P19357) and *Mitogen-activated protein kinase 3* (MAPK3; P21708) (Fig. 6A) or *Polyubiquitin-C* (Q63429) (Fig. 6B).

## Discussion

The small intestine is responsible for absorption of around 70–75% of F<sup>5,21</sup>. As consequence, gastrointestinal symptoms, such as abdominal pain, nausea, vomiting and diarrhea, are the most common occurrence in cases of excessive ingestion of F<sup>22–25</sup>. The mechanisms underlying these changes remain to be determined. Recently, our group took advantage of immunofluorescence and proteomics techniques to evaluate changes in the duodenum of rats after chronic exposure to F<sup>13</sup>. The group treated with 50 mgF/L had a significant decrease in the density of nNOS-IR neurons. Additionally, important morphological changes were seen in HUC/D-IR and nNOS-IR neurons, as well as in VIP-IR, CGRP-IR, and SP-IR varicosities for the groups treated with both 10 and 50 mgF/L. Moreover, profound proteomic alterations were observed in both treated groups. In the group treated with 10 mgF/L, most of the proteins with altered expression were upregulated. On the other hand, downregulation of several proteins was found in the group treated with the highest F concentration<sup>13</sup>.

Many proteins observed in the previous study were correlated with the neurotransmission process, which is essential for the function of the GIT through ENS control. For example, the pattern of intestinal smooth muscle contraction can be modified when the release of neurotransmitters stimulating muscle contraction, such

---

as SP<sup>26</sup> is increased or when the release of neurotransmitters promoting muscle relaxation, such as NO<sup>27</sup>, is decreased. In the present study, both conditions might have occurred, because we found a significance increase and decrease in the mean values of the SP varicosities area and the density of nNOS-IR neurons, respectively (Table 1), which is in accordance with our previous findings for the duodenum<sup>13</sup>. This finding can be also associated with the significant decrease in the density of HUC/D-IR neurons (Table 1), and it could contribute to the intestinal discomfort and symptoms, such as abdominal pain and diarrhea, observed upon excessive exposure to F.

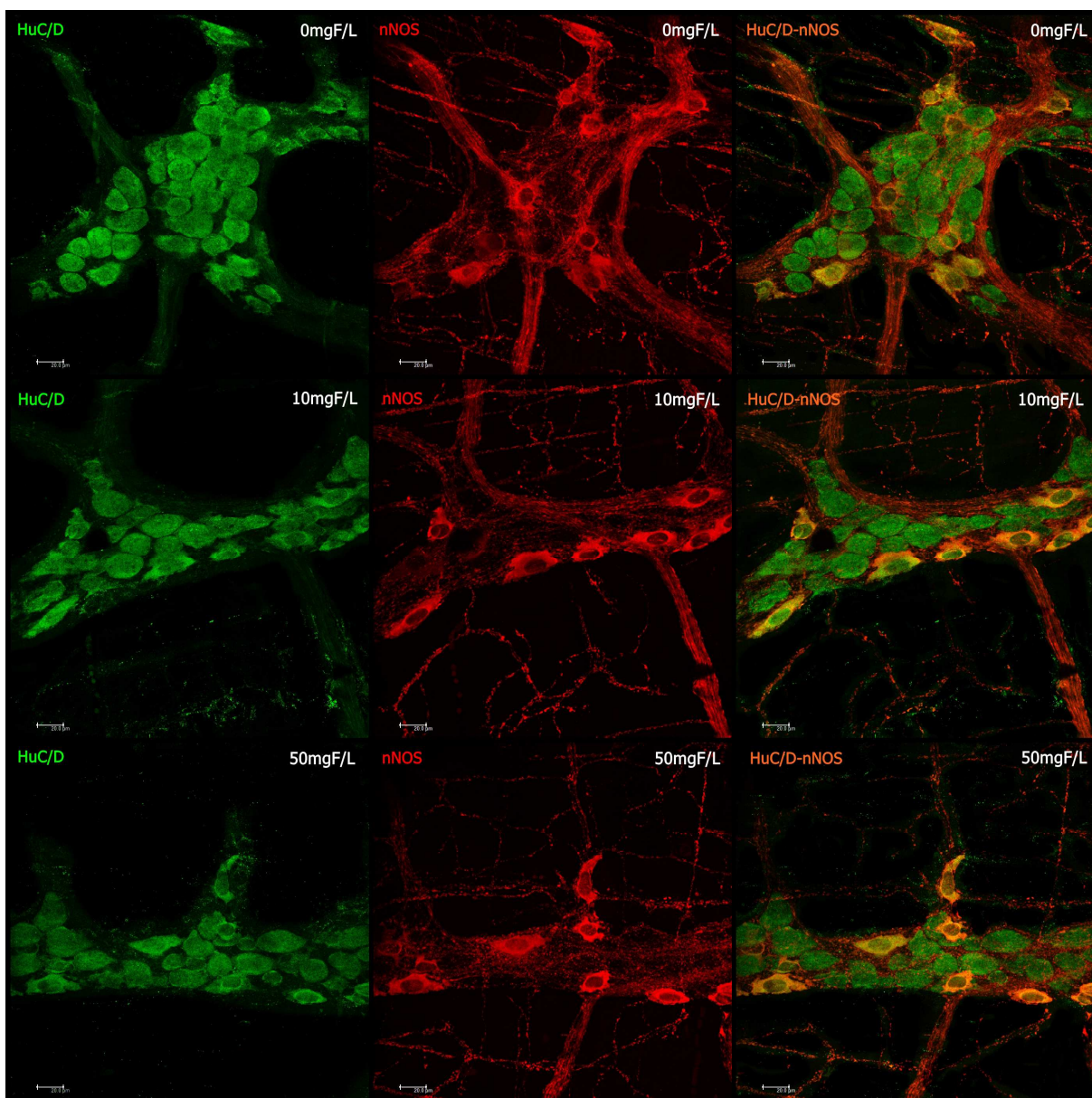


**Figure 1.** Photomicrography of myenteric neurons of the rats jejunum stained for HuC/D (green), nNOS (red), and double-labeling (HuC/D and nNOS) for the control group (0 mgF/L) and for the groups treated with 10 and 50 mgF/L. 20x Objective.

Another important neurotransmitter that also participates in the control of intestinal motility is VIP. In our study, it was observed a statistically significant increase in the mean value of the areas of VIP-IR myenteric varicosities in the 50 mgF/L group when compared with control. This finding is similar to what was observed in our previous study where duodenum was analyzed<sup>13</sup> and confirms that this dose of F can compromise the vipergic innervation of the small intestine. For the inhibitory control of motility, the main neurotransmitters involved are NO and VIP<sup>28</sup>, so basically any changes in the vipergic innervation can alter the intestinal motility, leading to a decrease in the tone of the intestinal smooth muscle, which could trigger diarrhea or even increased susceptibility to intestinal infections by decreased intestinal transit<sup>29</sup>. We can also suggest, in this case, that this increase may mean upregulation in the expression of the VIP, as a response to F toxicity since other processes such as axotomy and blocking of axonal transport or hypertrophic alterations promote upregulation of VIP in enteric neurons<sup>30</sup>. This increase can also be related to a neuroprotective role of VIP, because it acts as a potent anti-inflammatory molecule and presents an important antioxidant activity<sup>31–33</sup>. In addition to this, VIP is one of the most important elements involved in enteric neuroplasticity<sup>33</sup>, which is the ENS ability to adapt to any change in its microenvironment<sup>34</sup>. Due to the morphological changes that we observed in our study in the vipergic varicosities, we can suggest that F can induce important neuroplastic changes in the GIT.

Since alterations in the morphology of the intestinal wall infer important pathophysiological processes, we analyzed the total thickness of the intestinal wall, as well as the tunica muscularis separately. The group treated with 50 mgF/L presented a significant decrease in the total thickness of the intestinal wall and an increase in the thickness of the tunica muscularis, indicating that F can alter morphologically the jejunum wall. The finding for the tunica muscularis of the jejunum is in-line with our previous findings for the duodenum<sup>13</sup>, despite the total thickness of the duodenum wall was not altered. Changes in the number and morphology of myenteric cell bodies may be related to variations of the tunica muscularis thickness, which presents the structures responsible for the maintenance, development and plasticity of these neurons<sup>35</sup>. Similar increase in the thickness of the intestinal wall and tunica muscularis have been reported in the duodenum and jejunum of rats fed with a high fat diet for 8 weeks, where morphological alterations in the general population of enteric neurons

---

and in the nitrergic population were also detected<sup>36</sup>, emphasizing that intestinal physiology comprises many interconnected mechanisms.

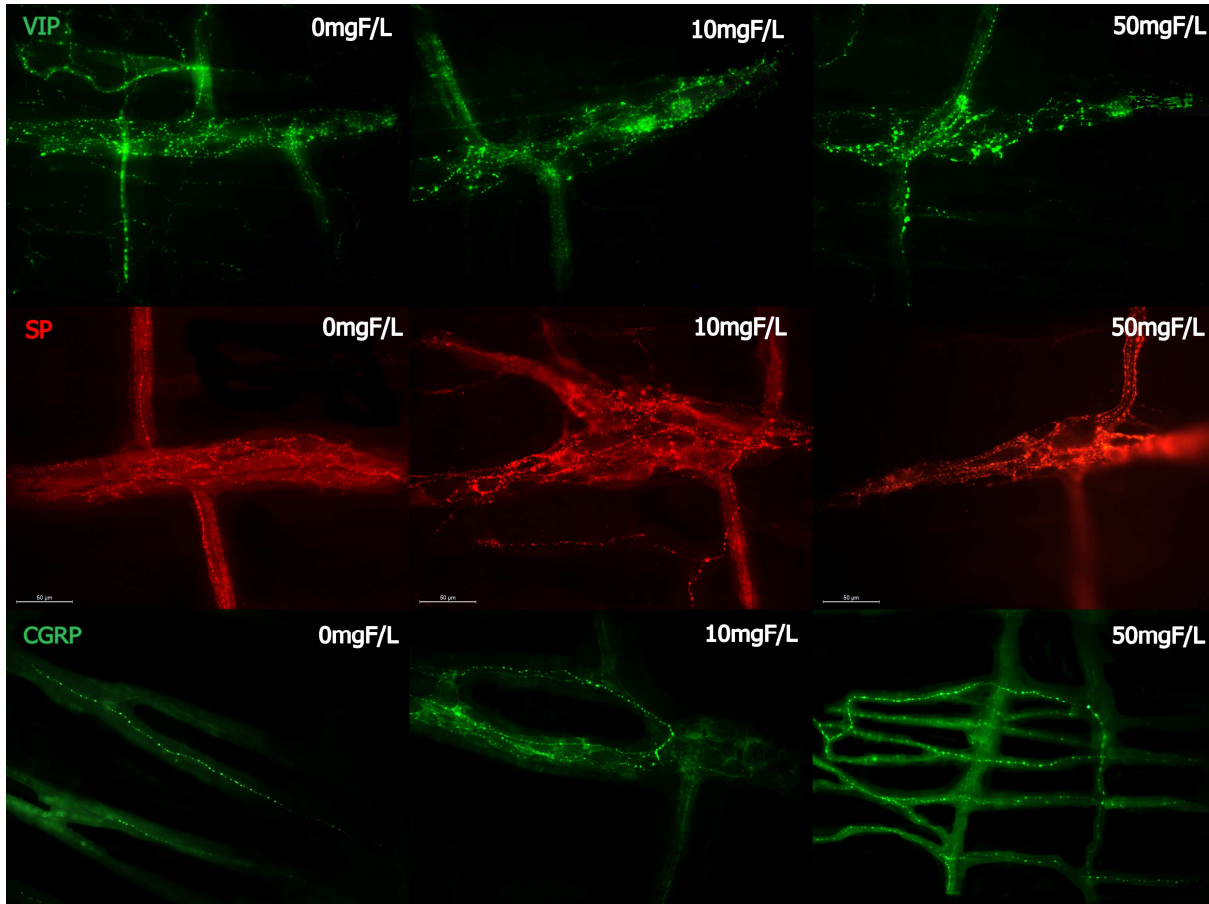


**Figure 2.** Photomicrography of myenteric varicosities of the rats jejunum after F chronic exposure (0, 10 or 50 mgF/L) for VIP-IR, SP-IR CGRP-IR. 40x Objective.



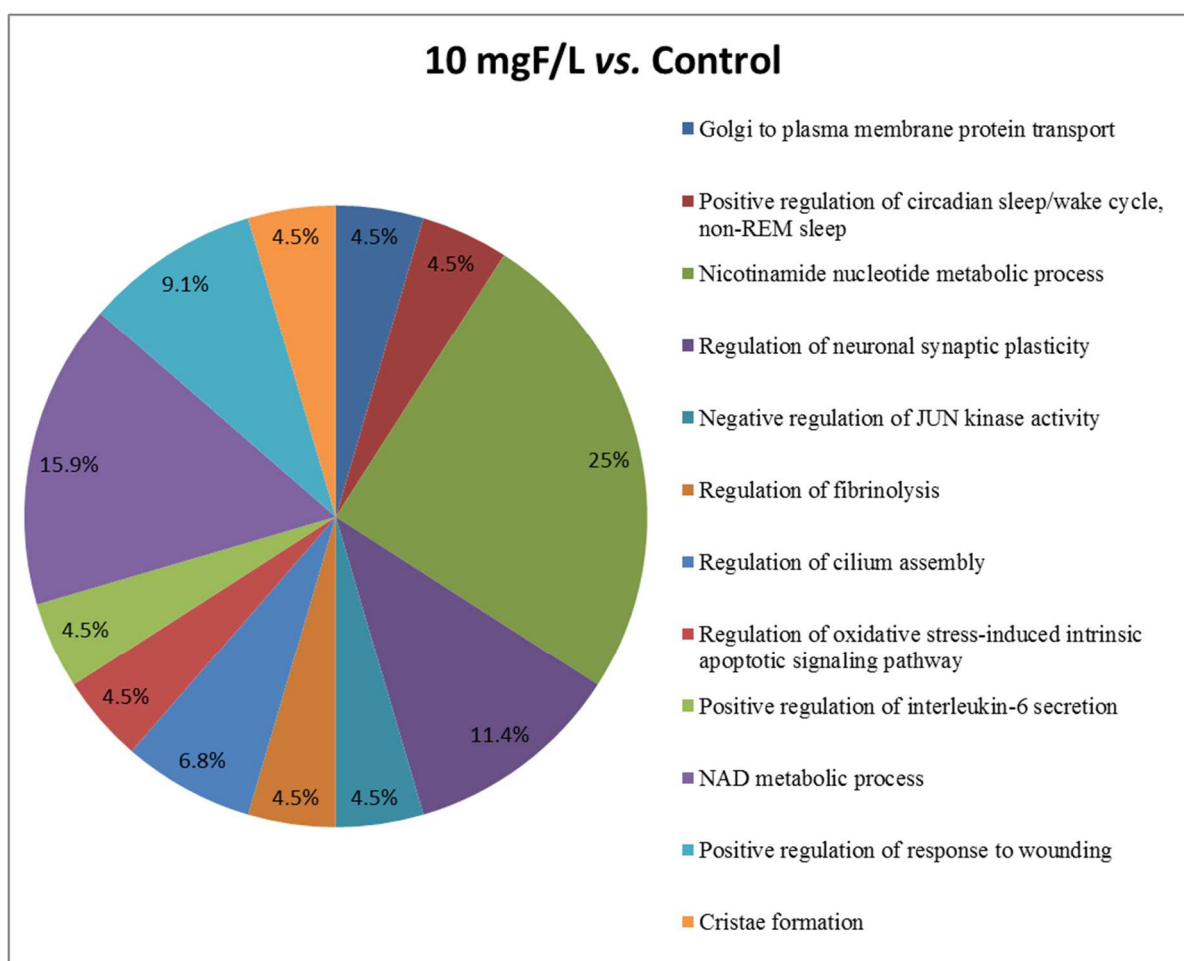


**Figure 3.** Functional distribution of proteins identified with differential expression in the jejunum of rats exposed to the chronic dose of 10 mgF/L vs. Control Group (0 mgF/L). Categories of proteins based on GO annotation Biological Process. Terms significant ( $Kappa = 0.04$ ) and distribution according to percentage of number of genes association. Proteins access number was provided by UNIPROT. The gene ontology was evaluated according to ClueGo® pluggins of Cytoscape® software 3.4.0<sup>89,90</sup>.

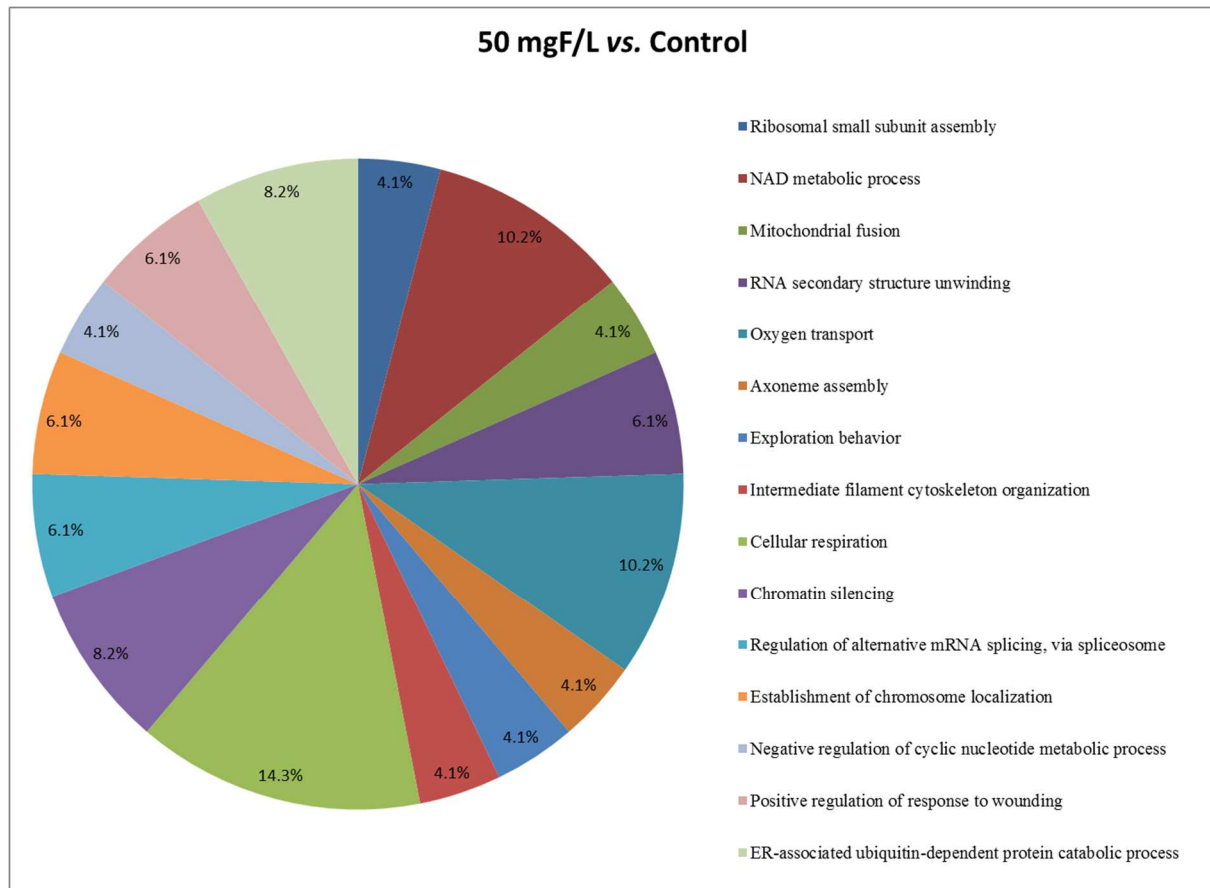


**Figure 4.** Functional distribution of proteins identified with differential expression in the jejunum of rats exposed to the chronic dose of 50 mgF/L vs. Control Group (0 mgF/L). Categories of proteins based on GO annotation Biological Process. Terms significant ( $Kappa = 0.04$ ) and distribution according to percentage of number of genes association. Proteins access number was provided by UNIPROT. The gene ontology was evaluated according to ClueGo® plugins of Cytoscape® software 3.4.089,90.

As in our study F caused morphological alterations in different enteric neuronal subtypes, which present several neurotransmitters involved in the GIT motility, it is possible that these alterations affect the GIT function, and promote the important symptomatology of F toxicity on the GIT, such as abdominal pain and diarrhea.

We also believe that our results are quite relevant regarding the ENS, since mechanisms of neurodegeneration associated to enteric neuropathies are characterized basically by alterations, damage or loss of enteric neurons, as observed in several important pathologies<sup>37</sup> and also in our study. Thus, in order to better investigate these findings involving the enteric innervation, we performed the proteomic analysis.

The proteomic approach revealed for both F doses that the majority of the proteins presenting changed expression interacted with *Solute carrier family 2, facilitated glucose transporter member 4* (GLUT4) (P19357) and *Polyubiquitin C*

(Q63429). In the network comparing 10 mgF/L vs. control groups, 17 members of the Ras-related *Rab* proteins (isoforms 1A, 1B, 3A, 3C, 3D, 4A, 4B, 5A, 8A, 8B, 10, 12, 14, 26, 35, 37, and 43) were uniquely found in the group treated with 10 mgF/L (Table S2), despite some not being present in the network. The GTPases *Rab* proteins are known as key regulators of intracellular membrane trafficking, from the formation of transport vesicles to their fusion with membranes. Rabs modulate between an inactive form (GDP-bound) and an active form (GTP-bound). The latter can attract to membranes distinct downstream effectors that will lead to vesicle formation, movement, tethering and fusion (UNIPROT). Generally, many studies report *Rab* proteins as molecules present in the CNS and their specific roles. Although marked differences distinguish the neuronal function between the ENS and CNS, their similarities allow the use of some principles established for the brain environment to be reapplied in the enteric context<sup>38</sup>. Several cellular processes can be altered and promote the enteric neuronal alterations caused by F effects through mechanisms involving the *Rab* proteins, which are considered neuronal regulators involved in the traffic and signaling of different molecules that promote neurons homeostasis, such as the neurotrophins family of growth factors. The neurotrophins-receptors complexes trigger important signaling pathways that promote development, survival and other neuronal functions through intracellular transport mechanisms mediate by the *Rab* proteins<sup>39</sup>.

*Rab 1A* is a regulator of specific vesicular trafficking from the ER to Golgi complex, and in dopaminergic neurons its expression presents a protective effect enhancing the control of motor function in surviving neurons of hemiparkinsonian animals<sup>40</sup>. From the family of the *Rab 3* proteins, 3 members were present in the 10 mgF/L group, *Rab 3A*, *Rab 3C*, and *Rab 3D*. The *Rab 3* family is observed in different cell types with high exocytic function<sup>41</sup>, in which they function as exocytosis regulators<sup>42</sup> correlated with neuronal traffic<sup>39</sup>, and are present in synaptic vesicles, modulating the neurotransmitter release<sup>42</sup>. *Rab 3A* is the most abundant isoform in the brain, where it presents a modulatory function in synaptic membrane fusion through a  $Ca^{2+}$ -dependent manner<sup>43</sup>. In the peripheral nervous system *Rab 3A* has increased expression in sciatic nerve lesion area associated to an increase in the expression of two other important proteins that contribute to neurotransmission, synaptophysin and synapsin I<sup>44</sup>. *Rab 3C* is highly expressed in primary hippocampal neurons, mediating regulated exocytosis<sup>45</sup> while *Rab 3D* is present in secretory granules and vesicles of

---

other cell types, such as adipocytes, exocrine glands, hematopoietic cells<sup>46</sup>, and low levels of expression were already identified in the duodenum, confirming its presence in exocrine cells of the GIT<sup>47</sup>.

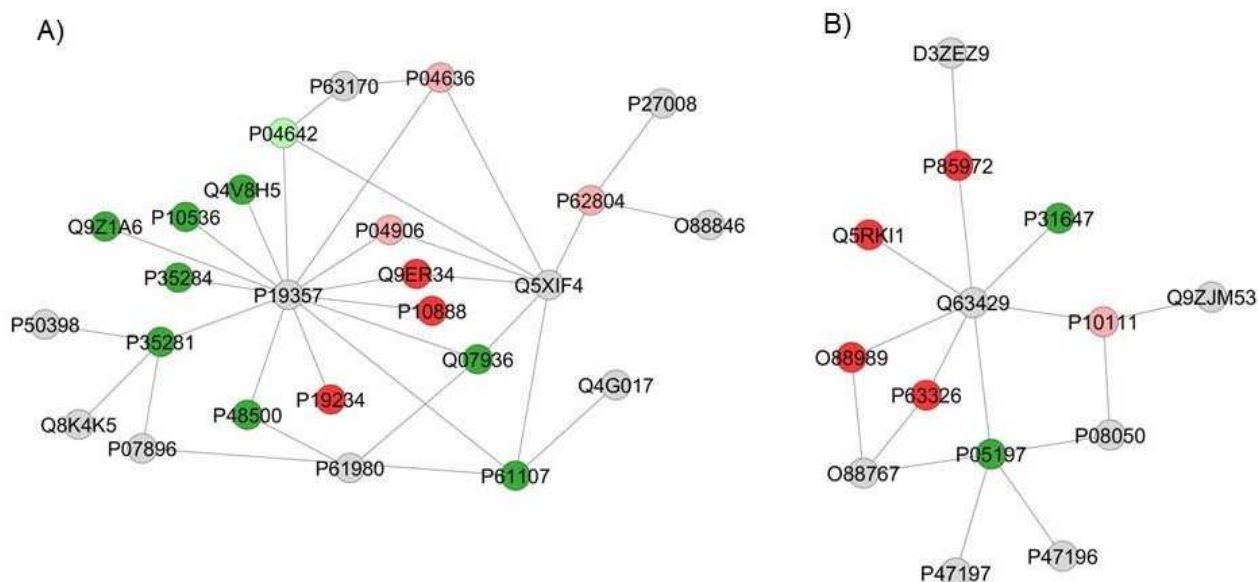


**Figure 5.** Subnetworks created by ClusterMark® to establish the interaction between proteins identified with differential expression in the 10 mgF/L group in relation to the control group. The color of the nodes indicates the differential expression of the respective named protein with its access code. The dark red and dark green nodes indicate proteins unique to the control and 10 mgF/L groups, respectively. The nodes in gray indicate the interaction proteins that are offered by CYTOSCAPE®, which were not identified in the present study and the light red and light green nodes indicate downregulation and upregulation, respectively. In (A), the access numbers in the gray nodes correspond to: Dynein light chain 1, cytoplasmic (P63170), Poly [ADP-ribose] polymerase 1 (P27008), E3 ubiquitin-protein ligase RNF4 (O88846), Small ubiquitin-related modifier 3 (Q5XIF4), Nischarin (Q4G017), Heterogeneous nuclear ribonucleoprotein K (P61980), Peroxisomal bifunctional enzyme (P07896), Lethal(2) giant larvae protein homolog 1 (Q8K4K5), Rab GDP dissociation inhibitor alpha (P50398) and Solute carrier family 2, facilitated glucose transporter member 4 (P19357). The access numbers of the unique proteins of the control (dark red nodes) correspond to: Aconitate hydratase, mitochondrial (Q9ER34), Cytochrome c oxidase subunit 4 isoform 1, mitochondrial (P10888) and NADH dehydrogenase [ubiquinone] flavoprotein 2, mitochondrial (P19234). The access numbers of the unique 10 mgF/L (dark green nodes) proteins correspond to: Aspartyl aminopeptidase (Q4V8H5), Ras-related protein Rab-1B (P10536), Vigilin (Q9Z1A6), Ras-related protein Rab-12 (P35284), Ras-related protein Rab-10 (P35281), Triosephosphate isomerase (P48500), Annexin A2 (Q07936) and Ras-related protein Rab-14 (P61107). The access numbers of the downregulated proteins (light red nodes) correspond to: Malate dehydrogenase, mitochondrial (P04636), Glutathione S-transferase P (P04906) and Histone H4 (P62804). The access numbers of the upregulated proteins (light green nodes) correspond to: L-lactate dehydrogenase A chain (P04642). In (B), the access numbers in the gray nodes correspond to: Protein Svitl (D3ZEZ9), Polyubiquitin-C (Q63429), Apoptosis-inducing factor 1, mitochondrial (Q9JM53), Protein deglycase DJ-1 (O88767), RAC-beta serine/threonine-protein kinase (P47197), RAC-alpha serine/threonine-protein kinase (P47196) and Gap junction alpha-1 protein (P08050). The access numbers of the unique proteins of the control (dark red nodes) correspond to: Vinculin (P85972), Eukaryotic initiation factor 4A-II (Q5RKI1), Malate dehydrogenase, cytoplasmic (O88989) and 40 S ribosomal

protein S10 (P63326). The accession numbers of the single 10 mgF/L (dark green nodes) proteins correspond to: Elongation factor 2 (P05197) and Sodium- and chloride-dependent GABA transporter 3 (P31647). The access numbers of the downregulated proteins (light red nodes) correspond to: Peptidyl-prolyl cis-trans isomerase A (P10111).

The Rabs 4A and 4B were also identified as exclusive for the 10 mgF/L, and Rab 4 is described as a regulator of early endosomes in the synapses, contributing to neurotransmitter receptor recycling through endosomes acting associated to other molecules in the later steps of the endocytic recycling pathway in dendrites, directing the neuronal membrane receptor trafficking<sup>48</sup>. This process is extremely important for the delivery of neurotransmitter receptors into the synaptic membrane, determining the synaptic function and plasticity. Rab 5A presents a role in axonal and dendritic endocytosis, contributing to the biogenesis of synaptic vesicles<sup>49</sup>. Rab 8 presents the same role as Rab 4, being required to direct into synapses neurotransmitter receptors as the AMPA-type glutamatergic receptors, presenting an important role in the control of synaptic function and plasticity at the postsynaptic membrane<sup>50</sup>.

Rab 10 is required for the secretion of neuropeptides through the release of dense core vesicles, which is a mechanism that modulates neuronal activity<sup>51</sup>. It is also a regulator of membrane trafficking during dendrite morphogenesis, and loss of RAB 10 decreases proximal dendritic arborization in the multi-dendritic PVD neurons<sup>52</sup>.

In the CNS Rab 12 is colocalized with M98K, and overexpression of the latter induces cell death in retinal glial cells, while knockdown of Rab 12 reduces M98K-induced cell death in the same cells through the autophagy mechanism<sup>53</sup>.

Rab 26 promotes in the brain the formation of clusters of vesicles in neuritis<sup>54</sup>, and the authors suggest a new mechanism for degradation of synaptic vesicles in which Rab 26 selectively conducts synaptic and secretory vesicles into preautophagosomal structures. In neuronal immortalized cells, Rab 35 promotes neurite differentiation and favors axon elongation in rat primary neurons in an activity-dependent manner<sup>55</sup>.

---

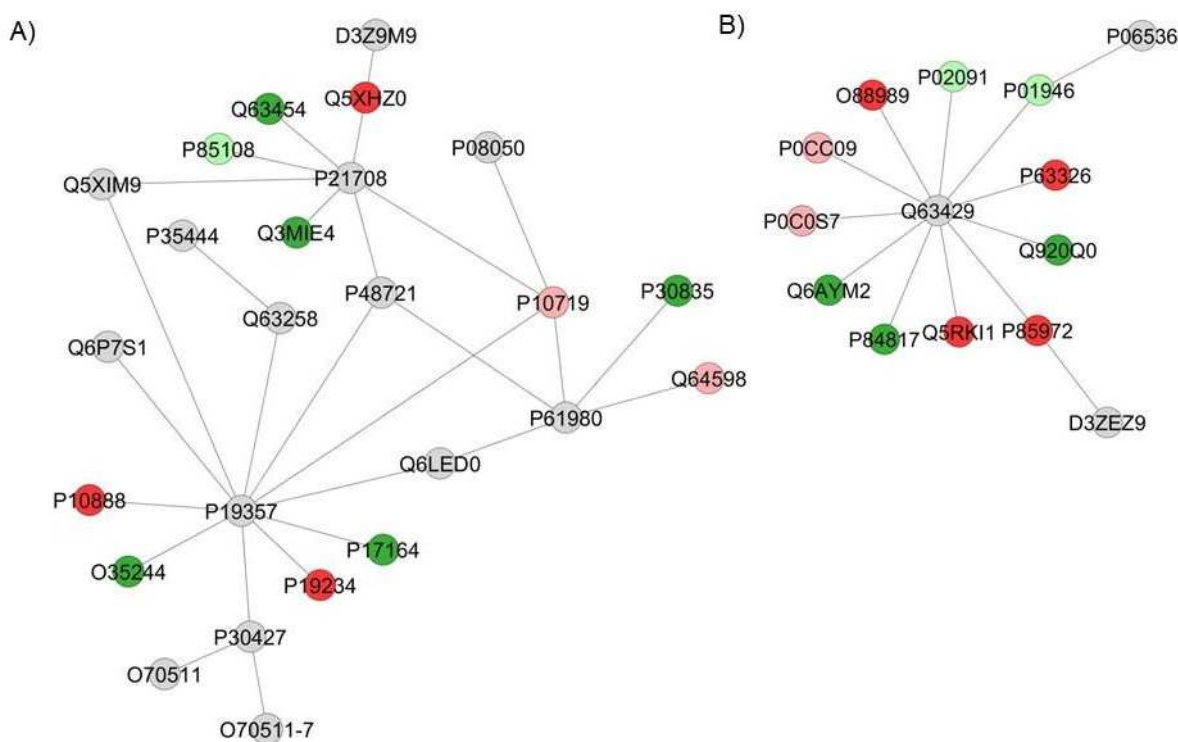


**Figure 6.** Subnetworks created by ClusterMark® to establish the interaction between proteins identified with differential expression in the 50 mgF/L group in relation to the control group. The color of the nodes indicates the differential expression of the respective named protein with its access code. The dark red and dark green nodes indicate proteins unique to the control and 50 mgF/L groups, respectively. The nodes in gray indicate the interaction proteins that are offered by CYTOSCAPE®, which were not identified in the present study and the light red and light green nodes indicate downregulation and upregulation, respectively. In (A), the access numbers in the gray nodes correspond to: PTEN induced putative kinase 1 (Predicted) (D3Z9M9), Mitogenactivated protein kinase 3 (P21708), T-complex protein 1 subunit beta (Q5XIM9), Gap junction alpha-1 protein (P08050), Cartilage oligomeric matrix protein (P35444), Acid ceramidase (Q6P7S1), Integrin alpha-7 (Q63258), Stress-70 protein, mitochondrial (P48721), Solute carrier family 2, facilitated glucose transporter member 4 (P19357), Histone H3.1 (Q6LED0), Heterogeneous nuclear ribonucleoprotein K (P61980), Ankyrin-3 (O70511), Plectin (P30427) and Ankyrin-3 (O70511-7). The access numbers of the unique proteins of the control (dark red nodes) correspond to: Malate dehydrogenase, cytoplasmic (O88989), 40 S ribosomal protein S10 (P63326), Eukaryotic initiation factor 4A-II (Q5RKI1) and Vinculin (P85972). The accession numbers of the unique 50 mgF/L (dark green nodes) proteins correspond to: Tektin-2 (Q6AYM2), Mitochondrial fission 1 protein (P84817) and Paralemmin-1 (Q920Q0). The access numbers of the downregulated proteins (light red nodes) correspond to: Histone H2A type 2-A (P0CC09) and Histone H2A.Z (P0C0S7). The accession numbers of the upregulated proteins (light green nodes) correspond to: Hemoglobin subunit beta-1 (P02091) and Hemoglobin subunit alpha-1/2 (P01946). In (B), the access numbers in the gray nodes correspond to: Polyubiquitin-C (Q63429), Protein Svit (D3ZEZ9) e Glucocorticoid receptor (P06536). The access numbers of the unique proteins of the control (dark red nodes) correspond to: Heat shock protein 75 kDa, mitochondrial (Q5XH20), Cytochrome c oxidase subunit 4 isoform 1, mitochondrial (P10888) and NADH dehydrogenase [ubiquinone] flavoprotein 2, mitochondrial (P19234). The accession numbers of the single 50 mgF/L (dark green nodes) proteins correspond to: Mitogen-activated protein kinase 4 (Q63454), Synaptic vesicle membrane protein VAT-1 homolog (Q3MIE4), ATP-dependent 6-phosphofructokinase, liver type (P30835), Tissue alpha-L-fucosidase (P17164) and

---

Peroxiredoxin-6 (O35244). The access numbers of the downregulated proteins (light red nodes) correspond to: ATP synthase subunit beta, mitochondrial (P10719) and e Histone H2A type 1-F (Q64598). The accession numbers of the upregulated proteins (light green nodes) correspond to: Tubulin beta-2A chain (P85108).

The fact that several members of the Rab proteins were expressed exclusively in the 10 mgF/L group might indicate that this F concentration could affect the neuronal functions, since different Rab proteins regulate distinct processes in the neuronal environment. Since the 10 mgF/L concentration caused a decrease in the enteric neuronal density, which can compromise the enteric neuronal activity, the expression of several Rab proteins can reflect an attempt to keep the neurotransmission unaltered in the presence of F. Besides the neuronal activity, other important biological mechanisms involve the Rab proteins action. In the network comparing 10 mgF/L vs. control groups, the isoforms 1B, 10, 12 and 14 interact with GLUT4, and especially Rab 10 and Rab 14, are required in GLUT4 translocation to the plasma membrane<sup>56,57</sup>. Their increased expression might help to explain the increased sensitivity to insulin recently reported to occur in rats with diabetes induced by streptozotocin exposed to 10 mgF/L in the drinking water<sup>58</sup>. The increased expression of Rab 10 and Rab 14 might facilitate glucose uptake. Rab 37 and Rab 3A, also present among the proteins exclusively expressed in the 10 mgF/L group, are involved in the insulin release. Rab 3A has an important role in the hormone release from pancreatic  $\beta$ -cells with a regulatory control on insulin-containing secretion<sup>59</sup>. Rab 37, with a high sequence homology with Rab 3A, has also been reported to participate in regulated secretion in mammalian cells in the control of insulin exocytosis through a different mechanism of Rab 3A<sup>60</sup>. According to the authors, impairment of Rab 37 expression may contribute to abnormal insulin release in pre-diabetic and diabetic conditions. We can infer that the expression of both proteins indicates that the insulin release mechanism could be altered with this F dose. We also observed an increase in *L-lactate dehydrogenase A chain (LDH)* (P04642) upon exposure to 10 mgF/L. This enzyme converts pyruvate to lactate with regeneration of NADH into NAD<sup>+</sup>. It is an alternative way to supply the lack of oxygen for aerobic oxidation of pyruvate and NADH produced in glycolysis<sup>61</sup>. In fact, the categories nicotinamide nucleotide metabolic process and NAD metabolic process were among the ones with the highest percentage of affected genes when the 10 mgF/L group was compared with control. Previous studies have reported increase in the LDH activity in the serum of infants who consumed water containing more than 2 mgF/L<sup>62</sup>. It was also overexpressed in the brain of rats treated with F<sup>63</sup>. When pyruvate

---

is converted into lactate by LDH, less pyruvate is available to enter into the mitochondria and form acetyl-CoA, which is consistent with the reduction of *Malate dehydrogenase, mitochondrial* (P04636) and of enzymes related to the oxidative phosphorylation, such as *Cytochrome c oxidase subunit 4 isoform 1, mitochondrial* (P10888) and *NADH dehydrogenase [ubiquinone] flavoprotein 2, mitochondrial* (P19234). According to Barbier, et al.<sup>3</sup>, F has an inhibitory effect on the activity of citric acid cycle enzymes, in agreement with our finding of reduction in Malate dehydrogenase, mitochondrial. Another protein with altered expression (downregulation) in the group treated with 10 mgF/L that interacts with GLUT4 was *Glutathione S-transferase P* (P04906) that was also found downregulated in the duodenum of rats treated with the same dose of F<sup>13</sup>. This enzyme is involved in the metabolism and detoxification of xenobiotics<sup>64</sup>. Many proteins with altered expression in the network comparing 10 mgF/L vs. control groups interact with *Polyubiquitin C* (Q63429), a highly conserved polypeptide that is covalently bound to other cellular proteins to signal processes such as protein degradation, protein/protein interaction and protein intracellular trafficking<sup>65</sup>. Among them are proteins related to translation, that were absent in the group treated with 10 mgF/L, such as *Eukaryotic initiation factor 4A-II* (Q5RK11) and *40 S ribosomal protein S10* (P63326). The latter was also reduced in the group treated with 50 mgF/L both in the present study and in a previous study where duodenum was analyzed<sup>13</sup>. In addition, *Peptidyl-prolyl cis-trans isomerase A* (P10111) was reduced in the group treated with 10 mgF/L compared to control, which might impair protein folding. Also involved in protein synthesis, *Elongation factor 2* (P05197) presented altered expression upon exposure to 10 mgF/L. This protein was present only in the group treated with 10 mgF/L, and catalyzes the GTP-dependent ribosomal translocation step during translation elongation (UNIPROT). Differences in expression of all these proteins indicate alterations in distinct steps of protein synthesis upon exposure to 10 mgF/L. Changes in protein synthesis might help to explain the alterations in the thickness of the jejunum wall observed in this group. Interestingly, Elongation factor 2 interacted with two of the 3 isoforms of the protein *kinase AKT*, namely *RAC-alpha serine/threonine-protein kinase* (AKT1; P47196) and *RAC-beta serine/threonine-protein kinase* (AKT2; P47197) that mediate protein synthesis and glucose metabolism<sup>66</sup>.

In the network comparing the 50 mgF/L vs. control groups (Fig. 6), some proteins with relevance for the neuronal homeostasis were expressed uniquely in the

---



---

50 mgF/L, such as *Tektin-2* (Q6AYM2), *Perforin-1* (Q5FVS5), and *Mitochondrial fission 1 protein* (Fis1-P84817). The *Tektins* family has significant expression in adult brain and in embryonic stages of the choroid plexus, the forming retina, and olfactory receptor neurons, and can be considered a molecular target for the comprehension of neural development<sup>67</sup>. Although not present in the subnetwork, *Perforin* participates in the CD8+ T cells response, promoting granule cytotoxicity leading to a fast cellular necrosis of the target cell in minutes<sup>68</sup> or apoptosis in a period of hours through a mechanism in which the target cell collaborates with perforin to deliver granzymes into the cytosol<sup>69</sup>. Using these mechanisms perforin-dependent, CD8+ T cells promote neuronal damage in inflammatory CNS disorders<sup>70</sup>.

*Mitochondrial fission* is implicated in the cell death through a pathway that involves caspase activation<sup>71</sup>, and *Mitochondrial fission 1 protein* (Fis1) is considered essential for mitochondrial fission<sup>72</sup>. Overexpression of Fis1 caused increase of mitochondrial fragmentation, which conducted to apoptosis or triggered autophagy<sup>73,74</sup>, and neuroprotective effects are correlated with inhibition of Fis1<sup>75</sup>.

The fact that these proteins presented increased expression in relation to the control group can reflect F neurotoxicity on the ENS with the concentration of 50 mgF/L, and could result in the decrease in the density of the general population of neurons since these 3 proteins are involved in pathways that conduct to cell death by distinct mechanisms.

Other proteins with altered expression interacted mainly with GLUT4 (P19357) and *Polyubiquitin C* (Q63429), which was also observed for the network comparing the 10 mgF/L vs. control groups (Fig. 5). In addition, *Mitogen-activated protein kinase 3* (MAPK3; P21708) was also an interacting partner as in the duodenum of rats treated with the same concentration of F in the drinking water<sup>13</sup>. Among the proteins that interacted with GLUT4, *Peroxiredoxin-6* (O35244) was present only in the group treated with 50 mgF/L, when compared with control (Fig. 6). This enzyme, located in the cytoplasm, protects cells against oxidative stress, in addition to modulating intracellular signaling pathways. Peroxiredoxins catalyze the reduction of H<sub>2</sub>O<sub>2</sub> and hydroxyperoxide in water and alcohol<sup>76</sup>. Thus, changes in these proteins expression could be linked to fluoride-induced oxidative stress that has been extensively described in the literature<sup>3,77-81</sup>. In the group treated with 50 mgF/L, there was a remarkable downregulation in several isoforms of Histones, in comparison with control (Fig. 6 and Table S5). The major role described for histones is DNA “packaging”, however, it is

---

also well described that these proteins confer variations in chromatin structure to ensure dynamic processes of transcriptional regulation in eukaryotes<sup>82</sup>. Epigenetic modifications of DNA and histones are fundamental mechanisms by which neurons adapt their transcriptional response to developmental and environmental factors. Modifications in the chromatin of neurons contribute dramatically to changes in the neuronal circuits, and it is possible that histone activity is involved in disorders that compromise neuronal function<sup>83</sup>. Thus, changes in the expression of histones might have contributed to the alterations found in the morphology of enteric neurons in response to F exposure. In addition, structural muscle proteins such as different isoforms of actin and myosin were increased or exclusive in the group treated with 50 mgF/L (Tables S3 and S5), which helps to explain the increase in the thickness of the jejunum tunica muscularis.

Probably the most remarkable finding of the present study was that when the groups treated with 10 and 50 mgF/L are compared with control, some proteins related to energetic metabolism presented similar alterations in expression, regardless the dose of F, such as: *Cytochrome c oxidase subunit 4 isoform 1, mitochondrial* (P10888), *NADH dehydrogenase [ubiquinone] flavoprotein 2, mitochondrial* (P19234), *Malate dehydrogenase, mitochondrial* (P04636), *Malate dehydrogenase, cytoplasmic* (O88989) and *L-lactate dehydrogenase A chain* (P04642). The absence of *Malate dehydrogenase, mitochondrial* (P04636), *Malate dehydrogenase, cytoplasmic* (O88989), that form *oxaloacetate*, absence of *NADH dehydrogenase [ubiquinone] flavoprotein 2, mitochondrial* (P19234) that transfers electrons from NADH to respiratory chain in both groups treated with F, as well as the reduction of *ATP synthase subunit beta, mitochondrial* (P10719) (only in the group treated with the highest F dose), as well as the increase in *L-lactate dehydrogenase A chain* (P04642) in both groups treated with F indicate an increase in anaerobic metabolism in attempt to obtain energy, since aerobic metabolism is impaired in the presence of F. However, the rate of production of ATP through anaerobic pathways is much lower than that of aerobic pathways, which is in-line with the reports of reduction in the production of ATP induced by exposure to high F doses<sup>3,84</sup>. It is important to highlight that these changes in the expression of proteins associated to energy metabolism induced by exposure to 10 and 50 mgF/L in the drinking water are more pronounced than those observed previously in other organs exposed to roughly the same doses of F<sup>58,63,80,85–88</sup>. This might be due to the fact that the small intestine is responsible for the absorption of

---

around 75% of ingested F<sup>5</sup>, which makes the cells of the intestinal wall exposed to higher doses of F than the cells from the other organs.

In conclusion, chronic exposure to F, especially to the highest concentration evaluated, increased the thickness of the tunica muscularis and altered the pattern of protein expression. Extensive downregulation of several isoforms of histones might have contributed to the alterations found in the morphology of enteric neurons in response to F exposure. Additionally, changes in proteins involved in energy metabolism indicate a shift from aerobic to anaerobic metabolism upon exposure to the highest F concentration. These findings provide new insights into the mechanisms involved in F toxicity in the intestine.

## REFERENCES

1. Yan, X. *et al.* Fluoride induces apoptosis and alters collagen I expression in rat osteoblasts. *Toxicol Lett* **200**, 133–138, <https://doi.org/10.1016/j.toxlet.2010.11.005> (2011).
2. Buzalaf, M. A., Pessan, J. P., Honorio, H. M. & ten Cate, J. M. Mechanisms of action of fluoride for caries control. *Monogr Oral Sci* **22**, 97–114, <https://doi.org/10.1159/000325151> (2011).
3. Barbier, O., Arreola-Mendoza, L. & Del Razo, L. M. Molecular mechanisms of fluoride toxicity. *Chem Biol Interact* **188**, 319–333, <https://doi.org/10.1016/j.cbi.2010.07.011> (2010).
4. Whitford, G. M. & Pashley, D. H. Fluoride absorption: the influence of gastric acidity. *Calcif Tissue Int* **36**, 302–307 (1984).
5. Nopakun, J., Messer, H. H. & Voller, V. Fluoride absorption from the gastrointestinal tract of rats. *J Nutr* **119**, 1411–1417 (1989).
6. Zheng, Y., Wu, J., Ng, J. C., Wang, G. & Lian, W. The absorption and excretion of fluoride and arsenic in humans. *Toxicol Lett* **133**, 77–82 (2002).
7. Susheela, A., Kumar, A., Bhatnagar, M. & Bahadur, R. Prevalence of endemic Fluorosis with gastrointestinal manifestations in People living in some North-Indian villages. *Fluoride* **26**, 97–104 (1993).
8. Susheela, A. *et al.* Fluoride ingestion and its correlation with gastrointestinal discomfort. *Fluoride* **25**, 5–22 (1992).
9. Sharma, J. D., Jain, P. & Sohu, D. Gastric Discomforts from Fluoride in Drinking Water in Sanganer Tehsil, Rajasthan, India. *Fluoride* **42**, 286–291 (2009).
10. Das, T. K., Susheela, A. K., Gupta, I. P., Dasarathy, S. & Tandon, R. K. Toxic Effects of Chronic Fluoride Ingestion on the Upper Gastrointestinal-Tract. *J Clin Gastroenterol* **18**, 194–199, <https://doi.org/10.1097/00004836-199404000-00004> (1994).

11. Furness, J. B. A comprehensive overview of all aspects of the enteric nervous system. *The Enteric Nervous System*. (Blackwell, 2006).
  12. Sand, E. *et al.* Structural and functional consequences of busserelin-induced enteric neuropathy in rat. *BMC Gastroenterol* **14**, 209, <https://doi.org/10.1186/s12876-014-0209-7> (2014).
  13. Melo, C. G. S. *et al.* Enteric innervation combined with proteomics for the evaluation of the effects of chronic fluoride exposure on the duodenum of rats. *Sci Rep* **7**, 1070, <https://doi.org/10.1038/s41598-017-01090-y> (2017).
  14. Guyton, A. C. & Hall, J. E. *Textbook of medical physiology*. 13 edn, (Elsevier Health Sciences, 2015).
  15. Dunipace, A. J. *et al.* Effect of aging on animal response to chronic fluoride exposure. *J Dent Res* **74**, 358–368, <https://doi.org/10.1177/00220345950740011201> (1995).
  16. Bradford, M. M. A rapid and sensitive method for the quantitation of microgram quantities of protein utilizing the principle of protein-dye binding. *Anal Biochem* **72**, 248–254 (1976).
  17. Lima Leite, A. *et al.* Proteomic analysis of gastrocnemius muscle in rats with streptozotocin-induced diabetes and chronically exposed to fluoride. *PLoS One* **9**, e106646, <https://doi.org/10.1371/journal.pone.0106646> (2014).
  18. Bauer-Mehren, A. Integration of genomic information with biological networks using Cytoscape. *Methods Mol Biol* **1021**, 37–61, [https://doi.org/10.1007/978-1-62703-450-0\\_3](https://doi.org/10.1007/978-1-62703-450-0_3) (2013).
  19. Millan, P. P. Visualization and analysis of biological networks. *Methods Mol Biol* **1021**, 63–88, [https://doi.org/10.1007/978-1-62703-450-0\\_4](https://doi.org/10.1007/978-1-62703-450-0_4) (2013).
  20. Orchard, S. Molecular interaction databases. *Proteomics* **12**, 1656–1662, <https://doi.org/10.1002/pmic.201100484> (2012).
  21. Nopakun, J. & Messer, H. H. Mechanism of fluoride absorption from the rat small intestine. *Nutr Res* **10**, 771–779 (1990).
  22. Vogt, R. L., Witherell, L., LaRue, D. & Klaucke, D. N. Acute fluoride poisoning associated with an on-site fluoridator in a Vermont elementary school. *Am J Public Health* **72**, 1168–1169 (1982).
  23. Augenstein, W. L. *et al.* Fluoride ingestion in children: a review of 87 cases. *Pediatrics* **88**, 907–912 (1991).
  24. Gessner, B. D., Beller, M., Middaugh, J. P. & Whitford, G. M. Acute fluoride poisoning from a public water system. *N Engl J Med* **330**, 95–99, <https://doi.org/10.1056/NEJM199401133300203> (1994).
  25. Akiniwa, K. Re-examination of acute toxicity of fluoride. *Fluoride* **30**, 89–104 (1997).
  26. Holzer, P. & Lippe, I. T. Substance P can contract the longitudinal muscle of the guinea-pig small intestine by releasing intracellular calcium. *Brit J Pharmacol* **82**, 259–267 (1984).
-

- 
27. Rivera, L. R., Poole, D. P., Thacker, M. & Furness, J. B. The involvement of nitric oxide synthase neurons in enteric neuropathies. *Neurogastroenterol Motil* **23**, 980–988, <https://doi.org/10.1111/j.1365-2982.2011.01780.x> (2011).
  28. Benarroch, E. E. Enteric nervous system: functional organization and neurologic implications. *Neurology* **69**, 1953–1957, <https://doi.org/10.1212/01.wnl.0000281999.56102.b5> (2007).
  29. Defani, M. A., Zanoni, J. N., Natali, M. R., Bazotte, R. B. & de Miranda-Neto, M. H. Effect of acetyl-L-carnitine on VIP-ergic neurons in the jejunum submucous plexus of diabetic rats. *Arq Neuropsiquiatr* **61**, 962–967 (2003).
  30. Ekelund, K. M. & Ekblad, E. Structural, neuronal, and functional adaptive changes in atrophic rat ileum. *Gut* **45**, 236–245 (1999).
  31. Hermes-Uliana, C. *et al.* Is L-glutathione more effective than L-glutamine in preventing enteric diabetic neuropathy? *Dig Dis Sci* **59**, 937–948, <https://doi.org/10.1007/s10620-013-2993-2> (2014).
  32. Veit, A. P. & Zanoni, J. N. Age-related changes in myosin-V myenteric neurons, CGRP and VIP immunoreactivity in the ileum of rats supplemented with ascorbic acid. *Histol Histopathol* **27**, 123–132, <https://doi.org/10.14670/HH-27.123> (2012).
  33. Ekblad, E. & Bauer, A. J. Role of vasoactive intestinal peptide and inflammatory mediators in enteric neuronal plasticity. *Neurogastroenterol Motil* **16**(Suppl 1), 123–128, <https://doi.org/10.1111/j.1743-3150.2004.00487.x> (2004).
  34. Oste, M. *et al.* The intestinal trophic response to enteral food is reduced in parenterally fed preterm pigs and is associated with more nitrergic neurons. *J Nutr* **135**, 2657–2663 (2005).
  35. Gabella, G. In *Physiology of the Gastrointestinal Tract*. (ed L. R. JOHNSON) 335–381 (Raven Press, 1987).
  36. Soares, A., Beraldi, E. J., Ferreira, P. E., Bazotte, R. B. & Buttow, N. C. Intestinal and neuronal myenteric adaptations in the small intestine induced by a high-fat diet in mice. *BMC Gastroenterol* **15**, 3, <https://doi.org/10.1186/s12876-015-0228-z> (2015).
  37. De Giorgio, R. *et al.* New insights into human enteric neuropathies. *Neurogastroenterol Motil* **16**(Suppl 1), 143–147, <https://doi.org/10.1111/j.1743-3150.2004.00491.x> (2004).
  38. Gershon, M. D. & Ratcliffe, E. M. Developmental biology of the enteric nervous system: pathogenesis of Hirschsprung's disease and other congenital dysmotilities. *Semin Pediatr Surg* **13**, 224–235 (2004).
  39. Bucci, C., Alifano, P. & Cogli, L. The role of rab proteins in neuronal cells and in the trafficking of neurotrophin receptors. *Membranes (Basel)* **4**, 642–677, <https://doi.org/10.3390/membranes4040642> (2014).
  40. Coune, P. G., Bensadoun, J. C., Aebischer, P. & Schneider, B. L. Rab1A over-expression prevents Golgi apparatus fragmentation and partially corrects motor deficits in an alpha-synuclein based rat model of Parkinson's disease. *J Parkinsons Dis* **1**, 373–387, <https://doi.org/10.3233/JPD-2011-11058> (2011).
  41. Lledo, P. M. *et al.* Rab3 proteins: key players in the control of exocytosis. *Trends Neurosci* **17**, 426–432 (1994).
-

42. Schlüter, O. M., Schmitz, F., Jahn, R., Rosenmund, C. & Südhof, T. C. A complete genetic analysis of neuronal Rab3 function. *J Neurosci* **24**, 6629–6637, <https://doi.org/10.1523/JNEUROSCI.1610-04.2004> (2004).
  43. Geppert, M., Goda, Y., Stevens, C. F. & Südhof, T. C. The small GTP-binding protein Rab3A regulates a late step in synaptic vesicle fusion. *Nature* **387**, 810–814, <https://doi.org/10.1038/42954> (1997).
  44. Li, J. Y., Jahn, R. & Dahlström, A. Rab3a, a small GTP-binding protein, undergoes fast anterograde transport but not retrograde transport in neurons. *Eur J Cell Biol* **67**, 297–307 (1995).
  45. van Vlijmen, T. *et al.* A unique residue in rab3c determines the interaction with novel binding protein Zwint-1. *FEBS Lett* **582**, 2838–2842, <https://doi.org/10.1016/j.febslet.2008.07.012> (2008).
  46. Pavlos, N. J. *et al.* Rab3D regulates a novel vesicular trafficking pathway that is required for osteoclastic bone resorption. *Mol Cell Biol* **25**, 5253–5269, <https://doi.org/10.1128/MCB.25.12.5253-5269.2005> (2005).
  47. Valentijn, J. A., van Weeren, L., Ultee, A. & Koster, A. J. Novel localization of Rab3D in rat intestinal goblet cells and Brunner's gland acinar cells suggests a role in early Golgi trafficking. *Am J Physiol Gastrointest Liver Physiol* **293**, G165–177, <https://doi.org/10.1152/ajpgi.00520.2006> (2007).
  48. Hoogenraad, C. C. *et al.* Neuron specific Rab4 effector GRASP-1 coordinates membrane specialization and maturation of recycling endosomes. *PLoS Biol* **8**, e1000283, <https://doi.org/10.1371/journal.pbio.1000283> (2010).
  49. de Hoop, M. J. *et al.* The involvement of the small GTP-binding protein Rab5a in neuronal endocytosis. *Neuron* **13**, 11–22 (1994).
  50. Gerges, N. Z., Backos, D. S. & Esteban, J. A. Local control of AMPA receptor trafficking at the postsynaptic terminal by a small GTPase of the Rab family. *J Biol Chem* **279**, 43870–43878, <https://doi.org/10.1074/jbc.M404982200> (2004).
  51. Sasidharan, N. *et al.* RAB-5 and RAB-10 cooperate to regulate neuropeptide release in *Caenorhabditis elegans*. *Proc Natl Acad Sci USA* **109**, 18944–18949, <https://doi.org/10.1073/pnas.1203306109> (2012).
  52. Zou, W., Yadav, S., DeVault, L., Nung Jan, Y. & Sherwood, D. R. RAB-10-Dependent Membrane Transport Is Required for Dendrite Arborization. *PLoS Genet* **11**, e1005484, <https://doi.org/10.1371/journal.pgen.1005484> (2015).
  53. Sirohi, K. *et al.* M98K-OPTN induces transferrin receptor degradation and RAB12-mediated autophagic death in retinal ganglion cells. *Autophagy* **9**, 510–527, <https://doi.org/10.4161/auto.23458> (2013).
  54. Binotti, B. *et al.* The GTPase Rab26 links synaptic vesicles to the autophagy pathway. *Elife* **4**, e05597, <https://doi.org/10.7554/eLife.05597> (2015).
  55. Villarroel-Campos, D. *et al.* Rab35 Functions in Axon Elongation Are Regulated by P53-Related Protein Kinase in a Mechanism That Involves Rab35 Protein Degradation and the Microtubule-Associated Protein 1B. *J Neurosci* **36**, 7298–7313, <https://doi.org/10.1523/JNEUROSCI.4064-15.2016> (2016).
-

- 
56. Sano, H. *et al.* Rab10, a target of the AS160 Rab GAP, is required for insulin-stimulated translocation of GLUT4 to the adipocyte plasma membrane. *Cell metabolism* **5**, 293–303, <https://doi.org/10.1016/j.cmet.2007.03.001> (2007).
57. Brewer, P. D., Habtemichael, E. N., Romenskaia, I., Coster, A. C. & Mastick, C. C. Rab14 limits the sorting of Glut4 from endosomes into insulin-sensitive regulated secretory compartments in adipocytes. *The Biochemical J* **473**, 1315–1327, <https://doi.org/10.1042/BCJ20160020> (2016).
58. Lobo, J. G. *et al.* Low-Level Fluoride Exposure Increases Insulin Sensitivity in Experimental Diabetes. *J Dent Res* **94**, 990–997, <https://doi.org/10.1177/0022034515581186> (2015).
59. Lang, J. Molecular mechanisms and regulation of insulin exocytosis as a paradigm of endocrine secretion. *Eur J Biochem* **259**, 3–17 (1999).
60. Ljubicic, S. *et al.* The GTPase Rab37 Participates in the Control of Insulin Exocytosis. *PLoS One* **8**, e68255, <https://doi.org/10.1371/journal.pone.0068255> (2013).
61. Lehninger, A. L., Nelson, D. L. & Cox, M. M. *Lehninger principles of biochemistry*. 3. ed. edn, 975 (2002).
62. Xiong, X. *et al.* Dose-effect relationship between drinking water fluoride levels and damage to liver and kidney functions in children. *Environ Res* **103**, 112–116, <https://doi.org/10.1016/j.envres.2006.05.008> (2007).
63. Ge, Y., Niu, R., Zhang, J. & Wang, J. Proteomic analysis of brain proteins of rats exposed to high fluoride and low iodine. *Arch Toxicol* **85**, 27–33, <https://doi.org/10.1007/s00204-010-0537-5> (2011).
64. Kaminsky, L. S. & Zhang, Q. Y. The small intestine as a xenobiotic-metabolizing organ. *Drug Metab Dispos* **31**, 1520–1525, <https://doi.org/10.1124/dmd.31.12.1520> (2003).
65. Ciechanover, A. & Schwartz, A. L. The ubiquitin-proteasome pathway: the complexity and myriad functions of proteins death. *Proc Natl Acad Sci USA* **95**, 2727–2730 (1998).
66. Bottermann, K., Reinartz, M., Barsoum, M., Kotter, S. & Godecke, A. Systematic Analysis Reveals Elongation Factor 2 and alpha-Enolase as Novel Interaction Partners of AKT2. *PLoS One* **8**, e66045, <https://doi.org/10.1371/journal.pone.0066045> (2013).
67. Norrander, J., Larsson, M., Ståhl, S., Höög, C. & Linck, R. Expression of ciliary tektins in brain and sensory development. *J Neurosci* **18**, 8912–8918 (1998).
68. Waterhouse, N. J. *et al.* Cytotoxic T lymphocyte-induced killing in the absence of granzymes A and B is unique and distinct from both apoptosis and perforin-dependent lysis. *J Cell Biol* **173**, 133–144, <https://doi.org/10.1083/jcb.200510072> (2006).
69. Pipkin, M. E. & Lieberman, J. Delivering the kiss of death: progress on understanding how perforin works. *Curr Opin Immunol* **19**, 301–308, <https://doi.org/10.1016/j.coi.2007.04.011> (2007).
70. Meuth, S. G. *et al.* Cytotoxic CD8+ T cell-neuron interactions: perforin-dependent electrical silencing precedes but is not causally linked to neuronal cell death. *J*
-

- Neurosci* **29**, 15397–15409, <https://doi.org/10.1523/JNEUROSCI.4339-09.2009> (2009).
71. Perfettini, J. L., Roumier, T. & Kroemer, G. Mitochondrial fusion and fission in the control of apoptosis. *Trends Cell Biol* **15**, 179–183, <https://doi.org/10.1016/j.tcb.2005.02.005> (2005).
72. Chen, H. & Chan, D. C. Emerging functions of mammalian mitochondrial fusion and fission. *Hum Mol Genet* **14 Spec No. 2**, R283–289, <https://doi.org/10.1093/hmg/ddi270> (2005).
73. James, D. I., Parone, P. A., Mattenberger, Y. & Martinou, J. C. hFis1, a novel component of the mammalian mitochondrial fission machinery. *J Biol Chem* **278**, 36373–36379, <https://doi.org/10.1074/jbc.M303758200> (2003).
74. Gomes, L. C. & Scorrano, L. High levels of Fis1, a pro-fission mitochondrial protein, trigger autophagy. *Biochim Biophys Acta* **1777**, 860–866, <https://doi.org/10.1016/j.bbabi.2008.05.442> (2008).
75. Wang, Y. *et al.* Neuroprotective Effect and Mechanism of Thiazolidinedione on Dopaminergic Neurons *In Vivo* and *In Vitro* in Parkinson's Disease. *PPAR Res* **2017**, 4089214, <https://doi.org/10.1155/2017/4089214> (2017).
76. Hofmann, B., Hecht, H. J. & Flohe, L. Peroxiredoxins. *Biol Chem* **383**, 347–364, <https://doi.org/10.1515/BC.2002.040> (2002).
77. Shanthakumari, D., Srinivasalu, S. & Subramanian, S. Effect of fluoride intoxication on lipidperoxidation and antioxidant status in experimental rats. *Toxicology* **204**, 219–228, <https://doi.org/10.1016/j.tox.2004.06.058> (2004).
78. Stirnimann, G., Kessebohmer, K. & Lauterburg, B. Liver injury caused by drugs: an update. *Swiss Med Wkly* **140**, w13080, <https://doi.org/10.4414/smw.2010.13080> (2010).
79. Zhan, X. A., Wang, M., Xu, Z. R., Li, W. F. & Li, J. X. Effects of fluoride on hepatic antioxidant system and transcription of Cu/Zn SOD gene in young pigs. *J Trace Elem Med Biol* **20**, 83–87, <https://doi.org/10.1016/j.jtemb.2005.11.003> (2006).
80. Pereira, H. A. *et al.* Proteomic analysis of liver in rats chronically exposed to fluoride. *PLoS One* **8**, e75343, <https://doi.org/10.1371/journal.pone.0075343> (2013).
81. Pereira, H. A. *et al.* Fluoride Intensifies Hypercaloric Diet-Induced ER Oxidative Stress and Alters Lipid Metabolism. *PLoS One* **11**, e0158121, <https://doi.org/10.1371/journal.pone.0158121> (2016).
82. Maze, I., Noh, K. M., Soshnev, A. A. & Allis, C. D. Every amino acid matters: essential contributions of histone variants to mammalian development and disease. *Nat Rev Genet* **15**, 259–271, <https://doi.org/10.1038/nrg3673> (2014).
83. Riccio, A. Dynamic epigenetic regulation in neurons: enzymes, stimuli and signaling pathways. *Nat Neurosci* **13**, 1330–1337, <https://doi.org/10.1038/nn.2671> (2010).
84. Strunecka, A., Patocka, J., Blaylock, R. & Chinoy, N. Fluoride interactions: from molecules to disease. *Current Signal Transduction Therapy* **2**, 190–213 (2007).
85. Xu, H. *et al.* Proteomic analysis of kidney in fluoride-treated rat. *Toxicol Lett* **160**, 69–75, <https://doi.org/10.1016/j.toxlet.2005.06.009> (2005).
-



86. Kobayashi, C. A. *et al.* Proteomic analysis of kidney in rats chronically exposed to fluoride. *Chem Biol Interact* **180**, 305–311, <https://doi.org/10.1016/j.cbi.2009.03.009> (2009).
87. Niu, R. *et al.* Proteomic analysis of hippocampus in offspring male mice exposed to fluoride and lead. *Biol Trace Elem Res* **162**, 227–233, <https://doi.org/10.1007/s12011-014-0117-2> (2014).
88. Carvalho, J. G. *et al.* Renal proteome in mice with different susceptibilities to fluorosis. *PLoS One* **8**, e53261, <https://doi.org/10.1371/journal.pone.0053261> (2013).
89. Bindea, G., Galon, J. & Mlecnik, B. CluePedia Cytoscape plugin: pathway insights using integrated experimental and in silico data. *Bioinformatics* **29**, 661–663, <https://doi.org/10.1093/bioinformatics/btt019> (2013).
90. Bindea, G. *et al.* ClueGO: a Cytoscape plug-in to decipher functionally grouped gene ontology and pathway annotation networks. *Bioinformatics* **25**, 1091–1093, <https://doi.org/10.1093/bioinformatics/btp101> (2009).

### Acknowledgements

This study was supported by FAPESP (2011/10233-7, 2012/16840-5 and 2016/09100-6).

### Author Contributions

C.M., M.B., J.Z., and J.P. conceived the experiments. A.D., C.M., J.P., S.S. and A.L. conducted the experiments. A.D., C.M., J.P., S.S., A.L., I.A., T.V., A.H., and J.S. participated in the research experiments. A.D., C. M., A.H., J.S., E.S. participated in the experiments analysis. A.D., C.M., M.B. drafted the article; analyzed and interpreted the results. All authors reviewed and approved the manuscript.

### Additional Information

**Supplementary information** accompanies this paper at <https://doi.org/10.1038/s41598-018-21533-4>.

**Competing Interests:** The authors declare no competing interests.

**Publisher's note:** Springer Nature remains neutral with regard to jurisdictional claims in published maps and institutional affiliations. **Open Access** This article is licensed under a Creative Commons Attribution 4.0 International License, which permits use, sharing, adaptation, distribution and reproduction in any medium or format, as long as you give appropriate credit to the original author(s) and the source, provide a link to the Creative Commons license, and indicate if changes were made. The images or other third party material in this article are included in the article's Creative Commons license, unless indicated otherwise in a credit line to the material. If material is not included in the article's Creative Commons

license and your intended use is not permitted by statutory regulation or exceeds the permitted use, you will need to obtain permission directly from the copyright holder. To view a copy of this license, visit <http://creativecommons.org/licenses/by/4.0/>.

**Supplementary Table S1.** Proteins identified exclusively in the jejunum of rats of control group.

<sup>a</sup> Access number	Protein name	PLGS Score
P63326	40S ribosomal protein S10	86.29
Q9ER34	Aconitate hydratase, mitochondrial	56.82
Q68FP8	Adenylate kinase 8	57.06
O09178	AMP deaminase 3	63.74
Q7TP90	Arrestin domain-containing protein 4	119.76
D3ZTV7	Ash2 (Absent, small, or homeotic)-like (Drosophila) (Predicted)	58.22
Q8K1M8	BMP/retinoic acid-inducible neural-specific protein 2	77.73
Q6AXW0	Borealin	85.75
Q6MGA9	Bromodomain-containing protein 2	36.96
Q5XIR8	Clathrin heavy chain linker domain-containing protein 1	45.92
A6JUQ6	Clavesin-2	125.81
Q6AY97	Coiled-coil domain-containing protein 91	59.96
F1LQC8	Cyclin-dependent kinase 7	106.02
P51952	Cyclin-dependent kinase 7 (Fragment)	106.02
P00173	Cytochrome b5	110.98
P10888	Cytochrome c oxidase subunit 4 isoform 1, mitochondrial	95.86
Q5PPJ4	Deoxyhypusine hydroxylase	97.36
Q9Z1Z3	Epsin-2	77.85
Q5RKI1	Eukaryotic initiation factor 4A-II	82.70
F1LM27	Gamma-aminobutyric acid receptor subunit pi	73.39
F8WFK6	Glutathione peroxidase	101.68
G3V6A8	Golgi autoantigen, golgin subfamily b, macrogolgin 1, isoform CRA_c	34.84
Q5XHZ0	Heat shock protein 75 kDa, mitochondrial	386.33
D3ZMT4	Histidine decarboxylase	60.20
M0RCB8	Histone H3 (Fragment)	61.07
Q4KLJ2	Integral membrane protein 2A	45.35
G3V667	Integrin, alpha 6, isoform CRA_a	42.01
Q63679	Lysine-specific demethylase 3A	37.26
O88989	Malate dehydrogenase, cytoplasmic	152.62
Q5EB94	Myocardial zonula adherens protein	63.78
P19234	NADH dehydrogenase [ubiquinone] flavoprotein 2, mitochondrial	85.87
A0JPJ0	Nicotinamide nucleotide adenyltransferase 1	157.53
Q78PB6	Nuclear distribution protein nudE-like 1	64.22
F1LUD2	Olfactory receptor	75.58
G3V7X0	Outer dense fiber of sperm tails 2, isoform CRA_e	52.20
Q63468	Phosphoribosyl pyrophosphate synthase-associated protein 1	40.67
P20961	Plasminogen activator inhibitor 1	110.43
P30427	Plectin	66.57

---



---

Q99PT0	Probable ATP-dependent RNA helicase DDX52	66.23
P10960	Prosaposin	101.41
D4A332	Protein Ankle1	67.55
D3ZUL3	Protein Col6a1	115.75
D4AD15	Protein Eif4g1	39.23
D3ZXM4	Protein Evi5l	163.14
D3Z8Z2	Protein Fam53b	41.90
D3ZQI9	Protein Iffo1	51.19
D4AE58	Protein Kank1	33.30
Q6IFW7	Protein Krt28	46.34
F1MAF7	Protein Krt33b	63.25
D3Z9W1	Protein LOC100271845	93.32
D3ZJY5	Protein LOC100360905	81.87
D4A609	Protein LOC100361741	53.06
D3ZET2	Protein LOC100910851	39.52
M0RC68	Protein LOC100911797	39.52
D3ZMU9	Protein LOC102547078 (Fragment)	92.54
D4A4U8	Protein LOC299277	110.61
D3ZBD0	Protein Msl1	78.45
F1M0Q9	Protein Pm20d1 (Fragment)	74.24
D4A404	Protein Psd3	91.46
D3Z8R4	Protein Rbm25l1	116.19
D3ZW64	Protein RGD1560556	43.61
D3ZH53	Protein RGD1561871	56.93
F1LT36	Protein RGD1564698	86.29
F1LVT5	Protein Rundc1	42.69
D4A4R7	Protein Serpina1f	70.53
M0R5B1	Protein Shisa8	78.09
D4A3B0	Protein Tln2	47.51
D3ZE22	Protein Tll3	46.14
D4A7F0	Protein Ubr3 (Fragment)	26.72
P85973	Purine nucleoside phosphorylase	111.91
D3ZXK9	Purine nucleoside phosphorylase (Fragment)	111.91
Q3B7T9	Rab11 family-interacting protein 1	65.46
P49797	Regulator of G-protein signaling 3	58.82
G3V9Q2	Regulator of G-protein signalling 3, isoform CRA_b	58.82
Q9R095	Sperm flagellar protein 2	51.95
D3ZTA9	Sulfotransferase	59.56
Q4V8I3	Tensin-4	41.40
F1LYK6	tRNA (guanine(37)-N1)-methyltransferase	60.45
P0CD94	Ubiquinol-cytochrome-c reductase complex assembly factor 3	153.05
P85972	Vinculin	96.17
Q5MYW4	Zinc finger protein 667	43.27

---

Identified proteins are organized according to the alphabetical order of proteins. The ID is based on protein ID from the UniProt protein database (<http://www.uniprot.org/>).

---

**Supplementary Table S2.** Proteins identified exclusively in the jejunum of rats chronically exposed to water containing 10 mgF/L.

<sup>a</sup> Access number	Protein name	PLGS Score
Q6AY33	Acrosin-binding protein	56.20
P38918	Aflatoxin B1 aldehyde reductase member 3	153.75
Q6PCU3	Aldoc protein	68.15
Q9JJH9	Alpha-2u globulin	53.82
D3ZVB9	Ankyrin repeat domain 23 (Predicted), isoform CRA_a	104.93
D3ZCC5	Ankyrin repeat domain 24 (Predicted), isoform CRA_d	59.06
Q07936	Annexin A2	117.91
Q4V8H5	Aspartyl aminopeptidase	90.11
Q8R4G8	BTB/POZ domain-containing protein KCTD1	60.79
O35783	Calumenin	127.44
Q66HA5	Coiled-coil and C2 domain-containing protein 1A	44.93
G3V927	Discs, large homolog-associated protein 4 (Drosophila)	52.25
P97839	Disks large-associated protein 4	54.65
Q63572	Dual specificity testis-specific protein kinase 1 Ectonucleotide pyrophosphatase/phosphodiesterase family member 2	95.42
Q64610	Elongation factor 2	85.33
P05197	Exocyst complex component 4	55.56
M0RBF8	Fructose-bisphosphate aldolase C	60.85
P09117	Germ cell-less homolog 1 (Drosophila), isoform CRA_a	95.90
Q5I287	Glucosamine-6-phosphate isomerase	60.01
B5DEZ6	Glycosylation-dependent cell adhesion molecule 1	97.01
Q04807	GTP-binding protein Rab-3D	151.29
Q63942	High density lipoprotein binding protein (Vigilin)	72.18
Q3KRF2	Immunoglobulin joining chain	39.09
G3V6G1	KH domain-containing, RNA-binding, signal transduction-associated protein 2	105.29
Q920F3	Leucine rich repeat containing 2	56.02
Q5U2S4	Leucine-rich repeat-containing protein 15	59.37
Q8R5M3	Metabotropic glutamate receptor 1	35.57
M0R476	Metabotropic glutamate receptor 5	35.57
P31424	Microtubule-associated protein	48.36
F1MAQ5	Microtubule-associated protein 2	26.44
P15146	Myelin basic protein	26.44
P02688	Myosin, heavy polypeptide 9, non-muscle	87.34
G3V6P7	Myosin-9	35.64
Q62812	Neuronal pentraxin-2	35.64
P97738	Nuclear prelamin A recognition factor	59.16
Q2YDU6	Olfactory receptor	61.54
D3ZLY6	Oligophrenin-1	121.70
P0CAX5	Ornithine carbamoyltransferase, mitochondrial	36.60
P00481	Oxysterol-binding protein	93.90
F1LRE5	Plexin-B3	37.41
D3ZLH5	Procollagen C-endopeptidase enhancer 1	41.08
O08628	Protein Adamts8	80.57
D4AAT1		60.31

---



---

D3ZZ20	Protein Afg3l1	58.65
F1LN92	Protein Afg3l2	50.73
D4A7K0	Protein Tmem242	144.96
D4AD05	Protein Crocc	32.25
Q5XI02	Protein disulfide-isomerase-like protein of the testis	37.97
D3ZRE8	Protein Efcc1	70.94
M0R5H1	Protein Etl4 (Fragment)	44.63
D3ZX40	Protein Fam65c	47.87
F1LSX0	Protein Gzmb12 (Fragment)	83.25
Q6IFV5	Protein Krt36	65.67
G3V6H0	Protein LOC100363782	72.18
F1LWE4	Protein LOC100910977	72.21
M0R620	Protein LOC100912565	270.84
F1M1G2	Protein Maneal	47.13
D3ZV75	Protein Mfsd1	71.46
D4AB60	Protein Mtbp	38.64
D3ZFU9	Protein Mylk	46.23
M0R915	Protein Naip6	47.42
D3Z8Y9	Protein Pnma3	88.38
D4A0G7	Protein Rab37	72.18
F1M8F0	Protein Rbm7	65.13
B2RYC3	Protein RGD1306746	53.17
F7FM32	Protein RGD1311345	78.42
D3ZYC4	Protein RGD1563680	112.27
D3ZN86	Protein RGD1565323	147.87
B5DFL9	Protein Sestd1	75.09
D4AC81	Protein Slc51a	59.38
F1M2T7	Protein Srrm4	49.73
D3ZAF7	Protein Tbc1d2b	51.81
B5DFD6	Protein Tie1	36.14
D4AA88	Protein Tp73	50.65
Q9EPJ1	Protein Twist1	112.96
F1M8H2	Protein Wars2	61.46
A0A096MIV6	Protein Wbscr17	54.48
B2RYB0	Protein Wdr25l	53.51
D4A365	Protein Zbtb40	42.10
Q5RKJ9	RAB10, member RAS oncogene family	72.18
Q62796	RalA-binding protein 1	50.87
Q9Z1C8	Rap guanine nucleotide exchange factor 3	41.18
P35281	Ras-related protein Rab-10	72.18
P35284	Ras-related protein Rab-12	72.18
P61107	Ras-related protein Rab-14	72.18
Q6NYB7	Ras-related protein Rab-1A	72.18
P10536	Ras-related protein Rab-1B	72.18
P51156	Ras-related protein Rab-26	72.18
Q5U316	Ras-related protein Rab-35	72.18
P63012	Ras-related protein Rab-3A	72.18
P62824	Ras-related protein Rab-3C	72.18
Q53B90	Ras-related protein Rab-43	72.18
P05714	Ras-related protein Rab-4A	72.18
P51146	Ras-related protein Rab-4B	72.18
M0RC99	Ras-related protein Rab-5A	84.73
P35280	Ras-related protein Rab-8A	72.18
P70550	Ras-related protein Rab-8B	72.18
D4AAM1	RCG48016, isoform CRA_c	395.50

---



---

Q5FVT1	RCG55460, isoform CRA_a	50.87
P81128	Rho GTPase-activating protein 35	69.97
R9PXY2	RIB43A domain with coiled-coils 2, isoform CRA_a	54.87
P20793	Serine/threonine-protein kinase MAK	64.55
P36394	Sex-determining region Y protein (Fragment)	63.97
D3ZED8	Protein Pmel	46.91
	Sodium- and chloride-dependent GABA transporter	
P31647	3	56.87
O35814	Stress-induced-phosphoprotein 1	115.58
G3V8I4	Syntaxin 4A (Placental), isoform CRA_a	52.26
Q08850	Syntaxin-4	52.26
Q68FW7	Threonine--tRNA ligase, mitochondrial	51.32
E9PTD9	Toll-like receptor	53.37
O08950	Transcription initiation factor IIA subunit 2	126.89
F1M7T6	Translocon-associated protein subunit gamma	154.77
Q03191	Trefoil factor 3	140.71
P48500	Triosephosphate isomerase	87.60
Q7TNK6	tRNA (guanine(10)-N2)-methyltransferase homolog	68.47
P63149	Ubiquitin-conjugating enzyme E2 B	117.61
Q5RJN9	Uncharacterized protein C14orf79 homolog	168.06
Q9Z1A6	Vigilin	44.45
	Voltage-dependent calcium channel gamma-2	
Q71RJ2	subunit	114.44
	WD repeat domain phosphoinositide-interacting	
Q5U2Y0	protein 4	65.00

Identified proteins are organized according to the alphabetical order of proteins. The ID is based on protein ID from the UniProt protein database (<http://www.uniprot.org/>).

**Supplementary Table S3.** Proteins identified exclusively in the jejunum of rats chronically exposed to water containing 50 mgF/L.

<sup>a</sup> Access number	Protein name	PLGS Score
Q63570	26S protease regulatory subunit 6B	97.66
P62198	26S protease regulatory subunit 8	61.88
Q6AYY8	Acetyl-coenzyme A transporter 1	56.97
Q6P7S1	Acid ceramidase	66.82
Q5U301	A-kinase anchor protein 2	118.01
D4ADM6	Alkaline phosphatase	55.07
Q63910	Alpha globin	59.39
G3V7W7	Aminopeptidase N	64.03
P15684	Aminopeptidase N	64.03
Q62901	Arginine-glutamic acid dipeptide repeats protein	26.94
B5DEX9	Arid3a protein	60.04
D3ZAF6	ATP synthase subunit f, mitochondrial	145.66
	ATP-binding cassette, sub-family G (WHITE),	
D3ZCM3	member 4	73.10
P30835	ATP-dependent 6-phosphofructokinase, liver type	60.62
D3ZXQ0	Carboxylic ester hydrolase	42.22
Q9WTT2	Caseinolytic peptidase B protein homolog	29.83
F1LMT2	Centlein	48.71
Q3B7T8	Centrosomal protein of 44 kDa	77.36
Q68EJ0	Cytochrome b5 reductase 4	46.55
D3Z7Y1	Cytochrome P450 2C7 (Fragment)	49.22

D3ZH41	Cytoskeleton-associated protein 4 (Predicted)	75.43
Q5M9G8	DDB1- and CUL4-associated factor 11	70.70
P60924	Death ligand signal enhancer	54.09
Q5U2T2	Dehydrodolichyl diphosphate synthase	54.29
Q5RK17	Diablo homolog (Drosophila)	69.43
Q3B8Q2	Eukaryotic initiation factor 4A-III	94.58
F1LMQ2	Farnesyl pyrophosphate synthase	65.62
D4ABB4	F-box/LRR-repeat protein 15	66.59
P43278	Histone H1.0	60.10
D3ZMG5	Hypothetical LOC300207 (Predicted)	90.09
D3ZFH4	Hypothetical LOC314467 (Predicted)	40.80
Q63258	Integrin alpha-7	44.08
D4A6K5	Interleukin 27 receptor, alpha (Predicted)	53.50
B2RYC8	Interleukin-1 receptor-associated kinase 3	65.66
Q6IFW6	Keratin, type I cytoskeletal 10	49.00
Q6IFW8	Keratin, type I cytoskeletal 27	108.44
D3ZIA5	Kinesin-like protein	73.68
Q62813	Limbic system-associated membrane protein	53.88
Q6QI46	LRRGT00162	61.29
P84817	Mitochondrial fission 1 protein	71.56
Q63454	Mitogen-activated protein kinase 4 (Fragment)	53.29
Q9WUJ3	Myomegalin	57.04
D4A3H8	NIMA (Never in mitosis gene a)-related kinase 11 (Predicted)	65.44
G3V8R1	Nucleobindin 2, isoform CRA_b	54.07
B5DFH4	Papss2 protein	121.84
Q920Q0	Paralemmin-1	63.67
Q5FVS5	Perforin 1 (Pore forming protein)	46.18
P35763	Perforin-1	46.18
O35244	Peroxioredoxin-6	87.65
D3ZTP9	Piwi-like protein	47.65
D3ZAN6	Poly(A) polymerase gamma (Predicted)	78.89
D4A8I8	Polymerase (DNA directed), iota (Predicted), isoform CRA_c	60.68
D3ZB30	Polypyrimidine tract binding protein 1, isoform CRA_c	53.14
Q00438	Polypyrimidine tract-binding protein 1	53.14
Q5PQT5	Progesterin and adipoQ receptor family member V	55.50
Q4V7A8	Protein ABHD18	55.91
D3ZTI3	Protein Cdh24	32.21
F1M7J7	Protein Cep250 (Fragment)	51.99
O88767	Protein deglycase DJ-1	79.83
F1LT14	Protein Frmd5	69.00
G3V8R3	Protein Hbz	59.39
G3V646	Protein Hsf2bp	50.15
M0R3X5	Protein L1td1	37.55
D4A7Z5	Protein LOC100360940	69.43
G3V8P7	Protein LOC100911794	31.65
M0R983	Protein LOC688320	70.10
F1M9Z7	Protein Lrrc3c	64.06
B0BNB4	Protein Meaf6	59.42
D4A7N2	Protein Mettl10	84.91
D3ZKF3	Protein Morc1	54.30
F1LMD5	Protein Mtf2	108.10
D3ZD36	Protein RGD1306739	41.58
G3V8I7	Protein RGD735029	54.09

D3ZC97	Protein Rgs9bp	66.61
F1LX07	Protein Slc25a12 (Fragment)	65.62
F1LYZ6	Protein Snapc4	65.30
M0R8U7	Protein Spata17 (Fragment)	173.95
D4A9F1	Protein Tango6	40.21
F1LV37	Protein Tnrc6b	28.69
F1LUG6	Protein Ttc24 (Fragment)	38.92
D4ACL2	Protein Ttc38	54.53
D4AA63	Protein Ubqln2	42.89
Q5J3K1	Protein Vom1r62	72.76
D3ZIN6	Protein Zfp27 (Fragment)	91.09
D4A1E1	Protein Zmynd15	52.35
Q921A2	Proton myo-inositol cotransporter	59.04
F1M7Z9	Regulating synaptic membrane exocytosis 4 Sarcoplasmic/endoplasmic reticulum calcium ATPase 1	111.56
Q64578		50.17
Q4FZX7	Signal recognition particle receptor subunit beta	106.18
P48721	Stress-70 protein, mitochondrial	57.24
P23739	Sucrase-isomaltase, intestinal	32.26
Q3MIE4	Synaptic vesicle membrane protein VAT-1 homolog	148.10
Q5XIM9	T-complex protein 1 subunit beta	56.14
Q6AYM2	Tektin-2	103.76
P49430	Thromboxane-A synthase	36.34
P17164	Tissue alpha-L-fucosidase	53.61
D4A556	Uncharacterized protein	55.91
Q3KRF3	Uncharacterized protein C1orf131 homolog	58.30
Q4V8C4	WD repeat-containing protein 5B	69.96

Identified proteins are organized according to the alphabetical order of proteins. The ID is based on protein ID from the UniProt protein database (<http://www.uniprot.org/>).

**Supplementary Table S4.** Proteins identified with significantly altered expression in the jejunum of rats treated with 10 mgF/L in the drinking water in comparison to control.

<sup>a</sup> Access number	Protein name	PLGS Score	Ratio 10 mg/L F: Control
O70177	Carboxylic ester hydrolase	77.78	1.79
P04642	L-lactate dehydrogenase A chain	185.71	1.65
F1LPR6	Protein Ighm(Fragment)	79.05	1.54
P42123	L-lactate dehydrogenase B chain	59.78	1.52
D4A2K1	Protein Hoga1	87.86	1.45
G3V9Y1	Myosin, heavy polypeptide 10, non-muscle, isoform CRA_b	68.24	1.34
P01946	Hemoglobin subunit alpha-1/2	579.84	1.27
Q63862	Myosin-11 (Fragments)	110.66	1.26
A0A0A0MY09	Endoplasmic reticulum chaperone protein 78kDa	82.66	1.25
F7FK40	Tropomyosin 1, alpha, isoform CRA_c	165.97	1.25
Q64122	Myosin regulatory light polypeptide 9	318.32	1.22
Q66HD0	Endoplasmic reticulum chaperone protein 78kDa	82.66	1.21
P13832	Myosin regulatory light chain RLC-A	205.79	1.20
B0BMS8	Myl9 protein	318.32	1.19
P06685	Sodium/potassium-transporting ATPase subunit alpha-1	100.28	1.19
P18666	Myosin regulatory light chain 12B	205.79	1.17



Q9ESV6	Glyceraldehyde-3-phosphate dehydrogenase, testis-specific	240.77	1.14
P00884	Fructose-bisphosphate aldolase B	391.00	1.13
Q66HT1	Fructose-bisphosphate aldolase	391.00	1.12
P04797	Glyceraldehyde-3-phosphate dehydrogenase	393.6	1.12
D3ZRN3	Protein Actb12	1720.7	1.06
P04636	Malate dehydrogenase, mitochondrial	1140.94	0.91
P02770	Serum albumin	478.3	0.89
P10111	Peptidyl-prolyl cis-trans isomerase A	567.27	0.82
D3ZJ08	Histone H3	139.14	0.79
P62804	Histone H4	1762.24	0.71
M0R6Y8	Phosphoglycerate kinase	440.19	0.54
P04906	Glutathione S-transferase P	130.58	0.54
Q9ERC0	Neuropeptide Y/peptide YY-Y2 receptor	77.69	0.53
D4A8D5	Filamin, beta (Predicted)	56.51	0.30

Identified proteins are organized according to the ratio score. The ID is based on protein ID from the UniProt protein database (<http://www.uniprot.org/>).

**Supplementary Table S5.** Proteins identified with significantly altered expression in the jejunum of rats treated with 50 mgF/L in the drinking water in comparison to control.

<sup>a</sup> Access number	Protein name	PLGS Score	Ratio 50 mg/L F: Control
F1LPR6	Protein Ighm (Fragment)	79.05	1.86
G3V741	Phosphate carrier protein, mitochondrial	58.81	1.84
Q00729	Histone H2B type 1-A	113.51	1.79
P01946	Hemoglobin subunit alpha-1/2	579.84	1.57
P04642	L-lactate dehydrogenase A chain	185.71	1.57
Q63862	Myosin-11 (Fragments)	110.66	1.36
Q64122	Myosin regulatory light polypeptide 9	318.32	1.27
P13832	Myosin regulatory light chain RLC-A	205.79	1.25
A0A0A0MY09	Endoplasmic	82.66	1.25
P68370	Tubulin alpha-1A chain	274.37	1.25
B0BMS8	Myl9 protein	318.32	1.23
Q66HD0	Endoplasmic	82.66	1.22
P85108	Tubulin beta-2A chain	453.08	1.22
P18666	Myosin regulatory light chain 12B	205.79	1.21
F7FK40	Tropomyosin 1, alpha, isoform CRA_c	165.97	1.21
P48675	Desmin	222.3	1.15
D4A2K1	Protein Hoga1	87.86	1.14
P02091	Hemoglobin subunit beta-1	1483.69	1.13
P00770	Mast cell protease 2	401.85	1.13
P11517	Hemoglobin subunit beta-2	615.47	1.11
P34058	Heat shock protein HSP 90-beta	202.44	1.11
O88752	Epsilon 1 globin	661.9	1.09
D3ZRN3	Protein Actb12	1720.70	1.05
P10719	ATP synthase subunit beta, mitochondrial	722.19	0.95
P04636	Malate dehydrogenase, mitochondrial	1140.94	0.93
P02262	Histone H2A type 1	863.45	0.88
Q64598	Histone H2A type 1-F	863.45	0.88
Q4FZT6	Histone H2A type 3	863.45	0.88

---

P0CC09	Histone H2A type 2-A	863.45	0.87
D3ZXP3	Histone H2A	863.45	0.87
P0C169	Histone H2A type 1-C	863.45	0.87
P0C170	Histone H2A type 1-E	863.45	0.87
Q00728	Histone H2A type 4	863.45	0.87
A9UMV8	Histone H2A.J	863.45	0.87
P0C0S7	Histone H2A.Z	863.45	0.87
P84245	Histone H3.3	139.14	0.66
Q6LED0	Histone H3.1	139.14	0.64
D3ZJ08	Histone H3	139.14	0.63
P62804	Histone H4	176.24	0.61
Q66H84	MAP kinase-activated protein kinase 3	119.36	0.53

---

Identified proteins are organized according to the ratio score. The ID is based on protein ID from the UniProt protein database (<http://www.uniprot.org/>).

---

---

## 2.2 Article 2

### **Intestinal changes associated to fluoride exposure: new insights from ileum analysis**

#### **Short Title: Fluoride alters the proteome of the ileum**

Aline Dionizio<sup>1</sup>, Carina Guimarães Souza Melo<sup>1</sup>, Isabela Tomazini Sabino-Arias<sup>1</sup>, Tamara Teodoro Araujo<sup>1</sup>, Talita Mendes Silva Ventura<sup>1</sup>, Aline Lima Leite<sup>1</sup>, Sara Raquel Garcia Souza<sup>2</sup>, Erika Xavier Santos<sup>2</sup>, Alessandro Domingues Heubel<sup>1</sup>, Juliana Gadelha Souza<sup>1</sup>, Juliana Vanessa Colombo Martins Perles<sup>2</sup>, Jacqueline Nelisis Zaroni<sup>2</sup> & Marília Afonso Rabelo Buzalaf<sup>1\*</sup>

1 Department of Biological Sciences, Bauru School of Dentistry, University of São Paulo, Bauru, Brazil.

2 Department of Morphophysiological Sciences, State University of Maringá, Maringá, Brazil.

\*Corresponding author

Marília Afonso Rabelo Buzalaf

Alameda Octávio Pinheiro Brisolla, 9-75

Bauru-SP, Brazil, 17012-901

Phone: # 55 14 3235-8346

Email: mbuzalaf@fob.usp.br

---

## Highlights

- 10mgF/L and 50mgF/L provokes morphological changes and alters in several proteins
- Morphological and proteomics alterations have similarity with Crohn's disease
- F decreases gastrotropin, what may be associated with diarrhea, a common symptom

## Abstract

Gastrointestinal symptoms such as nausea, vomiting, abdominal pain and especially diarrhea are the first signs of toxicity due to exposure to fluoride (F). In this work, rats chronically exposed to F had the ileum evaluated by proteomics, as well as by morphological analysis. Male rats received water containing 0, 10 or 50 mgF / L for 30 days. Treatment with F, regardless the dose, significantly decreased the density of nHuC/D-IR neurons, whereas the CGRP-IR and SP-IR varicosities were significantly increased compared to the control group. In addition, we found a significant increase in the ileum tunica muscularis, as well as in the total thickness of the ileum wall. Several proteins were altered in the presence of F. Upregulation in different isoforms of myosin might contribute for the observed increased in the thickness of the ileum tunica muscularis and in the total thickness of the ileum wall. F also caused decrease in *Gastrotopin* (confirmed by Western blotting), what may be associated with diarrhea, a common symptom found in cases of intoxication by F. Moreover, morphological alterations as well as changes in protein expression induced by F have similarity with Crohn's disease and this possible association should be investigated in further studies.

**Keywords:** Fluoride, gastrointestinal symptoms, diarrhea, Crohn's disease, ileum.

---

---

## INTRODUCTION

Fluoride (F) is an important ion for many physiological cellular processes in the organism [1] and is very utilized in dentistry to reduce dental caries [2]. However, when ingested excessively, F can induce oxidative stress [3, 4] and lipid peroxidation, alter intracellular homeostasis and cell cycle, disrupt cell communication and signal transduction, induce apoptosis [5] and morphological and proteomic alterations in the jejunum [6] and duodenum [7].

It is known that approximately 25% of the ingested F is absorbed in the stomach as hydrofluoric acid, a process that is directly related to pH [8], and the remaining, around 75%, is absorbed in the ionic form (F<sup>-</sup>) in the small intestine, in a pH-independent process [9, 10]. The gastrointestinal tract (GIT) is considered the main route of exposure to F [11], with gastrointestinal symptoms such as nausea, vomiting, diarrhea and abdominal pain being the initial signs of F toxicity [12-15].

The GIT is composed of an interconnected network of neurons arranged in the walls of the gut that controls its function, known as the Enteric Nervous System (ENS) [16]. Changes in this system can affect the absorption, secretion, permeability and motility of the GIT [17]. Recently, immunofluorescence and proteomic analysis techniques revealed important alterations in the morphology of the different enteric neuron types as well as changes in the expression of several proteins of duodenum [7] and jejunum [6] of rats after chronic exposure to F, providing the first insights for understanding the mechanisms involved in the effects of F in the intestine.

However, the effect of F on the ENS and proteome profile of the ileum has never been reported. Given that each segment of the small intestine has distinct anatomical, histological and physiological characteristics with functional implications [18], this study evaluated the morphology of distinct subtypes of enteric neurons of the ileum after chronic exposure to F. Proteomics tools were employed to evaluate the changes in the protein profile of the ileum after exposure to F, in attempt to provide mechanistic explanations as well as to try to understand possible causes of the symptoms commonly described in cases of toxicity caused by this ion.

---

## **MATERIAL AND METHODS**

### **Animals and treatment**

All experimental protocols were approved by the Ethics Committee for Animal Experiments of Bauru Dental School, University of São Paulo (protocols 014/2011 and 012/2016). Eighteen adult male rats (60 days of life - *Rattus norvegicus*, Wistar type) were housed individually in metabolic cages under controlled lighting schedule and temperature ( $22\pm 2^{\circ}\text{C}$ ), having access to water and food *ad libitum*. The animals were randomly divided into 3 groups ( $n=6$  per group), according to the F concentration (as sodium fluoride) in the drinking water that was administered for 30 days: 0, 10 or 50 mg/L. Since rodents metabolize F 5 times faster than humans, these F concentrations correspond to  $\sim 2$  and 10 mg/L in the drinking water of humans [19]. After the experimental period, animals had their blood collected for quantification of F described in a previous publication [7] and the ileum collected for histological, immunofluorescence and proteomic analysis. To collect the ileum, the cecum was first localized and 2 incisions for its removal were conducted: the first in the anterior portion of the ileocecal valve (distal incision) and the second, 10 centimeters proximally the first one.

### **Histological analysis and Myenteric plexus immunofluorescence, morphometric and quantitative analysis.**

These analyses were performed exactly as described by Melo, Perles, Zanoni, Souza, Santos, Leite, Heubel, CO, Souza and Buzalaf [7].

### **Proteomic analysis**

The procedures were performed exactly as previously described [6]. Briefly, the frozen ileum was homogenized in a cryogenic mill (model 6770, Spex, Metuchen, NJ, EUA). Samples from 2 animals were pooled and analyses were carried out in triplicates. Briefly, proteins were extracted by incubation in lysis buffer (7 M urea, 2 M thiourea, 40 mM DTT, all diluted in AMBIC solution) under constant stirring at  $4^{\circ}\text{C}$ . Samples were centrifuged at 14000 rpm for 30 min at  $4^{\circ}\text{C}$  and the supernatant was collected. Protein quantification was performed [20]. To 50  $\mu\text{L}$  of each sample (containing 50  $\mu\text{g}$  protein) 25  $\mu\text{L}$  of 0.2% Rapigest (Waters cat#186001861) were added, followed by agitation and then 10  $\mu\text{L}$  50 mM AMBIC were added. Samples were incubated for 30 min at  $37^{\circ}\text{C}$ . They were then reduced (2.5  $\mu\text{L}$  100 mM DTT;

---

BioRad, cat# 161-0611) and alkylated (2.5  $\mu$ L 300 mM IAA; GE, cat# RPN 6302V) under dark at room temperature for 30 min. Digestion was performed at 37°C overnight by adding 100 ng trypsin (Promega, cat #V5280). After digestion, 10  $\mu$ L of 5% TFA were added, incubated for 90 min at 37°C and sample was centrifuged (14000 rpm at 6°C for 30 min). Supernatant was purified using C 18 Spin columns (Pierce, cat #89870). Samples were resuspended in 200  $\mu$ L 3% acetonitrile.

### **LC-MS/MS and bioinformatics analyses**

The peptides identification was performed on a nanoAcquity UPLC-Xevo QToF MS system (Waters, Manchester, UK), as previously described [21]. Difference in expression among the groups was obtained using Protein Lynx Global Server (PLGS) software and expressed as  $p < 0.05$  for down-regulated proteins  $1 - p > 0.95$  for up-regulated proteins. Bioinformatics analysis was performed for comparison of the treated groups with the control group (Tables S1 and S2), as reported earlier [21-24]. The software CYTOSCAPE® 3.0.4 (Java®) was used to build networks of molecular interaction between the identified proteins, with the support of ClusterMarker application.

### **Western blotting analysis**

The Western blotting was performed as previously described (Yan, Gong, Guo, Lv, Guo, Zhuang, Zhang, Li and Zhang [25]). Ileum protein extracts were obtained by lysing homogenized tissue in lysis buffer (7 M urea, 2 M thiourea, 40 mM DTT, all diluted in AMBIC solution) supplemented with protease inhibitors (Roche Diagnostics, Mannheim, Germany). Protein samples (40  $\mu$ g) were resolved in 10% Tris-HCl polyacrylamide gels and subsequently transferred to a Polyvinylidene difluoride (PVDF) membrane. Membranes were probed with commercially available *Gastrotropin* (1:500 dilution) (Abcam, Cambridge, MA, USA), followed by HRP-conjugated anti-rabbit antibody (1:10000) for *Gastrotropin* and  $\alpha$ -*Actinin* (1:1000 dilution) (Cell Signaling, Danvers, MA, USA) and ECL Plus detection reagents (GE Biosciences, Piscataway, NJ, USA). Relative *Gastrotropin* and  $\alpha$ -*Actinin* band densities were determined by densitometrical analysis using the Image Studio Lite software from LICOR Corporate Offices-US (Lincoln, Nebraska USA). In all instances, density values of bands were corrected by subtraction of the background values. The results were expressed as the ratio of *Gastrotropin* to that of  $\alpha$ -*Actinin*.

---

### **Statistical analysis**

For Western blotting data, the software GraphPad Prism (version 7.0 for Windows, La Jolla, CA, USA) was used. Data were analyzed by One-way ANOVA. The level of significance was set at 5%.

## **RESULTS**

### **Morphological analysis of the ileum wall thickness**

Significant differences were observed among all the groups. Treatment with F significantly increased the thickness of the ileum *tunica muscularis*, as well as the total thickness of the ileum wall. Curiously, the concentration of 10 mgF/L led to the highest increase in both parameters (Bonferroni's test,  $p < 0.05$ ). The mean ( $\pm$ SD) thickness of the ileum *tunica muscularis* was  $111.8 \pm 1.8$ ,  $160.8 \pm 5.0$  and  $135.06 \pm 3.5$  for the 0, 10 and 50 mgF/L, respectively. The corresponding figures for the mean ( $\pm$ SD) total thickness of the ileum wall were  $774.05 \pm 9.5$ ,  $1165.8 \pm 10.7$  and  $833.6 \pm 10.1 \mu\text{m}^2$ , respectively.

### **Myenteric HuC/D – IR neurons analysis**

In the morphometric analysis of the general population of neurons of the ileum, the cell bodies areas ( $\mu\text{m}^2$ ) of the HuC/D–IR neurons did not significantly differ among the groups ( $p > 0.05$ ). However, in the quantitative analyses (neurons/ $\text{cm}^2$ ), a significant reduction in the treated groups was observed, in comparison with the control (Table 1).

### **Myenteric nNOS –IR neurons analysis**

In the morphometric analysis of the nitrenergic neurons of the ileum, the cell bodies areas ( $\mu\text{m}^2$ ) of the nNOS-IR neurons did not significantly differ among the groups ( $p > 0.05$ ). The same was observed for in the quantitative analysis (Table 1).

### **Myenteric varicosities VIP-IR, CGRP-IR and SP-IR morphometric analysis**

In the morphometric analyses of VIP-IR varicosity areas ( $\mu\text{m}^2$ ) of the ileum, a significant increase was detected in the group treated with 50 mgF/L in respect to the control group ( $p < 0.05$ ). For the CGRP-IR and SP-IR varicosities, a dose-response

---



effect was observed, with significant increments in the areas as the F concentration increased (Table 1).

Representative images of the immunofluorescences are displayed in the supplementary information (Supplementary Figs. S1 and S2).

**Table 1.** Means and standard errors of the values of the cell bodies areas and density of HuC/D-IR and nNOS-IR neurons and VIP-IR, CGRP-IR, and SP-IR values of myenteric neurons varicosities areas of the ileum of rats chronically exposed or not to fluoride in the drinking water.

ANALYSIS	Control	10 mgF/L	50 mgF/L
Cell bodies areas of the HuC/D-IR neurons ( $\mu\text{m}^2$ )	315.1 $\pm$ 4.0 <sup>a</sup>	311.8 $\pm$ 3.9 <sup>a</sup>	321.6 $\pm$ 3.6 <sup>a</sup>
Density HuC/D-IR neurons (neurons/ $\text{cm}^2$ )	16,626.7 $\pm$ 493.6 <sup>a</sup>	14,990.2 $\pm$ 419.1 <sup>b</sup>	14,615.6 $\pm$ 461.9 <sup>b</sup>
Cell bodies areas of the nNOS-IR neurons ( $\mu\text{m}^2$ )	293.1 $\pm$ 3.1 <sup>a</sup>	300.0 $\pm$ 3.4 <sup>a</sup>	290.2 $\pm$ 3.2 <sup>a</sup>
Density nNOS-IR neurons (neurons/ $\text{cm}^2$ )	4,563.4 $\pm$ 130.5 <sup>a</sup>	4,334.9 $\pm$ 119.6 <sup>a</sup>	4,353.9 $\pm$ 136.1 <sup>a</sup>
Area VIP-IR varicosities ( $\mu\text{m}^2$ )	3.5 $\pm$ 0,0 <sup>a</sup>	3.5 $\pm$ 0,0 <sup>a</sup>	4.7 $\pm$ 0,0 <sup>b</sup>
Area CGRP-IR varicosities ( $\mu\text{m}^2$ )	3.2 $\pm$ 0,0 <sup>a</sup>	3.4 $\pm$ 0,0 <sup>b</sup>	3.6 $\pm$ 0,0 <sup>c</sup>
Area SP-IR varicosities ( $\mu\text{m}^2$ )	2.9 $\pm$ 0,0 <sup>a</sup>	4.6 $\pm$ 0,0 <sup>b</sup>	4.6 $\pm$ 0,0 <sup>b</sup>

Means followed by different letters in the same line are significantly different according to Fisher's test (density HuC/D-IR and nNOS-IR neurons) or Tukey's test (other variables).  $p < 0.05$ .  $n = 6$ .

### **Proteomic analysis of the ileum**

The total numbers of proteins identified by mass spectrometry in the control, 10 and 50 mgF/L groups were 280, 276 and 285, respectively. Among them, 33, 69 and 40 proteins (Tables S1 and S2) were uniquely identified in the control, 10 mgF/L and 50 mgF/L groups, respectively. In the quantitative analysis of the 10 mgF/L vs. control group, 16 proteins with change in expression were detected (Table S1). As for the comparison 50 mgF/L vs. control group, 28 proteins with change in expression were found (Table S2). Most of the proteins with altered expression were upregulated in the group treated with 10 mgF/L when compared with the control group. As for the comparison 50 mgF/L vs. control group, most proteins with altered expression were downregulated in the treated group (Table S1 and S2).

Figures 1 and 2 show the subnetworks generated by ClusterMark® for the comparisons 10 mgF/L vs. control and 50 mgF/L vs. control, respectively. For the

animals exposed to 10 mgF/L (Fig. 1), most of the proteins with altered expression interacted with *Solute carrier family 2, facilitated glucose transporter member 4* (GLUT4, P19357), (Fig. 1A), *Mitogen-activated protein kinase 3* (MAPK3, P21708), *5'-AMP-activated protein kinase catalytic subunit alpha-1* (AMPK subunit alpha-1, P54645), *5'-AMP-activated protein kinase subunit beta-1* (AMPK subunit beta-1, P80386) and *Dystrophin* (P11530) (Fig.1B). As for the group treated with 50 mgF/L, most of the proteins with altered expression interacted with *AMPK subunit alpha-1* (P54645), *AMPK subunit beta-1* (P80386), *Tumor necrosis factor* (P16599), *Phosphoglycerate mutase 2* (P16290), *Calcium-activated potassium channel subunit alpha-1* (Q62976) and *Dynein light chain 1, cytoplasmic* (P63170) (Fig. 2A) or *GLUT4* (P19357), *MAPK3* (P21708), *Dystrophin* (P11530), *Calcium/calmodulin-dependent protein kinase kinase 1* (CaM-kinase kinase 1, P97756) and *Regulating synaptic membrane exocytosis protein 1* (Q9JIR4) (Fig. 2B).

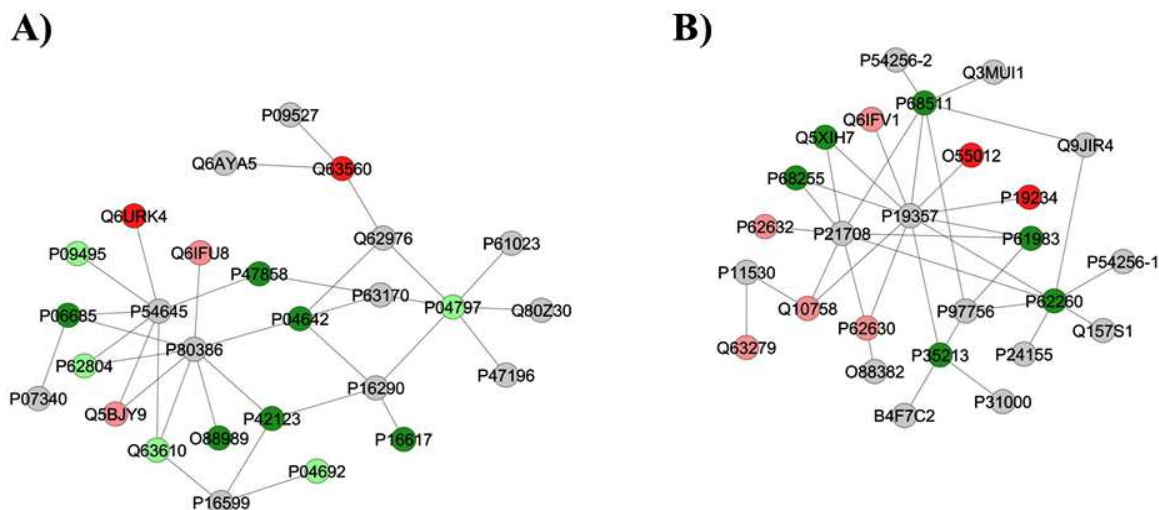


**Figure 1** – Subnetworks generated by ClusterMarker® for the comparison 10 mgF/L vs. Control (deionized water). The color of the nodes indicates the differential expression of the respective protein with its access code, available from UniProt protein database (<http://www.uniprot.org/>). The dark green and dark red nodes indicate proteins unique to 10 mgF/L and Control groups, respectively. The light red and light green nodes indicate down and upregulated proteins, respectively, in 10 mgF/L group in respect to Control. The gray nodes indicate the interaction proteins that are offered by CYTOSCAPE®, which were not identified in the present study.

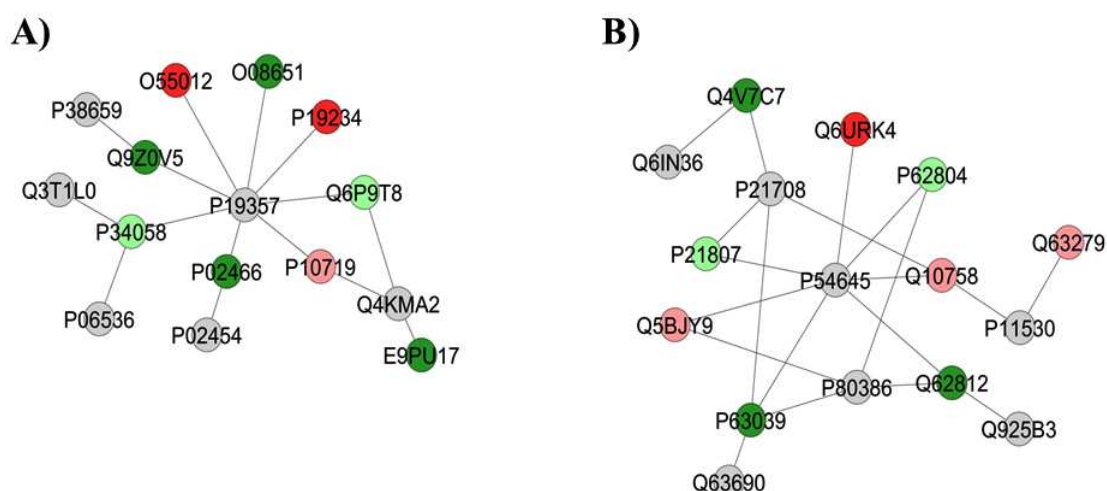


**Figure 2** – Subnetworks generated by ClusterMarker® for the comparison 50 mgF/L vs. Control (deionized water). The color of the nodes indicates the differential expression of the respective protein with its access code, available from UniProt protein database (<http://www.uniprot.org/>). The dark green and dark red nodes indicate proteins unique to 50 mgF/L and Control groups, respectively. The light red and light green nodes indicate down and upregulated proteins, respectively, in 50 mgF/L group in respect to Control. The gray nodes indicate the interaction proteins that are offered by CYTOSCAPE®, which were not identified in the present study.

### Western Blotting

Western blotting confirmed that *Gastrotropin* was significantly reduced upon exposure not F in a dose-response manner, as revealed by proteomic analysis (Fig. 3).

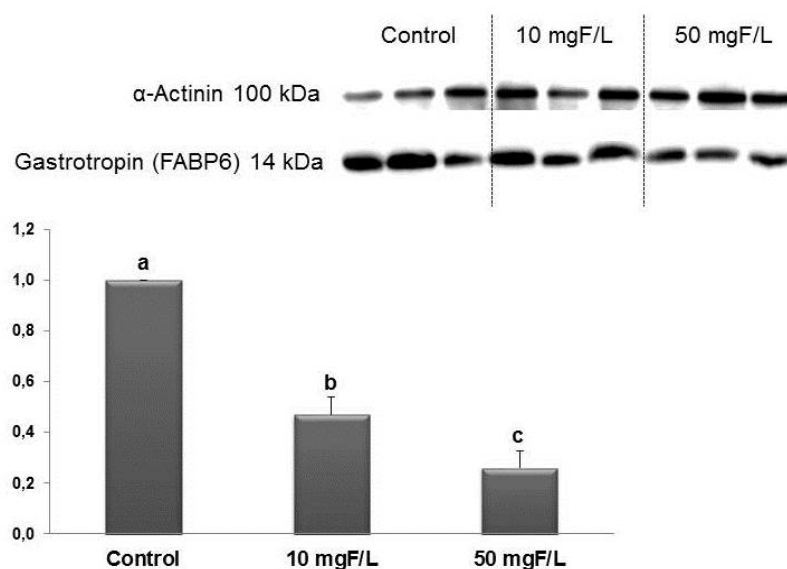


**Figure 3**- Representative expression of proteins *Gastrotropin* and of the constitutive protein  $\alpha$ -Actinin in samples of individual animals ( $n = 6$ ) from each group. Densitometric analysis was performed for 6 animals per group. Relative densitometry was analyzed using the software Image Studio Lite. For each type of diet, distinct letters denote significant differences between animals treated with 0 mgF/L, 10 mgF/L and 50 mgF/L (ANOVA one way,  $p < 0.05$ ) Bars indicate SD.  $n = 6$

## DISCUSSION

Considering that F is mainly absorbed from the small intestine [9, 10], gastrointestinal symptoms are often reported in cases of excessive ingestion of F [26-29]. In previous studies we evaluated the effects of chronic F exposure on the duodenum [7] and jejunum [6] of rats using morphological and proteomic analyses. The present study focuses on the ileum, since different segments of the small intestine have distinct anatomical, histological, physiological and functional characteristics [18].

A remarkable finding of the present study was the increase in thickness of the ileum *tunica muscularis*, as well as of the total thickness of the ileum wall upon exposure to both F concentrations. In our previous studies where duodenum and jejunum were evaluated, only the highest F concentration increased the thickness of the *tunica muscularis*, while F had no effect on the total thickness of these segments of the small intestine [6, 7]. In the present study, several proteins of the myosin family were upregulated in the 10 mgF/L group (Table S1) and 50 mgF/L group (Table S2). Increase in these proteins has been reported as a possible justification for the increase thickness of the ileum *tunica muscularis*, as well as the total thickness of the ileum wall [7, 30, 31]. Moreover, F has great affinity by  $Ca^{+2}$  and the low availability of  $Ca^{+2}$  might be related to the decrease in *Calmodulin-2*, since this protein was exclusively identified in the control group. Calcium binds to calmodulin, which activates the myosin light chain kinase in the muscle. Calmodulin is also responsible for initiating contraction by activating crossed myosin bridges [18]. Thus, increase in myosin family members in the groups treated with F might be a mechanism to counteract the lower availability of  $Ca^{+2}$ .

It should be noted that increase in the intestine wall thickness also occurs in Crohn's disease (CD) [32-35], a chronic inflammatory disorder that can affect any segment of the gastrointestinal tract, especially the terminal ileum and the ileocecal region [36] and in some cases can result in significant morbidity and disability [37]. The etiology of CD remains unknown, but is probably attributed to a response to environmental triggers (infection, drugs or other agents) in genetically susceptible individuals [38]. CD is characterized by the infiltration of inflammatory and immune cells (such as mast cells, neutrophils, T-lymphocytes and macrophages) that interact and release enzymes and cytokines [37, 39]. Another finding of the present study was an increase in the SP-IR varicosity area upon exposure to F, which was also observed for duodenum [7] and jejunum[6]. SP-IR was also reported to be intense in the

---

epithelium, granulomas, cells lining the mucosal fissure and in the muscle layers of the colon of patients with CD [40]. Moreover, a substantial increase in SP receptors was found in enteric neurons of the small and large bowel of CD patients, in comparison with controls and patients with ulcerative colitis (UC) [41]. Increased in SP were also reported in the serum of patients with CD [42]. SP has several effects throughout the central nervous system and the periphery, including strong nociceptive and proinflammatory properties [43]. It acts directly and indirectly on immune cascades and on the vasculature to cause plasma extravasation, edema, and pain [44]. It also stimulates intestinal smooth muscle contraction [45], which might be implicated in the increase in the thickness of the *tunica muscularis* of the ileum, observed in the present study. In addition to increase in SP-IR varicosity area upon exposure to F, increase in VIP-IR varicosity area was also observed in the ileum of the animals treated with 50 mgF/L, as observed in our previous studies in duodenum [7] and jejunum[6]. Increase density of VIP immunoreactive neurons in the submucosal plexus of inflamed regions has also been reported in paediatric patients with CD [46]. Changes in the vipergic innervation can change the intestinal motility, leading to a decrease in the tone of the intestinal smooth muscle, which could provoke diarrhea [47].

A decrease in *Gastrotopin* (P80020) was observed in the present study upon exposure to F, regardless the dose (Fig.4). This protein, also known as *Fatty acid binding protein 6*, is an important transport protein involved in the enterohepatic circulation of bile salts. It is expressed mainly in the ileum, acts in the absorption of B12 vitamin and binds to bile acids, potent detergents essential for efficient digestion and absorption of dietary fats [48-53]. The reduction in *Gastrotopin* leads to primary bile acid malabsorption [54, 55]. It is plausible that reduced bile acid transporter expression, without other evidence of damage, produces idiopathic bile acid malabsorption, since loss of expression is clearly the mechanism of malabsorption and diarrhea in ileal resection or inflammatory disease [54-56]. Inflammation of the ileum, as in CD or after radiation, causes secondary bile acid malabsorption and the presence of unabsorbed bile acids in the colon, then produces diarrhea (Fig.3), through stimulation of fluid and electrolyte secretion, since bile acids exert their effects on colonic fluid transport through both direct and indirect actions on the epithelium [54, 55, 57, 58].

---

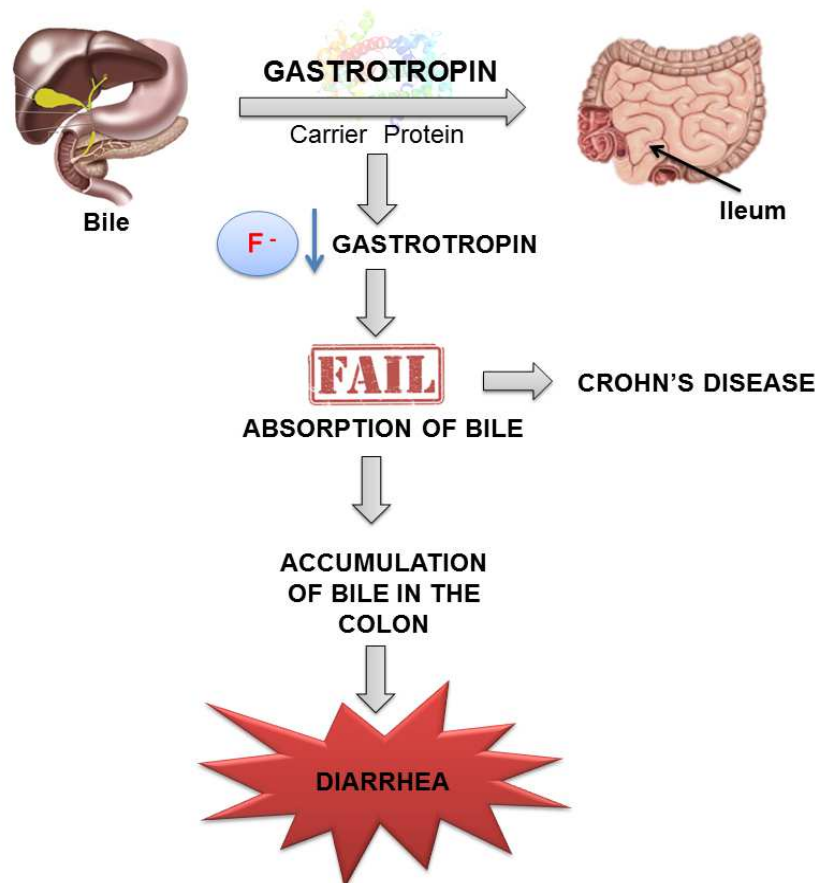


**Figure 4** – Possible mechanism by which excessive intake of fluoride (F) leads to diarrhea, the most common symptom in F intoxication. *Gastrotopin*, expressed mainly in the ileum, is very important for the enterohepatic circulation of bile salts. In the presence of F this protein is decreased, leading to poor absorption of bile by the small intestine, which leads to its accumulation in the colon, culminating with diarrhea.

In the present study, exposure to F led to various effects that are also found in CD, such as increase in the ileum wall thickness, increase in the SP-IR and VIP-IR varicosities, as well as decrease in bile acid transporters, such as *Gastrotopin*. These findings might help to explain common gastrointestinal symptoms shared in cases of exposure to high F levels and of CD, such as alteration in intestinal motility and diarrhea. A possible association between F exposure and inflammatory bowel disease (IBD) has been suggested, but the absence of direct studies on this association does not allow any definitive conclusion [59]. Despite these two identities share common features and symptoms, additional studies to provide unequivocal evidence on this relationship are necessary.

## Acknowledgements

This study was supported by FAPESP (2011/10233-7, 2012/16840-5 and 2016/09100-6).

## Conflict of interest

The authors declare that they have no conflict of interest.

## Additional Information

**Supplementary information** accompanies this paper.

## References

- [1] X. Yan, X. Yan, A. Morrison, T. Han, Q. Chen, J. Li, J. Wang, Fluoride induces apoptosis and alters collagen I expression in rat osteoblasts, *Toxicol Lett*, 200 (2011) 133-138.
  - [2] M.A. Buzalaf, G.M. Whitford, Fluoride metabolism, *Monogr Oral Sci*, 22 (2011) 20-36.
  - [3] H.A. Pereira, L. Leite Ade, S. Charone, J.G. Lobo, T.M. Cestari, C. Peres-Buzalaf, M.A. Buzalaf, Proteomic analysis of liver in rats chronically exposed to fluoride, *PLoS One*, 8 (2013) e75343.
  - [4] H.A. Pereira, A.S. Dionizio, M.S. Fernandes, T.T. Araujo, T.M. Cestari, C.P. Buzalaf, F.G. Iano, M.A. Buzalaf, Fluoride Intensifies Hypercaloric Diet-Induced ER Oxidative Stress and Alters Lipid Metabolism, *PLoS One*, 11 (2016) e0158121.
  - [5] O. Barbier, L. Arreola-Mendoza, L.M. Del Razo, Molecular mechanisms of fluoride toxicity, *Chem Biol Interact*, 188 (2010) 319-333.
  - [6] A.S. Dionizio, C.G.S. Melo, I.T. Sabino-Arias, T.M.S. Ventura, A.L. Leite, S.R.G. Souza, E.X. Santos, A.D. Heubel, J.G. Souza, J. Perles, J.N. Zanoni, M.A.R. Buzalaf, Chronic treatment with fluoride affects the jejunum: insights from proteomics and enteric innervation analysis, *Sci Rep*, 8 (2018) 3180.
  - [7] C.G.S. Melo, J. Perles, J.N. Zanoni, S.R.G. Souza, E.X. Santos, A.L. Leite, A.D. Heubel, E.S. CO, J.G. Souza, M.A.R. Buzalaf, Enteric innervation combined with proteomics for the evaluation of the effects of chronic fluoride exposure on the duodenum of rats, *Sci Rep*, 7 (2017) 1070.
  - [8] G.M. Whitford, D.H. Pashley, Fluoride absorption: the influence of gastric acidity, *Calcif Tissue Int*, 36 (1984) 302-307.
  - [9] J. Nopakun, H.H. Messer, Mechanism of fluoride absorption from the rat small intestine, *Nutr Res*, 10 (1990) 771-779.
  - [10] J. Nopakun, H.H. Messer, V. Voller, Fluoride absorption from the gastrointestinal tract of rats, *J Nutr*, 119 (1989) 1411-1417.
  - [11] Y. Zheng, J. Wu, J.C. Ng, G. Wang, W. Lian, The absorption and excretion of fluoride and arsenic in humans, *Toxicol Lett*, 133 (2002) 77-82.
  - [12] A. Susheela, A. Kumar, M. Bhatnagar, R. Bahadur, Prevalence of endemic Fluorosis with gastrointestinal manifestations in People living in some North-Indian villages, *Fluoride*, 26 (1993) 97-104.
-

- [13] T.K. Das, A.K. Susheela, I.P. Gupta, S. Dasarathy, R.K. Tandon, Toxic effects of chronic fluoride ingestion on the upper gastrointestinal tract, *Journal of clinical gastroenterology*, 18 (1994) 194-199.
- [14] A.e.a. Susheela, Fluoride ingestion and its correlation with gastrointestinal discomfort *Fluoride*, 25 (1992) 5-22.
- [15] J.D. Sharma, Jain, P. & Sohu, D. , Gastric Discomforts from Fluoride in Drinking Water in Sanganer Tehsil, Rajasthan, India. , *Fluoride*, 42 (2009) 286-291
- [16] J.B. Furness, A comprehensive overview of all aspects of the enteric nervous system, *The Enteric Nervous System.*, (Blackwell, 2006).
- [17] E. Sand, B. Roth, B. Westrom, P. Bonn, E. Ekblad, B. Ohlsson, Structural and functional consequences of busserelin-induced enteric neuropathy in rat, *BMC Gastroenterol*, 14 (2014) 209.
- [18] A.C. Guyton, J.E. Hall, *Textbook of medical physiology*, 13 ed., Elsevier Health Sciences, Philadelphia, 2015.
- [19] A.J. Dunipace, E.J. Brizendine, W. Zhang, M.E. Wilson, L.L. Miller, B.P. Katz, J.M. Warrick, G.K. Stookey, Effect of aging on animal response to chronic fluoride exposure, *J Dent Res*, 74 (1995) 358-368.
- [20] M.M. Bradford, A rapid and sensitive method for the quantitation of microgram quantities of protein utilizing the principle of protein-dye binding, *Anal Biochem*, 72 (1976) 248-254.
- [21] A. Lima Leite, J. Gualium Vaz Madureira Lobo, H.A. Barbosa da Silva Pereira, M. Silva Fernandes, T. Martini, F. Zucki, D.H. Sumida, A. Rigalli, M.A. Buzalaf, Proteomic analysis of gastrocnemius muscle in rats with streptozotocin-induced diabetes and chronically exposed to fluoride, *PLoS One*, 9 (2014) e106646.
- [22] A. Bauer-Mehren, Integration of genomic information with biological networks using Cytoscape, *Methods Mol Biol*, 1021 (2013) 37-61.
- [23] P.P. Millan, Visualization and analysis of biological networks, *Methods Mol Biol*, 1021 (2013) 63-88.
- [24] S. Orchard, Molecular interaction databases, *Proteomics*, 12 (2012) 1656-1662.
- [25] Y.X. Yan, Y.W. Gong, Y. Guo, Q. Lv, C. Guo, Y. Zhuang, Y. Zhang, R. Li, X.Z. Zhang, Mechanical strain regulates osteoblast proliferation through integrin-mediated ERK activation, *PLoS One*, 7 (2012) e35709.
- [26] R.L. Vogt, L. Witherell, D. LaRue, D.N. Klaucke, Acute fluoride poisoning associated with an on-site fluoridator in a Vermont elementary school, *Am J Public Health*, 72 (1982) 1168-1169.
- [27] B.D. Gessner, M. Beller, J.P. Middaugh, G.M. Whitford, Acute fluoride poisoning from a public water system, *N Engl J Med*, 330 (1994) 95-99.
- [28] W.L. Augenstein, D.G. Spoerke, K.W. Kulig, A.H. Hall, P.K. Hall, B.S. Riggs, M. el Saadi, B.H. Rumack, Fluoride ingestion in children: a review of 87 cases, *Pediatrics*, 88 (1991) 907-912.
- [29] K. Akiniwa, Re-examination of acute toxicity of fluoride, *Fluoride*, 30 (1997) 89-104.
- 
-



- [30] J. Chu, N.T. Pham, N. Olate, K. Kislitsyna, M.C. Day, P.A. LeTourneau, A. Kots, R.H. Stewart, G.A. Laine, C.S. Cox, Jr., K. Uray, Biphasic regulation of myosin light chain phosphorylation by p21-activated kinase modulates intestinal smooth muscle contractility, *J Biol Chem*, 288 (2013) 1200-1213.
- [31] A. Soares, E.J. Beraldi, P.E. Ferreira, R.B. Bazotte, N.C. Buttow, Intestinal and neuronal myenteric adaptations in the small intestine induced by a high-fat diet in mice, *BMC Gastroenterol*, 15 (2015) 3.
- [32] D.G. Rosenbaum, M.A. Conrad, D.M. Biko, E.D. Ruchelli, J.R. Kelsen, S.A. Anupindi, Ultrasound and MRI predictors of surgical bowel resection in pediatric Crohn disease, *Pediatric radiology*, 47 (2017) 55-64.
- [33] L. Chiorean, D. Schreiber-Dietrich, B. Braden, X. Cui, C.F. Dietrich, Transabdominal ultrasound for standardized measurement of bowel wall thickness in normal children and those with Crohn's disease, *Medical ultrasonography*, 16 (2014) 319-324.
- [34] H. Worlicek, H. Lutz, N. Heyder, W. Matek, Ultrasound findings in Crohn's disease and ulcerative colitis: a prospective study, *Journal of clinical ultrasound : JCU*, 15 (1987) 153-163.
- [35] B. Kang, S.Y. Choi, S. Chi, Y. Lim, T.Y. Jeon, Y.H. Choe, Baseline Wall Thickness Is Lower in Mucosa-Healed Segments 1 Year After Infliximab in Pediatric Crohn Disease Patients, *Journal of pediatric gastroenterology and nutrition*, 64 (2017) 279-285.
- [36] C.J. Ooi, G.K. Makharia, I. Hilmi, P.R. Gibson, K.M. Fock, V. Ahuja, K.L. Ling, W.C. Lim, K.T. Thia, S.C. Wei, W.K. Leung, P.K. Koh, R.B. Gearry, K.L. Goh, Q. Ouyang, J. Sollano, S. Manatsathit, H.J. de Silva, R. Rerknimitr, P. Pisespongsa, M.R. Abu Hassan, J. Sung, T. Hibi, C.C. Boey, N. Moran, R.W. Leong, D. Asia Pacific Association of Gastroenterology Working Group on Inflammatory Bowel, Asia-Pacific consensus statements on Crohn's disease. Part 2: Management, *Journal of gastroenterology and hepatology*, 31 (2016) 56-68.
- [37] S. Aniwan, S.H. Park, E.V. Loftus, Jr., Epidemiology, Natural History, and Risk Stratification of Crohn's Disease, *Gastroenterology clinics of North America*, 46 (2017) 463-480.
- [38] S. Ardizzone, G. Bianchi Porro, Inflammatory bowel disease: new insights into pathogenesis and treatment, *Journal of internal medicine*, 252 (2002) 475-496.
- [39] M. Gajendran, P. Loganathan, A.P. Catinella, J.G. Hashash, A comprehensive review and update on Crohn's disease, *Disease-a-month : DM*, (2017).
- [40] S. Mazumdar, K.M. Das, Immunocytochemical localization of vasoactive intestinal peptide and substance P in the colon from normal subjects and patients with inflammatory bowel disease, *The American journal of gastroenterology*, 87 (1992) 176-181.
- [41] C.R. Mantyh, S.R. Vigna, R.R. Bollinger, P.W. Mantyh, J.E. Maggio, T.N. Pappas, Differential expression of substance P receptors in patients with Crohn's disease and ulcerative colitis, *Gastroenterology*, 109 (1995) 850-860.
- [42] F. Tavano, F.F. di Mola, A. Latiano, O. Palmieri, F. Bossa, M.R. Valvano, T. Latiano, V. Annese, A. Andriulli, P. di Sebastiano, Neuroimmune interactions in

patients with inflammatory bowel diseases: disease activity and clinical behavior based on Substance P serum levels, *Journal of Crohn's & colitis*, 6 (2012) 563-570.

[43] F. Lembeck, The 1988 Ulf Euler Lecture. Substance P: from extract to excitement, *Acta physiologica Scandinavica*, 133 (1988) 435-454.

[44] P.W. Mantyh, Substance P and the inflammatory and immune response, *Annals of the New York Academy of Sciences*, 632 (1991) 263-271.

[45] P. Holzer, I.T. Lippe, Substance P can contract the longitudinal muscle of the guinea-pig small intestine by releasing intracellular calcium, *British journal of pharmacology*, 82 (1984) 259-267.

[46] L. Boyer, D. Sidpra, G. Jevon, A.M. Buchan, K. Jacobson, Differential responses of VIPergic and nitrergic neurons in paediatric patients with Crohn's disease, *Autonomic neuroscience : basic & clinical*, 134 (2007) 106-114.

[47] M.A. Defani, J.N. Zanoni, M.R. Natali, R.B. Bazotte, M.H. de Miranda-Neto, Effect of acetyl-L-carnitine on VIP-ergic neurons in the jejunum submucous plexus of diabetic rats, *Arq Neuropsiquiatr*, 61 (2003) 962-967.

[48] R.A. Davis, A.D. Attie, Deletion of the ileal basolateral bile acid transporter identifies the cellular sentinels that regulate the bile acid pool, *Proceedings of the National Academy of Sciences of the United States of America*, 105 (2008) 4965-4966.

[49] J.F. Landrier, J.J. Eloranta, S.R. Vavricka, G.A. Kullak-Ublick, The nuclear receptor for bile acids, FXR, transactivates human organic solute transporter-alpha and -beta genes, *American journal of physiology. Gastrointestinal and liver physiology*, 290 (2006) G476-485.

[50] C.A. Thompson, K. Wojta, K. Pulakanti, S. Rao, P. Dawson, M.A. Battle, GATA4 Is Sufficient to Establish Jejunal Versus Ileal Identity in the Small Intestine, *Cellular and molecular gastroenterology and hepatology*, 3 (2017) 422-446.

[51] J. Grober, I. Zaghini, H. Fujii, S.A. Jones, S.A. Kliewer, T.M. Willson, T. Ono, P. Besnard, Identification of a bile acid-responsive element in the human ileal bile acid-binding protein gene. Involvement of the farnesoid X receptor/9-cis-retinoic acid receptor heterodimer, *J Biol Chem*, 274 (1999) 29749-29754.

[52] G. Iizumi, Y. Sadoya, S. Hino, N. Shibuya, H. Kawabata, Proteomic characterization of the site-dependent functional difference in the rat small intestine, *Biochim Biophys Acta*, 1774 (2007) 1289-1298.

[53] L. Marvin-Guy, L.V. Lopes, M. Affolter, M.C. Courtet-Compondu, S. Wagniere, G.E. Bergonzelli, L.B. Fay, M. Kussmann, Proteomics of the rat gut: analysis of the myenteric plexus-longitudinal muscle preparation, *Proteomics*, 5 (2005) 2561-2569.

[54] S. Balesaria, R.J. Pell, L.J. Abbott, A. Tasleem, K.M. Chavele, N.F. Barley, U. Khair, A. Simon, K.J. Moriarty, W.G. Brydon, J.R. Walters, Exploring possible mechanisms for primary bile acid malabsorption: evidence for different regulation of ileal bile acid transporter transcripts in chronic diarrhoea, *European journal of gastroenterology & hepatology*, 20 (2008) 413-422.

[55] S.J. Keely, J.R. Walters, The Farnesoid X Receptor: Good for BAD, *Cellular and molecular gastroenterology and hepatology*, 2 (2016) 725-732.

---

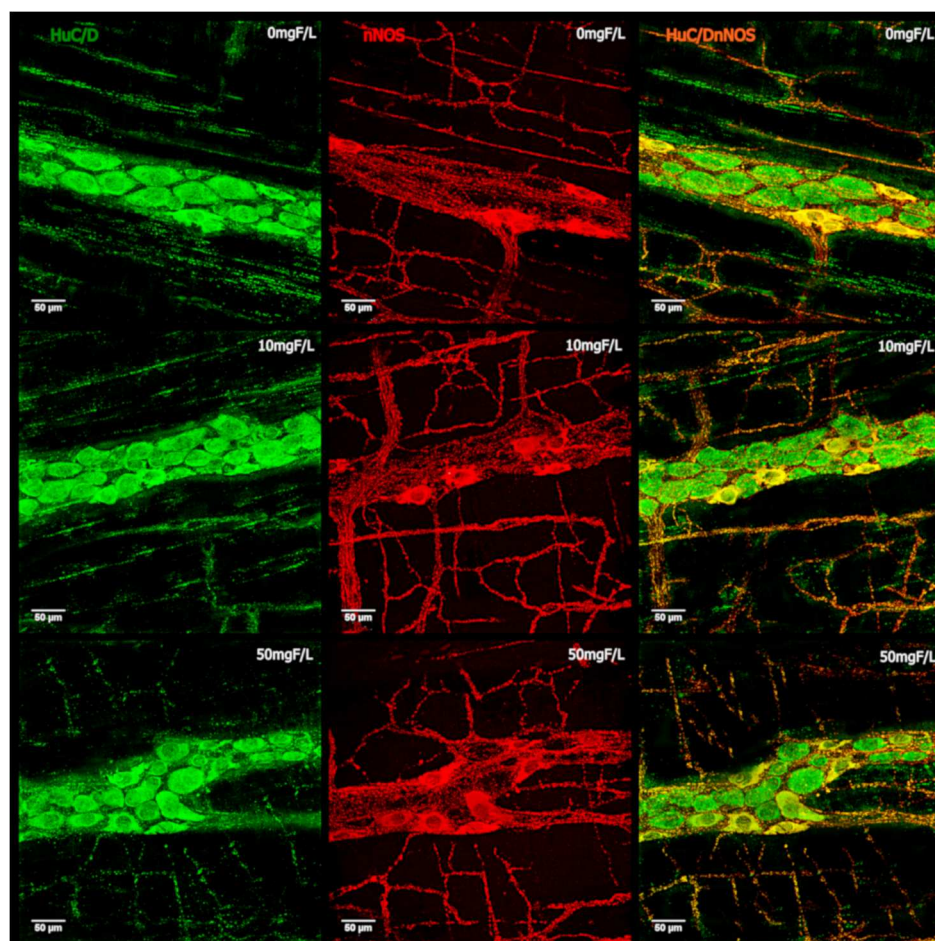
[56] D. Jung, A.C. Fantin, U. Scheurer, M. Fried, G.A. Kullak-Ublick, Human ileal bile acid transporter gene ASBT (SLC10A2) is transactivated by the glucocorticoid receptor, *Gut*, 53 (2004) 78-84.

[57] P. Rossel, H. Sortsoe Jensen, P. Qvist, A. Arveschoug, Prognosis of adult-onset idiopathic bile acid malabsorption, *Scandinavian journal of gastroenterology*, 34 (1999) 587-590.

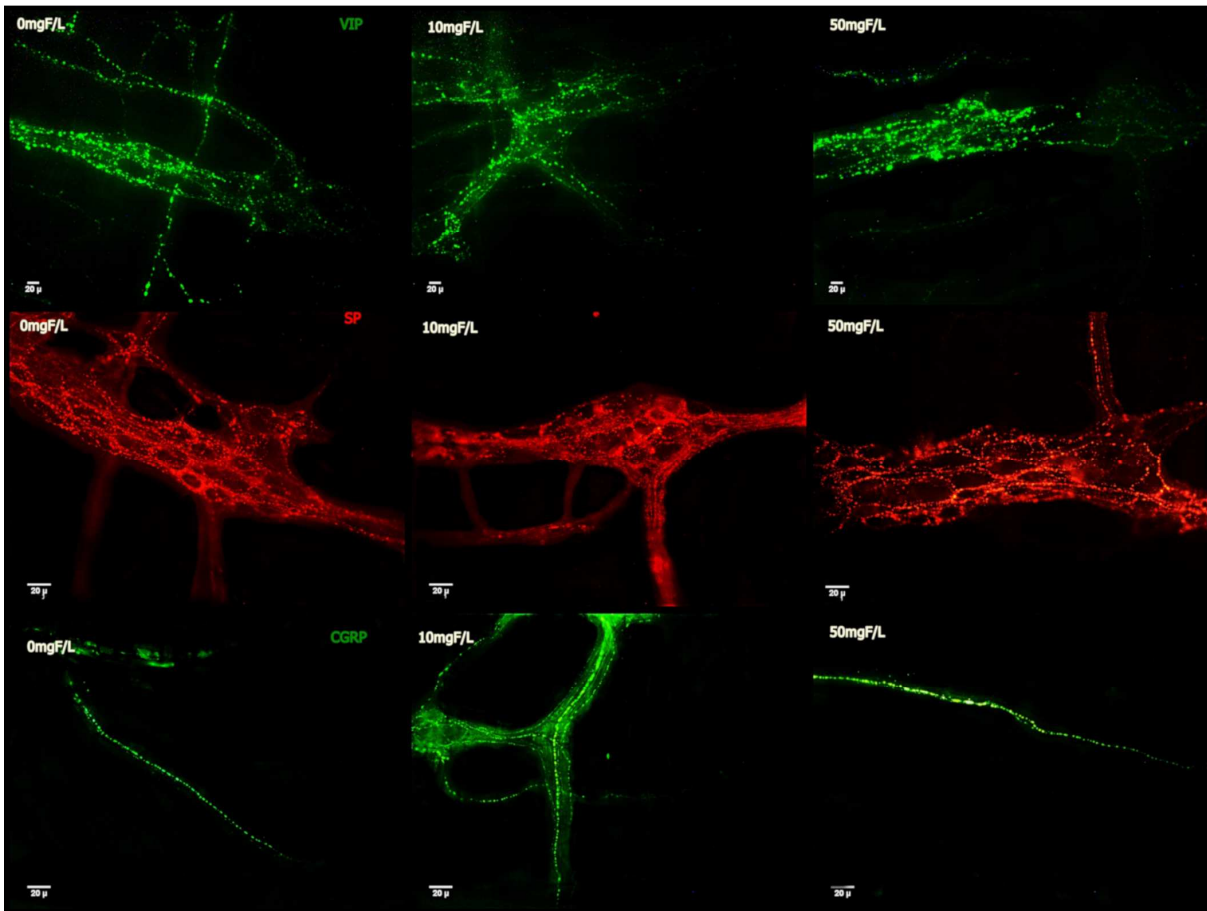
[58] W. Luman, A.J. Williams, M.V. Merrick, M.A. Eastwood, Idiopathic bile acid malabsorption: long-term outcome, *European journal of gastroenterology & hepatology*, 7 (1995) 641-645.

[59] B. Follin-Arbelet, B. Moum, Fluoride: a risk factor for inflammatory bowel disease?, *Scandinavian journal of gastroenterology*, 51 (2016) 1019-1024.

## SUPPLEMENTARY FIGURES AND TABLES



**Supplementary Fig. S1** - Photomicrography of myenteric neurons of the rats ileum stained for HuC/D (green), nNOS (red), and double-labeling (HuC/D and nNOS) for the control group (0 mgF/L) and for the groups treated with 10 and 50 mgF/L. 20x Objective.



**Supplementary Fig. S2** - Photomicrography of myenteric varicosities of the rats ileum after chronic F exposure (0, 10 or 50 mgF/L) for VIP-IR, SP-IR CGRP-IR. 40x Objective.

**Table S1. Proteins with expression significantly altered in the ileum of rats in the 10 mgF/L vs Control comparison.**

<sup>a</sup> Accession number	Protein name	PLGS Score	<sup>b</sup> Ratio 10 mgF/L:Control
Q6IG12	Keratin, type II cytoskeletal 7	72	1.70
P21807	Peripherin	76	1.45
P62804	Histone H4	550	1.35
P13832	Myosin regulatory light chain RLC-A	242	1.23
P18666	Myosin regulatory light chain 12B	242	1.23
Q6P9T8	Tubulin beta-4B chain	57	1.23
P00770	Mast cell protease 2	496	1.22
P34058	Heat shock protein HSP 90-beta	104	1.21
Q64122	Myosin regulatory light polypeptide 9	242	1.20
Q10758	Keratin, type II cytoskeletal 8	733	0.93
Q63279	Keratin, type I cytoskeletal 19	448	0.92
P10111	Peptidyl-prolyl cis-trans isomerase A	1088	0.90
P10719	ATP synthase subunit beta, mitochondrial	434	0.88
Q5BJY9	Keratin, type I cytoskeletal 18	207	0.87
P80020	Gastrotropin	877	0.72
Q68FR8	Tubulin alpha-3 chain	45	0.57
P97608	5-oxoprolinase	60	10 mgF/L*
P63039	60 kDa heat shock protein, mitochondrial	83	10 mgF/L
P20280	60S ribosomal protein L21	96	10 mgF/L
Q4V7C7	Actin-related protein 3	92	10 mgF/L
Q63072	ADP-ribosyl cyclase/cyclic ADP-ribose hydrolase 2	75	10 mgF/L
Q80YN4	Atrial natriuretic peptide-converting enzyme	48	10 mgF/L
P55213	Caspase-3	112	10 mgF/L
B0BNA5	Coactosin-like protein	272	10 mgF/L
P02466	Collagen alpha-2(I) chain	39	10 mgF/L
Q792H5	CUGBP Elav-like family member 2	51	10 mgF/L
Q9R1Q2	Cyclin-L1	90	10 mgF/L
P00406	Cytochrome c oxidase subunit 2	57	10 mgF/L
O08651	D-3-phosphoglycerate dehydrogenase	54	10 mgF/L
P06214	Delta-aminolevulinic acid dehydratase	78	10 mgF/L
Q9QYV8	DNA polymerase subunit gamma-1	42	10 mgF/L
Q4FZU2	Keratin, type II cytoskeletal 6A	64	10 mgF/L
P15650	Long-chain specific acyl-CoA dehydrogenase, mitochondrial	63	10 mgF/L
O55162	Ly6/PLAUR domain-containing protein 3	114	10 mgF/L
Q5FVQ5	Lymphocyte transmembrane adapter 1	124	10 mgF/L
P31421	Metabotropic glutamate receptor 2	47	10 mgF/L
Q62812	Myosin-9	44	10 mgF/L
Q9Z1A5	NEDD8-activating enzyme E1 regulatory subunit	53	10 mgF/L
F1M707	Neutrophil cytosolic factor 1	83	10 mgF/L

Q9Z0V5	Peroxiredoxin-4	70	10 mgF/L
E9PU17	Protein Abca17	46	10 mgF/L
Q66H38	Protein FAM71B	59	10 mgF/L
Q99MC0	Protein phosphatase 1 regulatory subunit 14A	187	10 mgF/L
Q5BK61	Sorting nexin-20	59	10 mgF/L
B2GV06	Succinyl-CoA:3-ketoacid coenzyme A transferase 1, mitochondrial	53	10 mgF/L
Q62747	Synaptotagmin-7	92	10 mgF/L
Q3ZBA0	Tectonin beta-propeller repeat-containing protein 1	39	10 mgF/L
Q03191	Trefoil factor 3	352	10 mgF/L
Q569C3	Ubiquitin carboxyl-terminal hydrolase 1	52	10 mgF/L
Q09426	2-hydroxyacylsphingosine 1-beta-galactosyltransferase	46	Control
Q5FVR4	3'-5' exoribonuclease 1	117	Control
O35167	Acetylcholinesterase collagenic tail peptide	33	Control
Q62875	Allergin-1	117	Control
P37091	Amiloride-sensitive sodium channel subunit gamma	53	Control
Q5M889	Apolipoprotein F	69	Control
Q792S6	Bcl-2-related ovarian killer protein	94	Control
Q78EJ9	Calpain-8	68	Control
P32038	Complement factor D	106	Control
Q5XHY4	Ecto-ADP-ribosyltransferase 5	29	Control
P10158	Fos-related antigen 1	99	Control
Q62833	G protein-coupled receptor kinase 5	51	Control
Q6URK4	Heterogeneous nuclear ribonucleoprotein A3	97	Control
P61980	Heterogeneous nuclear ribonucleoprotein K	66	Control
D3ZWE7	HORMA domain-containing protein 1	43	Control
O55165	Kinesin-like protein KIF3C	44	Control
Q62733	Lamina-associated polypeptide 2, isoform beta	85	Control
Q9ES73	Melanoma-associated antigen D1	445	Control
Q63560	Microtubule-associated protein 6	31	Control
P19234	NADH dehydrogenase [ubiquinone] flavoprotein 2, mitochondrial	121	Control
P63057	Noelin-3	70	Control
Q8R5M4	Optineurin	48	Control
A1BPI0	Ornithine decarboxylase antizyme 3	100	Control
O55012	Phosphatidylinositol-binding clathrin assembly protein	88	Control
Q66HR9	Protein phosphatase 1 regulatory subunit 32	64	Control
Q6MG48	Protein PRRC2A	53	Control
O88794	Pyridoxine-5'-phosphate oxidase	131	Control
B0K004	Solute carrier family 35 member G3	71	Control
A0JPP4	Sperm equatorial segment protein 1	84	Control

Q29YR5	Sulfotransferase family cytosolic 2B member 1	111	Control
Q66MI6	Testis-specific protein 10-interacting protein	66	Control
Q5BJT4	Thioredoxin domain-containing protein 15	73	Control
Q76LT8	Ubiquitin carboxyl-terminal hydrolase 48	36	Control
Q71RJ2	Voltage-dependent calcium channel gamma-2 subunit	99	Control

<sup>a</sup>Identification is based on proteins ID from UniProt protein database, reviewed only (<http://www.uniprot.org/>).

<sup>b</sup>Proteins with expression significantly altered are organized according to the ratio.

\*Indicates unique proteins in alphabetical order.

**Table S2.** Proteins with expression significantly altered in the ileum of rats in the 50 mgF/L vs Control comparison.

<sup>a</sup> Accession number	Protein name	PLGS Score	<sup>b</sup> Ratio 50 mgF/L:Control
Q01134	Choline kinase alpha	106	4.22
P04797	Glyceraldehyde-3-phosphate dehydrogenase	92	1.43
P62804	Histone H4	550	1.36
P34058	Heat shock protein HSP 90-beta	104	1.31
P58775	Tropomyosin beta chain	254	1.28
P04692	Tropomyosin alpha-1 chain	257	1.27
Q64122	Myosin regulatory light polypeptide 9	242	1.26
P09495	Tropomyosin alpha-4 chain	156	1.25
P18666	Myosin regulatory light chain 12B	242	1.23
P13832	Myosin regulatory light chain RLC-A	242	1.23
P11517	Hemoglobin subunit beta-2	1037	1.20
Q63610	Tropomyosin alpha-3 chain	198	1.19
P02091	Hemoglobin subunit beta-1	2209	1.08
P01946	Hemoglobin subunit alpha-1/2	1357	0.91
P02770	Serum albumin	514	0.90
P62632	Elongation factor 1-alpha 2	317	0.89
P62630	Elongation factor 1-alpha 1	317	0.88
Q10758	Keratin, type II cytoskeletal 8	734	0.88
Q61FV1	Keratin, type I cytoskeletal 14	89	0.87
Q63279	Keratin, type I cytoskeletal 19	449	0.87
P16409	Myosin light chain 3	473	0.86
Q64119	Myosin light polypeptide 6	732	0.85
P10111	Peptidyl-prolyl cis-trans isomerase A	1089	0.85
P10719	ATP synthase subunit beta, mitochondrial	435	0.85
Q61FU7	Keratin, type I cytoskeletal 42	95	0.84
Q61FU8	Keratin, type I cytoskeletal 17	89	0.84
Q5BJY9	Keratin, type I cytoskeletal 18	207	0.83
P80020	Gastrotropin	877	0.62
P35213	14-3-3 protein beta/alpha	55	50 mgF/L*

---

---

P62260	14-3-3 protein epsilon	55	50 mgF/L
P68511	14-3-3 protein eta	55	50 mgF/L
P61983	14-3-3 protein gamma	55	50 mgF/L
P68255	14-3-3 protein theta	55	50 mgF/L
Q66HF8	Aldehyde dehydrogenase X, mitochondrial	67	50 mgF/L
Q9Z1P2	Alpha-actinin-1	56	50 mgF/L
P47858	ATP-dependent 6-phosphofructokinase, muscle type	63	50 mgF/L
P43527	Caspase-1	45	50 mgF/L
P50339	Chymase	81	50 mgF/L
D3ZVN1	Colipase-like protein 2	142	50 mgF/L
Q9R1E9	Connective tissue growth factor	54	50 mgF/L
Q9R0L4	Cullin-associated NEDD8-dissociated protein 2	38	50 mgF/L
Q2Q0I9	Fibronectin type III domain-containing protein 1	35	50 mgF/L
Q9Z144	Galectin-2	318	50 mgF/L
P47819	Glial fibrillary acidic protein	28	50 mgF/L
D3ZQF4	Inactive peptidyl-prolyl cis-trans isomerase FKBP6	36	50 mgF/L
P04642	L-lactate dehydrogenase A chain	174	50 mgF/L
P42123	L-lactate dehydrogenase B chain	146	50 mgF/L
Q4V8A1	Lysophosphatidylcholine acyltransferase 2B	41	50 mgF/L
O88989	Malate dehydrogenase, cytoplasmic	129	50 mgF/L
P0C546	Mitochondrial coenzyme A transporter SLC25A42	67	50 mgF/L
Q9EQ10	PCNA-interacting partner	62	50 mgF/L
P16617	Phosphoglycerate kinase 1	354	50 mgF/L
A1A5S1	Pre-mRNA-processing factor 6	68	50 mgF/L
P67779	Prohibitin	126	50 mgF/L
Q5XIH7	Prohibitin-2	159	50 mgF/L
Q66HG8	Protein Red	34	50 mgF/L
B5DF21	Protein Smaug homolog 1	47	50 mgF/L
P35248	Pulmonary surfactant-associated protein D	151	50 mgF/L
P50399	Rab GDP dissociation inhibitor beta	130	50 mgF/L
Q80ZF7	Retinol dehydrogenase 10	82	50 mgF/L
Q9Z143	Semaphorin-4F	29	50 mgF/L
Q925F0	Small muscular protein	340	50 mgF/L
P06685	Sodium/potassium-transporting ATPase subunit alpha-1	53	50 mgF/L
Q6AXM9	Uncharacterized protein C12orf29 homolog	71	50 mgF/L
Q641W2	UPF0160 protein MYG1, mitochondrial	64	50 mgF/L
P85972	Vinculin	83	50 mgF/L
B2RYI0	WD repeat-containing protein 91	56	50 mgF/L
Q5U2Z0	Zinc finger protein 367	63	50 mgF/L
Q09426	2-hydroxyacylsphingosine 1-beta-galactosyltransferase	46	Control
Q5FVR4	3'-5' exoribonuclease 1	117	Control

---

---



O35167	Acetylcholinesterase collagenic tail peptide	33	Control
Q62875	Allergin-1	117	Control
P37091	Amiloride-sensitive sodium channel subunit gamma	53	Control
Q5M889	Apolipoprotein F	69	Control
Q792S6	Bcl-2-related ovarian killer protein	94	Control
Q78EJ9	Calpain-8	68	Control
P32038	Complement factor D	106	Control
Q5XHY4	Ecto-ADP-ribosyltransferase 5	29	Control
P10158	Fos-related antigen 1	99	Control
Q62833	G protein-coupled receptor kinase 5	51	Control
Q6URK4	Heterogeneous nuclear ribonucleoprotein A3	97	Control
P61980	Heterogeneous nuclear ribonucleoprotein K	66	Control
D3ZWE7	HORMA domain-containing protein 1	43	Control
O55165	Kinesin-like protein KIF3C	44	Control
Q62733	Lamina-associated polypeptide 2, isoform beta	85	Control
Q9ES73	Melanoma-associated antigen D1	445	Control
Q63560	Microtubule-associated protein 6	31	Control
P19234	NADH dehydrogenase [ubiquinone] flavoprotein 2, mitochondrial	121	Control
P63057	Noelin-3	70	Control
Q8R5M4	Optineurin	48	Control
A1BPI0	Ornithine decarboxylase antizyme 3	100	Control
O55012	Phosphatidylinositol-binding clathrin assembly protein	88	Control
Q66HR9	Protein phosphatase 1 regulatory subunit 32	64	Control
Q6MG48	Protein PRRC2A	53	Control
O88794	Pyridoxine-5'-phosphate oxidase	131	Control
B0K004	Solute carrier family 35 member G3	71	Control
A0JPP4	Sperm equatorial segment protein 1	84	Control
Q29YR5	Sulfotransferase family cytosolic 2B member 1	111	Control
Q66MI6	Testis-specific protein 10-interacting protein	66	Control
Q5BJT4	Thioredoxin domain-containing protein 15	73	Control
Q76LT8	Ubiquitin carboxyl-terminal hydrolase 48	36	Control
Q71RJ2	Voltage-dependent calcium channel gamma-2 subunit	99	Control

<sup>a</sup>Identification is based on proteins ID from UniProt protein database, reviewed only (<http://www.uniprot.org/>).

<sup>b</sup>Proteins with expression significantly altered are organized according to the ratio.

\*Indicates unique proteins in alphabetical order.



### 2.3 Article 3

#### **Effects of acute fluoride exposure on the jejunum and ileum of rats: Insights from proteomic and enteric innervation analysis**

Article formatted according to **Science of the Total Environment** Guidelines.

**Accepted June 20, 2020** (Aline Dionizio, Carina Guimarães Souza Melo, Isabela Tomazini Sabino-Arias, Tamara Teodoro Araujo, Talita Mendes Oliveira Ventura, Aline Lima Leite, Sara Raquel Garcia Souza, Erika Xavier Santos, Alessandro Domingues Heubel, Juliana Gadelha Souza, Juliana Vanessa Colombo Martins Perles, Jacqueline Nelisis Zanoni; Marília Afonso Rabelo Buzalaf. Effects of acute fluoride exposure on the jejunum and ileum of rats: Insights from proteomic and enteric innervation analysis. *Science of the Total Environment*, v. 741, e. 140419, 2020.). License by Creative Commons license

Aline Dionizio<sup>1</sup>, Carina Guimarães Souza Melo<sup>1</sup>, Isabela Tomazini Sabino-Arias<sup>1</sup>, Tamara Teodoro Araujo<sup>1</sup>, Talita Mendes Silva Ventura<sup>1</sup>, Aline Lima Leite<sup>1</sup>, Sara Raquel Garcia Souza<sup>2</sup>, Erika Xavier Santos<sup>2</sup>, Alessandro Domingues Heubel<sup>1</sup>, Juliana Gadelha Souza<sup>1</sup>, Juliana Vanessa Colombo Martins Perles<sup>2</sup>, Jacqueline Nelisis Zanoni<sup>2</sup> & Marília Afonso Rabelo Buzalaf<sup>1</sup>

1 Department of Biological Sciences, Bauru School of Dentistry, University of São Paulo, Bauru, Brazil.

2 Department of Morphophysiological Sciences, State University of Maringá, Maringá, Brazil.

Corresponding author

Marília Afonso Rabelo Buzalaf

Alameda Octávio Pinheiro Brisolla, 9-75

Bauru-SP, Brazil, 17012-901

Phone: # 55 14 3235-8346

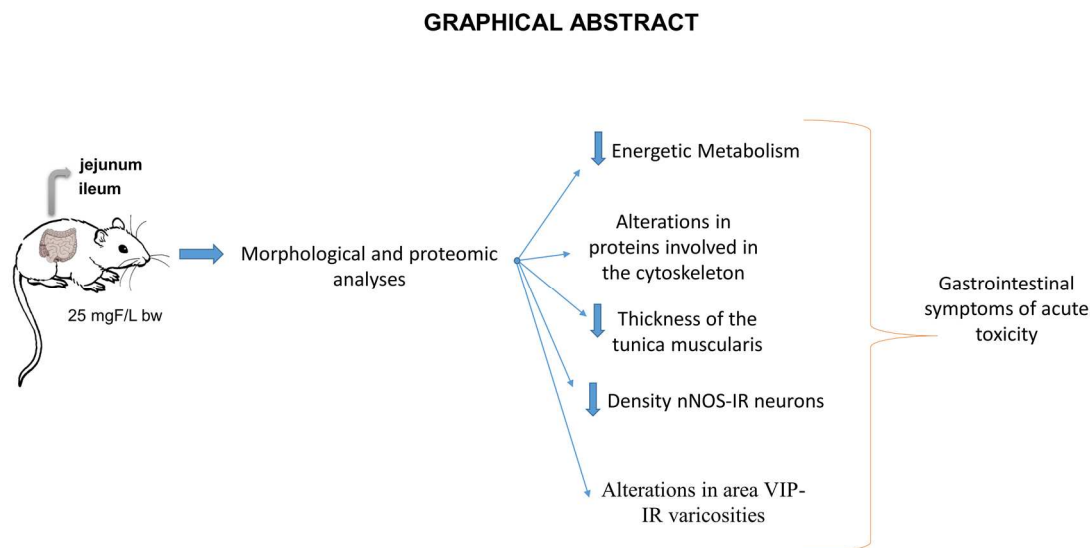
Email: mbuzalaf@fob.usp.br

---

## HIGHLIGHTS

- Water containing 25 mgF/Kg body weight fluoride provokes morphological changes and alters in several proteins in the jejunum and ileum of rats.
- After the acute exposure to F, the organism might not have had time to adapt to its toxic effect, which means that the loss of energy may have not been repaired.
- Morphological alterations in the gut, can be explained by alterations in the gut vipergic innervation and in proteins that regulate the cytoskeleton.

## GRAPHICAL ABSTRACT



## ABSTRACT

Fluoride (F) is largely employed in dentistry, in therapeutic doses, to control caries. However, excessive intake may lead to adverse effects in the body. Since F is absorbed mostly from the gastrointestinal tract (GIT), gastrointestinal symptoms are the first signs following acute F exposure. Nevertheless, little is known about the mechanistic events that lead to these symptoms. Therefore, the present study evaluated changes in the proteomic profile as well as morphological changes in the jejunum and ileum of rats upon acute exposure to F. Male rats received, by gastric gavage, a single dose of F containing 0 (control) or 25 mg/Kg for 30 days. Upon exposure to F, there was a decrease in the thickness of the tunic muscularis for both

segments and a decrease in the thickness of the wall only for the ileum. In addition, a decrease in the density of HuC/D-IR neurons and nNOS-IR neurons was found for the jejunum, but for the ileum only nNOS-IR neurons were decreased upon F exposure. Moreover, SP-IR varicosities were increased in both segments, while VIP-IR varicosities were increased in the jejunum and decreased in the ileum. As for the proteomic analysis, the proteins with altered expression were mostly negatively regulated and associated mainly with protein synthesis and energy metabolism. Proteomics also revealed alterations in proteins involved in oxidative/antioxidant defense, apoptosis and as well as in cytoskeletal proteins. Our results, when analyzed together, suggest that the gastrointestinal symptoms found in cases of acute F exposure might be related to the morphological alterations in the gut (decrease in the thickness of the tunica muscularis) that, at the molecular level, can be explained by alterations in the gut vipergic innervation and in proteins that regulate the cytoskeleton.

**Keyword:** Fluoride, Acute, Chronic, Ileum, Jejunum

**Abbreviations:** HuC/D-IR – immunoreactive to human proteins type C and D; nNOS-IR – immunoreactive to neural nitric oxide synthase; SP-IR – immunoreactive to substance P; VIP-IR – immunoreactive to intestinal vasoactive peptide; CGRP-IR – immunoreactive to calcitonin gene-related peptide.

## INTRODUCTION

Fluorine is one of the most abundant elements in the earth's crust (Shanthakumari et al., 2004) and is found in its ionic form (fluoride; F) in biological fluids and tissues as a trace element, in two different forms: inorganic and organic, being 99% accumulated in hard tissues (Suarez et al., 2008). F is widely used as a therapeutic agent against caries and can be found naturally in soil and water or in controlled doses at water supply stations (McDonagh et al., 2000; Wong et al., 2011). However, studies have shown that excessive intake of F can lead to side effects (Buzalaf et al., 2013; Whitford, 1996; Yan et al., 2011) perceived at the molecular level (Araujo et al., 2019; Barbier et al., 2010), as well as at the tissue level in several organs and structures, such as skeletal muscles, brain, spinal column (Mullenix et al., 1995),

---

liver (Dionizio et al., 2019; Pereira et al., 2018; Pereira et al., 2016; Pereira et al., 2013) and gut (Dionizio et al., 2018; Melo et al., 2017).

The toxic effect of F is related to the amount and duration of exposure (Araujo et al., 2019; Dionizio et al., 2019; Pereira et al., 2018) and can be classified into acute or chronic (He and Chen, 2006; Shanthakumari et al., 2004; Whitford, 1992). Acute toxicity occurs by ingesting a large amount of F at a single time (Whitford, 2011). Most of the studies evaluating acute F exposure report the effects at the molecular and histological levels in the kidney (Jimenez-Cordova et al., 2019; Mitsui et al., 2010; Santoyo-Sanchez et al., 2013) and heart (Mitsui et al., 2007; Panneerselvam et al., 2019). Considering that the gastrointestinal tract (GIT), especially the gut, is the main responsible for the absorption of F (Nopakun et al., 1989; Whitford, 2011; Whitford and Pashley, 1984), gastrointestinal manifestations are frequently reported in cases of acute F intoxication, such as vomiting with blood and diarrhea. These manifestations can occur in cases of professional application of F for caries prevention, especially in children, as well as in cases of poisoning (Whitford, 2011). However, little is known regarding the effects of acute F exposure in the GIT at the molecular level. This knowledge is important to allow an adequate treatment of patients submitted to acute F intoxication. In this sense, the present study attempted to shed light into the molecular mechanisms underlying acute F toxicity, by performing morphological analysis of the intestinal wall and myenteric neurons, as well as proteomic analysis of the jejunum and ileum of rats, after acute exposure to F.

## **MATERIAL AND METHODS**

### **Animals and treatment**

The work was performed on twelve adult male rats (60 days of life - *Rattus norvegicus*, Wistar type). The animals were individually housed in metabolic cages, with *ad libitum* access to deionized water and low-fluoride chow for 30 days. The illumination (12 h light/12 dark hours) and the ambient temperature were controlled ( $22 \pm 2$  °C). The animals were randomly divided into 2 groups (n = 6 per group), according with the treatment they received by gavage in the last day of the experiment. The experimental group received 25 mgF/kg body weight as sodium fluoride (NaF) dissolved in deionized water, while the control group received deionized water. As rodents metabolize F 5 times faster than humans (Dunipace et al., 1995), this dose of

---

F corresponds to ~ 5 mg/kg to humans, which corresponds to the probable toxic dose (PTD) (Whitford, 2011). After the treatment period, the plasma was obtained by centrifugation of blood at 800g for 5 min for quantification of F, as previously described (Melo et al., 2017). Then, the jejunum and ileum were collected as described by Dionizio et al. (2018), for morphological and proteomic analysis. Briefly, animal chow was removed from the animals 18 h prior to euthanasia, to reduce the volume of fecal material inside the small intestine, thus making easier the cleaning process for posterior analysis. After identifying the duodenojejunal flexure, one incision is made. Around 20 cm were despoised and then 15 cm of the jejunum were harvested. After localizing the cecum, two incisions were made to collect the ileum: one in the anterior portion of the ileocecal valve and the other 10 cm proximally to the first one. The jejunum and ileum segments were washed with phosphate buffered solution several times to remove residues of fecal material. All experimental protocols were approved by the Animal Experimentation Ethics Committee of the Faculty of Dentistry of Bauru of the University of São Paulo (protocols 014/2011 and 012/2016).

### **Histological analysis and Myenteric plexus immunofluorescence, morphometric and semi-quantitative analysis**

These analyses were performed exactly as described by Melo et al. (2017)

### **Proteomics and bioinformatics analyses**

The frozen jejunum and ileum were homogenized in a cryogenic mill (model 6770, Spex, Metuchen, NJ, EUA). Samples from 2 animals were pooled and analyses were carried out in triplicates, exactly as previously described (Dionizio et al., 2018). Briefly, protein extraction was performed by incubation in lysis buffer (7 M urea, 2 M thiourea, 40 mM DTT, all diluted in AMBIC solution) under constant stirring at 4°C. After centrifugation at 20,817g for 30 min at 4 °C, the supernatant was collected and total protein was quantified (Bradford, 1976). To 50 µL of each sample (containing 50 µg protein) 25 µL of 0.2% Rapigest (Waters cat#186001861) were added, followed by agitation and then 10 µL 50 mM AMBIC were added, followed by incubation for 30 min at 37 °C. Samples were then reduced (100 mM DTT; BioRad, cat# 161-0611) and alkylated (300 mM IAA; GE, cat# RPN 6302V) under dark at room temperature for 30 min. Digestion was performed at 37 °C overnight by adding 100 ng trypsin (Promega, cat #V5280). Then 10 µL of 5% TFA were added, samples were incubated for 90 min

---

at 37 °C and centrifuged (20,817 g at 6 °C for 30 min). Supernatant was purified using C 18 Spin columns (Pierce, cat #89870). Samples were then resuspended in 200 µL 3% acetonitrile.

The peptides identification was performed on a nanoAcquity UPLC-Xevo QToF MS system (Waters, Manchester, UK), as previously described (Lima Leite et al., 2014). The Protein Lynx Global Server (PLGS) software was used to detect difference in expression between the groups, which was expressed as  $p < 0.05$  and  $1 - p > 0.95$  for down- and up-regulated proteins, respectively. Bioinformatics analysis was performed for comparison of the treated group with the control group (Tables S1-S2), as earlier reported (Bauer-Mehren, 2013; Lima Leite et al., 2014; Millan, 2013; Orchard, 2012). The software CYTOSCAPE® 3.0.4 (Java®) was employed to build networks of molecular interaction between the identified proteins, with the support of ClusterMarker® application.

## RESULTS

### **Morphological analysis of the jejunum and ileum wall thickness**

The mean ( $\pm$  SD) thickness of the tunica muscularis was significantly decreased in the treated groups of jejunum ( $90.1 \pm 1.9 \mu\text{m}^2$ ) and ileum ( $134.0 \pm 2.5 \mu\text{m}^2$ ) when compared with the respective controls ( $116.4 \pm 3.7 \mu\text{m}^2$  and  $223.6 \pm 7.8 \mu\text{m}^2$ ) (Student's *t* test,  $p < 0.05$ ). The same was observed for the mean ( $\pm$  SD) total thickness of the wall, which was significantly reduced in the treated group ( $756.5 \pm 12.9 \mu\text{m}^2$ ) when compared with control ( $784.1 \pm 17.1 \mu\text{m}^2$ ) for ileum (Student's *t* test,  $p > 0.05$ ).

### **Myenteric neurons HuC/D – IR analysis.**

In the morphometric analysis of the general population of neurons, after treatment with fluoride, the cell bodies areas of the HuC/D–IR neurons of the ileum ( $\mu\text{m}^2$ ) were significantly increased, but no significant changes were seen in the jejunum ( $p > 0.05$ ). In the quantitative analyses, the treated group presented a significant decrease in the jejunum but was not significantly altered in the ileum ( $p > 0.05$ ). (Tables 1 and 2).

---



**Table 1.** Means and standard errors of the values of the cell bodies areas and density of HUC/D-IR, nNOS-IR and VIP-IR, CGRP-IR, and SP-IR values of myenteric neurons varicosities areas of the **jejunum** of rats exposed or not to acute dose of F. Animal groups: Control (deionized water - 0 mgF/L) and 25mgF/Kg bw.

ANALYSIS	Control	25mgF/Kg bw
Cell bodies areas of the HuC/D-IR neurons ( $\mu\text{m}^2$ )	319.5 $\pm$ 3.5 <sup>a</sup>	316.2 $\pm$ 3.9 <sup>a</sup>
Density HuC/D-IR neurons (neurons/cm <sup>2</sup> )	16,594.0 $\pm$ 343.1 <sup>a</sup>	13,848.4 $\pm$ 324.3 <sup>b</sup>
Cell bodies areas of the nNOS-IR neurons ( $\mu\text{m}^2$ )	288.7 $\pm$ 3.0 <sup>a</sup>	300.8 $\pm$ 3.0 <sup>b</sup>
Density nNOS-IR neurons (neurons/cm <sup>2</sup> )	5,959.9 $\pm$ 138.7 <sup>a</sup>	5,219.9 $\pm$ 151.6 <sup>b</sup>
Area VIP-IR varicosities ( $\mu\text{m}^2$ )	2.8 $\pm$ 0.0 <sup>a</sup>	3.0 $\pm$ 0.0 <sup>b</sup>
Area CGRP-IR varicosities ( $\mu\text{m}^2$ )	3.5 $\pm$ 0.0 <sup>a</sup>	3.5 $\pm$ 0.0 <sup>a</sup>
Area SP-IR varicosities ( $\mu\text{m}^2$ )	3.1 $\pm$ 0.0 <sup>a</sup>	4.8 $\pm$ 0.0 <sup>b</sup>

Means followed by different letters in the same column are significantly different according to Student's t-test ( $p < 0.05$ ). (N = 6).

#### **Myenteric neurons nNOS –IR analysis.**

In the morphometric analysis of the general population of neurons, the cell bodies areas of the nNOS-IR neurons ( $\mu\text{m}^2$ ) were significantly increased in the jejunum and significantly decreased in the ileum, in comparison with the respective controls ( $p < 0.05$ ). In the quantitative analyses, significant decreases were observed in the treated groups in respect to control, both for jejunum and ileum ( $p < 0.05$ ) (Tables 1 and 2).

**Table 2.** Means and standard errors of the values of the cell bodies areas and density of HuC/D-IR, nNOS-IR and VIP-IR, CGRP-IR, and SP-IR values of myenteric neurons varicosities areas of the **ileum** of rats exposed or not to acute dose of F. Animal groups: Control (deionized water - 0 mgF/L) and 25mgF/Kg bw.

ANALYSIS	Control	25mgF/Kg bw
Cell bodies areas of the HuC/D-IR neurons ( $\mu\text{m}^2$ )	298.0 $\pm$ 3.6 <sup>a</sup>	312.3 $\pm$ 4.0 <sup>b</sup>
Density HuC/D-IR neurons (neurons/cm <sup>2</sup> )	13,099.8 $\pm$ 420.9 <sup>a</sup>	12,756,9 $\pm$ 347.7 <sup>a</sup>
Cell bodies areas of the nNOS-IR neurons ( $\mu\text{m}^2$ )	300.4 $\pm$ 3.3 <sup>a</sup>	287.6 $\pm$ 3.1 <sup>b</sup>
Density nNOS-IR neurons (neurons/cm <sup>2</sup> )	4,657.1 $\pm$ 145.4 <sup>a</sup>	3,905.6 $\pm$ 129.7 <sup>b</sup>
Area VIP-IR varicosities ( $\mu\text{m}^2$ )	3.3 $\pm$ 0.0 <sup>a</sup>	3.1 $\pm$ 0.0 <sup>b</sup>
Area CGRP-IR varicosities ( $\mu\text{m}^2$ )	3.4 $\pm$ 0,0 <sup>a</sup>	3,2 $\pm$ 0,0 <sup>b</sup>
Area SP-IR varicosities ( $\mu\text{m}^2$ )	2.9 $\pm$ 0.0 <sup>a</sup>	4,515 $\pm$ 0,0 <sup>b</sup>

Means followed by different letters in the same line are significantly different according to Student's t-test ( $p < 0.05$ ). (N = 6).

### **Myenteric neurons VIP-IR, CGRP-IR and SP-IR morphometric analysis.**

In the morphometric analyses of the SP-IP varicosities ( $\mu\text{m}^2$ ) a significant increase was detected in the treated groups in respect to control, both for jejunum and ileum ( $p < 0.05$ ). CGRP-IR varicosities ( $\mu\text{m}^2$ ) were significantly reduced in the ileum after treatment with fluoride but were not significantly altered in the jejunum ( $p > 0.05$ ). The VIP-IR varicosities ( $\mu\text{m}^2$ ) were significantly increased in the jejunum and significantly decreased in the ileum upon treatment with fluoride ( $p < 0.05$ ) (Tables 1 and 2). Representative images of the immunofluorescences are displayed in supplementary information (Supplementary Figures 1-4).

### **Proteomic analysis**

The total numbers of proteins identified by mass spectrometry in jejunum of control and treated group were 282 and 227, respectively. Among them, 106 and 51 proteins were uniquely identified in the control and treated groups, respectively. In the quantitative analysis of treated vs. control group, 37 proteins with change in expression were detected. Most of the proteins with altered expression were downregulated in the group treated with F when compared with the control group (23 proteins), suggesting that acute exposure to F reduces protein synthesis (Table S1).

Figure 1 shows the subnetworks generated by ClusterMarker® for the comparison treated vs. control group of jejunum. Most of the proteins with altered expression interacted with *Dynein light chain 1, cytoplasmic* (P63170), *Solute carrier family 2, facilitated glucose transporter member 4* (P19357), *Polyubiquitin-C* (Q63429), *Gap junction alpha-1 protein* (P08050), *Protein deglycase DJ-1* (O88767), *Small ubiquitin-related modifier 3* (Q5XIF4) (Fig. 1A) or *Heterogeneous nuclear ribonucleoprotein K* (P61980) and *Mitogen-activated protein kinase 3* (P21708) (Fig. 1B).

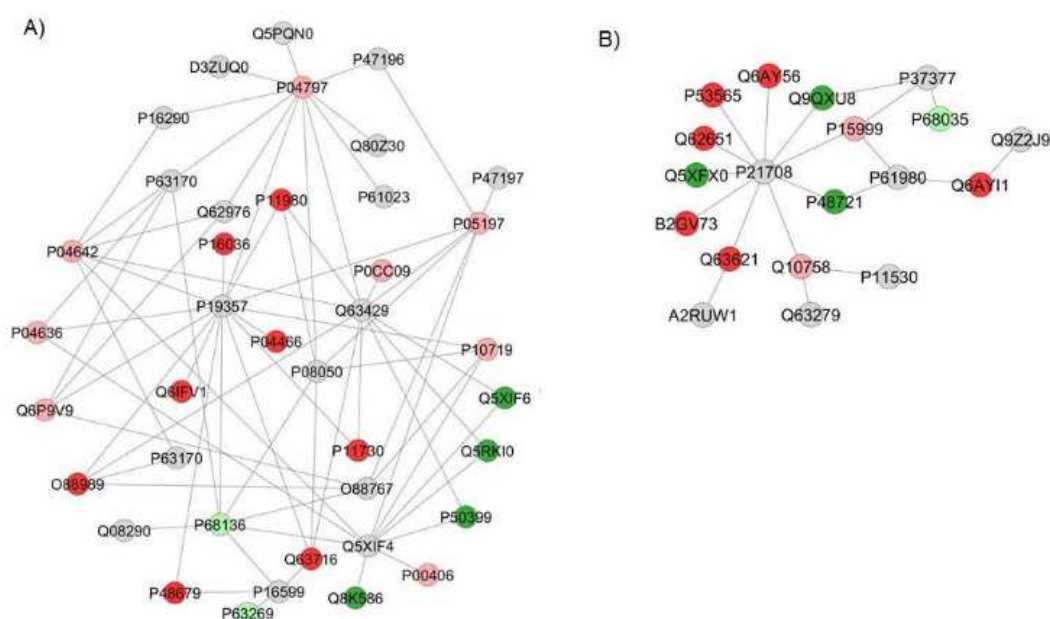


**Figure 1** - Subnetworks created by ClusterMarker® to establish the interaction between proteins identified with differential expression in the 25 mgF/Kg wb group in relation to the control group in jejunum. The color of the nodes indicates the differential expression of the respective named protein with its access code. The dark red and dark green nodes indicate proteins unique to the control and 25 mgF/Kg wb groups, respectively. The nodes in gray indicate the interaction proteins that are offered by CYTOSCAPE®, which were not identified in the present study and the light red and light green nodes indicate downregulation and upregulation, respectively. In **A** the access numbers in the gray nodes correspond to: *RAC-beta serine/threonine-protein kinase* (P47197), *RAC-alpha serine/threonine-protein kinase* (P47196), *Neurocalcin-delta* (Q5PQN0), *RILP-like protein 1* (D3ZUQ0), *Phosphoglycerate mutase 2* (P16290), *Dynein light chain 1, cytoplasmic* (P63170), *Calcium-activated potassium channel subunit alpha-1* (Q62976), *Protein phosphatase 1E* (Q80Z30), *Calcineurin B homologous protein 1* (P61023), *Solute carrier family 2, facilitated glucose transporter member 4* (P19357), *Polyubiquitin-C* (Q63429), *Gap junction alpha-1 protein* (P08050), *Dynein light chain 1, cytoplasmic* (P63170), *Protein deglycase DJ-1* (O88767), *Small ubiquitin-related modifier 3* (Q5XIF4), *Tumor necrosis factor* (P16599) and *Calponin-1* (Q08290). The access numbers of the unique proteins of the control (dark red nodes) correspond to the: *Pyruvate kinase PKM* (P11980), *Phosphate carrier protein, mitochondrial* (P16036), *Myosin regulatory light chain 2, skeletal muscle isoform* (P04466), *Keratin, type I cytoskeletal 14* (Q6IFV1), *Calcium/calmodulin-dependent protein kinase type II subunit gamma* (P11730), *Malate dehydrogenase, cytoplasmic* (O88989), *Peroxiredoxin-1* (Q63716) and *Prelamin-A/C* (P48679). The accession numbers of the unique 25 mgF/Kg wb (dark green nodes) proteins correspond to the: *Tubulin alpha-4A chain* (Q5XIF6), *WD repeat-containing protein 1* (Q5RKI0), *Rab GDP dissociation inhibitor beta* (P50399) and *GTP-binding nuclear protein Ran, testis-specific isoform* (Q8K586). The access numbers of the downregulated proteins (light red nodes) correspond to the: *Glyceraldehyde-3-phosphate dehydrogenase* (P04797), *L-lactate dehydrogenase A chain* (P04642), *Elongation factor 2* (P05197), *Histone H2A type 2-A* (P0CC09), *Malate dehydrogenase, mitochondrial* (P04636), *Tubulin*

*alpha-1B chain* (Q6P9V9), *ATP synthase subunit beta, mitochondrial* (P10719) and *Cytochrome c oxidase subunit 2* (P00406). The access numbers of the upregulated proteins (light green nodes) correspond to the: *Actin, gamma-enteric smooth muscle* (P63269) and *Actin, alpha skeletal muscle* (P68136). In **B** the access numbers in the gray nodes correspond to: *Alpha-synuclein* (P37377), *Runt-related transcription factor 2* (Q9Z2J9), *Heterogeneous nuclear ribonucleoprotein K* (P61980), *Mitogen-activated protein kinase 3* (P21708), *Dystrophin* (P11530), *Keratin, type I cytoskeletal 19* (Q63279) and *Toll-interacting protein* (A2RUW1). The access numbers of the unique proteins of the control (dark red nodes) correspond to the: *Tubulin alpha-8 chain* (Q6AY56), *Homeobox protein cut-like 1* (P53565), *Delta(3,5)-Delta(2,4)-dienoyl-CoA isomerase, mitochondrial* (Q62651), *Actin-related protein 2/3 complex subunit 3* (B2GV73), *Interleukin-1 receptor accessory protein* (Q63621) and *DEAD (Asp-Glu-Ala-Asp) box polypeptide 5* (Q6AY11). The accession numbers of the unique 25 mgF/Kg wb (dark green nodes) proteins correspond to the: *Cytoplasmic dynein 1 light intermediate chain 1* (Q9QXU8), *Transgelin-2* (Q5XFX0) and *Stress-70 protein, mitochondrial* (P48721). The access numbers of the downregulated proteins (light red nodes) correspond to the: *ATP synthase subunit alpha, mitochondrial* (P15999) and *Keratin, type II cytoskeletal 8* (Q10758). The access numbers of the upregulated proteins (light green nodes) correspond to the: *Actin, alpha cardiac muscle 1* (P68035).

Figure 2 shows the functional classification according to the biological process with the most significant term, for the comparison between treated vs. control group for jejunum. Among them, the categories with the highest percentages of genes were Actin filament binding (14.1%), Calmodulin binding (14.1%), Structural constituent of cytoskeleton (12.5%), Motor activity (10.9%) and Hydrogen ion transmembrane transporter activity (9.4%).

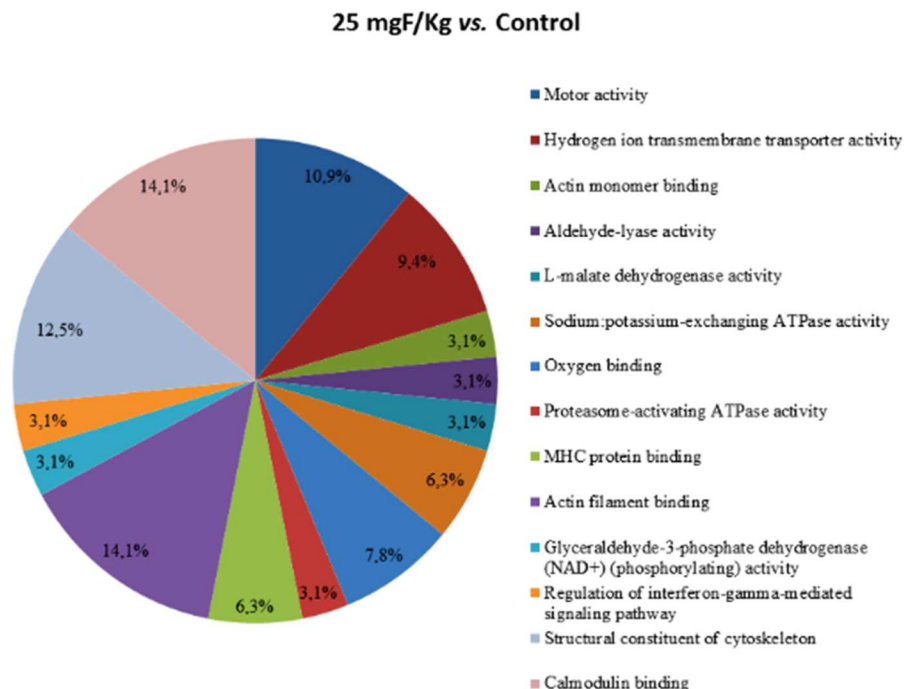


**Figure 2** - Functional distribution of proteins identified with differential expression in the jejunum of rats exposed acute dose of 25 mgF/Kg wb vs. Control Group (0 mgF/L). Categories of proteins based on GO annotation Biological Process. Terms significant ( $Kappa=0.04$ ) and distribution according to percentage of number of genes. Proteins access number was provided by the UNIPROT. The gene ontology was evaluated according to ClueGo® pluggins of Cytoscape® software 3.4.0 (Bindea et al., 2013; Bindea et al., 2009).

The total numbers of proteins identified by mass spectrometry in the ileum for control and treated groups were 195 and 183, respectively. Among them, 66 and 54 proteins were uniquely identified in the control and treated groups, respectively. In the quantitative analysis of the treated vs. control group, 36 proteins with change in expression were detected. Most of the proteins with altered expression were downregulated in the group treated with F when compared with the control group (22 proteins), suggesting that acute exposure to F reduces protein synthesis (Table S2).

Figure 3 shows the subnetworks generated by ClusterMarker® for the treated vs. control group of ileum. Most of the proteins with altered expression interacted with *Solute carrier family 2, facilitated glucose transporter member 4* (P19357), *Heterogeneous nuclear ribonucleoprotein K* (P61980), *UV excision repair protein RAD23 homolog B* (Q4KMA2), *Protein deglycase DJ-1* (O88767) and *Polyubiquitin-C* (Q63429) (Fig.3A) or *Mitogen-activated protein kinase 3* (P21708) and *Gap junction alpha-1 protein* (P08050) (Fig. 3B).

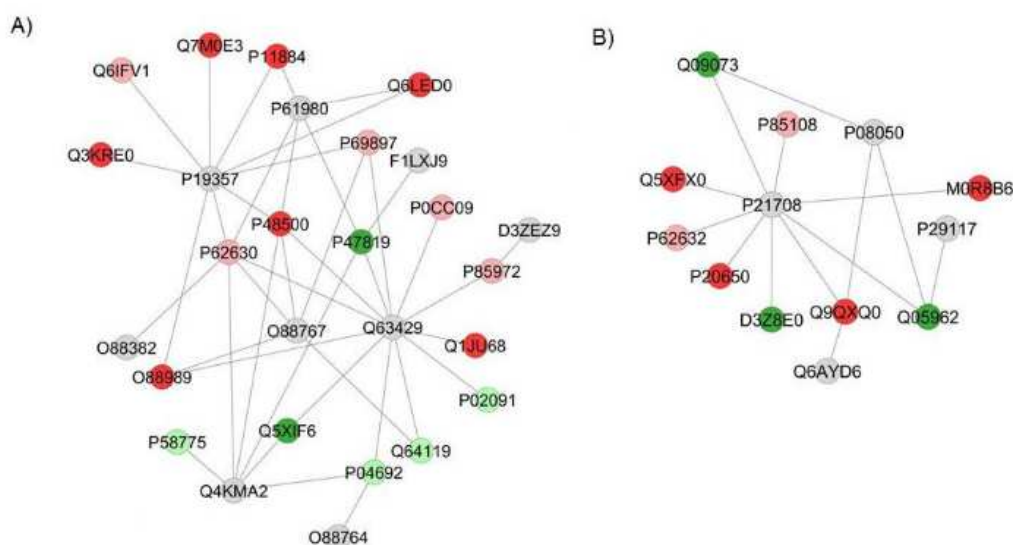


**Figure 3-** Subnetworks created by ClusterMarker® to establish the interaction between proteins identified with differential expression in the 25 mgF/Kg wb group in relation to the control group in ileum. The color of the nodes indicates the differential expression of the respective named protein with its access code. The dark red and dark green nodes indicate proteins unique to the control and 25 mgF/Kg wb groups, respectively. The nodes in gray indicate the interaction proteins that are offered by CYTOSCAPE®, which were not identified in the present study and the light red and light green nodes indicate downregulation and upregulation, respectively. In **A** the access numbers in the gray nodes correspond to: *Solute carrier family 2, facilitated glucose transporter member 4* (P19357), *Heterogeneous nuclear ribonucleoprotein K* (P61980), *Membrane-associated guanylate kinase, WW and PDZ domain-containing protein 2* (O88382), *UV excision repair protein RAD23 homolog B* (Q4KMA2), *Protein deglycase DJ-1* (O88767), *Death-associated protein kinase 3* (O88764), *Polyubiquitin-C* (Q63429), *Protein Ptprt* (F1LXJ9) and *Protein Svitl* (D3ZEZ9). The access numbers of the unique proteins of the control (dark red nodes) correspond to the: *Destrin* (Q7M0E3), *Aldehyde dehydrogenase, mitochondrial* (P11884), *Histone H3.1* (Q6LED0), *ATPase family AAA domain-containing protein 3* (Q3KRE0), *Triosephosphate isomerase* (P48500), *Malate dehydrogenase, cytoplasmic* (O88989) and *Eukaryotic translation initiation factor 3 subunit A* (Q1JU68). The accession numbers of the unique 25 mgF/Kg wb (dark green nodes) proteins correspond to the: *Glial fibrillary*

*acidic protein* (P47819) and *Tubulin alpha-4A chain* (Q5XIF6). The access numbers of the downregulated proteins (light red nodes) correspond to the: *Keratin, type I cytoskeletal 14* (Q61FV1), *Tubulin beta-5 chain* (P69897), *Histone H2A type 2-A* (P0CC09), *Vinculin* (P85972) and *Elongation factor 1-alpha 1* (P62630). The access numbers of the downregulated proteins (light green nodes) correspond to the: *Hemoglobin subunit beta-1* (P02091), *Myosin light polypeptide 6* (Q64119), *Tropomyosin alpha-1 chain* (P04692) and *Tropomyosin beta chain* (P58775). In **B** the access numbers in the gray nodes correspond to: *Peptidyl-prolyl cis-trans isomerase F, mitochondrial* (P29117), *PDZ and LIM domain protein 2* (Q6AYD6), *Mitogen-activated protein kinase 3* (P21708) and *Gap junction alpha-1 protein* (P08050). The access numbers of the unique proteins of the control (dark red nodes) correspond to the: *Transgelin-2* (Q5XFX0), *Protein phosphatase 1A* (P20650), *Alpha-actinin-4* (Q9QXQ0) and *Protein Tubb1* (M0R8B6). The accession numbers of the unique 25 mgF/Kg wb (dark green nodes) proteins correspond to the: *ADP/ATP translocase 2* (Q09073), *ADP/ATP translocase 1* (Q05962) and *Ribosomal protein S6 kinase* (D3Z8E0). The access numbers of the downregulated proteins (light red nodes) correspond to the: *Tubulin beta-2A chain* (P85108) and *Elongation factor 1-alpha 2* (P62632).

Figure 4 shows the functional classification according to the biological process with the most significant term, for the comparison between treated vs. control groups for ileum. Among them, the categories with the highest percentages of genes were Intermediate filament-based process (21%), Oxygen transport (12%), Regulation of mitochondrial membrane permeability involved in apoptotic process (9%), Positive regulation of lipid kinase activity (9%) and Cellular response to nitric oxide (6%).

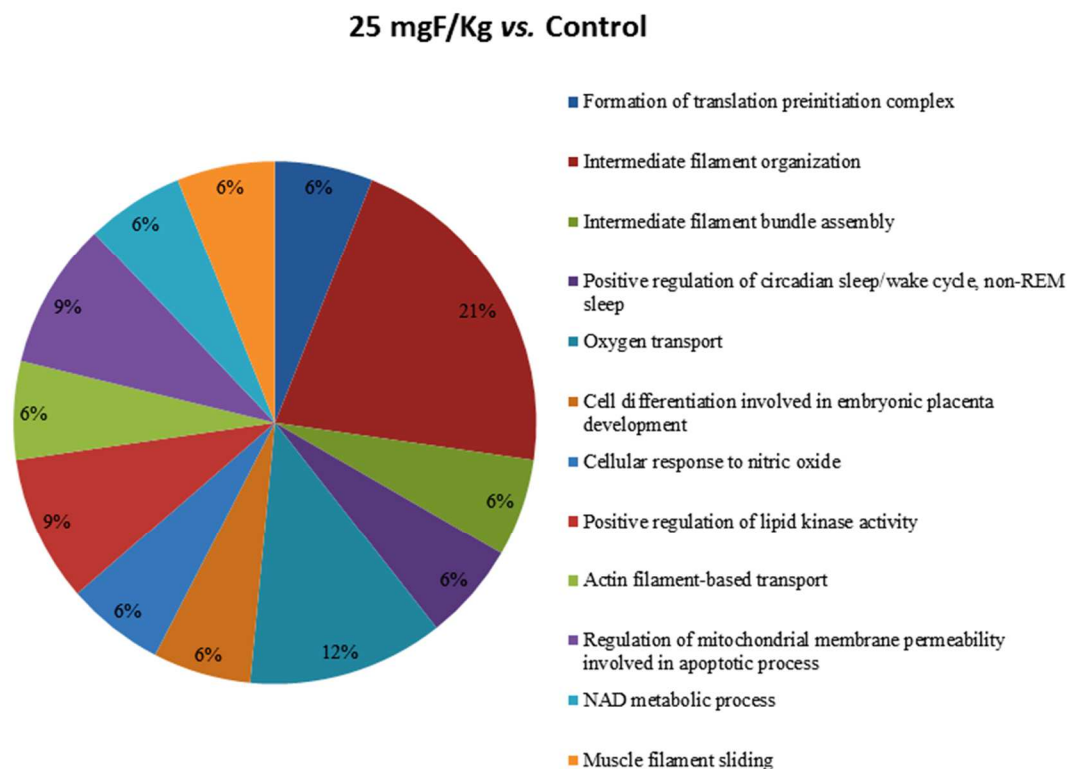


**Figure 4-** Functional distribution of proteins identified with differential expression in the ileum of rats exposed acute dose of 25 mgF/Kg wb vs. Control Group (0 mgF/L). Categories of proteins based on GO annotation Biological Process. Terms significant ( $Kappa=0.04$ ) and distribution according to percentage of number of genes. Proteins access number was provided by the UNIPROT. The gene

---

ontology was evaluated according to ClueGo® pluggins of Cytoscape® software 3.4.0 (Bindea et al., 2013; Bindea et al., 2009).

## DISCUSSION

The present study was designed to evaluate proteomic and morphological alterations in the jejunum after acute exposure to F. The dose we administered to rats (25 mgF/kg body weight) mimics the probable toxic dose (PTD) for humans, which is 5 mgF/Kg body weight (Whitford, 2011). This happens because rodents metabolize F 5 times faster than humans (Dunipace et al., 1995). We did not attempt to simulate the therapeutic doses of F for caries control, since in this case we usually have lower doses of fluoride administered along time, i.e., chronic exposure, which was evaluated in our previous studies (Dionizio et al., 2018; Melo et al., 2017). However, in cases of topical F application of fluoridated gels, especially in younger children, the PTD related to acute exposure can be reached and gastrointestinal signals and symptoms might be observed (Whitford, 2011).

Under acute exposure to F, the majority of the proteins with altered expression were downregulated, both in jejunum (Table S1) and ileum (Table S2). These results indicate that acute exposure to F reduced protein synthesis in distinct segments of the gut. The *subnetworks* for the comparison between the group treated with 25 mgF/Kg bw vs. control, both for jejunum (Fig. 1) and ileum (Fig. 3), revealed that most of the proteins with altered expression interacted with *Solute carrier family 2, facilitated glucose transporter member 4* (GLUT4; P19357), *Polyubiquitin-C* (Q63429), *Mitogen-activated protein kinase 3* (MAPK3; P21708) or *Heterogeneous nuclear ribonucleoprotein K* (P61980). Interestingly, the first 3 interacting partners were also present in the *subnetwork* comparing the proteins differentially expressed in the jejunum of rats chronically treated with 50 mgF/L F when compared with control (Dionizio et al., 2018). GLUT4 is involved in glucose transport. In a recent report by our group, in which proteomic analysis was conducted in the muscle and liver of diabetic rats, we observed that exposure to F altered many proteins that interacted with GLUT4 and could impair its function (Lima Leite et al., 2014; Lobo et al., 2015). In the present study, a plethora of proteins that interacted with GLUT4 and are involved in energy metabolism, especially of carbohydrates, were reduced or even absent in the jejunum upon acute exposure to F, such as *Malate dehydrogenase, mitochondrial* (P04636), *Malate dehydrogenase, cytoplasmic* (O88989), *L-lactate dehydrogenase A chain* (P04642), *Pyruvate kinase PKM* (P11980) and *Glyceraldehyde-3-phosphate*

---

*dehydrogenase* (GAPDH; P04797), while *Malate dehydrogenase, cytoplasmic* (O88989), *L-lactate dehydrogenase A chain* (P04642) and GAPDH (P04797) were also in the ileum upon exposure to F. These findings indicate a great impair in energy metabolism (especially of carbohydrates) in the jejunum and ileum of rats upon acute exposure to F, being the jejunum more affected than the ileum. These findings are somehow expected, since the enzymes involved in energy metabolism are highly affected by F, at least under chronic exposure to this ion (Araujo et al., 2019; Dionizio et al., 2018; Pereira et al., 2018). In addition, *ATP synthase subunit beta, mitochondrial* (P10719) and *ATP synthase subunit alpha, mitochondrial* (P15999), key enzymes in respiratory chain, were downregulated in the jejunum after acute F exposure, which corroborates the impair in the energy metabolism. It has been reported that expression of *ATP synthase subunit beta, mitochondrial* is reduced and correlated with ATP content in the livers of type 1 and type 2 diabetic mice, while hepatic overexpression of *ATP synthase subunit beta, mitochondrial* increases cellular ATP content and suppresses gluconeogenesis, leading to hyperglycemia amelioration (Wang et al., 2014).

*Polyubiquitin C* (Q63429) is a highly conserved polypeptide that is covalently bound to other cellular proteins to signal processes such as protein degradation, protein/protein interaction and protein intracellular trafficking (Ciechanover and Schwartz, 1998). In the present study, some of the above-mentioned proteins that interacted with GLUT4 also interacted with *Polyubiquitin C*. Another protein that interacted with *Polyubiquitin C* is Peroxiredoxin-1 (Q63716) that was absent in the jejunum upon acute exposure to F. Peroxiredoxin-1 plays an important role in cell protection against oxidative stress by detoxifying peroxides and acting as sensor of hydrogen peroxide-mediated signaling events (UniProt, 2019). In balance in the oxidant/antioxidant defense is a common effect of F (Araujo et al., 2019; Barbier et al., 2010; Iano et al., 2014).

MAPK3 (P21708) or extracellular-signal regulated kinases (ERK1) are a family of proteins that act as intermediaries in the signal transduction cascades triggered by extracellular signals at membrane receptors, through reversible protein phosphorylation, constituting one of the main mechanisms of cellular communication. They seem to be universal components of signal transduction mechanisms since multiple forms have been identified in a variety of organisms (Dinsmore and Soriano, 2018; Hymowitz and Malek, 2018). One of the proteins interacting with MAPK3 is

---



*Transgelin-2*. Increase in this protein is associated with the development of cancer, while its suppression leads to inhibition of cell proliferation, invasion and metastasis (Yakabe et al., 2016). Recently, transgelin was shown to be increased in colorectal cancer (Zhou et al., 2018) and was suggested as a potential biomarker for cancer as well as a potential new target for cancer treatment (Meng et al., 2017). In our studies, *Transgelin-2* was increased in the jejunum after acute exposure to F, but was absent in the ileum after acute exposure to F. The reason for this differential pattern of expression is not apparent at the moment but could possibly be related to the different characteristics in intestine segments, which should be evaluated in further studies. Interestingly, another protein involved in the control of cell proliferation (*Stress-70 protein, mitochondrial*; P48721) was identified exclusively in the jejunum after acute F exposure. In the jejunum, *Stress-70 protein, mitochondrial* also interacted with *Heterogeneous nuclear ribonucleoprotein K* that was also an interacting player in the ileum. This protein is one of the major pre-mRNA-binding proteins, playing an important role in p53/TP53 response to DNA damage, acting at the level of both transcription activation and repression, being necessary for the induction of apoptosis. In the jejunum, another identified protein that interacted with *Heterogeneous nuclear ribonucleoprotein K* was *DEAD (Asp-Glu-Ala-Asp) box polypeptide 5* (DDX5; Q6AY11), an RNA-binding protein overexpressed in various malignant tumors (Janknecht, 2010), since it causes growth (Saporita et al., 2011) and metastasis (Yang et al., 2006), through activation of several oncogenic pathways (Yang et al., 2006). In the present study, however, DDX5 was absent in the jejunum upon acute exposure to F. It has been reported that depletion of DDX5 causes apoptosis by inhibition of mammalian target of rapamycin complex 1 (mTORC1) (Taniguchi et al., 2016). Fluoride-induced apoptosis has been widely reported in the literature (Barbier et al., 2010; Ribeiro et al., 2017). In the ileum, *Elongation factor 1-alpha 1* (EF-1  $\alpha$ P62630) that interacted with *Heterogeneous nuclear ribonucleoprotein K* was reduced upon acute exposure to F, which is also related to induction of apoptosis, since elevated levels of EF-1  $\alpha$  are observed during neoplastic transformation and in tumors (Grant et al., 1992). In-line with this, *Aldehyde dehydrogenase, mitochondrial* (ALDH2; P11884) was absent upon acute exposure to F. Pharmacological inhibition of ALDH2 *per se* induces mitochondrial dysfunction and cell death (Mali et al., 2016). These findings are important because some reports incorrectly associate F exposure with the incidence of osteosarcoma (Bassin et al., 2006; Ramesh et al., 2001) and bladder cancer

---

(Grandjean et al., 1992). Our findings, however, give additional support to the safety of use of F on this aspect, since even when administered in a high dose as in the present study, F causes alterations in several proteins that lead to apoptosis instead of cell proliferation.

Most of the proteins that interacted with MAPK3 both in the jejunum and ileum are associated with cytoskeleton and some of them are actin-binding proteins (ABPs). Actin is one of the most abundant proteins in eukaryotic cells, participating in different cellular processes such as cell differentiation, proliferation, apoptosis, migration and signaling (Kristo et al., 2016). ABPs are highly abundant and directly participate in the modulation of cell processes through the regulation of actin cytoskeleton (Artman et al., 2014). Interestingly, *Transgelin-2* (Q5XFX0), an ABP, was absent in the ileum, but identified exclusively in the jejunum after acute exposure to F. This protein regulates the actin cytoskeleton through actin binding and sometimes participates in cytoskeleton remodeling (Dvorakova et al., 2014). In line with this, it is important to highlight that the categories with the highest percentage of associated genes, as revealed by functional classification, were acting filament binding (14.1%) and calmodulin binding (14.1%) for the jejunum (Fig. 2) and organization of intermediary filaments (21%) for the ileum (Fig. 4). Alterations in proteins involved in the cytoskeleton might explain some of the morphological findings of the present study. Both in the jejunum and ileum, the thickness of the tunica muscularis was significantly decreased in the group that received the acute dose of F, when compared with control. This alteration is considered as one of the possible explanations for the impairment of the intestinal motility upon exposure to F (Viteri and Schneider, 1974). For the inhibitory control of the motility, the main neurotransmitters involved are NO and VIP (Benarroch, 2007). In this sense, in our study NO was decreased in both segments, while VIP was increased in the jejunum and decreased in the ileum. These findings agree with those found by our group in the duodenum (Melo et al., 2017) and jejunum (Dionizio et al., 2018) of rats chronically treated with water containing 10 and 50 mgF/L.

Contrarily to which was seen in the chronic treatment of jejunum (Dionizio et al., 2018) and ileum (unpublished data), upon the acute exposure to F the organism might not have had time to adapt to its toxic effect, which means that the loss of energy may have not been repaired. According to the literature, some of the initial symptoms of acute toxicity are generalized weakness, drop in blood pressure and disorientation

---

(Buzalaf and Whitford, 2011; Whitford, 2011), which might be caused by decreased energy levels in the body.

In summary, our results, when analyzed in conjunction, suggest that the gastrointestinal symptoms found in cases of acute F exposure might be related to the morphological alterations in the gut (decrease in the thickness of the tunica muscularis) that, at the molecular level, can be explained by alterations in the gut vipergic innervation and in proteins that regulate the cytoskeleton. These findings help to explain the gastrointestinal signs and symptoms reported in cases of acute F toxicity.

### **Acknowledgements**

This study was supported by FAPESP (2011/10233-7, 2012/16840-5 and 2016/09100-6).

**CONFLICT OF INTEREST STATEMENT:** The authors have declared no conflict of interest.

### **Author Contributions**

#### **Author Contributions**

C.M., M.B., J.Z., and J.P. conceived the experiments. A.D., C.M., J.P., S.S. and A.L. conducted the experiments. A.D., C.M., T.T.A, J.P., S.S., A.L., I.A., T.V., A.H., and J.S. participated in the research experiments. A.D., T.T.A, C. M., A.H., J.S., E.S. participated in the experiment analyses. A.D., C.M., M.B. drafted the article; analyzed and interpreted the results. All authors reviewed and approved the manuscript.

### **Additional Information**

**Supplementary information** accompanies this paper.

### **References**

Araujo TT, Barbosa Silva Pereira HA, Dionizio A, Sanchez CDC, de Souza Carvalho T, da Silva Fernandes M, et al. Changes in energy metabolism induced by fluoride: Insights from inside the mitochondria. *Chemosphere* 2019; 236: 124357.

Artman L, Dormoy-Raclet V, von Roretz C, Gallouzi IE. Planning your every move: the role of beta-actin and its post-transcriptional regulation in cell motility. *Semin Cell Dev Biol* 2014; 34: 33-43.

---

Barbier O, Arreola-Mendoza L, Del Razo LM. Molecular mechanisms of fluoride toxicity. *Chem Biol Interact* 2010; 188: 319-33.

Bassin EB, Wypij D, Davis RB, Mittleman MA. Age-specific fluoride exposure in drinking water and osteosarcoma (United States). *Cancer Causes Control* 2006; 17: 421-8.

Bauer-Mehren A. Integration of genomic information with biological networks using Cytoscape. *Methods Mol Biol* 2013; 1021: 37-61.

Benarroch EE. Enteric Nervous System - Functional organization and neurologic implications. *Neurology* 2007; 69: 1953-1957.

Bindea, G, et al., Bernhard Mlecnik, Hubert Hackl, Pornpimol Charoentong, Marie Tosolini, Amos Kirilovsky, Wolf-Herman Fridman, Franck Pagès, Zlatko Trajanoski, Jérôme Galon, 2009. ClueGO: a Cytoscape plug-in to decipher functionally grouped gene ontology and pathway annotation networks. *Bioinformatics* 25 (8), 1091–1093. doi:doi.org/10.1093/bioinformatics/btp101.

Bindea, G, Jérôme G; Bernhard M, 2013. CluePedia Cytoscape plugin: pathway insights using integrated experimental and in silico data. *Bioinformatics* 29 (5), 661–663. doi:doi.org/10.1093/bioinformatics/btt019.

Bradford MM. A rapid and sensitive method for the quantitation of microgram quantities of protein utilizing the principle of protein-dye binding. *Anal Biochem* 1976; 72: 248-54.

Buzalaf MA, Moraes CM, Olympio KP, Pessan JP, Grizzo LT, Silva TL, et al. Seven years of external control of fluoride levels in the public water supply in Bauru, Sao Paulo, Brazil. *J Appl Oral Sci* 2013; 21: 92-8.

Buzalaf MA, Whitford GM. Fluoride metabolism. *Monogr Oral Sci* 2011; 22: 20-36.

Ciechanover A, Schwartz AL. The ubiquitin-proteasome pathway: the complexity and myriad functions of proteins death. *Proc Natl Acad Sci U S A* 1998; 95: 2727-30.

Dinsmore CJ, Soriano P. MAPK and PI3K Signaling: at the Crossroads of Neural Crest Development. *Dev Biol* 2018; Suppl 1: S79-S97.

Dionizio A, Pereira H, Araujo TT, Sabino-Arias IT, Fernandes MS, Oliveira KA, et al. Effect of Duration of Exposure to Fluoride and Type of Diet on Lipid Parameters and De Novo Lipogenesis. *Biol Trace Elem Res* 2019; 190: 157-171.

---

---

Dionizio AS, Melo CGS, Sabino-Arias IT, Ventura TMS, Leite AL, Souza SRG, et al. Chronic treatment with fluoride affects the jejunum: insights from proteomics and enteric innervation analysis. *Sci Rep* 2018; 8: 3180.

Dunipace AJ, Brizendine EJ, Zhang W, Wilson ME, Miller LL, Katz BP, et al. Effect of aging on animal response to chronic fluoride exposure. *J Dent Res* 1995; 74: 358-68.

Dvorakova M, Nenutil R, Bouchal P. Transgelins, cytoskeletal proteins implicated in different aspects of cancer development. *Expert Rev Proteomics* 2014; 11: 149-65.

Grandjean P, Olsen JH, Jensen OM, Juel K. Cancer incidence and mortality in workers exposed to fluoride. *J Natl Cancer Inst* 1992; 84: 1903-9.

Grant AG, Flomen RM, Tizard ML, Grant DA. Differential screening of a human pancreatic adenocarcinoma lambda gt11 expression library has identified increased transcription of elongation factor EF-1 alpha in tumour cells. *Int J Cancer* 1992; 50: 740-5.

He LF, Chen JG. DNA damage, apoptosis and cell cycle changes induced by fluoride in rat oral mucosal cells and hepatocytes. *World J Gastroenterol* 2006; 12: 1144-1148.

Hymowitz SG, Malek S. Targeting the MAPK Pathway in RAS Mutant Cancers. *Cold Spring Harb Perspect Med* 2018; 8: a031492.

Iano FG, Ferreira MC, Quaggio GB, Fernandes MS, Oliveira RC, Ximenes VF, et al. Effects of chronic fluoride intake on the antioxidant systems of the liver and kidney in rats. *J Fluorine Chem* 2014; 168: 212-217.

Janknecht R. Multi-talented DEAD-box proteins and potential tumor promoters: p68 RNA helicase (DDX5) and its paralog, p72 RNA helicase (DDX17). *Am J Transl Res* 2010; 2: 223-34.

Jimenez-Cordova MI, Gonzalez-Horta C, Ayllon-Vergara JC, Arreola-Mendoza L, Aguilar-Madrid G, Villareal-Vega EE, et al. Evaluation of vascular and kidney injury biomarkers in Mexican children exposed to inorganic fluoride. *Environ Res* 2019; 169: 220-228.

Kristo I, Bajusz I, Bajusz C, Borkuti P, Vilmos P. Actin, actin-binding proteins, and actin-related proteins in the nucleus. *Histochem Cell Biol* 2016; 145: 373-88.

---

Lima Leite A, Gualiume Vaz Madureira Lobo J, Barbosa da Silva Pereira HA, Silva Fernandes M, Martini T, Zucki F, et al. Proteomic analysis of gastrocnemius muscle in rats with streptozotocin-induced diabetes and chronically exposed to fluoride. *PLoS One* 2014; 9: e106646.

Lobo JG, Leite AL, Pereira HA, Fernandes MS, Peres-Buzalaf C, Sumida DH, et al. Low-Level Fluoride Exposure Increases Insulin Sensitivity in Experimental Diabetes. *J Dent Res* 2015; 94: 990-7.

Mali VR, Deshpande M, Pan G, Thandavarayan RA, Palaniyandi SS. Impaired ALDH2 activity decreases the mitochondrial respiration in H9C2 cardiomyocytes. *Cell Signal* 2016; 28: 1-6.

McDonagh MS, Whiting PF, Wilson PM, Sutton AJ, Chestnutt I, Cooper J, et al. Systematic review of water fluoridation. *BMJ* 2000; 321: 855-9.

Melo CGS, Perles J, Zanoni JN, Souza SRG, Santos EX, Leite AL, et al. Enteric innervation combined with proteomics for the evaluation of the effects of chronic fluoride exposure on the duodenum of rats. *Sci Rep* 2017; 7: 1070.

Meng T, Liu L, Hao R, Chen S, Dong Y. Transgelin-2: A potential oncogenic factor. *Tumour Biol* 2017; 39: 1010428317702650.

Millan PP. Visualization and analysis of biological networks. *Methods Mol Biol* 2013; 1021: 63-88.

Mitsui G, Dote T, Adachi K, Dote E, Fujimoto K, Shimbo Y, et al. Harmful effects and acute lethal toxicity of intravenous administration of low concentrations of hydrofluoric acid in rats. *Toxicol Ind Health* 2007; 23: 5-12.

Mitsui G, Dote T, Yamadori E, Imanishi M, Nakayama S, Ohnishi K, et al. Toxicokinetics and metabolism deteriorated by acute nephrotoxicity after a single intravenous injection of hydrofluoric acid in rats. *J Occup Health* 2010; 52: 395-9.

Mullenix PJ, Denbesten PK, Schunior A, Kernan WJ. Neurotoxicity of sodium fluoride in rats. *Neurotoxicol Teratol* 1995; 17: 169-77.

Nopakun J, Messer HH, Voller V. Fluoride absorption from the gastrointestinal tract of rats. *J Nutr* 1989; 119: 1411-7.

Orchard S. Molecular interaction databases. *Proteomics* 2012; 12: 1656-62.

---

Panneerselvam L, Raghunath A, Sundarraaj K, Perumal E. Acute fluoride exposure alters myocardial redox and inflammatory markers in rats. *Mol Biol Rep* 2019; 46: 6155-6164.

Pereira H, Dionizio AS, Araujo TT, Fernandes MDS, Iano FG, Buzalaf MAR. Proposed mechanism for understanding the dose- and time-dependency of the effects of fluoride in the liver. *Toxicol Appl Pharmacol* 2018; 358: 68-75.

Pereira HA, Dionizio AS, Fernandes MS, Araujo TT, Cestari TM, Buzalaf CP, et al. Fluoride Intensifies Hypercaloric Diet-Induced ER Oxidative Stress and Alters Lipid Metabolism. *PLoS One* 2016; 11: e0158121.

Pereira HA, Leite Ade L, Charone S, Lobo JG, Cestari TM, Peres-Buzalaf C, et al. Proteomic analysis of liver in rats chronically exposed to fluoride. *PLoS One* 2013; 8: e75343.

Ramesh N, Vuayaraghavan AS, Desai BS, Natarajan M, Murthy PB, Pillai KS. Low levels of p53 mutations in Indian patients with osteosarcoma and the correlation with fluoride levels in bone. *J Environ Pathol Toxicol Oncol* 2001; 20: 237-43.

Ribeiro DA, Cardoso CM, Yujra VQ, M DEBV, Aguiar O, Jr., Pisani LP, et al. Fluoride Induces Apoptosis in Mammalian Cells: In Vitro and In Vivo Studies. *Anticancer Res* 2017; 37: 4767-4777.

Santoyo-Sanchez MP, del Carmen Silva-Lucero M, Arreola-Mendoza L, Barbier OC. Effects of acute sodium fluoride exposure on kidney function, water homeostasis, and renal handling of calcium and inorganic phosphate. *Biol Trace Elem Res* 2013; 152: 367-72.

Saporita AJ, Chang HC, Winkeler CL, Apicelli AJ, Kladney RD, Wang J, et al. RNA helicase DDX5 is a p53-independent target of ARF that participates in ribosome biogenesis. *Cancer Res* 2011; 71: 6708-17.

Shanthakumari D, Srinivasalu S, Subramanian S. Effect of fluoride intoxication on lipidperoxidation and antioxidant status in experimental rats. *Toxicology* 2004; 204: 219-28.

Suarez P, Quintana MC, Hernandez L. Determination of bioavailable fluoride from sepiolite by "in vivo" digestibility assays. *Food Chem Toxicol* 2008; 46: 490-3.

---

Taniguchi T, Iizumi Y, Watanabe M, Masuda M, Morita M, Aono Y, et al. Resveratrol directly targets DDX5 resulting in suppression of the mTORC1 pathway in prostate cancer. *Cell Death Dis* 2016; 7: e2211.

UniProt C. UniProt: a worldwide hub of protein knowledge. *Nucleic Acids Res* 2019; 47: D506-D515.

Viteri, FE, Schneider RE, 1974. Gastrointestinal Alterations in Protein-Calorie Malnutrition. *Med Clin North Am* 58 (6), 1487–1505. doi:10.1016/s0025-7125(16)32085-5.

Wang C, Chen Z, Li S, Zhang Y, Jia S, Li J, et al. Hepatic overexpression of ATP synthase beta subunit activates PI3K/Akt pathway to ameliorate hyperglycemia of diabetic mice. *Diabetes* 2014; 63: 947-59.

Whitford GM. Acute and Chronic Fluoride Toxicity. *J Dent Res* 1992; 71: 1249-1254.

Whitford GM. The metabolism and toxicity of fluoride. *Monogr Oral Sci* 1996; 16 Rev 2: 1-153.

Whitford GM. Acute toxicity of ingested fluoride. *Monogr Oral Sci* 2011; 22: 66-80.

Whitford GM, Pashley DH. Fluoride absorption: the influence of gastric acidity. *Calcif Tissue Int* 1984; 36: 302-7.

Wong MC, Clarkson J, Glenny AM, Lo EC, Marinho VC, Tsang BW, et al. Cochrane reviews on the benefits/risks of fluoride toothpastes. *J Dent Res* 2011; 90: 573-9.

Yakabe K, Murakami A, Kajimura T, Nishimoto Y, Sueoka K, Sato S, et al. Functional significance of transgelin-2 in uterine cervical squamous cell carcinoma. *J Obstet Gynaecol Res* 2016; 42: 566-72.

Yan X, Yan X, Morrison A, Han T, Chen Q, Li J, et al. Fluoride induces apoptosis and alters collagen I expression in rat osteoblasts. *Toxicol Lett* 2011; 200: 133-8.

Yang L, Lin C, Liu ZR. P68 RNA helicase mediates PDGF-induced epithelial mesenchymal transition by displacing Axin from beta-catenin. *Cell* 2006; 127: 139-55.

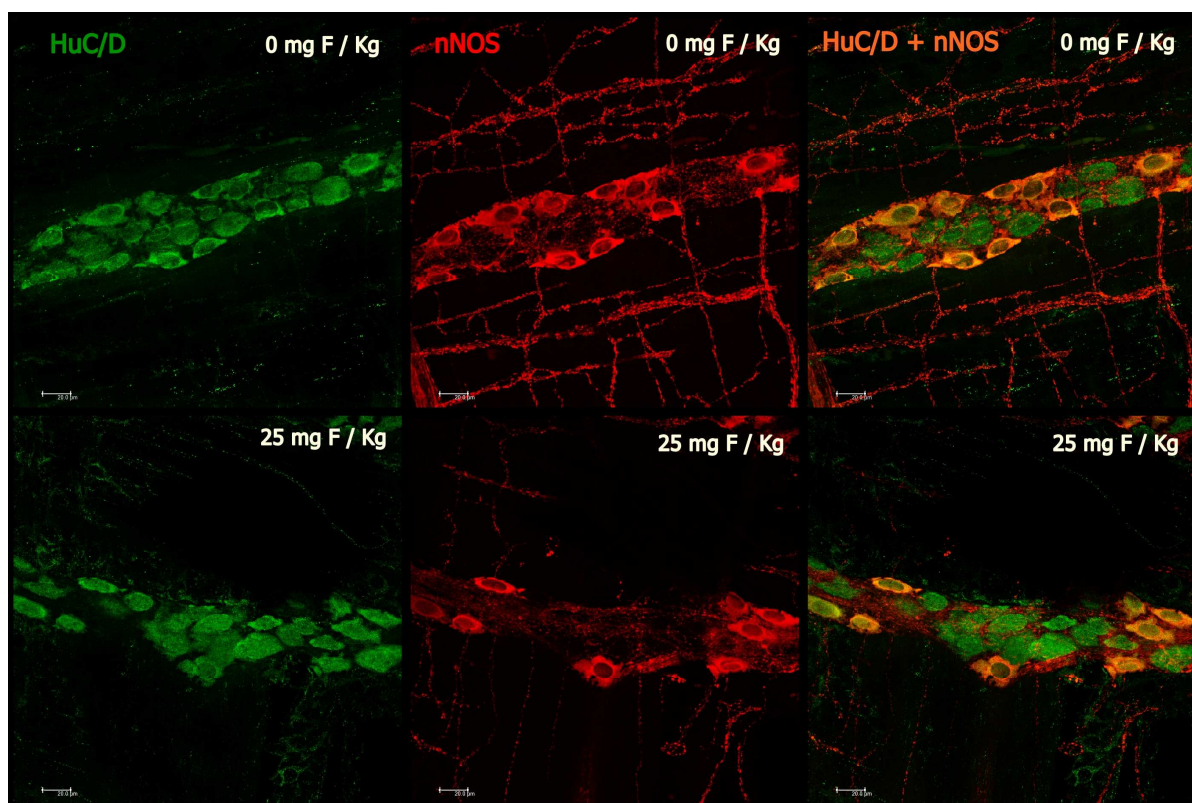
Zhou H, Zhang Y, Wu L, Xie W, Li L, Yuan Y, et al. Elevated transgelin/TNS1 expression is a potential biomarker in human colorectal cancer. *Oncotarget* 2018; 9: 1107-1113.

---

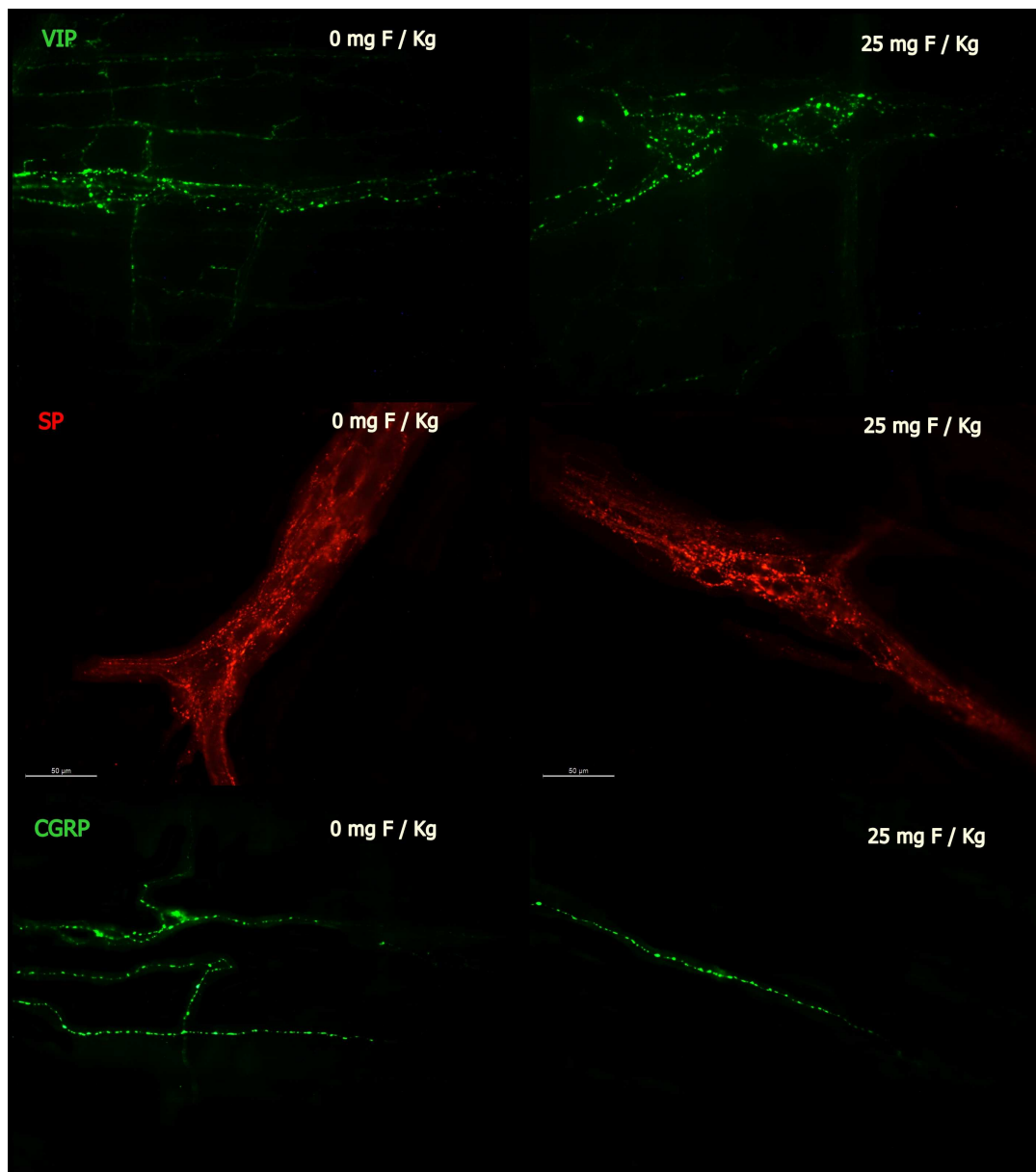
---



## SUPPLEMENTARY FIGURES AND TABLES

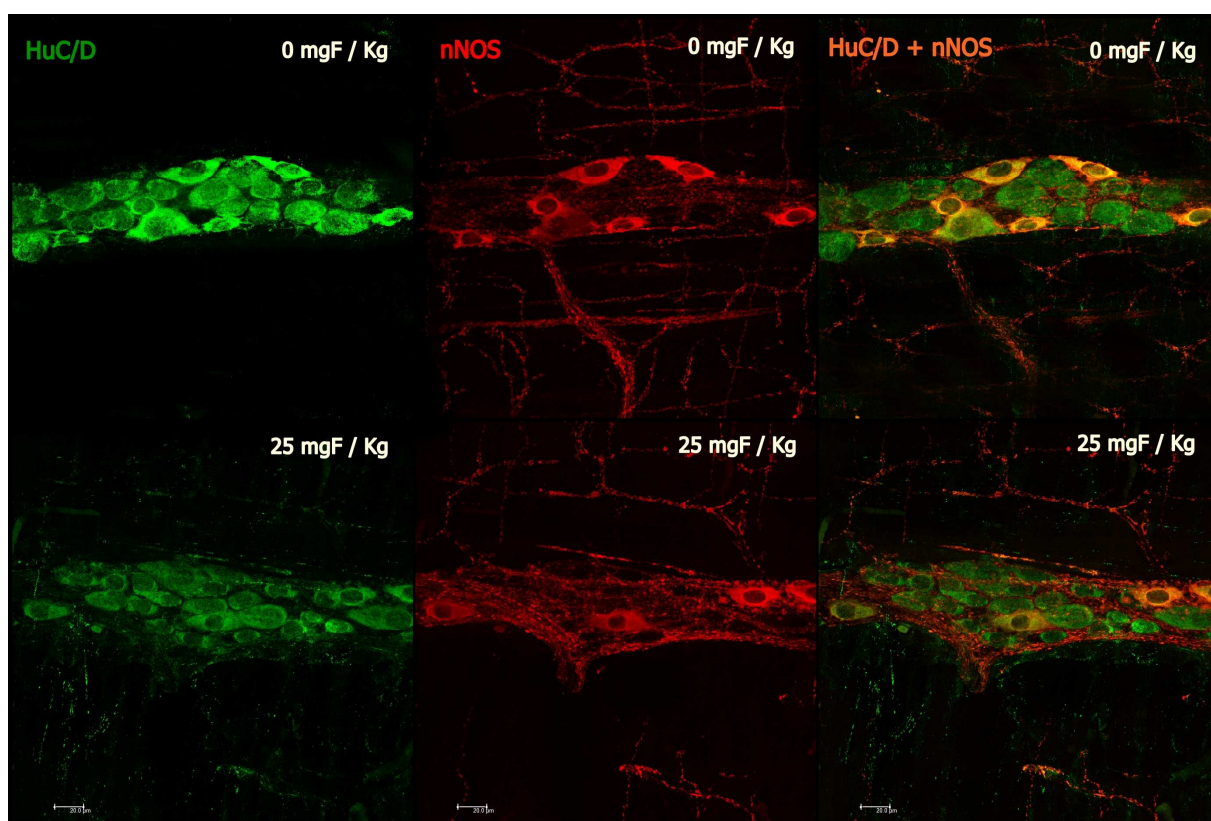


**Supplementary Figs. S1** - Photomicrography of myenteric neurons of the rats jejunum stained for HuC/D (green), nNOS (red), and double-labeling (HuC/D and nNOS) for the control group (0 mgF/L) and for the group treated with 25 mgF/Kg wb. 20X Objective.

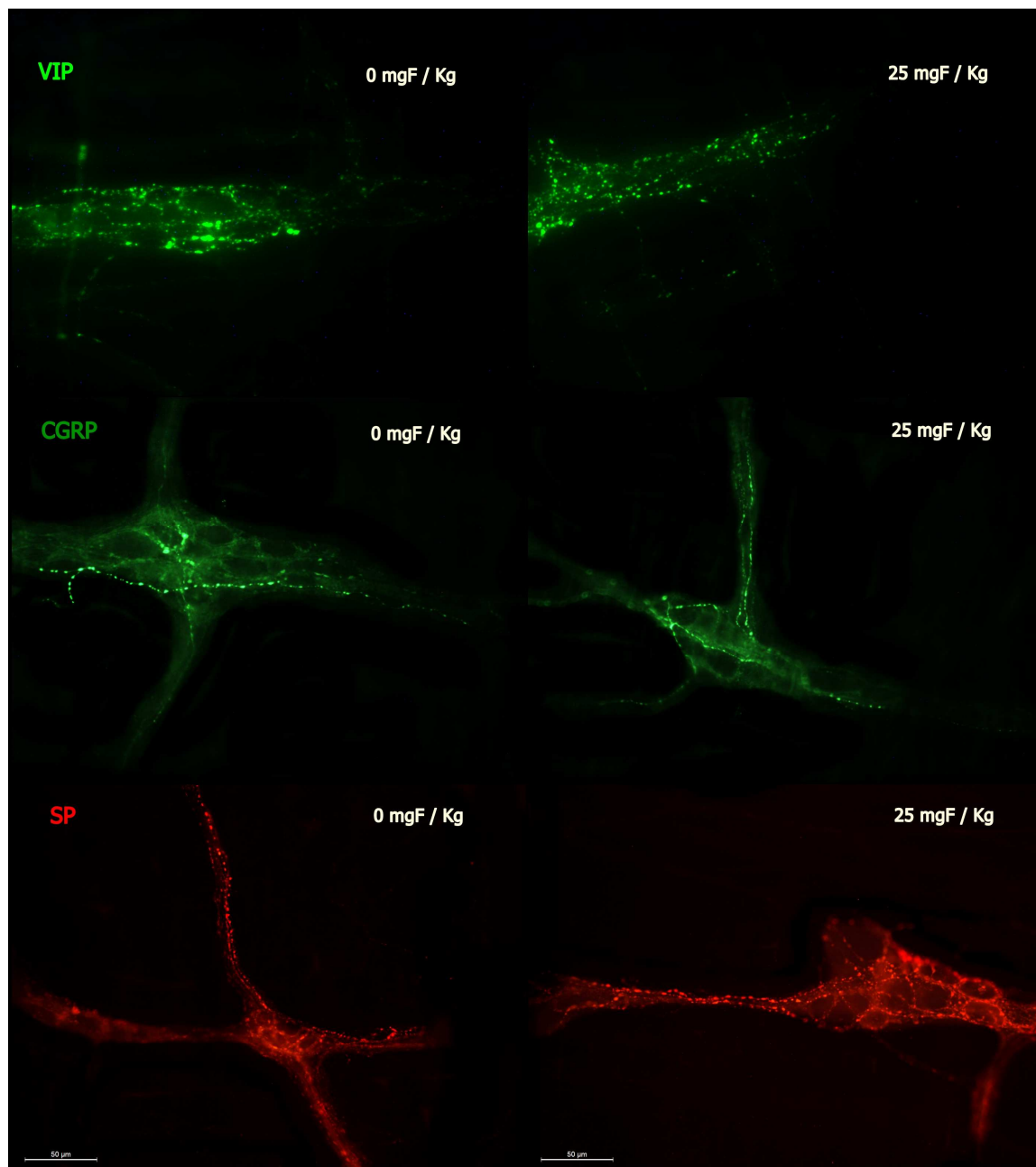


**Supplementary Figs. S2** - Photomicrography of myenteric varicosities of the rats jejunum after F acute exposure (25 mgF/Kg wb) for VIP-IR, SP-IR CGRP-IR. 40x Objective.

---



**Supplementary Figs. S3** - Photomicrography of myenteric neurons of the rats ileum stained for HuC/D (green), nNOS (red), and double-labeling (HuC/D and nNOS) for the control group (0 mgF/L) and for the group treated with 25 mgF/Kg wb. 20X Objective.



**Supplementary Figs. S4** - Photomicrography of myenteric varicosities of the rats ileum after F acute exposure (25 mgF/Kg wb) for VIP-IR, SP-IR CGRP-IR. 40x Objective.

**Table S1. Proteins with expression significantly altered in the jejunum of rats in the 25 mgF/Kg wb vs Control comparison.**

<sup>a</sup> Accession number	Protein name	PLGS Score	<sup>b</sup> Ratio 25 mgF/Kg:Control
D3ZNZ9	Histone H2B	1399	3.71
O88752	Epsilon 1 globin	557	2.83
P11517	Hemoglobin subunit beta-2	482	2.83
P02091	Hemoglobin subunit beta-1	851	2.64
P01946	Hemoglobin subunit alpha-1/2	295	2.14
D3ZVK7	Histone H2A	549	1.84
P02770	Serum albumin	186	1.21
P48675	Desmin	477	1.17
C0JPT7	Filamin alpha	83	1.17
Q9JLT0	Myosin-10	63	1.16
D3ZRN3	Protein Actb12	1615	1.08
P68035	Actin, alpha cardiac muscle 1	3780	1.07
P68136	Actin, alpha skeletal muscle	3190	1.07
P63269	Actin, gamma-enteric smooth muscle	3726	1.07
P34058	Heat shock protein HSP 90-beta	685	0.84
P62804	Histone H4	1079	0.83
P02262	Histone H2A type 1	549	0.80
P00406	Cytochrome c oxidase subunit 2	114	0.80
F1M2N4	Uncharacterized protein	275	0.80
P0CC09	Histone H2A type 2-A	549	0.79
A9UMV8	Histone H2A.J	549	0.79
D4A2K1	Protein Hoga1	134	0.79
G3V6D3	ATP synthase subunit beta	837	0.78
P10719	ATP synthase subunit beta, mitochondrial	837	0.76
Q9ESV6	Glyceraldehyde-3-phosphate dehydrogenase, testis-specific	308	0.76
P04797	Glyceraldehyde-3-phosphate dehydrogenase	433	0.75
Q6AYZ1	Tubulin alpha-1C chain	151	0.70
F1LP05	ATP synthase subunit alpha	286	0.70
P15999	ATP synthase subunit alpha, mitochondrial	286	0.69
P04642	L-lactate dehydrogenase A chain	450	0.64
Q10758	Keratin, type II cytoskeletal 8	762	0.63
P68370	Tubulin alpha-1A chain	151	0.59
Q6P9V9	Tubulin alpha-1B chain	151	0.59
Q8CJD3	Zymogen granule membrane protein 16	473	0.55
P04636	Malate dehydrogenase, mitochondrial	692	0.53
D4AAJ3	40S ribosomal protein S12	236	0.52
P05197	Elongation factor 2	94	0.40
Q9JLH5	CDK5 regulatory subunit-associated protein 2	81	25 mgF/Kg*
M0RC65	Cofilin 2, muscle (Predicted), isoform CRA_b	68	25 mgF/Kg
Q9Z1T4	Connector enhancer of kinase suppressor of ras 2	124	25 mgF/Kg
Q9QXU8	Cytoplasmic dynein 1 light intermediate chain 1	118	25 mgF/Kg
Q5FVP8	Diacylglycerol O-acyltransferase 2	69	25 mgF/Kg
B1H278	E3 ubiquitin-protein ligase TRIM11	25	25 mgF/Kg
Q9JMA8	Exostosins (Multiple)-like 3, isoform CRA_a	69	25 mgF/Kg
G3V9H9	Glycoprotein 5, platelet	112	25 mgF/Kg

Q8K586	GTP-binding nuclear protein Ran, testis-specific isoform	39	25 mgF/Kg
P20059	Hemopexin	41	25 mgF/Kg
P20760	Ig gamma-2A chain C region	107	25 mgF/Kg
P51886	Lumican	34	25 mgF/Kg
G3V6P7	Myosin, heavy polypeptide 9, non-muscle	83	25 mgF/Kg
Q62812	Myosin-9	83	25 mgF/Kg
Q6AY91	Nicotinamide riboside kinase 1	62	25 mgF/Kg
O08662	Phosphatidylinositol 4-kinase alpha	48	25 mgF/Kg
O08770	Platelet glycoprotein V	112	25 mgF/Kg
Q4V7D0	Polymerase (DNA-directed), delta 3, accessory subunit	111	25 mgF/Kg
D4A9W0	Protein Aim2	118	25 mgF/Kg
D3ZI35	Protein Cep135	31	25 mgF/Kg
F1M748	Protein Col24a1	19	25 mgF/Kg
D3ZPD6	Protein Fezf1	55	25 mgF/Kg
D4AA82	Protein Gpr179	52	25 mgF/Kg
M0R3V4	Protein Mydgf	260	25 mgF/Kg
D3ZJ56	Protein Gbp3	29	25 mgF/Kg
D3ZPF2	Protein Mcat	77	25 mgF/Kg
D4A913	Protein Med26	39	25 mgF/Kg
D3ZSU4	Protein Ms4a15	208	25 mgF/Kg
D3ZT79	Protein N4bp1	150	25 mgF/Kg
D3ZUN5	Protein O-fucosyltransferase 2 (Predicted), isoform CRA_a	79	25 mgF/Kg
D3ZZ81	Protein Ppfia1	59	25 mgF/Kg
D3ZVN9	Protein Rasgef1c	21	25 mgF/Kg
G3V970	Protein Six1	47	25 mgF/Kg
D3ZNC4	Protein Tcte3	253	25 mgF/Kg
D3Z9I0	Protein Tmem145	96	25 mgF/Kg
D3ZRN5	Protein Trove2	80	25 mgF/Kg
D3ZMN0	Protein Tsga13	47	25 mgF/Kg
P50399	Rab GDP dissociation inhibitor beta	94	25 mgF/Kg
P13668	Stathmin	92	25 mgF/Kg
P48721	Stress-70 protein, mitochondrial	73	25 mgF/Kg
P10960	Sulfated glycoprotein 1	70	25 mgF/Kg
F7EPE0	Sulfated glycoprotein 1	70	25 mgF/Kg
Q67ET3	Taste receptor type 2 member 120	138	25 mgF/Kg
P31232	Transgelin	205	25 mgF/Kg
Q5XFX0	Transgelin-2	509	25 mgF/Kg
Q5XIF6	Tubulin alpha-4A chain	44	25 mgF/Kg
P36511	UDP-glucuronosyltransferase 2B15	90	25 mgF/Kg
F1LN61	Uncharacterized protein	86	25 mgF/Kg
Q5RKI0	WD repeat-containing protein 1	35	25 mgF/Kg
Q63347	26S protease regulatory subunit 7	58	Control
P62198	26S protease regulatory subunit 8	53	Control
B2GV73	Actin-related protein 2/3 complex subunit 3	123	Control
Q5XIL7	Activating transcription factor 7 interacting protein 2	54	Control
P38918	Aflatoxin B1 aldehyde reductase member 3	98	Control
O35817	A-kinase anchor protein 14	54	Control
G3V9G3	Calcium/calmodulin-dependent protein kinase II, beta, isoform CRA_a	75	Control
P11275	Calcium/calmodulin-dependent protein kinase type II subunit alpha	75	Control

P08413	Calcium/calmodulin-dependent P06685protein kinase type II subunit beta	75	Control
P15791	Calcium/calmodulin-dependent protein kinase type II subunit delta	75	Control
P11730	Calcium/calmodulin-dependent protein kinase type II subunit gamma	75	Control
D3Z8E6	Calmodulin-regulated spectrin-associated protein 1	63	Control
O70177	Carboxylesterase	164	Control
G3V7J5	Carboxylesterase 5, isoform CRA_a	110	Control
M0R9W7	Carboxylic ester hydrolase	130	Control
B2RZ86	Coiled-coil domain-containing protein 89	46	Control
D3ZD09	Cytochrome c oxidase subunit 6B1	405	Control
Q6YFQ1	Cytochrome c oxidase subunit 6B2	228	Control
G3V861	Cytochrome P450, family 26, subfamily A, polypeptide 1	76	Control
Q6AYI1	DEAD (Asp-Glu-Ala-Asp) box polypeptide 5	61	Control
Q62651	Delta(3,5)-Delta(2,4)-dienoyl-CoA isomerase, mitochondrial	170	Control
D3ZCM4	DnaJ (Hsp40) homolog, subfamily C, member 15 (Predicted), isoform CRA_a	96	Control
Q8CH84	ELAV-like protein 2	93	Control
O09032	ELAV-like protein 4	93	Control
P09759	Ephrin type-B receptor 1	65	Control
O88753	Epsilon 2 globin	110	Control
D4AD21	Exonuclease 3'-5' domain-like 1 (Predicted)	65	Control
Q66HT1	Fructose-bisphosphate aldolase	149	Control
P00884	Fructose-bisphosphate aldolase B	149	Control
P39948	G1/S-specific cyclin-D1	85	Control
Q9Z144	Galectin-2	269	Control
Q5PPN0	Hairy and enhancer of split 6 (Drosophila)	112	Control
G3V7G6	Heat shock 27kDa protein 3	89	Control
Q9QZ58	Heat shock protein beta-3	89	Control
P53565	Homeobox protein cut-like 1	83	Control
D1M8S3	Interleukin 1 receptor accessory protein b	111	Control
Q63621	Interleukin-1 receptor accessory protein	111	Control
Q61FV4	Keratin, type I cytoskeletal 13	82	Control
Q61FV1	Keratin, type I cytoskeletal 14	78	Control
Q61FV3	Keratin, type I cytoskeletal 15	96	Control
Q61FU8	Keratin, type I cytoskeletal 17	83	Control
D3Z7Y6	Keratin, type I cytoskeletal 20	93	Control
Q5PQM2	Kinesin light chain 4	51	Control
Q2PQA9	Kinesin-1 heavy chain	71	Control
G3V8L3	Lamin A, isoform CRA_b	105	Control
O55162	Ly6/PLAUR domain-containing protein 3	96	Control
O88989	Malate dehydrogenase, cytoplasmic	134	Control
D3ZU82	Membrane frizzled-related protein (Predicted)	84	Control
Q6AXU8	Methyltransferase-like protein 6	67	Control
D4A1W8	Microsomal triglyceride transfer protein	75	Control
B5DF07	Mitochondrial ribonuclease P protein 3	47	Control
B1WC37	Mitochondrial tRNA-specific 2-thiouridylase 1	88	Control
P16409	Myosin light chain 3	190	Control
P04466	Myosin regulatory light chain 2, skeletal muscle isoform	90	Control
Q561S0	NADH dehydrogenase [ubiquinone] 1 alpha subcomplex subunit 10, mitochondrial	108	Control

D4ADM1	Olfactory receptor	133	Control
A1BPI0	Ornithine decarboxylase antizyme 3	316	Control
Q63716	Peroxiredoxin-1	135	Control
P16036	Phosphate carrier protein, mitochondrial	129	Control
P48679	Prelamin-A/C	105	Control
Q4KM35	Proteasome subunit beta type-10	115	Control
D3ZIF1	Protein Agr3	55	Control
F1M0U1	Protein Ccdc73	72	Control
F7F3M3	Protein Ces2a	110	Control
G3V9D8	Protein Ces2c	164	Control
D3ZXQ0	Protein Ces2g	130	Control
E9PT29	Protein Ddx17	67	Control
P11598	Protein disulfide-isomerase A3	160	Control
Q68FV5	Protein FAM71F1	79	Control
D3ZW92	Protein Fam78a	357	Control
D3ZLD5	Protein Golga3	36	Control
Q6AXZ7	Protein Hormad2	45	Control
G3V6Z0	Protein Hoxa11	68	Control
D4ACC2	Protein Kank2	60	Control
D4AC62	Protein Krt222	76	Control
D4A9I7	Protein Lrrc3b	123	Control
D4A1H7	Protein Mul1	84	Control
Q6MG75	Protein Nelfe	105	Control
Q9JKS6	Protein piccolo	113	Control
D3ZZL1	Protein Rad52	130	Control
D3ZCX6	Protein Rexo1	48	Control
D3ZBQ5	Protein Scarf2	54	Control
F1M155	Protein Svit	58	Control
Q6AXR1	Protein Tbc1d20	78	Control
Q9WVJ6	Protein Tgm2	54	Control
D4AC93	Protein Tmem223	82	Control
B5DFA0	Protein Vil1	133	Control
D4A7Z0	Protein Wdtdc1	66	Control
D3ZJ04	Protein Zfp322a	57	Control
M0RD14	Pyruvate kinase	142	Control
P11980	Pyruvate kinase PKM	142	Control
P70564	Serpin B5	79	Control
P06685	Sodium/potassium-transporting ATPase subunit alpha-1	93	Control
P06686	Sodium/potassium-transporting ATPase subunit alpha-2	54	Control
P06687	Sodium/potassium-transporting ATPase subunit alpha-3	60	Control
P57769	Sorting nexin-16	35	Control
P46462	Transitional endoplasmic reticulum ATPase	74	Control
Q03191	Trefoil factor 3	520	Control
Q6AY56	Tubulin alpha-8 chain	35	Control
B2RYI0	WD repeat-containing protein 91	71	Control

<sup>a</sup>Identification is based on proteins ID from UniProt protein database, reviewed only (<http://www.uniprot.org/>).

<sup>b</sup>Proteins with expression significantly altered are organized according to the ratio.

\*Indicates unique proteins in alphabetical order.



**Table S2. Proteins with expression significantly altered in the ileum of rats in the 25 mgF/Kg wb vs Control comparison.**

<sup>a</sup> Accession number	Protein name	PLGS Score	<sup>b</sup> Ratio 25 mgF/Kg:Control
P01946	Hemoglobin subunit alpha-1/2	392	1.90
P14650	Thyroid peroxidase	46	1.79
F1LN48	Thyroid peroxidase	52	1.70
P02091	Hemoglobin subunit beta-1	1007	1.35
O88752	Epsilon 1 globin	500	1.30
P11517	Hemoglobin subunit beta-2	500	1.30
P58775	Tropomyosin beta chain	266	1.30
F7FK40	Tropomyosin 1, alpha, isoform CRA_c	315	1.28
Q91XN6	Tropomyosin 1, alpha, isoform CRA_h	266	1.28
Q64119	Myosin light polypeptide 6	748	1.28
P04692	Tropomyosin alpha-1 chain	266	1.27
Q6AZ25	Tropomyosin 1, alpha	186	1.25
P48675	Desmin	349	1.22
D3ZRN3	Protein Actb12	733	1.15
M0RDM4	Histone H2A	552	0.89
Q63279	Keratin, type I cytoskeletal 19	173	0.89
P0CC09	Histone H2A type 2-A	552	0.88
Q6IFV1	Keratin, type I cytoskeletal 14	97	0.84
P62630	Elongation factor 1-alpha 1	186	0.83
P62632	Elongation factor 1-alpha 2	186	0.82
F1M6C2	Protein LOC103691939	186	0.82
M0R757	Elongation factor 1-alpha	186	0.81
P62804	Histone H4	2758	0.80
Q6IFU8	Keratin, type I cytoskeletal 17	85	0.75
P02770	Serum albumin	200	0.73
Q6IFV3	Keratin, type I cytoskeletal 15	162	0.73
P80020	Gastrotropin	829	0.72
Q6IFU7	Keratin, type I cytoskeletal 42	85	0.70
Q3KRE8	Tubulin beta-2B chain	173	0.65
Q6IFW5	Keratin, type I cytoskeletal 12	137	0.63
P85108	Tubulin beta-2A chain	173	0.63
Q4QRB4	Tubulin beta-3 chain	118	0.62
P69897	Tubulin beta-5 chain	173	0.61
E9PSN4	Protein Zc3h13	162	0.49
D3ZWE0	Histone H2A	497	0.44
P85972	Vinculin	48	0.42
P63102	14-3-3 protein zeta/delta	137	25 mgF/Kg*
G3V8A4	5-methyltetrahydrofolate-homocysteine methyltransferase, isoform CRA_b	69	25 mgF/Kg
Q05962	ADP/ATP translocase 1	43	25 mgF/Kg
Q09073	ADP/ATP translocase 2	49	25 mgF/Kg
P62161	Calmodulin	122	25 mgF/Kg
Q6MG22	Diffuse panbronchiolitis critical region protein 1 homolog	95	25 mgF/Kg
Q6AYU3	DnaJ homolog subfamily B member 6	64	25 mgF/Kg
B0BNA8	Docking protein 4	62	25 mgF/Kg
Q5RKG9	Eukaryotic translation initiation factor 4B	39	25 mgF/Kg

P47819	Glial fibrillary acidic protein	62	25 mgF/Kg
M0R4T9	Histone acetyltransferase	65	25 mgF/Kg
Q6IFW6	Keratin, type I cytoskeletal 10	117	25 mgF/Kg
Q6IFX1	Keratin, type I cytoskeletal 24	103	25 mgF/Kg
Q6IFW2	Keratin, type I cytoskeletal 40	103	25 mgF/Kg
Q6IG05	Keratin, type II cytoskeletal 75	41	25 mgF/Kg
Q5XI07	Lipoma-preferred partner homolog	76	25 mgF/Kg
F1LSJ6	Methionine sulfoxide reductase A	75	25 mgF/Kg
Q9Z2Q4	Methionine synthase	69	25 mgF/Kg
Q923M1	Mitochondrial peptide methionine sulfoxide reductase	75	25 mgF/Kg
Q5BK65	Negative regulator of reactive oxygen species	113	25 mgF/Kg
P09057	Ornithine decarboxylase	48	25 mgF/Kg
Q811R2	Peroxisome proliferator-activated receptor gamma coactivator 1-beta	51	25 mgF/Kg
Q64649	Phosphorylase b kinase regulatory subunit alpha, skeletal muscle isoform	52	25 mgF/Kg
D3ZGW2	Protein Ap1g2	72	25 mgF/Kg
F7FKK4	Protein Atxn7l2	41	25 mgF/Kg
D3ZJ52	Protein Fancm	88	25 mgF/Kg
D3ZT78	Protein Gm8225	99	25 mgF/Kg
D4A2F0	Protein Gnb1l	78	25 mgF/Kg
D3ZD85	Protein Kat6b	57	25 mgF/Kg
F1MAS0	Protein Krt32	103	25 mgF/Kg
F1MAF7	Protein Krt33b	113	25 mgF/Kg
Q6IFV6	Protein Krt35	103	25 mgF/Kg
Q6IFV5	Protein Krt36	113	25 mgF/Kg
F1M340	Protein LOC102557302	114	25 mgF/Kg
D3ZBD0	Protein Msl1	55	25 mgF/Kg
M0R5K7	Protein Pradc1	133	25 mgF/Kg
Q66HG8	Protein Red	44	25 mgF/Kg
D3ZB81	Protein Slc25a31	61	25 mgF/Kg
M0R887	Protein Stap2	72	25 mgF/Kg
F1M155	Protein Svll	132	25 mgF/Kg
F1LZT3	Protein Tbat	64	25 mgF/Kg
D4A3Z3	Protein Tbc1d24	53	25 mgF/Kg
Q3ZB99	Protein Tjp2	44	25 mgF/Kg
D3Z9B6	Protein Tmem200b	68	25 mgF/Kg
Q304F3	Protein Tnnc2	122	25 mgF/Kg
D3ZYY9	Protein Usp53	46	25 mgF/Kg
D3Z8E0	Ribosomal protein S6 kinase	50	25 mgF/Kg
A1A5P2	Ribosome biogenesis regulatory protein homolog	88	25 mgF/Kg
D3ZDL1	Sulfotransferase	80	25 mgF/Kg
Q5I0H4	Transmembrane and coiled-coil domains protein 1	98	25 mgF/Kg
Q68FR8	Tubulin alpha-3 chain	49	25 mgF/Kg
Q5XIF6	Tubulin alpha-4A chain	49	25 mgF/Kg
Q5FWT7	Ubiquitin-like domain-containing CTD phosphatase 1	56	25 mgF/Kg
P68255	14-3-3 protein theta	186	Control
D3ZVD3	5'-nucleotidase, cytosolic 1A (Predicted)	97	Control
O35167	Acetylcholinesterase collagenic tail peptide	55	Control

F1M6X2	Acetylcholinesterase collagenic tail peptide	55	Control
P11884	Aldehyde dehydrogenase, mitochondrial	67	Control
Q99JB3	Alpha-(1,3)-fucosyltransferase 9	47	Control
Q9Z1P2	Alpha-actinin-1	54	Control
Q9QXQ0	Alpha-actinin-4	59	Control
Q3KRE0	ATPase family AAA domain-containing protein 3	59	Control
P54258	Atrophin-1	75	Control
O88751	Calcium-binding protein 1	78	Control
Q5U2W3	Carboxypeptidase A5	58	Control
Q7M0E3	Destrin	157	Control
Q6AYE2	Endophilin-B1	61	Control
Q1JU68	Eukaryotic translation initiation factor 3 subunit A	48	Control
Q6MG20	General transcription factor II H, polypeptide 4	88	Control
P04797	Glyceraldehyde-3-phosphate dehydrogenase	221	Control
Q9ESV6	Glyceraldehyde-3-phosphate dehydrogenase, testis-specific	157	Control
D4A4S3	Heat shock cognate 71 kDa protein	140	Control
Q6URK4	Heterogeneous nuclear ribonucleoprotein A3	87	Control
D3ZJ08	Histone H3	366	Control
Q6LED0	Histone H3.1	366	Control
P84245	Histone H3.3	366	Control
D3ZP06	Integrin beta	59	Control
P25030	Keratin, type I cytoskeletal 20	85	Control
P04642	L-lactate dehydrogenase A chain	123	Control
Q6QI82	LRRGT00126	96	Control
Q6QI43	LRRGT00165	120	Control
Q6QI33	LRRGT00175	69	Control
O88989	Malate dehydrogenase, cytoplasmic	152	Control
Q66H84	MAP kinase-activated protein kinase 3	76	Control
P00770	Mast cell protease 2	316	Control
Q9R1J4	Myocilin	58	Control
Q9ERC0	Neuropeptide Y/peptide YY-Y2 receptor	128	Control
Q9EPI6	NMDA receptor synaptonuclear signaling and neuronal migration factor	95	Control
O54728	Phospholipase B1, membrane-associated	51	Control
F1LWB9	Protein Ankrd50	64	Control
D4A8N1	Protein Dpm1	70	Control
D3ZM69	Protein Epb41I2	50	Control
D3ZR63	Protein Gfod1	58	Control
Q62669	Protein Hbb-b1	111	Control
F1M4Q3	Protein Hmcn1	16	Control
Q6IFV0	Protein Ka11	117	Control
Q6IFU9	Protein Krt16	162	Control
D4AC62	Protein Krt222	85	Control
D4AEC9	Protein LOC100360330	58	Control
P20650	Protein phosphatase 1A	74	Control
D3ZNR0	Protein RGD1560927	165	Control
D4A4R7	Protein Serpina1f	79	Control

D3ZTT7	Protein Sun2	70	Control
D3ZLU5	Protein Tspyl5	155	Control
M0R8B6	Protein Tubb1	47	Control
E9PTE4	Protein Vom2r-ps125	53	Control
D3ZXJ3	Protein Zfp78	68	Control
P11345	RAF proto-oncogene serine/threonine-protein kinase	91	Control
Q5XFX0	Transgelin-2	101	Control
P48500	Triosephosphate isomerase	115	Control
A8WCF8	Tumor protein p63-regulated gene 1-like protein	82	Control
B5DEI4	Ubiquitin-conjugating enzyme E2 W	166	Control

---

<sup>a</sup>Identification is based on proteins ID from UniProt protein database, reviewed only (<http://www.uniprot.org/>).

<sup>b</sup>Proteins with expression significantly altered are organized according to the ratio.

\*Indicates unique proteins in alphabetical order.

---

## **3 DISCUSSION**

---



### 3 DISCUSSION

The doses of F administered chronically administered in the present study (10 mg/L and 50mg/L) are frequently employed in works of our research group (ARAUJO *et al.*, 2019; CARVALHO *et al.*, 2013; DIONIZIO *et al.*, 2019; LEITE ADE *et al.*, 2007; MELO *et al.*, 2017; PEREIRA *et al.*, 2018; PEREIRA *et al.*, 2016), since led to plasma F levels in rats corresponding to those found in humans drinking water containing 2 mgF/L and 10 mgF/L (levels associated with dental and skeletal fluorosis, respectively). This is due to the fact that rodents metabolize F 5 times faster than humans (DUNIPACE *et al.*, 1995). The World Health Organization has established 1.5 mgF/L as a safe limit in drinking water, with the average daily intake of F not exceeding 2 mg/day. However, in some regions of the world, in which there is already a high concentration of F naturally, due to the presence of this element in the groundwater from which the supply water is taken, it is estimated that the intake of F in some areas may reach up to 27 mg/day (DEY *et al.*, 2011). Besides some regions of Brazil, high concentrations of F can also be found in other areas of the world, as in the case of India (HUSSAIN; HUSSAIN; SHARMA, 2010). Therefore, the doses employed here mimic those consumed by humans in areas of endemic dental and skeletal fluorosis.

As for the study involving acute exposure to F, the dose employed (25 mgF/Kg body weight) corresponds to the probable toxic dose (PDT) for humans (5 mg/Kg body weight). The PDT is the “*minimum dose that could cause serious or life-threatening systemic signs and symptoms and that should trigger immediate therapeutic intervention and hospitalization*” (WHITFORD, 2011).

Considering that F is mainly absorbed by GIT, with roughly 70-75% of ingested F being absorbed in the small intestine (NOPAKUN; MESSER, 1990; NOPAKUN; MESSER; VOLLER, 1989), the intestinal cells are exposed to higher levels of F than the cells located in other organs/systems, which is in-line with the gastrointestinal symptoms (abdominal pain, nausea, vomiting and diarrhea) commonly reported in cases of excessive exposure to this ion (WHITFORD, 2011). Nonetheless, morphologic and proteomic F-induced are only scarcely reported in the literature. Recently, our research group employed morphological and proteomics approaches to assess the changes in the duodenum of rats after chronic (MELO *et al.*, 2017) and acute (MELO, 2015) F exposure.

---

Regarding the duodenum of chronically F treated animals: the group treated with 50 mgF/L had a significant decrease in the density of nNOS-IR neurons. In addition, significant morphological changes were observed in the HUC/D-IR and nNOS-IR neurons, as well as in the VIP-IR, CGRP-IR and SP-IR varicosities for the groups treated with 10 and 50 mgF/L. Profound proteomic changes were observed in the both F-treated groups. In the group treated with the lowest concentration of F, most of the proteins with altered expression were increased, while the largest F concentration mostly lead to downregulated proteins. Many altered proteins were correlated with the neurotransmission process, essential for the function of the GIT through the control of the ENS. In addition, the protein polymerization process was one of the most affected biological processes, which helps to explain the negative regulation of many proteins after exposure to 50 mgF/L. As for acute exposure to F, the most affected biological process in the duodenum of rats was “generation of precursor metabolites and energy”, in addition to the considerable histological and immunohistochemical changes found.

Knowing that the different segments of the small intestine (duodenum, jejunum and ileum) have different anatomical, histological, physiological and functional characteristics (GUYTON; HALL, 2015), this study evaluated proteomic changes in the jejunum and ileum segments of rats treated with chronic and/or acute doses of F, in order to correlate with the morphological and histological changes found in the study by our group (MELO, 2015). With this rationale in mind, the present thesis comprises three articles, divided as follows: 1) proteomic analysis of the jejunum of rats treated with chronic doses of F; 2) proteomic analysis of the ileum of rats treated with chronic doses of F and 3) proteomic analysis of the jejunum and ileum of animals treated with acute dose of F. The morphological analysis conducted in all these experiments in a previous thesis by our group (MELO, 2015) was included in each of these 3 articles, in order to, together with the proteomic analyses, provide insights on the mechanisms involved in the F toxicity.

The data taken together show that, regardless of the segment analyzed in the chronic treatment with both concentrations of F in the water, mostly an increase in the expression of proteins was observed in the presence of F, which might indicate an attempt of the body to fight F toxicity (Tables S1-S5 article 1; S1-S2 article 2). However, when F was administered in acute manner, there was a great reduction in protein

---



expression in comparison to the control groups (Tables S1-S2 article 3). This finding suggests an inhibition of protein synthesis by exposure to the acute dose of F.

Our proteomic data related to the chronic treatment with F, regardless of the intestinal segment, show a great impairment of biological processes such as energy metabolism, cellular respiration, NAD metabolic process, oxygen transport, in addition to pathways induced by oxidative stress, protein synthesis, involvement with the neural part, response to pain and injury, muscle and cytoskeleton changes (Article 1-2). This shows that intoxication cause by a non-lethal amount of F administered for a prolonged time affects the jejunum and ileum more broadly, altering distinct biological processes. These alterations suggest an attempt of the organism to combat this toxicity, which is in-line with studies conducted in other organs/organelles, such as liver (DIONIZIO *et al.*, 2019; PEREIRA *et al.*, 2018) and liver mitochondria (ARAUJO *et al.*, 2019).

As can be denoted from the analysis of the interaction networks, in the jejunum most of the proteins with altered expression in our study interact with proteins such as *GLUT4* and *Polyubiquitin-C* (Fig.5-6 article 1), and in the ileum with *5'-AMP-activated protein kinase catalytic subunit alpha-1*; *5'-AMP-activated protein kinase subunit beta-1* and *GLUT4* (Fig.1-2 article 2). *GLUT4* is a glucose transporter, which plays a key role in removing glucose from the circulation (UNIPROT, 2019). In the jejunum, several proteins related to energy metabolism interacted with it *GLUT4* such as *L-lactate dehydrogenase A chain (LDH)* (upregulated 10 mgF/L- Fig.5 and table S4 article 1); *malate dehydrogenase, mitochondrial* (downregulated 10 mgF/L- Fig.5 and table S4 article 1); *isoform 1 of cytochrome c oxidase 4* (only control group Fig 5. Table S1 article1) and *the mitochondrial and NADH dehydrogenase [ubiquinone] flavoprotein 2, mitochondrial* (only control group Fig.5 table S1 article 1). In addition, in the group treated with 50 mgF/L, the following alterations were found: *Malate dehydrogenase, mitochondrial* (downregulated 50 mgF/L Fig.6 Table S5 article 1); *Malate dehydrogenase, cytoplasmic* (only control group Fig 6. Table S1 article1); *NADH dehydrogenase [ubiquinone] flavoprotein 2, mitochondrial* (only control group Fig.5 table S1 article1); *ATP synthase beta, mitochondrial subunit* (downregulated 50 mgF/L Fig.6 table S5 article 1) and *L-lactate dehydrogenase A (LDH)* (upregulated 50 mgF/L Fig.6 table S5 article 1). It is also important to highlight some isoforms of *Rab proteins* such as *Rab 10* and *Rab 14*, which are necessary in the translocation of *GLUT4* to the plasma membrane, making it easier glucose absorption, as well as *Rab 3A*, which is involved in insulin release (BREWER *et al.*, 2016; LOBO *et al.*, 2015; SANO *et al.*,

---

2007). These three isoforms, in the jejunum, were only found in the group treated with 10 mgF/L (Table S2 article 1). This is in-line with previous studies from our group. In one of them, in which with rats with streptozotocin-induced diabetes were exposed to 10 mgF/L, increased insulin sensitivity was reported (LOBO *et al.*, 2015). In another one conducted with non-obese diabetic (NOD) that spontaneously develop type 1 diabetes along time, exposure to water containing 10 mgF/L reduced glycemia (MALVEZZI *et al.*, 2019), which might also be related to our current findings involving the *Rab* proteins. In the Malvezzi *et al.* study (MALVEZZI *et al.*, 2019), an increase in antioxidant proteins in the liver upon exposure to F was possibly related to the anti-diabetic effects of F, since oxidative damage in the pancreatic islets is associated with the onset of diabetes (BOGDANI *et al.*, 2013), but this needs to be better addressed in future studies. In the present study, *peroxiredoxin-6* was upregulated in the jejunum in the group treated with 50 mgF/L (table S5; article 1). This protein helps to protect the body against oxidative stress (HOFMANN; HECHT; FLOHE, 2002). It is well known in the literature that F provokes oxidative stress (DIONIZIO *et al.*, 2019; PEREIRA *et al.*, 2016). Moreover, in the gastrocnemius muscle of mice treated with 10 mg/L and 50 mgF/L, and in the liver of mice treated with 10 mgF/L, increased expression in proteins involved in the energy metabolism was found, which can be related to the lower plasma glucose levels found (MALVEZZI *et al.*, 2019). Regarding alterations in proteins involved in energy metabolism, it is believed that an increase in *LDH* (increased in the jejunum upon exposure to both F doses), which is an enzyme responsible for converting pyruvate into lactate with regeneration of NADH into NAD<sup>+</sup>, may be an alternative way for the body to provide the lack of oxygen for aerobic oxidation of pyruvate and NADH produced in glycolysis (LEHNINGER; NELSON; COX, 2002). Increased *LDH* activity in the serum of infants who consumed water containing more than 2 mg/L was already reported (XIONG *et al.*, 2007), in-line with our findings. This increase in LDH is a response of the organism upon decrease in enzymes related to oxidative phosphorylation and proteins belonging to the Krebs' cycle that are largely affected by F (ARAUJO *et al.*, 2019). However, the rate of ATP production through anaerobic pathways is much lower than that of aerobic pathways, in-line with reports of reduced ATP production induced by exposure to high doses of F (BARBIER; ARREOLA-MENDOZA; DEL RAZO, 2010; STRUNECKA *et al.*, 2007).

In the ileum, proteins related to the energy metabolism were also altered, such as *NADH dehydrogenase [ubiquinone] flavoprotein 2, mitochondrial* (only control group

---

Fig.1-2 table S1-S2 article 2); *ATP synthase subunit beta, mitochondrial* (downregulated 10 mgF/L Fig 1 table S1 article 2 ) and *Phosphatidylinositol-binding clathrin assembly protein* (regulation of protein transport - (only control group Fig.1-2 table S1-S2 article 2)). This might be compensated by an increase in *Heat shock protein HSP 90-beta* (transcription regulatory proteins; ATP binding) (UNIPROT, 2019) - upregulated 10 mgF/L Fig 1 table S1 article 2), *Peroxiredoxin-4* (helps protecting against oxidative stress (HOFMANN; HECHT; FLOHE, 2002) - only 10 mgF/L Fig 1 table S1 article 2), and *D-3-phosphoglycerate dehydrogenase* (only 10 mgF/L Fig 1 table S1 article 2), which is responsible for catalyzing reversible oxidation of *3-phospho-D-glycerate in 3-phosphonoxy pyruvate* (UNIPROT, 2019). F also affected other proteins involved in the energy metabolism in the ileum, such as *14-3-3 protein theta* and *14-3-3 protein eta*, *Prohibitin-2*, *4-3-3 protein gamma*, *14-3-3 protein epsilon* (exclusively found in the 50 mgF/L Fig 2 table S2 article 2). Despite proteins related in energy metabolism were also altered by F in the ileum, the alterations in the jejunum were more pronounced and the rationale for this should be addressed in future studies. It should be highlighted these changes in metabolism-related proteins were more evident in the jejunum and ileum than in other organs in studies evaluating F doses similar to the ones employed in the present study (GE *et al.*, 2011; KOBAYASHI *et al.*, 2009; LOBO *et al.*, 2015; NIU *et al.*, 2014; PEREIRA *et al.*, 2018; PEREIRA *et al.*, 2016; PEREIRA *et al.*, 2013; XU *et al.*, 2005). The reason for this is the fact of most of the F ingested is absorbed from the small intestine (NOPAKUN; MESSER, 1990; NOPAKUN; MESSER; VOLLER, 1989), which makes cells in the intestinal wall exposed to higher doses of F than cells in other organs.

Due to the important role of the ENS to control the function of the GIT (FURNESS *et al.*, 2004), morphological data related to the ENS obtained in a previous study (MELO, 2015), were in the 3 articles here presented, correlated to the proteomics data. In the jejunum, several proteins of the *Rab family* were expressed exclusively in the group treated with 10 mgF/L (Table S2 article 1). This may indicate that this concentration of F can affect neuronal functions, since several *Rabs* regulate different processes in the neuronal environment. In the study by MELO (2015), 10 mgF/L decreased enteric neuronal density (Density HuC/D-IR neurons), which can compromise enteric neuronal activity. The several *Rabs* proteins expressed exclusively in this group may reflect an attempt by the organism to keep neurotransmission unchanged in the presence of F (HOLZER; HOLZER-PETSCHKE,

---

1997; HOLZER; LIPPE, 1984; MELO *et al.*, 2017; RIVERA *et al.*, 2011). In addition, proteins involved in neural homeostasis, were found exclusively in the group treated with 50 mgF/L (Table S3 article 1), such as *Tektin-2*; *Perforin 1* and *Mitochondrial fission 1 protein*. This may reflect a toxic effect of F on the ENS, reflecting in decreased density of the general population of neurons (density of HuC/D-IR), as well as in a decreasing density of nNOS-IR neurons, both of which was also reported by our group (MELO, 2015). Interestingly, these three proteins are also involved in pathways that lead to cell death (UNIPROT, 2019).

Changes in the chromatin of neurons strongly contribute to changes in neuronal circuits and it is possible that histone activity is involved in disorders that compromise neuronal function. Thus, changes in the expression of histones (downregulated in the jejunum upon exposure to 50 mgF/L; Table S5 article 1) may have contributed for the changes found in the morphology of enteric neurons in response to exposure F in the jejunum (MAZE *et al.*, 2014; MELO, 2015; RICCIO, 2010). In addition, structural muscle proteins, such as different isoforms of actin and myosin, were increased or exclusively found in the group treated with 50 mgF/L (Tables S3 and S5 article 1), which helps to explain the increase in the thickness of the tunica muscularis and jejunum wall (CHU *et al.*, 2013; MELO *et al.*, 2017; SOARES *et al.*, 2015).

In the ileum, both doses of F lead to an increase in the thickness of the ileum tunica muscularis, as well as in the total thickness of the wall (MELO, 2015). In this segment, positive regulation of several proteins of the myosin family was also found, both doses of F (Table S1 - S2-article 2). The increase in these proteins has been reported as a possible justification for the increase in the the thickness of the ileum tunica muscularis, as well as the in total thickness of the ileum wall (CHU *et al.*, 2013; MELO *et al.*, 2017; SOARES *et al.*, 2015). Moreover, it is widely known that F, the most electronegative component of the periodic table, has great affinity for  $\text{Ca}^{+2}$ , thus binding to this ion (BUZALAF; WHITFORD, 2011). The low availability of free  $\text{Ca}^{+2}$  may be related to the decrease in Calmodulin-2, since this protein was identified exclusively in the control group. Calmodulin is also responsible for initiating muscle contraction, activating myosin cross-bridges (GUYTON; HALL, 2015). Thus, the increase in members of the myosin family in the groups treated with F may be a mechanism to neutralize the lower availability of  $\text{Ca}^{+2}$ , but interestingly this protein was only found in the ileum (Table S1-S1 article 2 and Table S2 article 3), which should be further investigated.

---

In the jejunum and ileum an increase in SP-IR was found in both doses. Moreover, in the jejunum a decrease in NO-IR was also found in the 50 mgF/L group. This may result in a change in the contraction of the intestinal smooth muscle. Together with VIP and NO, SP makes is one of the neurotransmitters responsible for controlling intestinal motility. In both segments, upon treatment with 50 mgF/L, there was an increase in VIP. Vipergic alterations can lead to a decrease in the tonus of the intestinal smooth muscles. These findings may result in diarrhea or even increased susceptibility to intestinal infections, possibly due to reduced intestinal transit (HOLZER; HOLZER-PETSCHKE, 1997; HOLZER; LIPPE, 1984; MELO *et al.*, 2017; RIVERA *et al.*, 2011).

Remarkably, this is the first study to provide a molecular rationale to explain the occurrence in diarrhea, which is the main signal in people intoxicated by F. Gastrotropin protein is mainly expressed in the ileum and is important for transporting bile salts into the ileum (DAVIS; ATTIE, 2008; GROBER *et al.*, 1999; IIZUMI *et al.*, 2007; LANDRIER *et al.*, 2006; MARVIN-GUY *et al.*, 2005; THOMPSON *et al.*, 2017). The reduction of this protein can lead to the primary malabsorption of bile acids (BALESARIA *et al.*, 2008; JUNG *et al.*, 2004; KEELY; WALTERS, 2016). It is plausible that the reduced expression of the bile acid transporter, without other evidence of damage, produces idiopathic bile acid malabsorption, since the loss of expression is clearly the mechanism of malabsorption and diarrhea in ileal resection or inflammatory disease (BALESARIA *et al.*, 2008; JUNG *et al.*, 2004; KEELY; WALTERS, 2016). The presence of unabsorbed bile acids in the colon leads to diarrhea, by stimulating the secretion of liquids and electrolytes, since the Bile acids exert their effects on the transport of colonic fluid through direct and indirect actions on the epithelium (BALESARIA *et al.*, 2008; KEELY; WALTERS, 2016; LUMAN *et al.*, 1995; ROSSEL *et al.*, 1999) (Fig. 3 article 2). In the present study, the chronic exposure of the ileum to F led to several effects also found in Crohns' disease (CD), such as increased thickness of the ileum wall, increased SP-IR and VIP-IR varicosities, as well as a decrease in bile acid transporters, such as *Gastrotropin* for both F doses. These findings might help to explain common gastrointestinal symptoms shared in cases of exposure to high levels of F and CD, such as changes in the intestinal motility and diarrhea. A possible association between exposure to F and inflammatory bowel disease (IBD) has been suggested, but the absence of direct studies on this association does not allow any definitive conclusions (FOLLIN-ARBELET; MOUM, 2016). Although these two

---

identities share common characteristics and symptoms, additional studies are needed to provide unambiguous evidence about this relationship.

The proteomic changes found in the ileum and jejunum of animals treated with an acute dose of F, as well as the morphological changes found in our previous work (MELO, 2015), mostly reflect alterations in structural proteins, as well as in proteins involved in the apoptotic process, which together may be related to the main gastrointestinal symptoms in cases of acute F toxicity. In other words, since a large dose of F is ingested at one time, the organism does not have any change to adapt to the effects of F, which explains the alterations in structural and apoptotic proteins, differently to which is observed when chronic doses of F are ingested along time. As found in the chronic treatment, several proteins interacted with *GLUT4* and are involved in energy metabolism, in this case mainly carbohydrates metabolism. These proteins were reduced or even absent in the jejunum after acute exposure to F, such as *mitochondrial malate dehydrogenase*, *cytoplasmic chain dehydrogenase*, *L-lactate dehydrogenase A*, *PKM pyruvate kinase* and *glyceraldehyde-3-phosphate dehydrogenase* (Fig. 1- Table S1 article 3), while *Malate dehydrogenase*, *cytoplasmic chain* and *GAPDH* were also decreased or absent in the ileum after exposure to F (Fig.3 - Table S2 article 3). Again, we noticed a greater impairment of the jejunum when compared with the ileum. In addition, the *beta subunits of ATP synthase*, *mitochondrial* and *alpha subunit of ATP synthase*, *mitochondrial*, key enzymes in the respiratory chain, were downregulated in the jejunum after acute exposure to F (Fig. 1- Table S1 article 3), which corroborates the impairment in energy metabolism. Contrarily to which was seen in the chronic treatment, upon the acute exposure to F the organism might not have had time to adapt to its toxic effect, which means that the the loss of energy may have not been repaired. According to the literature, some of the initial symptoms of acute toxicity are generalized weakness, drop in blood pressure and disorientation (BUZALAF; WHITFORD, 2011; WHITFORD, 2011), which might be caused by decreased energy levels in the body.

Some proteins involved in the control of cell proliferation were differentially expressed upon acute exposure to F. *Transgelin-2* was increased in the jejunum (Table S1 article 3) and absent in the ileum (Table S2 article 3). The increase in this protein is associated with the development of cancer, while its suppression leads to inhibition of cell proliferation, invasion and metastasis (RIVERA *et al.*, 2011; YAKABE *et al.*, 2016). Recently, *transgelin* has been shown to be increased in colorectal cancer

---

(ZHOU *et al.*, 2018) and has been suggested as a potential biomarker for cancer, as well as a potential new target for cancer treatment (MENG *et al.*, 2017; RIVERA *et al.*, 2011). In addition, *Stress-70 protein, mitochondrial* identified exclusively in the jejunum after acute exposure to F (Table S1 article 3). In the jejunum, the *Stress-70 protein*, the mitochondria also interacted with the *heterogeneous nuclear ribonucleoprotein K*, which was also an interaction partner in the ileum. This protein is one of the main pre-mRNA binding proteins, playing an important role in the response of p53/TP53 to DNA damage, acting on the level of activation and repression of transcription, being necessary for the induction of apoptosis. In the jejunum, another identified protein that interacted with *heterogeneous nuclear ribonucleoprotein K* was *DEAD box polypeptide 5 (Asp-Glu-Ala-Asp) (DDX5)*, an RNA-binding protein overexpressed in various malignant tumors (JANKNECHT, 2010), since it causes growth (SAPORITA *et al.*, 2011) and metastasis (YANG; LIN; LIU, 2006), through the activation of several oncogenic pathways (YANG; LIN; LIU, 2006). In the present study, however, *DDX5* was absent in the jejunum after acute exposure to F (Table S1 article 3). *DDX5* depletion has been reported to cause apoptosis by inhibiting the target of rapamycin complex 1 (mTORC1) mammals (TANIGUCHI *et al.*, 2016). Fluoride-induced apoptosis has been widely reported in the literature (BARBIER; ARREOLA-MENDOZA; DEL RAZO, 2010; RIBEIRO *et al.*, 2017). In the ileum, the stretching *factor 1-alpha 1 (EF-1  $\alpha$ )* that interacted with the *heterogeneous nuclear ribonucleoprotein K* was reduced with acute exposure to F in ileum (Fig. 2- Table S2 article 3), which is also related to the induction of apoptosis, since elevated levels of EF-1  $\alpha$  are observed during neoplastic transformation and in tumors (GRANT *et al.*, 1992). Accordingly, *aldehyde dehydrogenase mitochondrial (ALDH2)* was absent after acute exposure to F (Table S2 article 3). Pharmacological inhibition of ALDH2 alone induces mitochondrial dysfunction and cell death (MALI *et al.*, 2016). These findings are important because some reports incorrectly associate exposure to F with the incidence of osteosarcoma (BASSIN *et al.*, 2006; RAMESH *et al.*, 2001) and bladder cancer (GRANDJEAN *et al.*, 1992). Our findings, however, provide additional support for the safety of using F in this regard, since, even when administered in high doses, as in the present study, F causes changes in several proteins that lead to apoptosis instead of cell proliferation.

There were also altered proteins associated with the cytoskeleton in both segments, some of which are linked to actin. Actin is one of the most abundant proteins

---

in eukaryotic cells, participating in different cellular processes, such as cell differentiation, proliferation, apoptosis, migration, signaling (KRISTO *et al.*, 2016) and regulation of the actin cytoskeleton (ARTMAN *et al.*, 2014). In line with this, it is important to highlight that the categories with the highest percentage of associated genes, revealed by the functional classification, were “actin filament binding (14.1%), “calmodulin binding” (14.1%) and “structural constituent of the cytoskeleton” for the jejunum (Fig. 2 article 3) and “intermediate filament-based process” (21%) for the ileum (Fig. 4 article 3). Changes in proteins involved in the cytoskeleton may explain some of the morphological findings of the present study. Both in the jejunum and in the ileum, the thickness of the tunica muscularis decreased significantly in the group that received the acute dose of F, when compared to the control. In contrast, when administered chronically, an increase in the tunica muscularis was observed for both segments, which is believed to be due to increased expression of structural proteins, which was not seen in the acute exposure to F. This change is considered one of the possible explanations for the impairment of intestinal motility after exposure to F (VITERI; SCHNEIDER, 1974). For the inhibitory control of motility, the main neurotransmitters involved are NO and VIP (BENARROCH, 2007), which were reduced in the group exposed to F in the ileum and increased in the jejunum. These findings agree with those found by our group in the duodenum (MELO *et al.*, 2017) and jejunum (DIONIZIO *et al.*, 2018) of rats treated chronically with water containing 10 and 50 mgF/L.

In conclusion, proteomics combined with morphologic analysis, both in cases of acute and chronic exposure to F, allowed us to provide mechanistic rationales for the signs and symptoms commonly reported in cases of F intoxication.

---



# REFERENCES

---

---



## REFERENCES

ARAUJO, T. T.; BARBOSA SILVA PEREIRA, H. A.; DIONIZIO, A.; SANCHEZ, C. D. C. *et al.* Changes in energy metabolism induced by fluoride: Insights from inside the mitochondria. **Chemosphere**, 236, p. 124357, Jul 12 2019.

ARTMAN, L.; DORMOY-RACLET, V.; VON RORETZ, C.; GALLOUZI, I. E. Planning your every move: the role of beta-actin and its post-transcriptional regulation in cell motility. **Semin Cell Dev Biol**, 34, p. 33-43, Oct 2014.

BALESARIA, S.; PELL, R. J.; ABBOTT, L. J.; TASLEEM, A. *et al.* Exploring possible mechanisms for primary bile acid malabsorption: evidence for different regulation of ileal bile acid transporter transcripts in chronic diarrhoea. **Eur J Gastroenterol Hepatol**, 20, n. 5, p. 413-422, May 2008.

BARBIER, O.; ARREOLA-MENDOZA, L.; DEL RAZO, L. M. Molecular mechanisms of fluoride toxicity. **Chem Biol Interact**, 188, n. 2, p. 319-333, Nov 5 2010.

BASSIN, E. B.; WYPIJ, D.; DAVIS, R. B.; MITTLEMAN, M. A. Age-specific fluoride exposure in drinking water and osteosarcoma (United States). **Cancer Causes Control**, 17, n. 4, p. 421-428, May 2006.

BENARROCH, E. E. Enteric Nervous System - Functional organization and neurologic implications. **Neurology**, 69, n. 20, p. 1953-1957, Nov 13 2007.

BOGDANI, M.; HENSCHER, A. M.; KANSRA, S.; FULLER, J. M. *et al.* Biobreeding rat islets exhibit reduced antioxidative defense and N-acetyl cysteine treatment delays type 1 diabetes. **J Endocrinol**, 216, n. 2, p. 111-123, Feb 2013.

BRASIL. Lei nº 6.050, de 24 de maio de 1974. Dispõe sobre a obrigatoriedade da fluoretação das águas em sistemas de abastecimento. SAÚDE, M. d. Brasília - Distrito Federal: Diário oficial da República Federativa do Brasil. 8: 687-688 p. 1974.

BRASIL. Decreto nº 76.872, de 22 de dezembro de 1975. Regulamenta a Lei nº 6.050, de 24 de maio de 1974, que dispõe sobre a fluoretação da água em sistemas públicos de abastecimento. SAÚDE, M. d. Brasília - Distrito Federal: Coleção das Leis de 1975. 8: 687-688 p. 1976.

BREWER, P. D.; HABTEMICHAEL, E. N.; ROMENSKAIA, I.; COSTER, A. C. *et al.* Rab14 limits the sorting of Glut4 from endosomes into insulin-sensitive regulated

---

secretory compartments in adipocytes. **Biochem J**, 473, n. 10, p. 1315-1327, May 15 2016.

BUZALAF, M. A. R. Review of Fluoride Intake and Appropriateness of Current Guidelines. **Adv Dent Res**, 29, n. 2, p. 157-166, Mar 2018.

BUZALAF, M. A. R.; WHITFORD, G. M. Fluoride metabolism. **Monogr Oral Sci**, 22, p. 20-36, 2011.

CARVALHO, J. G.; LEITE ADE, L.; PERES-BUZALAF, C.; SALVATO, F. *et al.* Renal proteome in mice with different susceptibilities to fluorosis. **PLoS One**, 8, n. 1, p. e53261, 2013.

CHAUHAN, S. S.; OJHA, S.; MAHMOOD, A. Modulation of lipid peroxidation and antioxidant defense systems in rat intestine by subchronic fluoride and ethanol administration. **Alcohol**, 45, n. 7, p. 663-672, Nov 2011.

CHOUHAN, S.; FLORA, S. J. Effects of fluoride on the tissue oxidative stress and apoptosis in rats: biochemical assays supported by IR spectroscopy data. **Toxicology**, 254, n. 1-2, p. 61-67, Dec 5 2008.

CHU, J.; PHAM, N. T.; OLATE, N.; KISLITSYNA, K. *et al.* Biphasic regulation of myosin light chain phosphorylation by p21-activated kinase modulates intestinal smooth muscle contractility. **J Biol Chem**, 288, n. 2, p. 1200-1213, Jan 11 2013.

COOKE, H. J. Neurotransmitters in neuronal reflexes regulating intestinal secretion. **Ann N Y Acad Sci**, 915, p. 77-80, 2000.

DAVIS, R. A.; ATTIE, A. D. Deletion of the ileal basolateral bile acid transporter identifies the cellular sentinels that regulate the bile acid pool. **Proc Natl Acad Sci U S A**, 105, n. 13, p. 4965-4966, Apr 1 2008.

DE CARVALHO, C. A.; ZANLORENZI NICODEMO, C. A.; FERREIRA MERCADANTE, D. C.; DE CARVALHO, F. S. *et al.* Dental fluorosis in the primary dentition and intake of manufactured soy-based foods with fluoride. **Clin Nutr**, 32, n. 3, p. 432-437, Jun 2013.

DENBESTEN, P.; LI, W. Chronic fluoride toxicity: dental fluorosis. **Monogr Oral Sci**, 22, p. 81-96, 2011.

---

---

DEY, S.; SWARUP, D.; SAXENA, A.; DAN, A. In vivo efficacy of tamarind (*Tamarindus indica*) fruit extract on experimental fluoride exposure in rats. **Res Vet Sci**, 91, n. 3, p. 422-425, Dec 2011.

DIONIZIO, A.; PEREIRA, H.; ARAUJO, T. T.; SABINO-ARIAS, I. T. *et al.* Effect of Duration of Exposure to Fluoride and Type of Diet on Lipid Parameters and De Novo Lipogenesis. **Biol Trace Elem Res**, 190, n. 1, p. 157-171, Jul 2019.

DIONIZIO, A. S.; MELO, C. G. S.; SABINO-ARIAS, I. T.; VENTURA, T. M. S. *et al.* Chronic treatment with fluoride affects the jejunum: insights from proteomics and enteric innervation analysis. **Sci Rep**, 8, n. 1, p. 3180, Feb 16 2018.

DUNIPACE, A. J.; KELLY, S. A.; WILSON, M. E.; ZHANG, W. *et al.* Correlation of Fluoride Levels in Human Plasma, Urine and Saliva. **Journal of Dental Research**, 74, p. 134-134, 1995.

FOLLIN-ARBELET, B.; MOUM, B. Fluoride: a risk factor for inflammatory bowel disease? **Scand J Gastroenterol**, 51, n. 9, p. 1019-1024, Sep 2016.

FURNESS, J. B.; JOHNSON, P. J.; POMPOLO, S.; BORNSTEIN, J. C. Evidence that enteric motility reflexes can be initiated through entirely intrinsic mechanisms in the guinea-pig small intestine. **Neurogastroenterol Motil**, 7, n. 2, p. 89-96, Jun 1995.

FURNESS, J. B.; JONES, C.; NURGALI, K.; CLERC, N. Intrinsic primary afferent neurons and nerve circuits within the intestine. **Prog Neurobiol**, 72, n. 2, p. 143-164, Feb 2004.

GE, Y.; NIU, R.; ZHANG, J.; WANG, J. Proteomic analysis of brain proteins of rats exposed to high fluoride and low iodine. **Arch Toxicol**, 85, n. 1, p. 27-33, Jan 2011.

GRANDJEAN, P.; OLSEN, J. H.; JENSEN, O. M.; JUEL, K. Cancer incidence and mortality in workers exposed to fluoride. **J Natl Cancer Inst**, 84, n. 24, p. 1903-1909, Dec 16 1992.

GRANT, A. G.; FLOMEN, R. M.; TIZARD, M. L.; GRANT, D. A. Differential screening of a human pancreatic adenocarcinoma lambda gt11 expression library has identified increased transcription of elongation factor EF-1 alpha in tumour cells. **Int J Cancer**, 50, n. 5, p. 740-745, Mar 12 1992.

GROBER, J.; ZAGHINI, I.; FUJII, H.; JONES, S. A. *et al.* Identification of a bile acid-responsive element in the human ileal bile acid-binding protein gene. Involvement of the farnesoid X receptor/9-cis-retinoic acid receptor heterodimer. **J Biol Chem**, 274, n. 42, p. 29749-29754, Oct 15 1999.

---

GUYTON, A. C.; HALL, J. E. **Textbook of medical physiology**. 13 ed. Philadelphia: Elsevier Health Sciences, 2015. 1264 p.

HOFMANN, B.; HECHT, H. J.; FLOHE, L. Peroxiredoxins. **Biol Chem**, 383, n. 3-4, p. 347-364, Mar-Apr 2002.

HOLZER, P.; HOLZER-PETSCHKE, U. Tachykinins in the gut. Part II. Roles in neural excitation, secretion and inflammation. **Pharmacol Ther**, 73, n. 3, p. 219-263, 1997.

HOLZER, P.; LIPPE, I. T. Substance P can contract the longitudinal muscle of the guinea-pig small intestine by releasing intracellular calcium. **Br J Pharmacol**, 82, n. 1, p. 259-267, May 1984.

HUSSAIN, J.; HUSSAIN, I.; SHARMA, K. C. Fluoride and health hazards: community perception in a fluorotic area of central Rajasthan (India): an arid environment. **Environ Monit Assess**, 162, n. 1-4, p. 1-14, Mar 2010.

IHEOZOR-EJIOFOR, Z.; WORTHINGTON, H. V.; WALSH, T.; O'MALLEY, L. *et al.* Water fluoridation for the prevention of dental caries. **Cochrane Database Syst Rev**, n. 6, p. CD010856, Jun 18 2015.

IIIZUMI, G.; SADOYA, Y.; HINO, S.; SHIBUYA, N. *et al.* Proteomic characterization of the site-dependent functional difference in the rat small intestine. **Biochim Biophys Acta**, 1774, n. 10, p. 1289-1298, Oct 2007.

INKIELEWICZ-STEPNIAK, I.; CZARNOWSKI, W. Oxidative stress parameters in rats exposed to fluoride and caffeine. **Food Chem Toxicol**, 48, n. 6, p. 1607-1611, Jun 2010.

JANKNECHT, R. Multi-talented DEAD-box proteins and potential tumor promoters: p68 RNA helicase (DDX5) and its paralog, p72 RNA helicase (DDX17). **Am J Transl Res**, 2, n. 3, p. 223-234, May 5 2010.

JUNG, D.; FANTIN, A. C.; SCHEURER, U.; FRIED, M. *et al.* Human ileal bile acid transporter gene ASBT (SLC10A2) is transactivated by the glucocorticoid receptor. **Gut**, 53, n. 1, p. 78-84, Jan 2004.

KEELY, S. J.; WALTERS, J. R. The Farnesoid X Receptor: Good for BAD. **Cell Mol Gastroenterol Hepatol**, 2, n. 6, p. 725-732, Nov 2016.

---

---

KHAN, Z. N.; SABINO, I. T.; DE SOUZA MELO, C. G.; MARTINI, T. *et al.* Liver Proteome of Mice with Distinct Genetic Susceptibilities to Fluorosis Treated with Different Concentrations of F in the Drinking Water. **Biol Trace Elem Res**, 187, n. 1, p. 107-119, Jan 2019.

KOBAYASHI, C. A.; LEITE, A. L.; PERES-BUZALAF, C.; CARVALHO, J. G. *et al.* Bone response to fluoride exposure is influenced by genetics. **PLoS One**, 9, n. 12, p. e114343, 2014.

KOBAYASHI, C. A.; LEITE, A. L.; SILVA, T. L.; SANTOS, L. D. *et al.* Proteomic analysis of kidney in rats chronically exposed to fluoride. **Chem Biol Interact**, 180, n. 2, p. 305-311, Jul 15 2009.

KRISHNAMACHARI, K. A. Skeletal fluorosis in humans: a review of recent progress in the understanding of the disease. **Prog Food Nutr Sci**, 10, n. 3-4, p. 279-314, 1986.

KRISTO, I.; BAJUSZ, I.; BAJUSZ, C.; BORKUTI, P. *et al.* Actin, actin-binding proteins, and actin-related proteins in the nucleus. **Histochem Cell Biol**, 145, n. 4, p. 373-388, Apr 2016.

LANDRIER, J. F.; ELORANTA, J. J.; VAVRICKA, S. R.; KULLAK-UBLICK, G. A. The nuclear receptor for bile acids, FXR, transactivates human organic solute transporter-alpha and -beta genes. **Am J Physiol Gastrointest Liver Physiol**, 290, n. 3, p. G476-485, Mar 2006.

LEHNINGER, A. L.; NELSON, D. L.; COX, M. M. **Lehninger principles of biochemistry**. 3. ed. ed. São Paulo: 2002.

LEITE ADE, L.; SANTIAGO, J. F., Jr.; LEVY, F. M.; MARIA, A. G. *et al.* Absence of DNA damage in multiple organs (blood, liver, kidney, thyroid gland and urinary bladder) after acute fluoride exposure in rats. **Hum Exp Toxicol**, 26, n. 5, p. 435-440, May 2007.

LIMA LEITE, A.; GUALIUME VAZ MADUREIRA LOBO, J.; BARBOSA DA SILVA PEREIRA, H. A.; SILVA FERNANDES, M. *et al.* Proteomic analysis of gastrocnemius muscle in rats with streptozotocin-induced diabetes and chronically exposed to fluoride. **PLoS One**, 9, n. 9, p. e106646, 2014.

LOBO, J. G.; LEITE, A. L.; PEREIRA, H. A.; FERNANDES, M. S. *et al.* Low-Level Fluoride Exposure Increases Insulin Sensitivity in Experimental Diabetes. **J Dent Res**, 94, n. 7, p. 990-997, Jul 2015.

---

LUMAN, W.; WILLIAMS, A. J.; MERRICK, M. V.; EASTWOOD, M. A. Idiopathic bile acid malabsorption: long-term outcome. **Eur J Gastroenterol Hepatol**, 7, n. 7, p. 641-645, Jul 1995.

MALI, V. R.; DESHPANDE, M.; PAN, G.; THANDAVARAYAN, R. A. *et al.* Impaired ALDH2 activity decreases the mitochondrial respiration in H9C2 cardiomyocytes. **Cell Signal**, 28, n. 2, p. 1-6, Feb 2016.

MALVEZZI, M.; PEREIRA, H.; DIONIZIO, A.; ARAUJO, T. T. *et al.* Low-level fluoride exposure reduces glycemia in NOD mice. **Ecotoxicol Environ Saf**, 168, p. 198-204, Jan 30 2019.

MARVIN-GUY, L.; LOPES, L. V.; AFFOLTER, M.; COURTET-COMPONDU, M. C. *et al.* Proteomics of the rat gut: analysis of the myenteric plexus-longitudinal muscle preparation. **Proteomics**, 5, n. 10, p. 2561-2569, Jul 2005.

MAZE, I.; NOH, K. M.; SOSHNEV, A. A.; ALLIS, C. D. Every amino acid matters: essential contributions of histone variants to mammalian development and disease. **Nat Rev Genet**, 15, n. 4, p. 259-271, Apr 2014.

MELO, C. G. d. S. **Avaliação da inervação entérica e análise proteômica do intestino delgado de ratos expostos à dose aguda ou crônica de fluoreto**. 2015. 456 f. (Doutorado) - Faculdade de Odontologia de Bauru. , Universidade de São Paulo, Bauru.

MELO, C. G. S.; PERLES, J.; ZANONI, J. N.; SOUZA, S. R. G. *et al.* Enteric innervation combined with proteomics for the evaluation of the effects of chronic fluoride exposure on the duodenum of rats. **Sci Rep**, 7, n. 1, p. 1070, Apr 21 2017.

MENG, T.; LIU, L.; HAO, R.; CHEN, S. *et al.* Transgelin-2: A potential oncogenic factor. **Tumour Biol**, 39, n. 6, p. 1010428317702650, Jun 2017.

NIU, R.; LIU, S.; WANG, J.; ZHANG, J. *et al.* Proteomic analysis of hippocampus in offspring male mice exposed to fluoride and lead. **Biol Trace Elem Res**, 162, n. 1-3, p. 227-233, Dec 2014.

NOPAKUN, J.; MESSER, H. H. Mechanism of fluoride absorption from the rat small intestine. **Nutr Res**, 10, p. 771-779, 1990.

NOPAKUN, J.; MESSER, H. H.; VOLLER, V. Fluoride absorption from the gastrointestinal tract of rats. **J Nutr**, 119, n. 10, p. 1411-1417, Oct 1989.

---



PEREIRA, H.; DIONIZIO, A. S.; ARAUJO, T. T.; FERNANDES, M. D. S. *et al.* Proposed mechanism for understanding the dose- and time-dependency of the effects of fluoride in the liver. **Toxicol Appl Pharmacol**, 358, p. 68-75, Nov 1 2018.

PEREIRA, H. A.; DIONIZIO, A. S.; FERNANDES, M. S.; ARAUJO, T. T. *et al.* Fluoride Intensifies Hypercaloric Diet-Induced ER Oxidative Stress and Alters Lipid Metabolism. **PLoS One**, 11, n. 6, p. e0158121, 2016.

PEREIRA, H. A.; LEITE ADE, L.; CHARONE, S.; LOBO, J. G. *et al.* Proteomic analysis of liver in rats chronically exposed to fluoride. **PLoS One**, 8, n. 9, p. e75343, 2013.

RAMESH, N.; VUAYARAGHAVAN, A. S.; DESAI, B. S.; NATARAJAN, M. *et al.* Low levels of p53 mutations in Indian patients with osteosarcoma and the correlation with fluoride levels in bone. **J Environ Pathol Toxicol Oncol**, 20, n. 3, p. 237-243, 2001.

RIBEIRO, D. A.; CARDOSO, C. M.; YUJRA, V. Q.; M, D. E. B. V. *et al.* Fluoride Induces Apoptosis in Mammalian Cells: In Vitro and In Vivo Studies. **Anticancer Res**, 37, n. 9, p. 4767-4777, Sep 2017.

RICCIO, A. Dynamic epigenetic regulation in neurons: enzymes, stimuli and signaling pathways. **Nat Neurosci**, 13, n. 11, p. 1330-1337, Nov 2010.

RIVERA, L. R.; POOLE, D. P.; THACKER, M.; FURNESS, J. B. The involvement of nitric oxide synthase neurons in enteric neuropathies. **Neurogastroenterol Motil**, 23, n. 11, p. 980-988, Nov 2011.

ROSSEL, P.; SORTSOE JENSEN, H.; QVIST, P.; ARVESCHOUG, A. Prognosis of adult-onset idiopathic bile acid malabsorption. **Scand J Gastroenterol**, 34, n. 6, p. 587-590, Jun 1999.

SANO, H.; EGUEZ, L.; TERUEL, M. N.; FUKUDA, M. *et al.* Rab10, a target of the AS160 Rab GAP, is required for insulin-stimulated translocation of GLUT4 to the adipocyte plasma membrane. **Cell Metab**, 5, n. 4, p. 293-303, Apr 2007.

SAPORITA, A. J.; CHANG, H. C.; WINKELER, C. L.; APICELLI, A. J. *et al.* RNA helicase DDX5 is a p53-independent target of ARF that participates in ribosome biogenesis. **Cancer Res**, 71, n. 21, p. 6708-6717, Nov 1 2011.

SCHAFFER, K. H.; VAN GINNEKEN, C.; COPRAY, S. Plasticity and neural stem cells in the enteric nervous system. **Anat Rec (Hoboken)**, 292, n. 12, p. 1940-1952, Dec 2009.

---

SHANTHAKUMARI, D.; SRINIVASALU, S.; SUBRAMANIAN, S. Effect of fluoride intoxication on lipidperoxidation and antioxidant status in experimental rats. **Toxicology**, 204, n. 2-3, p. 219-228, Nov 15 2004.

SOARES, A.; BERARDI, E. J.; FERREIRA, P. E.; BAZOTTE, R. B. *et al.* Intestinal and neuronal myenteric adaptations in the small intestine induced by a high-fat diet in mice. **BMC Gastroenterol**, 15, p. 3, Jan 22 2015.

STRUNECKA, A.; PATOCKA, J.; BLAYLOCK, R.; CHINOY, N. Fluoride interactions: from molecules to disease. **Current Signal Transduction Therapy**, 2, n. 3, p. 190-213, 2007.

TANIGUCHI, T.; IIZUMI, Y.; WATANABE, M.; MASUDA, M. *et al.* Resveratrol directly targets DDX5 resulting in suppression of the mTORC1 pathway in prostate cancer. **Cell Death Dis**, 7, p. e2211, May 5 2016.

THOMPSON, C. A.; WOJTA, K.; PULAKANTI, K.; RAO, S. *et al.* GATA4 Is Sufficient to Establish Jejunal Versus Ileal Identity in the Small Intestine. **Cell Mol Gastroenterol Hepatol**, 3, n. 3, p. 422-446, May 2017.

UNIPROT, C. UniProt: a worldwide hub of protein knowledge. **Nucleic Acids Res**, 47, n. D1, p. D506-D515, Jan 8 2019.

VITERI, F. E.; SCHNEIDER, R. E. Gastrointestinal alterations in protein-calorie malnutrition. **Med Clin North Am**, 58, n. 6, p. 1487-1505, Nov 1974.

WHITFORD, G. M. Acute and Chronic Fluoride Toxicity. **Journal of Dental Research**, 71, n. 5, p. 1249-1254, May 1992.

WHITFORD, G. M. The metabolism and toxicity of fluoride. **Monogr Oral Sci**, 16 Rev 2, p. 1-153, 1996.

WHITFORD, G. M. Acute toxicity of ingested fluoride. **Monogr Oral Sci**, 22, p. 66-80, 2011.

XIONG, X.; LIU, J.; HE, W.; XIA, T. *et al.* Dose-effect relationship between drinking water fluoride levels and damage to liver and kidney functions in children. **Environ Res**, 103, n. 1, p. 112-116, Jan 2007.

XU, H.; HU, L. S.; CHANG, M.; JING, L. *et al.* Proteomic analysis of kidney in fluoride-treated rat. **Toxicol Lett**, 160, n. 1, p. 69-75, Dec 30 2005.

---

---

YAKABE, K.; MURAKAMI, A.; KAJIMURA, T.; NISHIMOTO, Y. *et al.* Functional significance of transgelin-2 in uterine cervical squamous cell carcinoma. **J Obstet Gynaecol Res**, 42, n. 5, p. 566-572, May 2016.

YAN, X.; YAN, X.; MORRISON, A.; HAN, T. *et al.* Fluoride induces apoptosis and alters collagen I expression in rat osteoblasts. **Toxicol Lett**, 200, n. 3, p. 133-138, Feb 05 2011.

YANG, L.; LIN, C.; LIU, Z. R. P68 RNA helicase mediates PDGF-induced epithelial mesenchymal transition by displacing Axin from beta-catenin. **Cell**, 127, n. 1, p. 139-155, Oct 6 2006.

ZHOU, H.; ZHANG, Y.; WU, L.; XIE, W. *et al.* Elevated transgelin/TNS1 expression is a potential biomarker in human colorectal cancer. **Oncotarget**, 9, n. 1, p. 1107-1113, Jan 2 2018.

---

---



**ANNEX**

---



ANEXO A – APROVAÇÃO PELO COMITE DE ÉTICA



**Universidade de São Paulo  
Faculdade de Odontologia de Bauru**

Comissão de Ética no Ensino e Pesquisa em  
Animais

**PROTOCOLO DE RECEBIMENTO**

*Proc. Nº 012/2016*

**Título do Projeto de Pesquisa ou Roteiro de Aula:** *Análise proteômica do jejuno e íleo em ratos expostos a dose aguda ou crônica de fluoreto*

**Pesquisador Responsável:** Marília Afonso Rabelo Buzalaf

**Pesquisador Executor:** Aline Salgado Dionizio

**Colaboradores:** Letícia Alves de Lima Ferrari

**Data de entrega :** 25 de maio de 2016

**Reunião da CEEPA :** 17 de junho de 2016

**Maristela Petenuci Ferrari**

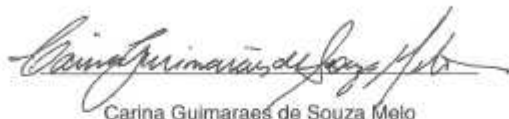
Secretária da Comissão de Ética no Ensino e Pesquisa em Animais

## ANEXO B - CARTA DE DOAÇÃO DAS PEÇAS ANATÔMICAS

### TERMO DE DOAÇÃO DE PEÇAS ANATÔMICAS

Carina Guimaraes de Souza Melo, inscrita no CPF 304430188-20, situada(o) à Av. Affonso Jose aielo, 8-200, Condominio Villaggio III casa D-19, na cidade de Bauru, estado de Sao Paulo, telefone (14) 32392569, e-mail carinamgs@yahoo.com.br, DOA, por este instrumento, a quantidade de 30 (trinta) ileo e 30 (trinta) jejuno (parte do intestino delgado) de ratos Wistar macho, obtidas no projeto de pesquisa aprovado pela CEEPA (Proc. CEEPA n° 014/2011), sob responsabilidade do Profa. Dra. Marília Afonso Rabelo Buzalaf, para desenvolvimento da pesquisa, intitulada "Análise proteômica do jejuno e ileo em ratos expostos a dose aguda ou crônica de fluoreto.", sob responsabilidade do pesquisador Profa. Dra. Marília Afonso Rabelo Buzalaf.

Bauru, 24 de Maio de 2016.




Carina Guimaraes de Souza Melo



## ANEXO C – ARTIGO PUBLICADO SCIENTIFIC REPORTS (ARTIGO 1)

www.nature.com/scientificreports

# SCIENTIFIC REPORTS



**OPEN** **Chronic treatment with fluoride affects the jejunum: insights from proteomics and enteric innervation analysis**

Received: 7 September 2017  
Accepted: 6 February 2018  
Published online: 16 February 2018

Aline Salgado Dionizio<sup>1</sup>, Carina Guimarães Souza Melo<sup>2</sup>, Isabela Tomazini Sabino-Arias<sup>2</sup>, Talita Mendes Silva Ventura<sup>2</sup>, Aline Lima Leite<sup>2</sup>, Sara Raquel Garcia Souza<sup>2</sup>, Erika Xavier Santos<sup>2</sup>, Alessandro Domingues Heibel<sup>2</sup>, Juliana Gadelha Souza<sup>2</sup>, Juliana Vanessa Colombo Martins Perles<sup>2</sup>, Jacqueline Nelisis Zanoni<sup>2</sup> & Marília Afonso Rabelo Buzalaf<sup>2</sup>

Gastrointestinal symptoms are the first signs of fluoride (F) toxicity. In the present study, the jejunum of rats chronically exposed to F was evaluated by proteomics, as well as by morphological analysis. *Wistar* rats received water containing 0, 10 or 50 mgF/L during 30 days. HuC/D, neuronal Nitric Oxide (nNOS), Vasoactive Intestinal Peptide (VIP), Calcitonin Gene Related Peptide (CGRP), and Substance P (SP) were detected in the myenteric plexus of the jejunum by immunofluorescence. The density of nNOS-IR neurons was significantly decreased (compared to both control and 10 mgF/L groups), while the VIP-IR varicosities were significantly increased (compared to control) in the group treated with the highest F concentration. Significant morphological changes were seen observed in the density of HuC/D-IR neurons and in the area of SP-IR varicosities for F-treated groups compared to control. Changes in the abundance of various proteins correlated with relevant biological processes, such as protein synthesis, glucose homeostasis and energy metabolism were revealed by proteomics.

Fluoride (F) is considered one of the essential elements for the maintenance of the normal cellular processes in the organism<sup>1</sup> and is largely employed in dentistry to control dental caries<sup>2</sup>. However, when excessive amounts are ingested, F can induce oxidative stress and lipid peroxidation, alter intracellular homeostasis and cell cycle, disrupt communication between cells and signal transduction and induce apoptosis<sup>3</sup>.

Nearly 25% of ingested F is absorbed from the stomach as an undissociated molecule (HF) in a process that is inversely related to pH<sup>4</sup>, while the remainder is absorbed in the ionic form (F<sup>-</sup>) from the small intestine, in a pH-independent manner<sup>5</sup>. Due to its major role in F absorption, the gastrointestinal tract (GIT) is regarded as the principal way of exposure to F<sup>6</sup>. Thus, gastrointestinal symptoms, including motion sickness, vomiting, diarrhea and abdominal pain are the first signs of F toxicity<sup>7–10</sup>.

The Enteric Nervous System (ENS) is an interlinked network of neurons disposed in the intestinal walls that controls the function of the GIT<sup>11</sup>. Due to its control function, changes in ENS affect the absorption, secretion, permeability and motility of the GIT<sup>12</sup>. Recently, immunofluorescence techniques revealed important alterations in the morphology of different types of enteric neurons and proteomic analysis demonstrated changes in the expression of several proteins of the duodenum of rats<sup>13</sup> after chronic exposure to F, providing the first insights for the comprehension of the mechanisms underlying the actions of F on the bowel. However, the effect of F on the ENS and proteomic profile of the jejunum has never been reported. Considering that each segment of the small intestine has distinct anatomical, histological and physiological characteristics with functional implications<sup>14</sup>, this study evaluated the morphology of distinct subtypes of enteric neurons of the jejunum after chronic exposure to F. Quantitative label-free proteomics tools were employed to evaluate the changes on the pattern of protein profile of the jejunum, after exposure to F, in attempt to provide mechanistic explanations for the effects of this ion in the intestine.

<sup>1</sup>Department of Biological Sciences, Bauru School of Dentistry, University of São Paulo, Bauru, Brazil. <sup>2</sup>Department of Morphophysiological Sciences, State University of Maringá, Maringá, Brazil. Correspondence and requests for materials should be addressed to M.A.R.B. (email: mbuzalaf@fob.usp.br)

SCIENTIFIC REPORTS | (2018) 8:3780 | DOI:10.1038/s41598-018-21533-4

1

## Material and Methods

**Animals and treatment.** The Ethics Committee for Animal Experiments of Bauru Dental School, University of São Paulo approved all experimental protocols (#014/2011 and #012/2016). All experimental protocols were approved by. The assays conformed with the guidelines of the National Research Council. Eighteen adult male rats (60 days of life - *Rattus norvegicus*, Wistar type) were randomly assigned to 3 groups ( $n = 6/\text{group}$ ). They remained one by one in metabolic cages, having access to water and food *ad libitum* under standard conditions of light and temperature. The animals received deionized water (0 mgF/L), 10 mgF/L and 50 mgF/L for 30 days as sodium fluoride (NaF) dissolved in deionized water, in order to simulate chronic intoxication with F. Since rodents metabolize F 5 times faster than humans, these F concentrations correspond to ~2 and 10 mg/L in the drinking water of humans<sup>15</sup>. After the experimental period, the animals received an intramuscular injection of anesthetic and muscle relaxant (ketamine chlorhydrate and xylazine chlorhydrate, respectively). While the rats were anesthetized, the peritoneal and thoracic cavities were exposed, and the heart was punctured for blood collection, using a heparinized syringe. Plasma was obtained by centrifugation at 800 g for 5 minutes for quantification of F, described in a previous publication<sup>15</sup>. After blood collection, the jejunum was collected for histological, immunofluorescence and proteomic analysis. For the collection of the jejunum, animal chow was removed from the animals 18 hours prior the euthanasia to decrease the volume of fecal material inside the small intestine, facilitating the cleaning process for posterior processing. After laparotomy, to remove the jejunum, initially the small intestine was localized, and the jejunum proximal limit was identified by the portion after the duodenojejunal flexure that is attached to the posterior abdominal wall by the ligament of Treitz. After incisions in the flexure and ligament, 20 centimeters distally to the incision were despoised and then 15 centimeters of the jejunum were harvested for processing. After harvesting, the jejunum was washed with PBS solution applied several times with a syringe in the lumen to remove completely any residue of fecal material.

**Histological analysis.** This analysis was performed exactly as described by Melo, et al.<sup>11</sup>.

**Myenteric plexus immunohistochemistry, morphometric and semi-quantitative analysis.** These analyses were performed exactly as described by Melo, et al.<sup>15</sup>.

**Proteomic analysis.** The frozen jejunum was homogenized in a cryogenic mill (model 6770, SPEX, Metuchen, NJ, EUA). Samples from 2 animals were pooled and analyses were carried out in triplicates. Protein extraction was performed by incubation in lysis buffer (7 M urea, 2 M thiourea, 40 mM DTT, all diluted in AMBIC solution) under constant stirring at 4 °C. Samples were centrifuged at 14000 rpm for 30 min at 4 °C and the supernatant was collected. Protein quantification was performed<sup>16</sup>. To 50  $\mu\text{L}$  of each sample (containing 50  $\mu\text{g}$  protein) 25  $\mu\text{L}$  of 0.2% Rapigest (WATERS cat#186001861) was added, followed by agitation and then 10  $\mu\text{L}$  50 mM AMBIC were added. Samples were incubated for 30 min at 37 °C. Samples were reduced (2.5  $\mu\text{L}$  100 mM DTT; BIORAD, cat# 161-0611) and alkylated (2.5  $\mu\text{L}$  300 mM IAA; GE, cat# RPN 6302 V) under dark at room temperature for 30 min. Digestion was performed at 37 °C overnight by adding 100 ng trypsin (PROMEGA, cat #V5280). After digestion, 10  $\mu\text{L}$  of 5% TFA were added, incubated for 90 min at 37 °C and sample was centrifuged (14000 rpm at 6 °C for 30 min). Supernatant was purified using C 18 Spin columns (PIERCCE, cat #89870). Samples were resuspended in 200  $\mu\text{L}$  3% acetonitrile.

**LC-MS/MS and bioinformatics analyses.** The peptides identification was done on a nanoAcquity UPLC-Xevo QTof MS system (WATERS, Manchester, UK), using the PLGS software, as previously described<sup>17</sup>. Difference in abundance among the groups was obtained using the Monte-Carlo algorithm in the ProteinLynx Global Server (PLGS) software and displayed as  $p < 0.05$  for down-regulated proteins and  $1 - p > 0.95$  for up-regulated proteins. Bioinformatics analysis was done to compare the treated groups with the control group (Tables S1–S5), as previously reported<sup>17–20</sup>. The software CYTOSCAPE 3.0.4 (JAVA) was used to build networks of molecular interaction between the identified proteins, with the aid of ClueGo and ClusterMarker applications.

## Results

**Morphological analysis of the jejunum wall thickness.** The mean ( $\pm$ SD) thickness of the jejunum tunica muscularis was significantly higher in the 50 mgF/L ( $93.0 \pm 1.4 \mu\text{m}^2$ ) when compared to control ( $81.5 \pm 1.1 \mu\text{m}^2$ ) and 10 mgF/L ( $84.2 \pm 2.5 \mu\text{m}^2$ ) groups (Bonferroni's test,  $p < 0.05$ ). The total thickness of the jejunum wall was significantly lower in the 50 mgF/L ( $742.25 \pm 7.8 \mu\text{m}^2$ ) and 10 mgF/L ( $734.4 \pm 11.8 \mu\text{m}^2$ ) when compared to control ( $783.15 \pm 5.8 \mu\text{m}^2$ ) (Bonferroni's test,  $p < 0.05$ ).

**Myenteric HuC/D – IR neurons analysis.** When the general population of neuron was morphometrically analyzed, the cell bodies areas ( $\mu\text{m}^2$ ) of the HuC/D – IR neurons were not significantly different among the groups ( $p > 0.05$ ). In the semi-quantitative analyses (neurons/cm<sup>2</sup>), a significant decrease in the density was observed in the treated groups when compared with control ( $p < 0.05$ ) (Table 1).

**Myenteric nNOS – IR neurons analysis.** The cell bodies areas ( $\mu\text{m}^2$ ) of the nNOS – IR neurons did not present a significant difference among the groups ( $p > 0.05$ ) in the morphometric analysis. As for the semi-quantitative analyses, a decrease in the mean value of the density for the group treated with 50 mgF/L when compared with the other groups was observed ( $p < 0.05$ ; Table 1).

**Myenteric varicosities VIP-IR, CGRP-IR or SP-IR morphometric analysis.** A significant increase in the VIP-IR varicosity areas ( $\mu\text{m}^2$ ) was detected in the group treated with 50 mgF/L when compared with the control group ( $p < 0.05$ ). For the CGRP-IR varicosity areas, the groups did not differ significantly ( $p > 0.05$ ). However, SP-IP varicosity areas were significantly increased in the treated groups when compared with control.

ANALYSIS	Control	10 mgF/L	50 mgF/L
Cell bodies area of the HuC/D-IR neurons ( $\mu\text{m}^2$ )	304.9 $\pm$ 3.5*	310.7 $\pm$ 3.8*	304.8 $\pm$ 3.8*
Density HuC/D-IR neurons (neurons/ $\text{cm}^2$ )	16,968 $\pm$ 390*	15,620 $\pm$ 392*	15,230 $\pm$ 380*
Cell bodies area of the nNOS-IR neurons ( $\mu\text{m}^2$ )	291.4 $\pm$ 3.2*	296.6 $\pm$ 3.5*	289.6 $\pm$ 2.9*
Density nNOS-IR neurons (neurons/ $\text{cm}^2$ )	5,725 $\pm$ 123*	5,559 $\pm$ 134*	5,176 $\pm$ 146*
Area VIP-IR varicosities ( $\mu\text{m}^2$ )	3.08 $\pm$ 0.52*	3.98 $\pm$ 0.03*	4.46 $\pm$ 0.04*
Area CGRP-IR varicosities ( $\mu\text{m}^2$ )	3.31 $\pm$ 0.03*	3.25 $\pm$ 0.04*	3.38 $\pm$ 0.03*
Area SP-IR varicosities ( $\mu\text{m}^2$ )	2.81 $\pm$ 0.01*	4.86 $\pm$ 0.03*	4.64 $\pm$ 0.03*

**Table 1.** Means and standard errors of the values of the cell bodies areas and density of HUC/D-IR and nNOS-IR neurons and VIP-IR, CGRP-IR, and SP-IR values of myenteric neurons varicosities areas of the jejunum of rats chronically exposed or not to fluoride in the drinking water. Means followed by different letters in the same line are significantly different according to Fisher's test (density HuC/D-IR and nNOS-IR neurons) or Tukey's test (other variables).  $p < 0.05$ .  $n = 6$ .

In addition, the group treated with 10 mgF/L presented an area significantly higher than the group treated with 50 mgF/L (Table 1).

Typical images of the immunofluorescences are shown in Figs 1 and 2.

**Proteomic analysis of the jejunum.** The total numbers of proteins identified in the control, 10 and 50 mgF/L groups were 294, 343 and 322, respectively. These proteins were present in the 3 pooled samples for each group. Among them, 81 (Table S1), 120 (Table S2) and 99 (Table S3) proteins were uniquely identified in the control, 10 mgF/L and 50 mgF/L groups, respectively. In the quantitative analysis of the 10 mgF/L vs. control group, 30 proteins with change in expression were detected (Table S4). As for the comparison 50 mgF/L vs. control group, 40 proteins with change in expression were found (Table S5). Most of the proteins with changed expression were upregulated in the groups treated with F when compared with the control group (21 and 23 proteins in the groups treated with 10 mgF/L and 50 mgF/L, Tables S4 and S5, respectively).

Figures 3 and 4 show the functional classification according to the biological process with the most significant term, for the comparisons 10 mgF/L vs. control and 50 mgF/L vs. control, respectively. The group exposed to the highest F concentration had the largest alteration, with change in 15 functional categories (Fig. 4). Among them, the categories with the highest percentage of associated genes were: Cellular respiration (14.3%), NAD metabolic process (10.2%), Oxygen transport (10.2%), Chromatin silencing (8.2%) and ER-associated ubiquitin-dependent protein catabolic process (8.2%). Exposure to the lowest F concentration influenced 12 functional categories (Fig. 3). The biological processes with the highest percentage of affected genes were: Nicotinamide nucleotide metabolic process (25%), Regulation of neuronal synaptic plasticity (11.4%), NAD metabolic process (15.9%) and Positive regulation of response to wounding (9.1%). It should be highlighted that Regulation of oxidative stress-induced intrinsic apoptotic signaling pathway was also identified, with 4.5% of affected genes (4.5%).

Figures 5 and 6 show the subnetworks created by CLUSTERMARK for the comparisons 10 mgF/L vs. control and 50 mgF/L vs. control, respectively. For the 10 mgF/L group (Fig. 5), most of the proteins with change in expression interacted with *Solute carrier family 2, facilitated glucose transporter member 4* (GLUT4; P19357) and *Small ubiquitin-related modifier 3* (Q5XIF4) (Fig. 5A) or with *Polyubiquitin-C* (Q63429) and *Elongation factor 2* (P05197) (Fig. 5B). As for the group treated with 50 mgF/L, most of the proteins with change in expression interacted with GLUT4 (P19357) and *Mitogen-activated protein kinase 3* (MAPK3; P21708) (Fig. 6A) or *Polyubiquitin-C* (Q63429) (Fig. 6B).

## Discussion

The small intestine is responsible for absorption of around 70–75% of  $\text{F}^{1,21}$ . As consequence, gastrointestinal symptoms, such as abdominal pain, nausea, vomiting and diarrhea, are the most common occurrence in cases of excessive ingestion of  $\text{F}^{22-25}$ . The mechanisms underlying these changes remain to be determined. Recently, our group took advantage of immunofluorescence and proteomics techniques to evaluate changes in the duodenum of rats after chronic exposure to  $\text{F}^{11}$ . The group treated with 50 mgF/L had a significant decrease in the density of nNOS-IR neurons. Additionally, important morphological changes were seen in HUC/D-IR and nNOS-IR neurons, as well as in VIP-IR, CGRP-IR, and SP-IR varicosities for the groups treated with both 10 and 50 mgF/L. Moreover, profound proteomic alterations were observed in both treated groups. In the group treated with 10 mgF/L, most of the proteins with altered expression were upregulated. On the other hand, downregulation of several proteins was found in the group treated with the highest F concentration<sup>11</sup>.

Many proteins observed in the previous study were correlated with the neurotransmission process, which is essential for the function of the GIT through ENS control. For example, the pattern of intestinal smooth muscle contraction can be modified when the release of neurotransmitters stimulating muscle contraction, such as  $\text{SP}^{26}$  is increased or when the release of neurotransmitters promoting muscle relaxation, such as  $\text{NO}^{27}$ , is decreased. In the present study, both conditions might have occurred, because we found a significance increase and decrease in the mean values of the SP varicosities area and the density of nNOS-IR neurons, respectively (Table 1), which is in accordance with our previous findings for the duodenum<sup>11</sup>. This finding can be also associated with the significant decrease in the density of HUC/D-IR neurons (Table 1), and it could contribute to the intestinal discomfort and symptoms, such as abdominal pain and diarrhea, observed upon excessive exposure to F.

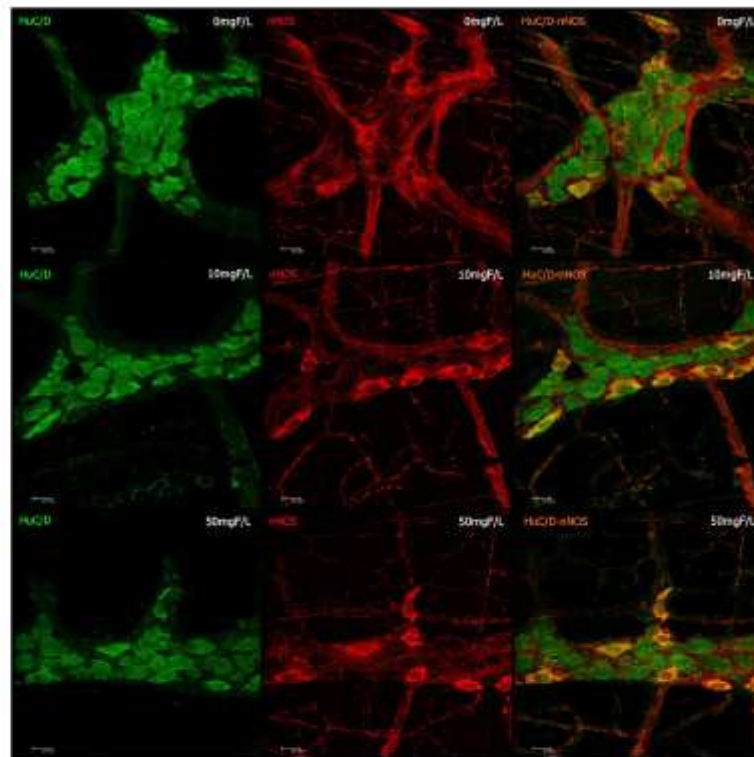


**Figure 1.** Photomicrography of myenteric neurons of the rats jejunum stained for HuC/D (green), nNOS (red), and double-labeling (HuC/D and nNOS) for the control group (0 mgF/L) and for the groups treated with 10 and 50 mgF/L. 20x Objective.

Another important neurotransmitter that also participates in the control of intestinal motility is VIP. In our study, it was observed a statistically significant increase in the mean value of the areas of VIP-IR myenteric varicosities in the 50 mgF/L group when compared with control. This finding is similar to what was observed in our previous study where duodenum was analyzed<sup>11</sup> and confirms that this dose of F can compromise the vipergic innervation of the small intestine. For the inhibitory control of motility, the main neurotransmitters involved are NO and VIP<sup>20</sup>, so basically any changes in the vipergic innervation can alter the intestinal motility, leading to a decrease in the tone of the intestinal smooth muscle, which could trigger diarrhea or even increased susceptibility to intestinal infections by decreased intestinal transit<sup>20</sup>. We can also suggest, in this case, that this increase may mean upregulation in the expression of the VIP, as a response to F toxicity since other processes such as axotomy and blocking of axonal transport or hypertrophic alterations promote upregulation of VIP in enteric neurons<sup>21</sup>. This increase can also be related to a neuroprotective role of VIP, because it acts as a potent anti-inflammatory molecule and presents an important antioxidant activity<sup>21–23</sup>. In addition to this, VIP is one of the most important elements involved in enteric neuroplasticity<sup>23</sup>, which is the ENS ability to adapt to any change in its microenvironment<sup>24</sup>. Due to the morphological changes that we observed in our study in the vipergic varicosities, we can suggest that F can induce important neuroplastic changes in the GIT.

Since alterations in the morphology of the intestinal wall infer important pathophysiological processes, we analyzed the total thickness of the intestinal wall, as well as the tunica muscularis separately. The group treated with 50 mgF/L presented a significant decrease in the total thickness of the intestinal wall and an increase in the thickness of the *tunica muscularis*, indicating that F can alter morphologically the jejunum wall. The finding for the *tunica muscularis* of the jejunum is in-line with our previous findings for the duodenum<sup>11</sup>, despite the total thickness of the duodenum wall was not altered. Changes in the number and morphology of myenteric cell bodies may be related to variations of the *tunica muscularis* thickness, which presents the structures responsible for the

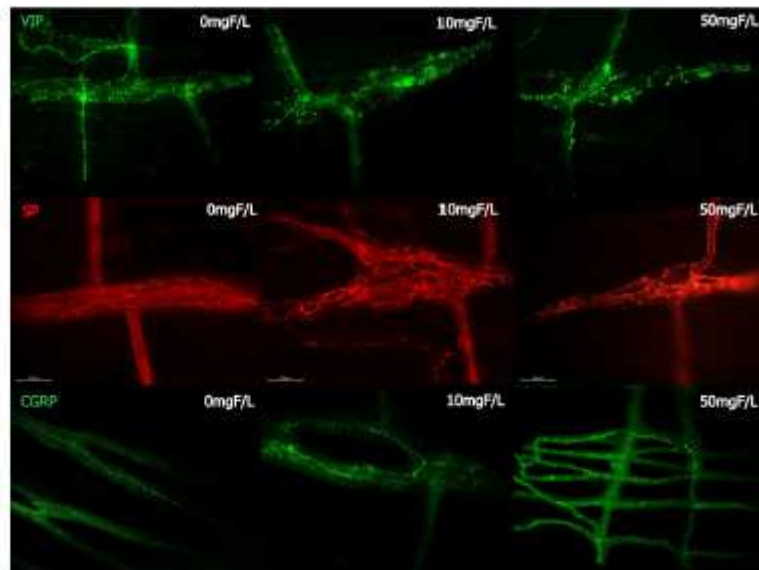


**Figure 2.** Photomicrography of myenteric varicosities of the rats jejunum after F chronic exposure (0, 10 or 50 mgF/L) for VIP-IR, SP-IR CGRP-IR. 40x Objective.

#### 10 mgF/L vs. Control

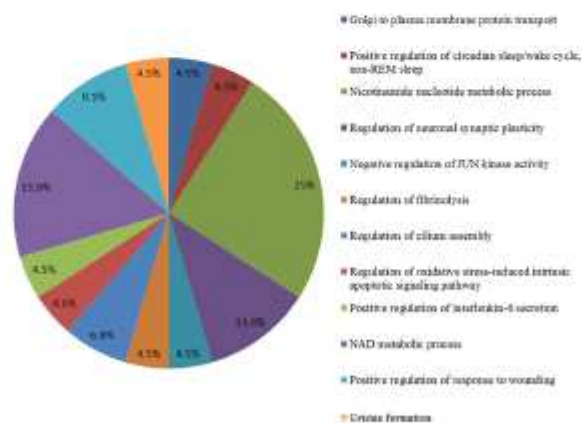


**Figure 3.** Functional distribution of proteins identified with differential expression in the jejunum of rats exposed to the chronic dose of 10 mgF/L vs. Control Group (0 mgF/L). Categories of proteins based on GO annotation Biological Process. Terms significant (Kappa = 0.04) and distribution according to percentage of number of genes association. Proteins access number was provided by UNIPROT. The gene ontology was evaluated according to ClueGo<sup>®</sup> plugins of Cytoscape<sup>®</sup> software 3.4.0<sup>26,27</sup>.

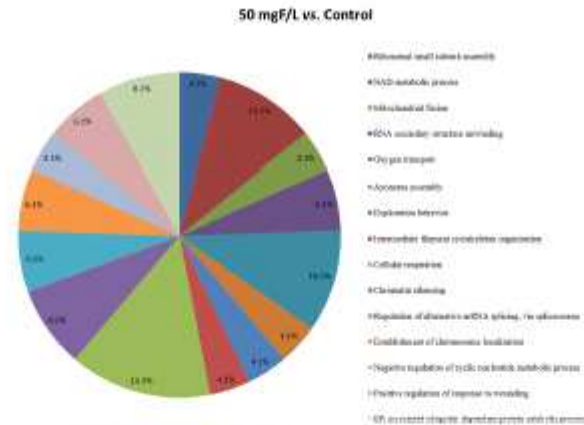


**Figure 4.** Functional distribution of proteins identified with differential expression in the jejunum of rats exposed to the chronic dose of 50 mgF/L vs. Control Group (0 mgF/L). Categories of proteins based on GO annotation Biological Process. Terms significant ( $Kappa = 0.04$ ) and distribution according to percentage of number of genes association. Proteins access number was provided by UNIPROT. The gene ontology was evaluated according to ClueGo<sup>®</sup> plugins of Cytoscape<sup>®</sup> software 3.4.0<sup>40,41</sup>.

maintenance, development and plasticity of these neurons<sup>31</sup>. Similar increase in the thickness of the intestinal wall and *tunica muscularis* have been reported in the duodenum and jejunum of rats fed with a high fat diet for 8 weeks, where morphological alterations in the general population of enteric neurons and in the nitregic population were also detected<sup>30</sup>, emphasizing that intestinal physiology comprises many interconnected mechanisms.

As in our study *F* caused morphological alterations in different enteric neuronal subtypes, which present several neurotransmitters involved in the GIT motility, it is possible that these alterations affect the GIT function, and promote the important symptomatology of *F* toxicity on the GIT, such as abdominal pain and diarrhea. We also believe that our results are quite relevant regarding the ENS, since mechanisms of neurodegeneration associated to enteric neuropathies are characterized basically by alterations, damage or loss of enteric neurons, as observed in several important pathologies<sup>37</sup> and also in our study. Thus, in order to better investigate these findings involving the enteric innervation, we performed the proteomic analysis.

The proteomic approach revealed for both *F* doses that the majority of the proteins presenting changed expression interacted with *Solute carrier family 2, facilitated glucose transporter member 4* (GLUT4) (P19357) and *Polyubiquitin C* (Q63429). In the network comparing 10 mgF/L vs. control groups, 17 members of the Ras-related Rab proteins (isoforms 1A, 1B, 3A, 3C, 3D, 4A, 4B, 5A, 8A, 8B, 10, 12, 14, 26, 35, 37, and 43) were uniquely found in the group treated with 10 mgF/L (Table S2), despite some not being present in the network. The GTPases Rab proteins are known as key regulators of intracellular membrane trafficking, from the formation of transport vesicles to their fusion with membranes. Rabs modulate between an inactive form (GDP-bound) and an active form (GTP-bound). The latter can attract to membranes distinct downstream effectors that will lead to vesicle formation, movement, tethering and fusion (UNIPROT). Generally, many studies report Rab proteins as molecules present in the CNS and their specific roles. Although marked differences distinguish the neuronal function between the ENS and CNS, their similarities allow the use of some principles established for the brain environment to be reapplied in the enteric context<sup>38</sup>. Several cellular processes can be altered and promote the enteric neuronal alterations caused by *F* effects through mechanisms involving the Rab proteins, which are considered neuronal regulators involved in the traffic and signaling of different molecules that promote neurons homeostasis, such as the neurotrophins family of growth factors. The neurotrophins-receptors complexes trigger important signaling pathways that promote development, survival and other neuronal functions through intracellular transport mechanisms mediated by the Rab proteins<sup>39</sup>.

Rab 1A is a regulator of specific vesicular trafficking from the ER to Golgi complex, and in dopaminergic neurons its expression presents a protective effect enhancing the control of motor function in surviving neurons of hemiparkinsonian animals<sup>40</sup>. From the family of the Rab 3 proteins, 3 members were present in the 10 mgF/L group, Rab 3A, Rab 3C, and Rab 3D. The Rab 3 family is observed in different cell types with high exocytic function<sup>41</sup>, in which they function as exocytosis regulators<sup>42</sup> correlated with neuronal traffic<sup>39</sup>, and are present in synaptic vesicles, modulating the neurotransmitter release<sup>43</sup>. Rab 3A is the most abundant isoform in the brain, where it presents a modulatory function in synaptic membrane fusion through a  $Ca^{2+}$ -dependent manner<sup>43</sup>. In the peripheral nervous system Rab 3A has increased expression in sciatic nerve lesion area associated to an increase in the expression of two other important proteins that contribute to neurotransmission, synaptophysin and synapsin I<sup>44</sup>. Rab 3C is highly expressed in primary hippocampal neurons, mediating regulated exocytosis<sup>45</sup>.

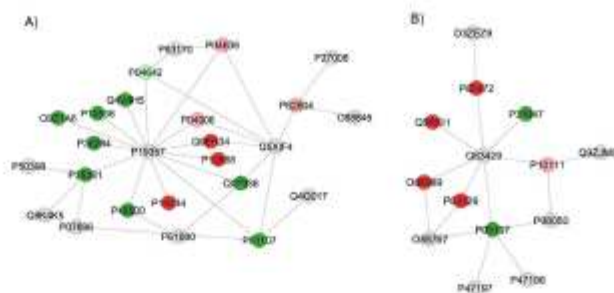


**Figure 5.** Subnetworks created by ClusterMark<sup>®</sup> to establish the interaction between proteins identified with differential expression in the 10 mg F/L group in relation to the control group. The color of the nodes indicates the differential expression of the respective named protein with its access code. The dark red and dark green nodes indicate proteins unique to the control and 10 mg F/L groups, respectively. The nodes in gray indicate the interaction proteins that are offered by CYTOSCAPE<sup>®</sup>, which were not identified in the present study and the light red and light green nodes indicate downregulation and upregulation, respectively. In (A), the access numbers in the gray nodes correspond to: *Dynein light chain 1, cytoplasmic* (P63170), *Poly [ADP-ribose] polymerase 1* (P27008), *E3 ubiquitin-protein ligase RNF4* (O88846), *Small ubiquitin-related modifier 3* (Q5XIF4), *Nischarin* (Q4G017), *Heterogeneous nuclear ribonucleoprotein K* (P61980), *Periaxonal bifunctional enzyme* (P07896), *Lethal(2) giant larvae protein homolog 1* (Q8K4K5), *Rab GDP dissociation inhibitor alpha* (P50398) and *Solute carrier family 2, facilitated glucose transporter member 4* (P19357). The access numbers of the unique proteins of the control (dark red nodes) correspond to: *Aconitate hydratase, mitochondrial* (Q9ER34), *Cytochrome c oxidase subunit 4 isoform 1, mitochondrial* (P10888) and *NADH dehydrogenase [ubiquinone] flavoprotein 2, mitochondrial* (P19234). The accession numbers of the unique 10 mg F/L (dark green nodes) proteins correspond to: *Asparyl aminopeptidase* (Q4V8H5), *Ras-related protein Rab-1B* (P10536), *Vigilin* (Q9Z1A6), *Ras-related protein Rab-12* (P35284), *Ras-related protein Rab-10* (P35281), *Triosephosphate isomerase* (P48500), *Annexin A2* (Q07936) and *Ras-related protein Rab-14* (P61107). The access numbers of the downregulated proteins (light red nodes) correspond to: *Malate dehydrogenase, mitochondrial* (P04636), *Glutathione S-transferase P* (P04906) and *Histone H4* (P62804). The accession numbers of the upregulated proteins (light green nodes) correspond to: *L-lactate dehydrogenase A chain* (P04642). In (B), the access numbers in the gray nodes correspond to: *Protein Svit* (D3ZEZ9), *Polyubiquitin-C* (Q63429), *Apoptosis-inducing factor 1, mitochondrial* (Q9JMS3), *Protein dephosphatase DJ-1* (O88767), *RAC-beta serine/threonine-protein kinase* (P47197), *RAC-alpha serine/threonine-protein kinase* (P47196) and *Gap junction alpha-1 protein* (P08050). The access numbers of the unique proteins of the control (dark red nodes) correspond to: *Vinculin* (P85972), *Eukaryotic initiation factor 4A-II* (Q5RKL1), *Malate dehydrogenase, cytoplasmic* (O88989) and *40S ribosomal protein S10* (P63326). The accession numbers of the single 10 mg F/L (dark green nodes) proteins correspond to: *Elongation factor 2* (P05197) and *Sodium- and chloride-dependent GABA transporter 3* (P31647). The access numbers of the downregulated proteins (light red nodes) correspond to: *Peptidyl-prolyl cis-trans isomerase A* (P10111).

while Rab 3D is present in secretory granules and vesicles of other cell types, such as adipocytes, exocrine glands, hematopoietic cells<sup>45</sup>, and low levels of expression were already identified in the duodenum, confirming its presence in exocrine cells of the GIT<sup>47</sup>.

The Rabs 4A and 4B were also identified as exclusive for the 10 mg F/L, and Rab4 is described as a regulator of early endosomes in the synapses, contributing to neurotransmitter receptor recycling through endosomes acting associated to other molecules in the later steps of the endocytic recycling pathway in dendrites, directing the neuronal membrane receptor trafficking<sup>48</sup>. This process is extremely important for the delivery of neurotransmitter receptors into the synaptic membrane, determining the synaptic function and plasticity. Rab 5A presents a role in axonal and dendritic endocytosis, contributing to the biogenesis of synaptic vesicles<sup>49</sup>. Rab 8 presents the same role as Rab 4, being required to direct into synapses neurotransmitter receptors as the AMPA-type glutamatergic receptors, presenting an important role in the control of synaptic function and plasticity at the postsynaptic membrane<sup>50</sup>.

Rab 10 is required for the secretion of neuropeptides through the release of dense core vesicles, which is a mechanism that modulates neuronal activity<sup>51</sup>. It is also a regulator of membrane trafficking during dendrite morphogenesis, and loss of RAB 10 decreases proximal dendritic arborization in the multi-dendritic PVD neurons<sup>52</sup>. In the CNS Rab 12 is colocalized with M98K, and overexpression of the latter induces cell death in retinal glial cells, while knockdown of Rab 12 reduces M98K-induced cell death in the same cells through the autophagy mechanism<sup>53</sup>.

Rab 26 promotes in the brain the formation of clusters of vesicles in neuritis<sup>54</sup>, and the authors suggest a new mechanism for degradation of synaptic vesicles in which Rab 26 selectively conducts synaptic and secretory

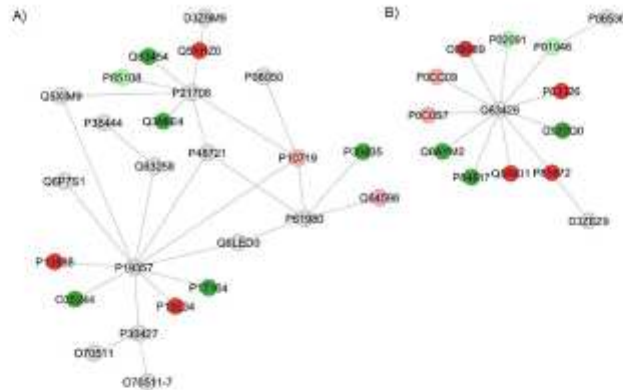


**Figure 6.** Subnetworks created by ClusterMark<sup>®</sup> to establish the interaction between proteins identified with differential expression in the 50 mg F/L group in relation to the control group. The color of the nodes indicates the differential expression of the respective named protein with its access code. The dark red and dark green nodes indicate proteins unique to the control and 50 mg F/L groups, respectively. The nodes in gray indicate the interaction proteins that are offered by CYTOSCAPE<sup>®</sup>, which were not identified in the present study and the light red and light green nodes indicate downregulation and upregulation, respectively. In (A), the access numbers in the gray nodes correspond to: *PTEN induced putative kinase 1 (Predicted)* (D3Z29M9), *Mitogen-activated protein kinase 3* (P21708), *T-complex protein 1 subunit beta* (Q5XIM9), *Gap junction alpha-1 protein* (P08050), *Cartilage oligomeric matrix protein* (P35444), *Acid ceramidase* (Q6P7S1), *Integrin alpha-7* (Q63258), *Stress-70 protein, mitochondrial* (P48721), *Solute carrier family 2, facilitated glucose transporter member 4* (P19357), *Histone H3.1* (Q6LED0), *Heterogeneous nuclear ribonucleoprotein K* (P61980), *Ankyrin-3* (C070511), *Plectin* (P30427) and *Ankyrin-3* (O70511-7). The access numbers of the unique proteins of the control (dark red nodes) correspond to: *Malate dehydrogenase, cytoplasmic* (O88989), *40S ribosomal protein S10* (P63326), *Eukaryotic initiation factor 4A-II* (Q5RKK1) and *Vinculin* (P85972). The accession numbers of the unique 50 mg F/L (dark green nodes) proteins correspond to: *Tektin-2* (Q6AYM2), *Mitochondrial fission 1 protein* (P84817) and *Paralemmin-1* (Q920Q0). The access numbers of the downregulated proteins (light red nodes) correspond to: *Histone H2A type 2-A* (P0CC09) and *Histone H2A.Z* (P0C0S7). The accession numbers of the upregulated proteins (light green nodes) correspond to: *Hemoglobin subunit beta-1* (P02091) and *Hemoglobin subunit alpha-1/2* (P01946). In (B), the access numbers in the gray nodes correspond to: *Polyubiquitin-C* (Q63429), *Protein Svitl (D3ZEZ9)* e *Glucocorticoid receptor* (P06536). The access numbers of the unique proteins of the control (dark red nodes) correspond to: *Heat shock protein 75 kDa, mitochondrial* (Q5XHZ0), *Cytochrome c oxidase subunit 4 isoform 1, mitochondrial* (P10888) and *NADH dehydrogenase [ubiquinone] flavoprotein 2, mitochondrial* (P19234). The accession numbers of the single 50 mg F/L (dark green nodes) proteins correspond to: *Mitogen-activated protein kinase 4* (Q63454), *Synaptic vesicle membrane protein VAT-1 homolog* (Q3MIE4), *ATP-dependent 6-phosphofructokinase, liver type* (P30835), *Tissue alpha-L-fucosidase* (P17164) and *Peroxiredoxin-6* (O35244). The access numbers of the downregulated proteins (light red nodes) correspond to: *ATP synthase subunit beta, mitochondrial* (P10719) and *e Histone H2A type 1-F* (Q64598). The accession numbers of the upregulated proteins (light green nodes) correspond to: *Tubulin beta-2A chain* (P85108).

vesicles into preautophagosomal structures. In neuronal immortalized cells, Rab 35 promotes neurite differentiation and favors axon elongation in rat primary neurons in an activity-dependent manner<sup>55</sup>.

The fact that several members of the Rab proteins were expressed exclusively in the 10 mg F/L group might indicate that this F concentration could affect the neuronal functions, since different Rab proteins regulate distinct processes in the neuronal environment. Since the 10 mg F/L concentration caused a decrease in the enteric neuronal density, which can compromise the enteric neuronal activity, the expression of several Rab proteins can reflect an attempt to keep the neurotransmission unaltered in the presence of E. Besides the neuronal activity, other important biological mechanisms involve the Rab proteins action. In the network comparing 10 mg F/L vs. control groups, the isoforms 1B, 10, 12 and 14 interact with GLUT4, and especially Rab 10 and Rab 14, are required in GLUT4 translocation to the plasma membrane<sup>56,57</sup>. Their increased expression might help to explain the increased sensitivity to insulin recently reported to occur in rats with diabetes induced by streptozotocin exposed to 10 mg F/L in the drinking water<sup>58</sup>. The increased expression of Rab 10 and Rab 14 might facilitate glucose uptake. Rab 37 and Rab 3A, also present among the proteins exclusively expressed in the 10 mg F/L group, are involved in the insulin release. Rab 3A has an important role in the hormone release from pancreatic  $\beta$ -cells with a regulatory control on insulin-containing secretion<sup>59</sup>. Rab 37, with a high sequence homology with Rab 3A, has also been reported to participate in regulated secretion in mammalian cells in the control of insulin exocytosis



through a different mechanism of Rab 3A<sup>60</sup>. According to the authors, impairment of Rab 37 expression may contribute to abnormal insulin release in pre-diabetic and diabetic conditions. We can infer that the expression of both proteins indicates that the insulin release mechanism could be altered with this F dose. We also observed an increase in *L-lactate dehydrogenase A chain* (LDH) (P04642) upon exposure to 10 mgF/L. This enzyme converts pyruvate to lactate with regeneration of NADH into NAD<sup>+</sup>. It is an alternative way to supply the lack of oxygen for aerobic oxidation of pyruvate and NADH produced in glycolysis<sup>61</sup>. In fact, the categories nicotinamide nucleotide metabolic process and NAD metabolic process were among the ones with the highest percentage of affected genes when the 10 mgF/L group was compared with control. Previous studies have reported increase in the LDH activity in the serum of infants who consumed water containing more than 2 mgF/L<sup>62</sup>. It was also overexpressed in the brain of rats treated with F<sup>63</sup>. When pyruvate is converted into lactate by LDH, less pyruvate is available to enter into the mitochondria and form acetyl-CoA, which is consistent with the reduction of *Malate dehydrogenase, mitochondrial* (P04636) and of enzymes related to the oxidative phosphorylation, such as *Cytochrome c oxidase subunit 4 isoform 1, mitochondrial* (P10888) and *NADH dehydrogenase [ubiquinone] flavoprotein 2, mitochondrial* (P19234). According to Barbier, et al.<sup>3</sup>, F has an inhibitory effect on the activity of citric acid cycle enzymes, in agreement with our finding of reduction in *Malate dehydrogenase, mitochondrial*. Another protein with altered expression (downregulation) in the group treated with 10 mgF/L that interacts with GLUT4 was *Glutathione S-transferase P* (P04906) that was also found downregulated in the duodenum of rats treated with the same dose of F<sup>64</sup>. This enzyme is involved in the metabolism and detoxification of xenobiotics<sup>64</sup>. Many proteins with altered expression in the network comparing 10 mgF/L vs. control groups interact with *Polyubiquitin C* (Q63429), a highly conserved polypeptide that is covalently bound to other cellular proteins to signal processes such as protein degradation, protein/protein interaction and protein intracellular trafficking<sup>65</sup>. Among them are proteins related to translation, that were absent in the group treated with 10 mgF/L, such as *Eukaryotic initiation factor 4A-II* (Q5RKL1) and *40S ribosomal protein S10* (P63326). The latter was also reduced in the group treated with 50 mgF/L both in the present study and in a previous study where duodenum was analyzed<sup>11</sup>. In addition, *Peptidyl-prolyl cis-trans isomerase A* (P10111) was reduced in the group treated with 10 mgF/L compared to control, which might impair protein folding. Also involved in protein synthesis, *Elongation factor 2* (P05197) presented altered expression upon exposure to 10 mgF/L. This protein was present only in the group treated with 10 mgF/L, and catalyzes the GTP-dependent ribosomal translocation step during translation elongation (UNIPROT). Differences in expression of all these proteins indicate alterations in distinct steps of protein synthesis upon exposure to 10 mgF/L. Changes in protein synthesis might help to explain the alterations in the thickness of the jejunum wall observed in this group. Interestingly, *Elongation factor 2* interacted with two of the 3 isoforms of the protein kinase AKT, namely *RAC-alpha serine/threonine-protein kinase* (AKT1; P47196) and *RAC-beta serine/threonine-protein kinase* (AKT2; P47197) that mediate protein synthesis and glucose metabolism<sup>66</sup>.

In the network comparing the 50 mgF/L vs. control groups (Fig. 6), some proteins with relevance for the neuronal homeostasis were expressed uniquely in the 50 mgF/L, such as *Tektin-2* (Q6AYM2), *Perforin-1* (Q5FV55), and *Mitochondrial fission 1 protein* (Fis1; P84817). The Tektins family has significant expression in adult brain and in embryonic stages of the choroid plexus, the forming retina, and olfactory receptor neurons, and can be considered a molecular target for the comprehension of neural development<sup>67</sup>. Although not present in the subnetwork, Perforin participates in the CD8<sup>+</sup> T cells response, promoting granule cytotoxicity leading to a fast cellular necrosis of the target cell in minutes<sup>68</sup> or apoptosis in a period of hours through a mechanism in which the target cell collaborates with perforin to deliver granzymes into the cytosol<sup>68</sup>. Using these mechanisms perforin-dependent, CD8<sup>+</sup> T cells promote neuronal damage in inflammatory CNS disorders<sup>69</sup>.

Mitochondrial fission is implicated in the cell death through a pathway that involves caspase activation<sup>70</sup>, and *Mitochondrial fission 1 protein* (Fis1) is considered essential for mitochondrial fission<sup>71</sup>. Overexpression of Fis1 caused increase of mitochondrial fragmentation, which conducted to apoptosis or triggered autophagy<sup>72,73</sup>, and neuroprotective effects are correlated with inhibition of Fis1<sup>74</sup>.

The fact that these proteins presented increased expression in relation to the control group can reflect F neurotoxicity on the ENS with the concentration of 50 mgF/L, and could result in the decrease in the density of the general population of neurons since these 3 proteins are involved in pathways that conduct to cell death by distinct mechanisms.

Other proteins with altered expression interacted mainly with GLUT4 (P19357) and *Polyubiquitin C* (Q63429), which was also observed for the network comparing the 10 mgF/L vs. control groups (Fig. 5). In addition, *Mitogen-activated protein kinase 3* (MAPK3; P21708) was also an interacting partner as in the duodenum of rats treated with the same concentration of F in the drinking water<sup>11</sup>. Among the proteins that interacted with GLUT4, *Peroxioredoxin-6* (O35244) was present only in the group treated with 50 mgF/L, when compared with control (Fig. 6). This enzyme, located in the cytoplasm, protects cells against oxidative stress, in addition to modulating intracellular signaling pathways. Peroxioredoxins catalyze the reduction of H<sub>2</sub>O<sub>2</sub> and hydroxyperoxide in water and alcohol<sup>75</sup>. Thus, changes in these proteins expression could be linked to fluoride-induced oxidative stress that has been extensively described in the literature<sup>177-81</sup>. In the group treated with 50 mgF/L, there was a remarkable downregulation in several isoforms of Histones, in comparison with control (Fig. 6 and Table S5). The major role described for histones is DNA "packaging", however, it is also well described that these proteins confer variations in chromatin structure to ensure dynamic processes of transcriptional regulation in eukaryotes<sup>82</sup>. Epigenetic modifications of DNA and histones are fundamental mechanisms by which neurons adapt their transcriptional response to developmental and environmental factors. Modifications in the chromatin of neurons contribute dramatically to changes in the neuronal circuits, and it is possible that histone activity is involved in disorders that compromise neuronal function<sup>83</sup>. Thus, changes in the expression of histones might have contributed to the alterations found in the morphology of enteric neurons in response to F exposure. In addition, structural muscle proteins such as different isoforms of actin and myosin were increased or exclusive

in the group treated with 50 mg F/L (Tables S3 and S5), which helps to explain the increase in the thickness of the jejunum tunica muscularis.

Probably the most remarkable finding of the present study was that when the groups treated with 10 and 50 mg F/L are compared with control, some proteins related to energetic metabolism presented similar alterations in expression, regardless the dose of F, such as: *Cytochrome c oxidase subunit 4 isoform 1, mitochondrial* (P10888), *NADH dehydrogenase [ubiquinone] flavoprotein 2, mitochondrial* (P19234), *Malate dehydrogenase, mitochondrial* (P04636), *Malate dehydrogenase, cytoplasmic* (O88989) and *L-lactate dehydrogenase A chain* (P04642). The absence of *Malate dehydrogenase, mitochondrial* (P04636), *Malate dehydrogenase, cytoplasmic* (O88989), that form oxaloacetate, absence of *NADH dehydrogenase [ubiquinone] flavoprotein 2, mitochondrial* (P19234) that transfers electrons from NADH to respiratory chain in both groups treated with F, as well as the reduction of *ATP synthase subunit beta, mitochondrial* (P10719) (only in the group treated with the highest F dose), as well as the increase in *L-lactate dehydrogenase A chain* (P04642) in both groups treated with F indicate an increase in anaerobic metabolism in attempt to obtain energy, since aerobic metabolism is impaired in the presence of F. However, the rate of production of ATP through anaerobic pathways is much lower than that of aerobic pathways, which is in-line with the reports of reduction in the production of ATP induced by exposure to high F doses<sup>15,6</sup>. It is important to highlight that these changes in the expression of proteins associated to energy metabolism induced by exposure to 10 and 50 mg F/L in the drinking water are more pronounced than those observed previously in other organs exposed to roughly the same doses of F<sup>19,6,20,21</sup>. This might be due to the fact that the small intestine is responsible for the absorption of around 75% of ingested F<sup>2</sup>, which makes the cells of the intestinal wall exposed to higher doses of F than the cells from the other organs.

In conclusion, chronic exposure to F, especially to the highest concentration evaluated, increased the thickness of the tunica muscularis and altered the pattern of protein expression. Extensive downregulation of several isoforms of histones might have contributed to the alterations found in the morphology of enteric neurons in response to F exposure. Additionally, changes in proteins involved in energy metabolism indicate a shift from aerobic to anaerobic metabolism upon exposure to the highest F concentration. These findings provide new insights into the mechanisms involved in F toxicity in the intestine.

## References

1. Yan, X. et al. Fluoride induces apoptosis and alters collagen I expression in rat osteoblasts. *Toxicol Lett* 200, 133–138, <https://doi.org/10.1016/j.toxlet.2010.11.005> (2011).
2. Buzalaf, M. A., Pawan, J. P., Honorio, H. M. & Ien Cate, J. M. Mechanisms of action of fluoride for caries control. *Monogr Ora/Sci* 22, 97–114, <https://doi.org/10.1159/000325151> (2011).
3. Barbier, O., Arrocha-Mendoza, L. & Del Razo, L. M. Molecular mechanisms of fluoride toxicity. *Chem Biol Interact* 188, 319–333, <https://doi.org/10.1016/j.cbil.2010.07.011> (2010).
4. Whitford, G. M. & Pasley, D. H. Fluoride absorption: the influence of gastric acidity. *Calk J Bone Int* 36, 302–307 (1984).
5. Nopaku, J., Messer, H. H. & Volter, V. Fluoride absorption from the gastrointestinal tract of rats. *J Nutr* 119, 1411–1417 (1989).
6. Zheng, Y., Wu, J. C., Wang, G. & Lian, W. The absorption and excretion of fluoride and arsenic in humans. *Toxicol Lett* 133, 77–82 (2002).
7. Sushoda, A., Kumar, A., Bhalnagar, M. & Bahadur, R. Prevalence of endemic fluorosis with gastrointestinal manifestations in People living in some North-Indian villages. *Fluoride* 26, 97–104 (1993).
8. Sushoda, A. et al. Fluoride ingestion and its correlation with gastrointestinal discomfort. *Fluoride* 25, 5–22 (1992).
9. Sharma, J. D., Jain, P. & Soha, D. Gastric Discomforts from Fluoride in Drinking Water in Sanganeer Taluk, Rajasthan, India. *Fluoride* 42, 286–291 (2009).
10. Das, T. K., Sushoda, A. K., Gupta, I. P., Dasarathy, S. & Tandon, R. K. Toxic Effects of Chronic Fluoride Ingestion on the Upper Gastrointestinal Tract. *J Clin Gastroenterol* 18, 194–199, <https://doi.org/10.1097/00004836-199404000-00004> (1994).
11. Furness, J. B. A comprehensive overview of all aspects of the enteric nervous system. *The Enteric Nervous System*. (Blackwell, 2006).
12. Sand, E. et al. Structural and functional consequences of bisphenol-A-induced enteric neuropathy in rat.  *BMC Gastroenterol* 14, 209, <https://doi.org/10.1186/s12876-014-0209-7> (2014).
13. Melo, C. G. S. et al. Enteric innervation combined with proteomics for the evaluation of the effects of chronic fluoride exposure on the duodenum of rats. *Sci Rep* 7, 1070, <https://doi.org/10.1038/s41598-017-01990-y> (2017).
14. Guyton, A. C. & Hall, J. E. *Textbook of medical physiology*. 13 edn. (Elsevier Health Sciences, 2015).
15. Duntzka, A. J. et al. Effect of aging on animal response to chronic fluoride exposure. *J Dent Res* 74, 358–368, <https://doi.org/10.1177/00220349950740011201> (1995).
16. Bradford, M. M. A rapid and sensitive method for the quantitation of microgram quantities of protein utilizing the principle of protein-dye binding. *Anal Biochem* 72, 248–254 (1976).
17. Lima Letta, A. et al. Proteomic analysis of gastrocnemius muscle in rats with streptozotocin-induced diabetes and chronically exposed to fluoride. *PLoS One* 9, e106646, <https://doi.org/10.1371/journal.pone.0106646> (2014).
18. Bauer-Mehren, A. Integration of genomic information with biological networks using Cytoscape. *Methods Mol Biol* 1021, 37–61, [https://doi.org/10.1007/978-1-42703-450-0\\_3](https://doi.org/10.1007/978-1-42703-450-0_3) (2013).
19. Milan, P. P. Visualization and analysis of biological networks. *Methods Mol Biol* 1021, 63–88, [https://doi.org/10.1007/978-1-42703-450-0\\_4](https://doi.org/10.1007/978-1-42703-450-0_4) (2013).
20. Orchard, S. Molecular interaction databases. *Proteomics* 12, 1656–1662, <https://doi.org/10.1002/pmic.201100484> (2012).
21. Nopaku, J. & Messer, H. H. Mechanism of fluoride absorption from the rat small intestine. *Nutr Res* 10, 771–779 (1990).
22. Vogt, R. L., Wilbered, L., Laffue, D. & Klauke, D. N. Acute fluoride poisoning associated with an on-site fluoridator in a Vermont elementary school. *Am J Public Health* 72, 1168–1169 (1982).
23. Augenstein, W. I. et al. Fluoride ingestion in children: a review of 87 cases. *Pediatrics* 88, 907–912 (1991).
24. Gosner, B. D., Beller, M., Muddaigh, J. P. & Whitford, G. M. Acute fluoride poisoning from a public water system. *N Engl J Med* 330, 95–99, <https://doi.org/10.1056/NEJM199401133300203> (1994).
25. Akitawa, K. Re-examination of acute toxicity of fluoride. *Fluoride* 30, 89–104 (1997).
26. Holzer, P. & Lippe, L. T. Substance P can contract the longitudinal muscle of the guinea-pig small intestine by releasing intracellular calcium. *Br J Pharmacol* 82, 259–267 (1984).
27. Rivera, L. R., Poole, D. B., Thacker, M. & Furness, J. B. The involvement of nitric oxide synthase neurons in enteric neuropathies. *Neurogastroenterol Motil* 23, 980–988, <https://doi.org/10.1111/j.1365-2982.2011.01780.x> (2011).
28. Benarroch, E. E. Enteric nervous system: functional organization and neurologic implications. *Neurology* 69, 1953–1957, <https://doi.org/10.1212/01.wnl.0000281998.56102.26> (2007).

29. Defani, M. A., Zanoni, J. N., Natali, M. R., Razzola, R. H. & de Miranda-Neto, M. H. Effect of acetyl-L-carnitine on VIP-ergic neurons in the jejunum submucosal plexus of diabetic rats. *Arq Neuropsiquiatr* **61**, 962–967 (2003).
30. Ekblad, K. M. & Ekblad, E. Structural, neuronal, and functional adaptive changes in atrophic rat ileum. *Gut* **45**, 236–245 (1999).
31. Hermus-Uitana, C. et al. Is L-glutathione more effective than L-glutamine in preventing enteric diabetic neuropathy? *Dig Dis Sci* **59**, 937–948, <https://doi.org/10.1007/s10620-013-2993-2> (2014).
32. Veil, A. P. & Zanoni, J. N. Age-related changes in myosin V myenteric neurons, CGRP and VIP immunoreactivity in the ileum of rats supplemented with ascorbic acid. *Histo Histopathol* **27**, 123–132, <https://doi.org/10.14670/HH.27.123> (2012).
33. Ekblad, E. & Bauer, A. J. Role of vasoactive intestinal peptide and inflammatory mediators in enteric neuronal plasticity. *Neurogastroenterol Motil* **16**(Suppl 1), 123–128, <https://doi.org/10.1111/j.1743-3150.2004.00487.x> (2004).
34. Ost, M. et al. The intestinal trophic response to enteral food is reduced in parenterally fed preterm pigs and is associated with more nitroergic neurons. *J Nutr* **135**, 2657–2663 (2005).
35. Gabella, G. In Physiology of the Gastrointestinal Tract. (ed L. R. JOHNSON) 335–381 (Raven Press, 1987).
36. Soares, A., Heraldo, E. J., Ferreira, P. E., Razzola, R. H. & Ballow, N. C. Intestinal and neuronal myenteric adaptations in the small intestine induced by a high-fat diet in mice. *BMC Gastroenterol* **15**, 3, <https://doi.org/10.1186/s12876-015-0228-x> (2015).
37. De Giorgio, R. et al. New insights into human enteric neuropathies. *Neurogastroenterol Motil* **16**(Suppl 1), 143–147, <https://doi.org/10.1111/j.1743-3150.2004.00491.x> (2004).
38. Gershon, M. D. & Ruitledge, E. M. Developmental biology of the enteric nervous system: pathogenesis of Hirschsprung disease and other congenital dysmotilities. *Semin Pediatr Surg* **13**, 224–235 (2004).
39. Iucci, C., Allilano, P. & Cogli, L. The role of rab proteins in neuronal cells and in the trafficking of neurotrophin receptors. *Membranes (Basel)* **4**, 642–677, <https://doi.org/10.3390/membranes4040642> (2014).
40. Cosme, P. G., Hensadoun, J. C., Aebischer, P. & Schneider, H. L. Rab1A over-expression prevents Golgi apparatus fragmentation and partially corrects motor deficits in an alpha-synuclein based rat model of Parkinson disease. *J Parkinsons Dis* **1**, 373–387, <https://doi.org/10.3233/JPD-2011-11058> (2011).
41. Lledo, P. M. et al. Rab3 proteins: key players in the control of exocytosis. *Trends Neurosci* **17**, 426–432 (1994).
42. Schlüter, G. M., Schmitz, E., Jahn, R., Rosenmund, C. & Südhof, T. C. A complete genetic analysis of neuronal Rab3 function. *J Neurosci* **24**, 6629–6637, <https://doi.org/10.1523/JNEUROSCI.1610-04.2004> (2004).
43. Geppert, M., Goda, Y., Stevens, C. E. & Südhof, T. C. The small GTP-binding protein Rab3A regulates a late step in synaptic vesicle fusion. *Nature* **387**, 810–814, <https://doi.org/10.1038/42054> (1997).
44. Li, J. Y., Jahn, R. & Dahlström, A. Rab32, a small GTP-binding protein, undergoes fast anterograde transport but not retrograde transport in neurons. *Eur J Cell Biol* **67**, 297–307 (1995).
45. van Vlijmen, T. et al. A unique residue in rab32c determines the interaction with novel binding protein Zwint-1. *FEBS Lett* **582**, 2838–2842, <https://doi.org/10.1016/j.febslet.2008.07.012> (2008).
46. Pavlov, N. J. et al. Rab3D regulates a novel vesicular trafficking pathway that is required for osteoclastic bone resorption. *Mol Cell Biol* **25**, 5253–5260, <https://doi.org/10.1128/MCB.25.12.5253-5260.2005> (2005).
47. Valentijn, J. A., van Weeren, L., Ultee, A. & Koster, A. J. Novel localization of Rab3D in rat intestinal goblet cells and Brunner's gland acinar cells suggests a role in early Golgi trafficking. *Am J Physiol Gastrointest Liver Physiol* **293**, G165–177, <https://doi.org/10.1152/ajpgi.00210.2006> (2007).
48. Hoogenraad, C. C. et al. Neuron specific Rab4 effector GRASP-1 coordinates membrane specialization and maturation of recycling endosomes. *PLoS Biol* **8**, e1000283, <https://doi.org/10.1371/journal.pbio.1000283> (2010).
49. de Hoop, M. J. et al. The involvement of the small GTP-binding protein Rab5a in neuronal endocytosis. *Neuron* **13**, 11–22 (1994).
50. Gerges, N. Z., Backos, D. S. & Eskin, J. A. Local control of AMPA receptor trafficking at the postsynaptic terminal by a small GTPase of the Rab family. *J Biol Chem* **279**, 43870–43878, <https://doi.org/10.1074/jbc.M404982004> (2004).
51. Sathidharan, N. et al. RAB-5 and RAB-10 cooperate to regulate neuropeptide release in *Caenorhabditis elegans*. *Proc Natl Acad Sci USA* **106**, 18944–18949, <https://doi.org/10.1073/pnas.1209306109> (2012).
52. Zou, W., Yadav, S., DeVaull, L., Nung Jan, Y. & Sherwood, D. B. RAB-10-Dependent Membrane Transport Is Required for Dendrite Arborization. *PLoS Genet* **11**, e1005484, <https://doi.org/10.1371/journal.pgen.1005484> (2015).
53. Strobl, K. et al. M98K-DPTN induces transferrin receptor degradation and RAB12-mediated autophagic death in retinal ganglion cells. *Autophagy* **9**, 510–527, <https://doi.org/10.4161/auto.23458> (2013).
54. Ilmotto, H. et al. The GTPase Rab26 links synaptic vesicles to the autophagy pathway. *Elife* **4**, e05597, <https://doi.org/10.7554/eLife.05597> (2015).
55. Villarsel-Campos, D. et al. Rab35 Functions in Axon Elongation Are Regulated by P53-Related Protein Kinase in a Mechanism That Involves Rab35 Protein Degradation and the Microtubule-Associated Protein 1B. *J Neurosci* **36**, 7298–7313, <https://doi.org/10.1523/JNEUROSCI.4064-15.2016> (2016).
56. Sano, H. et al. Rab10, a target of the AS160/Rab GAP, is required for insulin-stimulated translocation of GLUT4 to the adipocyte plasma membrane. *Cell Metabolism* **5**, 293–303, <https://doi.org/10.1016/j.cmet.2007.05.001> (2007).
57. Brewer, P. D., Habtemichael, E. N., Rotenski, I., Costler, A. C. & Mastick, C. C. Rab14 limits the sorting of Glu4 from endosomes into insulin-sensitive regulated secretory compartments in adipocytes. *The Biochemical J* **473**, 1315–1327, <https://doi.org/10.1042/BJC20160020> (2016).
58. Lobo, J. C. et al. Low-Level Fluoride Exposure Increases Insulin Sensitivity in Experimental Diabetes. *J Dent Res* **94**, 990–997, <https://doi.org/10.1177/0022034515581186> (2015).
59. Lang, J. Molecular mechanisms and regulation of insulin exocytosis as a paradigm of endocrine secretion. *Eur J Biochem* **259**, 3–17 (1999).
60. Ijehick, S. et al. The GTPase Rab37 Participates in the Control of Insulin Exocytosis. *PLoS One* **8**, e68255, <https://doi.org/10.1371/journal.pone.0068255> (2013).
61. Lehninger, A. L., Nelson, D. L. & Cox, M. M. *Lehninger principles of biochemistry*. 3. ed. edn, 975 (2002).
62. Xiong, X. et al. Dose-effect relationship between drinking water fluoride levels and damage in liver and kidney functions in children. *Environ Res* **103**, 112–116, <https://doi.org/10.1016/j.envres.2006.05.008> (2007).
63. Ge, Y., Niu, R., Zhang, J. & Wang, J. Proteomic analysis of brain proteins of rats exposed to high fluoride and low iodine. *Arch Toxicol* **85**, 27–33, <https://doi.org/10.1007/s00204-010-0537-5> (2011).
64. Kaminsky, L. S. & Zhang, Q. Y. The small intestine as a xenobiotic-metabolizing organ. *Drug Metab Dispos* **31**, 1520–1525, <https://doi.org/10.1124/dmd.31.12.1520> (2003).
65. Ciechanover, A. & Schwartz, A. L. The ubiquitin-proteasome pathway: the complexity and myriad functions of protein death. *Proc Natl Acad Sci USA* **95**, 2727–2730 (1998).
66. Bottermann, K., Reimartz, M., Barsom, M., Kottler, S. & Godecke, A. Systematic Analysis Reveals Elongation Factor 2 and alpha-Inolase as Novel Interaction Partners of AKT2. *PLoS One* **8**, e66045, <https://doi.org/10.1371/journal.pone.0066045> (2013).
67. Norrander, J., Larsson, M., Sjöbl, S., 1986, C. & Linck, B. Expression of olfactory lectins in brain and sensory development. *J Neurosci* **18**, 8912–8918 (1998).
68. Waterhouse, N. J. et al. Cytotoxic T lymphocyte-induced killing in the absence of granzymes A and B is unique and distinct from both apoptosis and perforin-dependent lysis. *J Cell Biol* **173**, 133–144, <https://doi.org/10.1083/jcb.200510072> (2006).
69. Pipkin, M. E. & Lieberman, J. Delivering the kiss of death: progress on understanding how perforin works. *Curr Opin Immunol* **19**, 301–308, <https://doi.org/10.1016/j.coi.2007.04.011> (2007).

70. Meuth, S. G. et al. Cytotoxic CD8+ T cell-neuron interactions: perlecan-dependent electrical silencing precedes but is not causally linked to neuronal cell death. *J Neurosci* **29**, 15397–15409, <https://doi.org/10.1523/JNEUROSCI.4339-09.2009> (2009).
71. Perletti, L., Roumier, T. & Kroemer, G. Mitochondrial fusion and fission in the control of apoptosis. *Trends Cell Biol* **15**, 179–183, <https://doi.org/10.1016/j.tcb.2005.02.005> (2005).
72. Chen, H. & Chan, D. C. Emerging functions of mammalian mitochondrial fusion and fission. *Hum Mol Genet* **14** (Spec. No. 2), R283–289, <https://doi.org/10.1093/hmg/ddi270> (2005).
73. James, D. L., Parone, P. A., Malenberger, Y. & Martinova, J. C. hFis1, a novel component of the mammalian mitochondrial fission machinery. *J Biol Chem* **278**, 36373–36379, <https://doi.org/10.1074/jbc.M303738200> (2003).
74. Gomes, L. C. & Scorrano, L. High levels of Fis1, a pro-fission mitochondrial protein, trigger autophagy. *Biochim Biophys Acta* **1777**, 860–866, <https://doi.org/10.1016/j.bbab.2008.05.042> (2008).
75. Wang, Y. et al. Neuroprotective Effect and Mechanism of Thiazolidinedione on Dopaminergic Neurons In Vivo and In Vitro in Parkinson Disease. *PPAR Res* **2017**, 4089214, <https://doi.org/10.1155/2017/4089214> (2017).
76. Hofmann, H., Hacht, H. J. & Fehle, L. Peroxiredoxin. *Biol Chem* **383**, 347–364, <https://doi.org/10.1515/BC.2002.040> (2002).
77. Shanthakumari, D., Srinivasulu, S. & Subramanian, S. Effect of fluoride intoxication on lipid peroxidation and antioxidant status in experimental rats. *Toxicology* **204**, 219–228, <https://doi.org/10.1016/j.tox.2004.06.058> (2004).
78. Strimmann, G., Keschobek, K. & Laakerburg, B. Liver injury caused by drugs: an update. *Stets Med Wkly* **140**, w13080, <https://doi.org/10.4414/owm.2010.13080> (2010).
79. Zhan, X. A., Wang, M., Xu, Z. H., Li, W. F. & Li, J. X. Effects of fluoride on hepatic antioxidant system and transcription of Cu/Zn SOD gene in young pigs. *J Trace Elem Med Biol* **20**, 83–87, <https://doi.org/10.1016/j.jtemb.2005.11.003> (2006).
80. Pereira, H. A. et al. Proteomic analysis of liver in rats chronically exposed to fluoride. *PLoS One* **8**, e73343, <https://doi.org/10.1371/journal.pone.0073343> (2013).
81. Pereira, H. A. et al. Fluoride Increases Hypercortisol: Diet-Induced ER, Oxidative Stress and Alters Lipid Metabolism. *PLoS One* **11**, e0158121, <https://doi.org/10.1371/journal.pone.0158121> (2016).
82. Marx, I., Noh, K. M., Soshnev, A. A. & Allis, C. D. Every amino acid matters: essential contributions of histone variants to mammalian development and disease. *Nat Rev Genet* **15**, 259–271, <https://doi.org/10.1038/nrg3673> (2014).
83. Rocchi, A. Dynamic epigenetic regulation in neurons: enzymes, stimuli and signaling pathways. *Nat Neurosci* **13**, 1330–1337, <https://doi.org/10.1038/nn.2671> (2010).
84. Strunecka, A., Patocka, J., Slaylock, H. & Chinoy, N. Fluoride interactions: from molecules to disease. *Current Signal Transduction Therapy* **2**, 190–213 (2007).
85. Xu, H. et al. Proteomic analysis of kidney in fluoride-treated rat. *Toxicol Lett* **160**, 69–75, <https://doi.org/10.1016/j.toxlet.2005.06.009> (2005).
86. Kobayashi, C. A. et al. Proteomic analysis of kidney in rats chronically exposed to fluoride. *Chem Biol Interact* **180**, 305–311, <https://doi.org/10.1016/j.cbi.2009.03.009> (2009).
87. Niu, H. et al. Proteomic analysis of hippocampus in offspring male mice exposed to fluoride and lead. *Biol Trace Elem Res* **162**, 227–233, <https://doi.org/10.1007/s12011-014-0117-2> (2014).
88. Carvalho, J. G. et al. Renal proteome in mice with different susceptibilities to fluorosis. *PLoS One* **8**, e53261, <https://doi.org/10.1371/journal.pone.0053261> (2013).
89. Bindea, C., Galan, J. & Micsink, B. CluePedia Cytoscape plugin: pathway insights using integrated experimental and in silico data. *Bioinformatics* **29**, 661–663, <https://doi.org/10.1093/bioinformatics/btt019> (2013).
90. Bindea, C. et al. ClueGO: a Cytoscape plug-in to decipher functionally grouped gene ontology and pathway annotation networks. *Bioinformatics* **25**, 1091–1093, <https://doi.org/10.1093/bioinformatics/btp111> (2009).

#### Acknowledgements

This study was supported by FAPESP (2011/10233-7, 2012/16840-5 and 2016/09100-6).

#### Author Contributions


C.M., M.B., J.Z., and J.P. conceived the experiments. A.D., C.M., J.P., S.S. and A.L. conducted the experiments. A.D., C.M., J.P., S.S., A.L., L.A., T.V., A.H., and J.S. participated in the research experiments. A.D., C.M., A.H., J.S., E.S. participated in the experiments analysis. A.D., C.M., M.B. drafted the article; analyzed and interpreted the results. All authors reviewed and approved the manuscript.

#### Additional Information

**Supplementary information** accompanies this paper at <https://doi.org/10.1038/s41598-018-21533-4>.

**Competing Interests:** The authors declare no competing interests.

**Publisher's note:** Springer Nature remains neutral with regard to jurisdictional claims in published maps and institutional affiliations.

 **Open Access** This article is licensed under a Creative Commons Attribution 4.0 International License, which permits use, sharing, adaptation, distribution and reproduction in any medium or format, as long as you give appropriate credit to the original author(s) and the source, provide a link to the Creative Commons license, and indicate if changes were made. The images or other third party material in this article are included in the article's Creative Commons license, unless indicated otherwise in a credit line to the material. If material is not included in the article's Creative Commons license and your intended use is not permitted by statutory regulation or exceeds the permitted use, you will need to obtain permission directly from the copyright holder. To view a copy of this license, visit <http://creativecommons.org/licenses/by/4.0/>.

© The Author(s) 2018

## ANEXO D – ARTIGO PUBLICADO SCIENCE OF THE TOTAL ENVIRONMENT (ARTIGO 3)

Science of the Total Environment 741 (2020) 140419

Contents lists available at ScienceDirect

**Science of the Total Environment**

Journal homepage: [www.elsevier.com/locate/scitotenv](http://www.elsevier.com/locate/scitotenv)






### Effects of acute fluoride exposure on the jejunum and ileum of rats: Insights from proteomic and enteric innervation analysis

Aline Dionizio<sup>a</sup>, Carina Guimarães Souza Melo<sup>a</sup>, Isabela Tomazini Sabino-Arias<sup>a</sup>, Tamara Teodoro Araujo<sup>a</sup>, Talita Mendes Oliveira Ventura<sup>a</sup>, Aline Lima Leite<sup>a</sup>, Sara Raquel Garcia Souza<sup>b</sup>, Erika Xavier Santos<sup>b</sup>, Alessandro Domingues Heubel<sup>a</sup>, Juliana Gadelha Souza<sup>a</sup>, Juliana Vanessa Colombo Martins Perles<sup>b</sup>, Jacqueline Nelisis Zanoni<sup>b</sup>, Marília Afonso Rabelo Buzalaf<sup>a,\*</sup>

<sup>a</sup> Department of Biological Sciences, Bauru School of Dentistry, University of São Paulo, Bauru, Brazil  
<sup>b</sup> Department of Morphophysiological Sciences, State University of Maringá, Maringá, Brazil

---

#### HIGHLIGHTS

- Water containing 25 mgF/Kg bw F provokes morphological changes and alters in several proteins in the jejunum and ileum;
- Organism might not have had time to adapt to its toxic effect. Therefore, the loss of energy may have not been repaired.
- Morphological changes in the gut, can be explained by alterations in VIP-IR and in proteins that regulate the cytoskeleton.

#### GRAPHICAL ABSTRACT



---

#### ARTICLE INFO

**Article history:**  
Received 27 March 2020  
Received in revised form 4 June 2020  
Accepted 20 June 2020  
Available online 22 June 2020

**Editor:** Lofli Aleya

**Keywords:**  
Fluoride  
Acute  
Chronic  
Ileum  
Jejunum

#### ABSTRACT

Fluoride (F) is largely employed in dentistry, in therapeutic doses, to control caries. However, excessive intake may lead to adverse effects in the body. Since F is absorbed mostly from the gastrointestinal tract (GIT), gastrointestinal symptoms are the first signs following acute F exposure. Nevertheless, little is known about the mechanistic events that lead to these symptoms. Therefore, the present study evaluated changes in the proteomic profile as well as morphological changes in the jejunum and ileum of rats upon acute exposure to F. Male rats received, by gastric gavage, a single dose of F containing 0 (control) or 25 mg/Kg for 30 days. Upon exposure to F, there was a decrease in the thickness of the tunica muscularis for both segments and a decrease in the thickness of the wall only for the ileum. In addition, a decrease in the density of HuC/D-IR neurons and nNOS-IR neurons was found for the jejunum, but for the ileum only nNOS-IR neurons were decreased upon F exposure. Moreover, SP-IR varicosities were increased in both segments, while VIP-IR varicosities were increased in the jejunum and decreased in the ileum. As for the proteomic analysis, the proteins with altered expression were mostly negatively regulated and associated mainly with protein synthesis and energy metabolism. Proteomics also revealed alterations in proteins involved in oxidative/antioxidant defense, apoptosis and as well as in cytoskeletal proteins. Our results, when analyzed together, suggest that the gastrointestinal symptoms found in cases of acute F exposure might be related to the morphological alterations in the gut (decrease in the thickness of the tunica muscularis).

---

**Abbreviations:** HuC/D-IR, immunoreactive to human protein type C and D; nNOS-IR, immunoreactive to neural nitric oxide synthase; SP-IR, immunoreactive to substance P; VIP-IR, immunoreactive to intestinal vasoactive peptide; CCRP-IR, immunoreactive to calcitonin gene-related peptide.

\* Corresponding author at: Alameda Octávio Pinheiro Brisolla, 9-75, Bauru, SP 17012-901, Brazil.  
E-mail address: [mbuzalaf@fob.usp.br](mailto:mbuzalaf@fob.usp.br) (M.A.R. Buzalaf).

<http://dx.doi.org/10.1016/j.scitotenv.2020.140419>  
0048-9697/© 2020 Elsevier B.V. All rights reserved.

that, at the molecular level, can be explained by alterations in the gut vagal innervation and in proteins that regulate the cytoskeleton.

© 2020 Elsevier B.V. All rights reserved.

## 1. Introduction

Fluorine is one of the most abundant elements in the earth's crust (Shanthakumari et al., 2004) and is found in its ionic form (fluoride; F) in biological fluids and tissues as a trace element, in two different forms: inorganic and organic, being 99% accumulated in hard tissues (Suarez et al., 2008). F is widely used as a therapeutic agent against caries and can be found naturally in soil and water or in controlled doses at water supply stations (McDonagh et al., 2000; Wong et al., 2011). However, studies have shown that excessive intake of F can lead to side effects (Buzalaf et al., 2013; Whitford, 1996; Yan et al., 2011) perceived at the molecular level (Araujo et al., 2019; Barbier et al., 2010), as well as at the tissue level in several organs and structures, such as skeletal muscles, brain, spinal column (Mullenix et al., 1995), liver (Dionizio et al., 2019; Pereira et al., 2018; Pereira et al., 2016; Pereira et al., 2013) and gut (Dionizio et al., 2018; Melo et al., 2017).

The toxic effect of F is related to the amount and duration of exposure (Araujo et al., 2019; Dionizio et al., 2019; Pereira et al., 2018) and can be classified into acute or chronic (He and Chen, 2006; Shanthakumari et al., 2004; Whitford, 1992). Acute toxicity occurs by ingesting a large amount of F at a single time (Whitford, 2011). Most of the studies evaluating acute F exposure report the effects at the molecular and histological levels in the kidney (Jimenez-Cordova et al., 2019; Mitsui et al., 2010; Santoyo-Sanchez et al., 2013) and heart (Mitsui et al., 2007; Panneerselvam et al., 2019). Considering that the gastrointestinal tract (GIT), especially the gut, is the main responsible for the absorption of F (Nopakun et al., 1989; Whitford, 2011; Whitford and Pashley, 1984), gastrointestinal manifestations are frequently reported in cases of acute F intoxication, such as vomiting with blood and diarrhea. These manifestations can occur in cases of professional application of F for caries prevention, especially in children, as well as in cases of poisoning (Whitford, 2011). However, little is known regarding the effects of acute F exposure in the GIT at the molecular level. This knowledge is important to allow an adequate treatment of patients submitted to acute F intoxication. In this sense, the present study attempted to shed light into the molecular mechanisms underlying acute F toxicity, by performing morphological analysis of the intestinal wall and myenteric neurons, as well as proteomic analysis of the jejunum and ileum of rats, after acute exposure to F.

## 2. Material and methods

### 2.1. Animals and treatment

The work was performed on twelve adult male rats (60 days of life - *Rattus norvegicus*, Wistar type). The animals were individually housed in metabolic cages, with *ad libitum* access to deionized water and low-fluoride chow for 30 days. The illumination (12 h light/12 dark hours) and the ambient temperature were controlled ( $22 \pm 2$  °C). The animals were randomly divided into 2 groups ( $n = 6$  per group), according with the treatment they received by gavage in the last day of the experiment. The experimental group received 25 mgF/kg body weight as sodium fluoride (NaF) dissolved in deionized water, while the control group received deionized water. As rodents metabolize F 5 times faster than humans (Dunipace et al., 1995), this dose of F corresponds to ~5 mg/kg to humans, which corresponds to the probable toxic dose (PTD) (Whitford, 2011). After the treatment period, the plasma was obtained by centrifugation of blood at 800g for 5 min for quantification of F, as previously described (Melo et al., 2017). Then, the jejunum and

ileum were collected as described by Dionizio et al. (2018), for morphological and proteomic analysis. Briefly, animal chow was removed from the animals 18 h prior to euthanasia, to reduce the volume of fecal material inside the small intestine, thus making easier the cleaning process for posterior analysis. After identifying the duodenojejunal flexure, one incision is made. Around 20 cm were despised and then 15 cm of the jejunum were harvested. After localizing the cecum, two incisions were made to collect the ileum: one in the anterior portion of the ileocecal valve and the other 10 cm proximally to the first one. The jejunum and ileum segments were washed with phosphate buffered solution several times to remove residues of fecal material. All experimental protocols were approved by the Animal Experimentation Ethics Committee of the Faculty of Dentistry of Bauru of the University of São Paulo (protocols 014/2011 and 012/2016).

### 2.2. Histological analysis and myenteric plexus immunohistochemistry, morphometric and semi-quantitative analysis

These analyses were performed exactly as described by Melo et al. (2017)

### 2.3. Proteomics and bioinformatics analyses

The frozen jejunum and ileum were homogenized in a cryogenic mill (model 6770, Spex, Metuchen, NJ, EUA). Samples from 2 animals were pooled and analyses were carried out in triplicates, exactly as previously described (Dionizio et al., 2018). Briefly, protein extraction was performed by incubation in lysis buffer (7 M urea, 2 M thiourea, 40 mM DTT, all diluted in AMBIC solution) under constant stirring at 4 °C. After centrifugation at 20,817g for 30 min at 4 °C, the supernatant was collected and total protein was quantified (Bradford, 1976). To 50 µl of each sample (containing 50 µg protein) 25 µl of 0.2% Rapigest (Waters cat#186001861) were added, followed by agitation and then 10 µl 50 mM AMBIC were added, followed by incubation for 30 min at 37 °C. Samples were then reduced (100 mM DTT; BioRad, cat# 161-0611) and alkylated (300 mM IAA; GE, cat# RPN 6302 V) under dark at room temperature for 30 min. Digestion was performed at 37 °C overnight by adding 100 ng trypsin (Promega, cat#V5280). Then 10 µl of 5% TFA were added, samples were incubated for 90 min at 37 °C and centrifuged (20,817 g at 6 °C for 30 min). Supernatant was purified using C18 Spin columns (Pierce, cat #89870). Samples were then resuspended in 200 µl 3% acetonitrile.

The peptides identification was performed on a nanoAcquity UPLC-Xevo QToF MS system (Waters, Manchester, UK), as previously described (Lima Leite et al., 2014). The Protein Lynx Global Server (PLGS) software was used to detect difference in expression between the groups, which was expressed as  $p < 0.05$  and  $1-p > 0.95$  for down- and up-regulated proteins, respectively. Bioinformatics analysis was performed for comparison of the treated group with the control group (Tables S1–S2), as earlier reported (Bauer-Mehren, 2013; Lima Leite et al., 2014; Millan, 2013; Orchard, 2012). The software CYTOSCAPE@ 3.0.4 (Java®) was employed to build networks of molecular interaction between the identified proteins, with the support of ClusterMarker® application.

### 3. Results

#### 3.1. Morphological analysis of the jejunum and ileum wall thickness

The mean ( $\pm$ SD) thickness of the tunica muscularis was significantly decreased in the treated groups of jejunum ( $90.1 \pm 1.9 \mu\text{m}^2$ ) and ileum ( $134.0 \pm 2.5 \mu\text{m}^2$ ) when compared with the respective controls ( $116.4 \pm 3.7 \mu\text{m}^2$  and  $223.6 \pm 7.8 \mu\text{m}^2$ ) (Student's t-test,  $p < 0.05$ ). The same was observed for the mean ( $\pm$ SD) total thickness of the wall, which was significantly reduced in the treated group ( $756.5 \pm 12.9 \mu\text{m}^2$ ) when compared with control ( $784.1 \pm 17.1 \mu\text{m}^2$ ) for ileum (Student's t-test,  $p > 0.05$ ).

#### 3.2. Myenteric neurons HuC/D-IR analysis

In the morphometric analysis of the general population of neurons, after treatment with fluoride, the cell bodies areas of the HuC/D-IR neurons of the ileum ( $\mu\text{m}^2$ ) were significantly increased, but no significant changes were seen in the jejunum ( $p > 0.05$ ). In the quantitative analyses, the treated group presented a significant decrease in the jejunum but was not significantly altered in the ileum ( $p > 0.05$ ), (Tables 1 and 2).

#### 3.3. Myenteric neurons nNOS-IR analysis

In the morphometric analysis of the general population of neurons, the cell bodies areas of the nNOS-IR neurons ( $\mu\text{m}^2$ ) were significantly increased in the jejunum and significantly decreased in the ileum, in comparison with the respective controls ( $p < 0.05$ ). In the quantitative analyses, significant decreases were observed in the treated groups in respect to control, both for jejunum and ileum ( $p < 0.05$ ) (Tables 1 and 2).

#### 3.4. Myenteric neurons VIP-IR, CGRP-IR and SP-IR morphometric analysis

In the morphometric analyses of the SP-IP varicosities ( $\mu\text{m}^2$ ) a significant increase was detected in the treated groups in respect to control, both for jejunum and ileum ( $p < 0.05$ ). CGRP-IR varicosities ( $\mu\text{m}^2$ ) were significantly reduced in the ileum after treatment with fluoride but were not significantly altered in the jejunum ( $p > 0.05$ ). The VIP-IR varicosities ( $\mu\text{m}^2$ ) were significantly increased in the jejunum and significantly decreased in the ileum upon treatment with fluoride ( $p < 0.05$ ) (Tables 1 and 2). Representative images of the immunofluorescences are displayed in supplementary information (Supplementary Figs S1–S4).

**Table 1**

Means and standard errors of the values of the cell bodies areas and density of HuC/D-IR, nNOS-IR and VIP-IR, CGRP-IR, and SP-IR values of myenteric neurons varicosities areas of the jejunum of rats exposed or not to acute dose of F. Animal groups: Control (deionized water - 0 mgF/L) and 25mgF/kg bw.

Analysis	Control	25mgF/kg bw
Cell bodies areas of the HuC/D-IR neurons ( $\mu\text{m}^2$ )	319.5 $\pm$ 3.5 <sup>a</sup>	316.2 $\pm$ 3.9 <sup>a</sup>
Density HuC/D-IR neurons (neurons/cm <sup>2</sup> )	16,094.0 $\pm$ 343.1 <sup>a</sup>	13,848.4 $\pm$ 324.3 <sup>b</sup>
Cell bodies areas of the nNOS-IR neurons ( $\mu\text{m}^2$ )	288.7 $\pm$ 3.0 <sup>a</sup>	300.8 $\pm$ 3.0 <sup>a</sup>
Density nNOS-IR neurons (neurons/cm <sup>2</sup> )	5959.9 $\pm$ 138.7 <sup>a</sup>	5219.9 $\pm$ 151.6 <sup>b</sup>
Area VIP-IR varicosities ( $\mu\text{m}^2$ )	2.8 $\pm$ 0.0 <sup>a</sup>	3.0 $\pm$ 0.0 <sup>a</sup>
Area CGRP-IR varicosities ( $\mu\text{m}^2$ )	3.5 $\pm$ 0.0 <sup>a</sup>	3.5 $\pm$ 0.0 <sup>a</sup>
Area SP-IR varicosities ( $\mu\text{m}^2$ )	3.1 $\pm$ 0.0 <sup>a</sup>	4.8 $\pm$ 0.0 <sup>a</sup>

Means followed by different letters in the same column are significantly different according to Student's t-test ( $p < 0.05$ ), (N = 6).

**Table 2**

Means and standard errors of the values of the cell bodies areas and density of HuC/D-IR, nNOS-IR and VIP-IR, CGRP-IR, and SP-IR values of myenteric neurons varicosities areas of the ileum of rats exposed or not to acute dose of F. Animal groups: Control (deionized water - 0 mgF/L) and 25mgF/kg bw.

Analysis	Control	25mgF/kg bw
Cell bodies areas of the HuC/D-IR neurons ( $\mu\text{m}^2$ )	298.0 $\pm$ 3.6 <sup>a</sup>	312.3 $\pm$ 4.0 <sup>b</sup>
Density HuC/D-IR neurons (neurons/cm <sup>2</sup> )	13,099.8 $\pm$ 420.9 <sup>a</sup>	12,756.9 $\pm$ 347.7 <sup>a</sup>
Cell bodies areas of the nNOS-IR neurons ( $\mu\text{m}^2$ )	300.4 $\pm$ 3.3 <sup>a</sup>	287.6 $\pm$ 3.1 <sup>b</sup>
Density nNOS-IR neurons (neurons/cm <sup>2</sup> )	4657.1 $\pm$ 145.4 <sup>a</sup>	3905.6 $\pm$ 129.7 <sup>b</sup>
Area VIP-IR varicosities ( $\mu\text{m}^2$ )	3.3 $\pm$ 0.0 <sup>a</sup>	3.1 $\pm$ 0.0 <sup>a</sup>
Area CGRP-IR varicosities ( $\mu\text{m}^2$ )	3.4 $\pm$ 0.0 <sup>a</sup>	3.2 $\pm$ 0.0 <sup>a</sup>
Area SP-IR varicosities ( $\mu\text{m}^2$ )	2.9 $\pm$ 0.0 <sup>a</sup>	4.515 $\pm$ 0.0 <sup>b</sup>

Means followed by different letters in the same line are significantly different according to Student's t-test ( $p < 0.05$ ), (N = 6).

#### 3.5. Proteomic analysis

The total numbers of proteins identified by mass spectrometry in jejunum of control and treated group were 282 and 227, respectively. Among them, 106 and 51 proteins were uniquely identified in the control and treated groups, respectively. In the quantitative analysis of treated vs. control group, 37 proteins with change in expression were detected. Most of the proteins with altered expression were downregulated in the group treated with F when compared with the control group (23 proteins), suggesting that acute exposure to F reduces protein synthesis (Table S1).

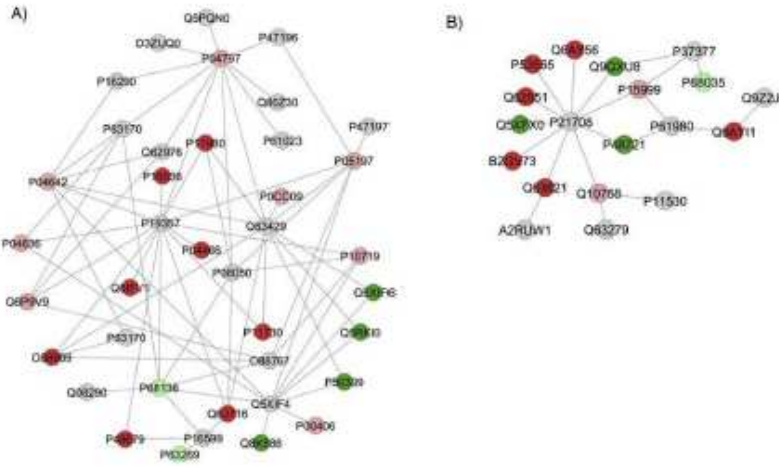
Fig. 1 shows the subnetworks generated by ClusterMarker® for the comparison treated vs. control group of jejunum. Most of the proteins with altered expression interacted with *Dynein light chain 1, cytoplasmic* (P63170), *Solute carrier family 2, facilitated glucose transporter member 4* (P19357), *Polyubiquitin-C* (Q63429), *Gap junction alpha-1 protein* (P08050), *Protein deglycase DJ-1* (O88767), *Small ubiquitin-related modifier 3* (Q5XIF4) (Fig. 1A) or *Heterogeneous nuclear ribonucleoprotein K* (P61980) and *Mitogen-activated protein kinase 3* (P21708) (Fig. 1B).

Fig. 2 shows the functional classification according to the biological process with the most significant term, for the comparison between treated vs. control group for jejunum. Among them, the categories with the highest percentages of genes were Actin filament binding (14.1%), Calmodulin binding (14.1%), Structural constituent of cytoskeleton (12.5%), Motor activity (10.9%) and Hydrogen ion transmembrane transporter activity (9.4%).

The total numbers of proteins identified by mass spectrometry in the ileum for control and treated groups were 195 and 183, respectively. Among them, 66 and 54 proteins were uniquely identified in the control and treated groups, respectively. In the quantitative analysis of the treated vs. control group, 36 proteins with change in expression were detected. Most of the proteins with altered expression were downregulated in the group treated with F when compared with the control group (22 proteins), suggesting that acute exposure to F reduces protein synthesis (Table S2).

Fig. 3 shows the subnetworks generated by ClusterMarker® for the treated vs. control group of ileum. Most of the proteins with altered expression interacted with *Solute carrier family 2, facilitated glucose transporter member 4* (P19357), *Heterogeneous nuclear ribonucleoprotein K* (P61980), *UV excision repair protein in RAD23 homolog B* (Q4KM42), *Protein deglycase DJ-1* (O88767) and *Polyubiquitin-C* (Q63429) (Fig. 3A) or *Mitogen-activated protein kinase 3* (P21708) and *Gap junction alpha-1 protein* (P08050) (Fig. 3B).

Fig. 4 shows the functional classification according to the biological process with the most significant term, for the comparison between treated vs. control groups for ileum. Among them, the categories with the highest percentages of genes were Intermediate filament-based



**Fig. 1.** Subnetworks created by ClusterMakerX to establish the interaction between proteins identified with differential expression in the 25 mgF/kg bw group in relation to the control group in jejunum. The color of the nodes indicates the differential expression of the respective named protein with its accession code. The dark red and dark green nodes indicate proteins unique to the control and 25 mgF/kg bw groups, respectively. The nodes in gray indicate the interaction proteins that are offered by CYTOSCAPEX, which were not identified in the present study and the light red and light green nodes indicate downregulation and upregulation, respectively. In A the accession numbers in the gray nodes correspond to: *α*-*RAC*-beta serine/threonine-protein kinase (P47197), *RAC*-alpha serine/threonine-protein kinase (P47196), Neurocalcin delta (Q5RQJ0), *MLP*-like protein 1 (D3ZLQ0), *Phosphoglycerate mutase 2* (P16290), *Dynein light chain 1, cytoplasmic* (P63170), *Calcium-activated potassium channel subunit alpha-1* (Q62976), *Protein phosphatase 1E* (Q80230), *Calcineurin B homologous protein 1* (P63023), *Solute carrier family 2, facilitated glucose transporter member 4* (P19357), *Polyubiquitin-C* (Q63429), *Gap junction alpha-1 protein* (P08860), *Dynein light chain 1, cytoplasmic* (P63170), *Protein deglycase DJ-1* (O88767), *Small ubiquitin-related modifier 3* (Q63044), *Tumor necrosis factor* (P16599) and *Calponin-1* (Q08290). The accession numbers of the unique proteins of the control (dark red nodes) correspond to the: *Pyruvate kinase PKM* (P11980), *Phosphate carrier protein, mitochondrial* (P16036), *Myosin regulatory light chain 2, skeletal muscle isoform* (R04466), *Keratin, type I cytoskeletal 14* (Q61FV1), *Calcium/calmodulin-dependent protein kinase type II subunit gamma* (P11730), *Malate dehydrogenase, cytoplasmic* (O88989), *Peracineclatin-1* (Q63716) and *Prelamin-A/C* (P48679). The accession numbers of the unique 25 mgF/kg bw (dark green nodes) proteins correspond to the: *Tubulin alpha-4A chain* (Q53046), *WD repeat-containing protein 1* (Q5RKK0), *Rab GDP dissociation inhibitor beta* (P50399) and *GTP-binding nuclear protein Ran, testis-specific isoform* (Q8K586). The accession numbers of the downregulated proteins (light red nodes) correspond to the: *Glyceraldehyde-3-phosphate dehydrogenase* (P04797), *L-lactate dehydrogenase A chain* (P04642), *Elongation factor 2* (P05197), *Histone H2A type 2-A* (P00C09), *Malate dehydrogenase, mitochondrial* (P04636), *Tubulin alpha-1B chain* (Q6P9V9), *ATP synthase subunit beta, mitochondrial* (P10719) and *Cytochrome c oxidase subunit 2* (P00406). The accession numbers of the upregulated proteins (light green nodes) correspond to the: *Actin, gamma-enteric smooth muscle* (P63269) and *Actin, alpha skeletal muscle* (P68136). In B the accession numbers in the gray nodes correspond to: *Alpha-synuclein* (P97377), *Runt-related transcription factor 2* (Q9Z2J9), *Heterogeneous nuclear ribonucleoprotein K* (P61980), *Mitogen-activated protein kinase 3* (P21708), *Dystrophin* (P11530), *Keratin, type I cytoskeletal 19* (Q63279) and *Toll-interacting protein* (A2R1W1). The accession numbers of the unique proteins of the control (dark red nodes) correspond to the: *Tubulin alpha-8 chain* (Q6AVS6), *Homonobax protein cas-like 1* (P53565), *Delta(3,5)-Delta(2,4)-diene-yl-CoA isomerase, mitochondrial* (Q62651), *Actin-related protein 2/3 complex subunit 3* (B2GV73), *Interleukin-1 receptor accessory protein* (Q63621) and *DEAD (Asp-Glu-Ala-Asp) box polypeptide 5* (Q6AV11). The accession numbers of the unique 25 mgF/kg bw (dark green nodes) proteins correspond to the: *Cytoplasmic dynein 1 light intermediate chain 1* (Q9QXL8), *Transthylin-2* (Q5XF20) and *Stress-70 protein, mitochondrial* (P48721). The accession numbers of the downregulated proteins (light red nodes) correspond to the: *ATP synthase subunit alpha, mitochondrial* (P15999) and *Keratin, type II cytoskeletal 8* (Q10758). The accession numbers of the upregulated proteins (light green nodes) correspond to the: *Actin, alpha cardiac muscle 1* (R68035). (For interpretation of the references to color in this figure legend, the reader is referred to the web version of this article.)

process (21%), Oxygen transport (12%), Regulation of mitochondrial membrane permeability involved in apoptotic process (9%), Positive regulation of lipid kinase activity (9%) and Cellular response to nitric oxide (8%).

**4. Discussion**

The present study was designed to evaluate proteomic and morphological alterations in the jejunum after acute exposure to F. The dose we administered to rats (25 mgF/kg body weight) mimics the probable toxic dose (PTD) for humans, which is 5 mgF/kg body weight (Whitford, 2011). This happens because rodents metabolize F 5 times faster than humans (Dunipace et al., 1995). We did not attempt to simulate the therapeutic doses of F for canines control, since in this case we usually have lower doses of fluoride administered along time, i.e., chronic exposure, which was evaluated in our previous studies (Dionizio et al., 2018; Melo et al., 2017). However, in cases of topical F application of fluoridated gels, especially in younger children, the PTD related to acute exposure can be reached and gastrointestinal signals and symptoms might be observed (Whitford, 2011).

Under acute exposure to F, the majority of the proteins with altered expression were downregulated, both in jejunum (Table S1) and ileum (Table S2). These results indicate that acute exposure to F reduced

protein synthesis in distinct segments of the gut. The subnetworks for the comparison between the group treated with 25 mgF/kg bw vs control, both for jejunum (Fig. 1) and ileum (Fig. 3), revealed that most of the proteins with altered expression interacted with *Solute carrier family 2 facilitated glucose transporter member 4* (GLUT4; P19357), *Polyubiquitin-C* (Q63429), *Mitogen-activated protein kinase 3* (MAPK3; P21708) or *Heterogeneous nuclear ribonucleoprotein K* (P61980). Interestingly, the first 3 interacting partners were also present in the subnetwork comparing the proteins differentially expressed in the jejunum of rats chronically treated with 50 mgF/LF when compared with control (Dionizio et al., 2018). GLUT4 is involved in glucose transport. In a recent report by our group, in which proteomic analysis was conducted in the muscle and liver of diabetic rats, we observed that exposure to F altered many proteins that interacted with GLUT4 and could impair its function (Lima Leite et al., 2014; Lobo et al., 2015). In the present study, a plethora of proteins that interacted with GLUT4 and are involved in energy metabolism, especially of carbohydrates, were reduced or even absent in the jejunum upon acute exposure to F, such as *Malate dehydrogenase, mitochondrial* (P04636), *Malate dehydrogenase, cytoplasmic* (O88989), *L-lactate dehydrogenase A chain* (P04642), *Pyruvate kinase PKM* (P11980) and *Glyceraldehyde-3-phosphate dehydrogenase* (GAPDH; P04797), while *Malate dehydrogenase, cytoplasmic* (O88989), *L-lactate dehydrogenase A chain* (P04642) and *GAPDH* (P04797) were



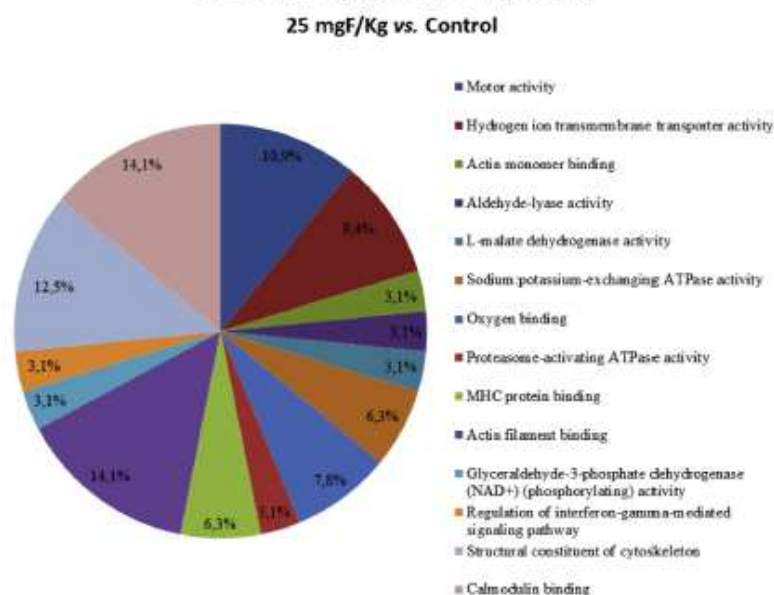


Fig. 2. Functional distribution of proteins identified with differential expression in the jejunum of rats exposed acute dose of 25 mgF/kg vs. Control Group (0 mgF/l). Categories of proteins based on GO annotation Biological Process. Terms significant ( $Kappa = 0.04$ ) and distribution according to percentage of number of genes. Proteins access number was provided by the UNIPROT. The gene ontology was evaluated according to ClustGoR2 plugin of CYTOSCAPE software 3.4.0 (Bindea et al., 2009, 2013).

also in the ileum upon exposure to F. These findings indicate a great impair in energy metabolism (especially of carbohydrates) in the jejunum and ileum of rats upon acute exposure to F, being the jejunum more affected than the ileum. These findings are somehow expected, since the enzymes involved in energy metabolism are highly affected by F, at least under chronic exposure to this ion (Araujo et al., 2019; Dionizio et al., 2018; Pereira et al., 2018). In addition, *ATP synthase subunit beta, mitochondrial* (P10719) and *ATP synthase subunit alpha, mitochondrial* (P15999), key enzymes in respiratory chain, were downregulated in the jejunum after acute F exposure, which corroborates the impair in the energy metabolism. It has been reported that expression of *ATP synthase subunit beta, mitochondrial* is reduced and correlated with ATP content in the livers of type 1 and type 2 diabetic mice, while hepatic overexpression of *ATP synthase subunit beta, mitochondrial* increases cellular ATP content and suppresses gluconeogenesis, leading to hyperglycemia amelioration (Wang et al., 2014).

*Polyubiquitin C* (Q63429) is a highly conserved polypeptide that is covalently bound to other cellular proteins to signal processes such as protein degradation, protein/protein interaction and protein intracellular trafficking (Ciechanover and Schwartz, 1998). In the present study, some of the above-mentioned proteins that interacted with *GLUT4* also interacted with *Polyubiquitin C*. Another protein that interacted with *Polyubiquitin C* is *Peroxiredoxin-1* (Q63716) that was absent in the jejunum upon acute exposure to F. *Peroxiredoxin-1* plays an important role in cell protection against oxidative stress by detoxifying peroxides and acting as sensor of hydrogen peroxide-mediated signaling events (UniProt, 2019). In balance in the oxidant/antioxidant defense is a common effect of F (Araujo et al., 2019; Barbier et al., 2010; Iano et al., 2014).

*MAPK3* (P21708) or extracellular-signal regulated kinases (ERK1) are a family of proteins that act as intermediaries in the signal transduction cascades triggered by extracellular signals at membrane receptors, through reversible protein phosphorylation, constituting one of the main mechanisms of cellular communication. They seem to be universal

components of signal transduction mechanisms since multiple forms have been identified in a variety of organisms (Dinsmore and Soriano, 2018; Hymowitz and Malek, 2018). One of the proteins interacting with *MAPK3* is *Transgelin-2*. Increase in this protein is associated with the development of cancer, while its suppression leads to inhibition of cell proliferation, invasion and metastasis (Yakabe et al., 2016). Recently, *transgelin* was shown to be increased in colorectal cancer (Zhou et al., 2018) and was suggested as a potential biomarker for cancer as well as a potential new target for cancer treatment (Meng et al., 2017). In our studies, *Transgelin-2* was increased in the jejunum after acute exposure to F, but was absent in the ileum after acute exposure to F. The reason for this differential pattern of expression is not apparent at the moment but could possibly be related to the different characteristics in intestine segments, which should be evaluated in further studies. Interestingly, another protein involved in the control of cell proliferation (*Stress-70 protein, mitochondrial*; P48721) was identified exclusively in the jejunum after acute F exposure. In the jejunum, *Stress-70 protein, mitochondrial* also interacted with *Heterogeneous nuclear ribonucleoprotein K* that was also an interacting player in the ileum. This protein is one of the major pre-mRNA-binding proteins, playing an important role in p53/TP53 response to DNA damage, acting at the level of both transcription activation and repression, being necessary for the induction of apoptosis. In the jejunum, another identified protein that interacted with *Heterogeneous nuclear ribonucleoprotein K* was *DEAD (Asp-Glu-Ala-Asp) box polypeptide 5* (DDX5; Q6AY11), an RNA-binding protein overexpressed in various malignant tumors (Janknecht, 2010), since it causes growth (Saporita et al., 2011) and metastasis (Yang et al., 2006), through activation of several oncogenic pathways (Yang et al., 2006). In the present study, however, DDX5 was absent in the jejunum upon acute exposure to F. It has been reported that depletion of DDX5 causes apoptosis by inhibition of mammalian target of rapamycin complex 1 (mTORC1) (Taniguchi et al., 2016). Fluoride-induced apoptosis has been widely reported in the literature (Barbier et al., 2010; Ribeiro et al., 2017). In the ileum, *Elongation*

6

A. Dionizio et al. / Science of the Total Environment 741 (2020) 140419

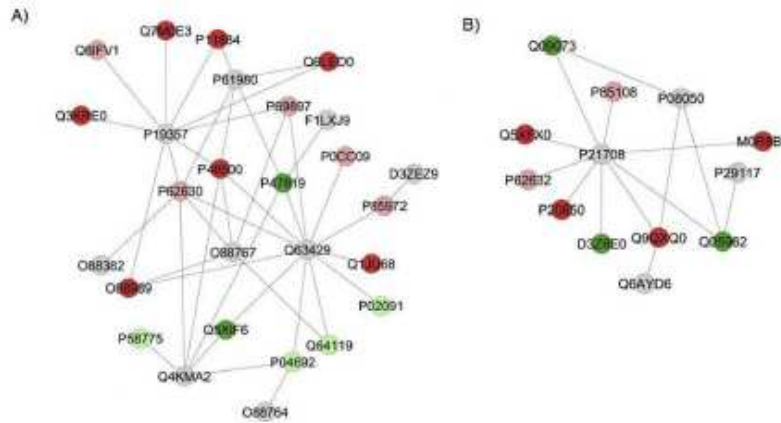


**Fig. 3.** Subnetworks created by ClusterMaker® to establish the interaction between proteins identified with differential expression in the 25 mg/kg wb group in relation to the control group in ileum. The color of the nodes indicates the differential expression of the respective named protein with its access code. The dark red and dark green nodes indicate proteins unique to the control and 25 mg/kg wb groups, respectively. The nodes in gray indicate the interaction proteins that are offered by CYTOSCAPE®, which were not identified in the present study and the light red and light green nodes indicate downregulation and upregulation, respectively. In A the access numbers in the gray nodes correspond to: *Solute carrier family 2, facilitated glucose transporter member 4* (P19357), *Heterogeneous nuclear ribonucleoprotein K* (P61980), *Membrane-associated guanylate kinase, WW and PI3K domain-containing protein 2* (O88382), *UV oxidin repair protein XPD3 homolog B* (Q4KMA2), *Protein deglycase D1-1* (O88767), *Death-associated protein kinase 3* (O88764), *Polyubiquitin-C* (Q63429), *Protein Hprt* (F1LXJ9) and *Protein Svt1* (D3ZE29). The access numbers of the unique proteins of the control (dark red nodes) correspond to the: *Destrin* (Q7MRE3), *Aldehyde dehydrogenase, mitochondrial* (P11884), *Histone H3.1* (Q6LEDO), *ATPase family AAA domain-containing protein 3* (Q3KRE0), *Trisphosphate isomerase* (P48500), *Malate dehydrogenase, cytoplasmic* (O88989) and *Eukaryotic translation initiation factor 3 subunit A* (Q1J088). The accession numbers of the unique 25 mg/kg wb (dark green nodes) proteins correspond to the: *Gliad fibrillary acidic protein* (P47819) and *Tubulin alpha-4A chain* (Q5X0F6). The access numbers of the downregulated proteins (light red nodes) correspond to the: *Keratin, type I cytoskeletal 14* (Q68FV1), *Tubulin beta-5 chain* (P68897), *Histone H2A type 2-A* (R0CC08), *Vinculin* (P85972) and *Elongation factor 1-alpha 1* (P62630). The access numbers of the upregulated proteins (light green nodes) correspond to the: *Hemoglobin subunit beta-1* (P03091), *Myosin light polypeptide 6* (Q641B), *Tropomyosin alpha-1 chain* (P04692) and *Tropomyosin beta chain* (P58775). In B the access numbers in the gray nodes correspond to: *Peptidyl-prolyl cis-trans isomerase F, mitochondrial* (P29117), *PI3K and LIM domain protein 2* (Q6AYD6), *Mitogen-activated protein kinase 3* (P21708) and *Gap junction alpha-1 protein* (P08050). The access numbers of the unique proteins of the control (dark red nodes) correspond to the: *Transgelin-2* (Q5XFX0), *Protein phosphatase 1A* (P20630), *Alpha-actinin-4* (Q9QXQ0) and *Protein Tubb1* (M0R886). The access numbers of the unique 25 mg/kg wb (dark green nodes) proteins correspond to the: *ADP/ATP translocase 2* (Q09073), *ADP/ATP translocase 1* (Q05962) and *Ribosomal protein S6 kinase* (D3Z8E0). The access numbers of the downregulated proteins (light red nodes) correspond to the: *Tubulin beta-2A chain* (P85108) and *Elongation factor 1-alpha 2* (P62632). (For interpretation of the references to color in this figure legend, the reader is referred to the web version of this article.)

*factor 1-alpha 1* (EF-1  $\alpha$  P62630) that interacted with *Heterogeneous nuclear ribonucleoprotein K* was reduced upon acute exposure to F, which is also related to induction of apoptosis, since elevated levels of EF-1  $\alpha$  are observed during neoplastic transformation and in tumors (Grant et al., 1992). In-line with this, *Aldehyde dehydrogenase, mitochondrial* (ALDH2; P11884) was absent upon acute exposure to F. Pharmacological inhibition of ALDH2 *per se* induces mitochondrial dysfunction and cell death (Mali et al., 2016). These findings are important because some reports incorrectly associate F exposure with the incidence of osteosarcoma (Bassin et al., 2006; Rameshet al., 2001) and bladder cancer (Grandjean et al., 1992). Our findings, however, give additional support to the safety of use of F on this aspect, since even when administered in a high dose as in the present study, F causes alterations in several proteins that lead to apoptosis instead of cell proliferation.

Most of the proteins that interacted with MAPK3 both in the jejunum and ileum are associated with cytoskeleton and some of them are actin-binding proteins (ABPs). Actin is one of the most abundant proteins in eukaryotic cells, participating in different cellular processes such as cell differentiation, proliferation, apoptosis, migration and signaling (Kristo et al., 2016). ABPs are highly abundant and directly participate in the modulation of cell processes through the regulation of actin cytoskeleton (Artman et al., 2014). Interestingly, *Transgelin-2* (Q5XFX0), an ABP, was absent in the ileum, but identified exclusively in the jejunum after acute exposure to F. This protein regulates the actin cytoskeleton through actin binding and sometimes participates in cytoskeleton remodeling (Dvorakova et al., 2014). In line with this, it is important to highlight that the categories with the highest percentage of associated genes, as revealed by functional classification, were

acting filament binding (14.1%) and calmodulin binding (14.1%) for the jejunum (Fig. 2) and organization of intermediary filaments (21%) for the ileum (Fig. 4). Alterations in proteins involved in the cytoskeleton might explain some of the morphological findings of the present study. Both in the jejunum and ileum, the thickness of the tunica muscularis was significantly decreased in the group that received the acute dose of F, when compared with control. This alteration is considered as one of the possible explanations for the impairment of the intestinal motility upon exposure to F (Viteri and Schneider, 1974). For the inhibitory control of the motility, the main neurotransmitters involved are NO and VIP (Benarroch, 2007). In this sense, in our study NO was decreased in both segments, while VIP was increased in the jejunum and decreased in the ileum. These findings agree with those found by our group in the duodenum (Melo et al., 2017) and jejunum (Dionizio et al., 2018) of rats chronically treated with water containing 10 and 50 mg/kg/L.

Contrarily to which was seen in the chronic treatment of jejunum (Dionizio et al., 2018) and ileum (unpublished data), upon the acute exposure to F the organism might not have had time to adapt to its toxic effect, which means that the loss of energy may have not been repaired. According to the literature, some of the initial symptoms of acute toxicity are generalized weakness, drop in blood pressure and disorientation (Buzalaf and Whitford, 2011; Whitford, 2011), which might be caused by decreased energy levels in the body.

In summary, our results, when analyzed in conjunction, suggest that the gastrointestinal symptoms found in cases of acute F exposure might be related to the morphological alterations in the gut (decrease in the thickness of the tunica muscularis) that, at the molecular level, can be explained by alterations in the gut vidergic innervation and in proteins

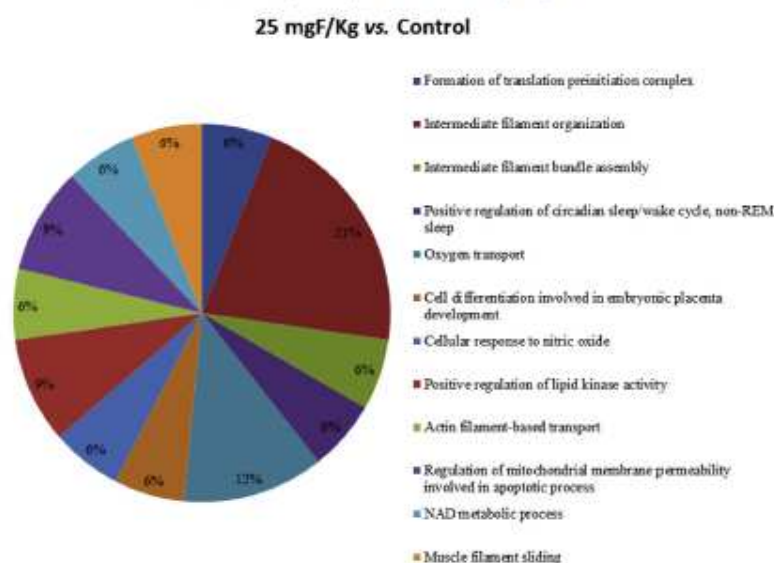


**Fig. 4.** Functional distribution of proteins identified with differential expression in the serum of rats exposed acute dose of 25 mgF/Kg vs. Control Group (0 mgFA). Categories of proteins based on GO annotation Biological Process. Terms significant (Kappa = 0.04) and distribution according to percentage of number of genes. Proteins access number was provided by the UNIPROT. The gene ontology was evaluated according to ClueGO® plugins of CYTOSCAPE® software 3.4.0 (Bindea et al., 2009, 2013).

that regulate the cytoskeleton. These findings help to explain the gastrointestinal signs and symptoms reported in cases of acute F toxicity.

Supplementary data to this article can be found online at <http://doi.org/10.1016/j.scitotenv.2020.140419>.

#### CRediT authorship contribution statement

**Aline Dionizio:** Writing - review & editing, Writing - original draft, Formal analysis, Validation, Investigation, Data curation, Funding acquisition, Methodology. **Carina Guimarães Souza Melo:** Writing - original draft, Formal analysis, Investigation, Methodology, Funding acquisition. **Isabela Tomazini Sabino-Arias:** Data curation, Formal analysis. **Tamara Teodoro Araujo:** Data curation, Formal analysis. **Talita Mendes Silva Ventura:** Data curation, Formal analysis. **Aline Lima Leite:** Data curation, Formal analysis. **Sara Raquel Garcia Souza:** Data curation, Formal analysis. **Erika Xavier Santos:** Data curation, Formal analysis. **Alessandro Domingues Heibel:** Data curation, Formal analysis. **Juliana Gadelha Souza:** Data curation, Formal analysis. **Juliana Vanessa Colombo Martins Perles:** Data curation, Formal analysis, Investigation, Methodology. **Jacqueline Nelis Zanoni:** Data curation, Formal analysis, Investigation, Methodology. **Marília Afonso Rabelo Buzalaf:** Writing - review & editing, Formal analysis, Writing - original draft, Methodology, Funding acquisition, Project administration, Supervision.

#### Declaration of competing interest

The authors declare that they have no known competing financial interests or personal relationships that could have appeared to influence the work reported in this paper.

#### Acknowledgements

This study was supported by FAPESP (2011/10233-7, 2012/16840-5 and 2016/09100-6).

#### References

- Araujo, T.T., Barbosa Silva Pereira, H.A., Dionizio, A., Sanchez, C.D.C., de Souza Carvalho, T., da Silva Fernandes, M., et al., 2019. Changes in energy metabolism induced by fluoride: insights from inside the mitochondria. *Chemosphere* 236, 124357.
- Arman, L., Dormoy-Radlet, V., von Roretz, C., Gallou, L.E., 2014. Planning your every move: the role of beta-actin and its post-transcriptional regulation in cell motility. *Semin. Cell Dev. Biol.* 34, 33–43.
- Barbier, O., Areola-Mendoza, L., Del Razo, L.M., 2010. Molecular mechanisms of fluoride toxicity. *Chem. Biol. Interact.* 188, 319–333.
- Bassin, E.B., Wypij, D., Davis, R.B., Mittelman, M.A., 2006. Age-specific fluoride exposure in drinking water and osteosarcoma (United States). *Cancer Causes Control* 17, 421–428.
- Bauer-Mehren, A., 2013. Integration of genomic information with biological networks using Cytoscape. *Methods Mol. Biol.* 1021, 37–61.
- Benarisch, E.E., 2007. Enteric nervous system - functional organization and neurologic implications. *Neurology* 69, 1953–1957.
- Bindea, C., Bernhard, M., Hubert, H., Pompl, C., Marie, T., Amos, K., Wolf-Herman, E., Franck, P., Zaidi, T., Bindea, C., Galon, J., 2009. ClueGO: a Cytoscape plug-in to decipher functionally grouped gene ontology and pathway annotation networks. *Bioinformatics* 25 (8), 1091–1093. <https://doi.org/10.1093/bioinformatics/btp101>.
- Bindea, C., Galon, J., Mlecnik, B., 2013. CluePedia Cytoscape plugin: pathway insights using integrated experimental and in silico data. *Bioinformatics* 29 (5), 661–663. <https://doi.org/10.1093/bioinformatics/btt019>.
- Bradford, M.M., 1976. A rapid and sensitive method for the quantitation of microgram quantities of protein utilizing the principle of protein-dye binding. *Anal. Biochem.* 72, 248–254.
- Buzalaf, M.A., Whitford, C.M., 2011. Fluoride metabolism. *Monogr. Oral Sci.* 22, 20–36.
- Buzalaf, M.A., Moraes, C.M., Olympio, K.P., Pessan, J.P., Grizzo, L.T., Silva, T.L., et al., 2013. Seven years of external control of fluoride levels in the public water supply in Bauri, São Paulo, Brazil. *J. Appl. Oral Sci.* 21, 92–98.
- Clechanover, A., Schwartz, A.L., 1998. The ubiquitin-proteasome pathway: the complexity and myriad functions of p-proteins death. *Proc. Natl. Acad. Sci. U. S. A.* 95, 2727–2730.
- Dinmore, C.J., Soriano, P., 2018. MAPK and PI3K signaling: at the crossroads of neural crest development. *Dev. Biol. (Suppl. 1)*, S29–S92.
- Dionizio, A., Pereira, H., Araujo, T.T., Sabino-Arias, I.T., Fernandes, M.S., Oliveira, K.A., et al., 2019. Effect of duration of exposure to fluoride and type of diet on lipid parameters and de novo lipogenesis. *Biol. Trace Elem. Res.* 190, 157–171.
- Dionizio, A.S., Melo, C.C.S., Sabino-Arias, I.T., Ventura, T.M.S., Leite, A.J., Souza, S.R.G., et al., 2018. Chronic treatment with fluoride affects the jejunal um: insights from proteomics and enteric innervation analysis. *Sci. Rep.* 8, 3180.
- Dunipac, A.J., Brizendine, E.J., Zhang, W., Wilson, M.E., Miller, L.L., Katz, B.P., et al., 1995. Effect of aging on animal response to chronic fluoride exposure. *J. Dent. Res.* 74, 358–368.

- Dvorakova, M., Nemtil, R., Bouchal, P., 2014. Transgelins, cytoskeletal proteins implicated in different aspects of cancer development. *Expert Rev Proteomics* 11, 149–165.
- Grandjean, P., Olsen, J.H., Jensen, O.M., Jus, K., 1992. Cancer incidence and mortality in workers exposed to fluoride. *J. Natl. Cancer Inst.* 84, 1903–1909.
- Grant, A.G., Flomen, R.M., Tizabi, M.L., Grant, D.A., 1992. Differential screening of a human pancreatic adenocarcinoma lambda gt11 expression library has identified increased transcription of elongation factor EF-1 alpha in tumour cells. *Int. J. Cancer* 50, 740–745.
- He, L.F., Chen, J.G., 2006. DNA damage, apoptosis and cell cycle changes induced by fluoride in rat oral mucosal cells and hepatocytes. *World J. Gastroenterol.* 12, 1144–1148.
- Hymowitz, S.C., Malek, S., 2018. Targeting the MAPK pathway in RAS mutant cancers. *Cold Spring Harb Perspect Med* 8, a031492.
- Iano, F.G., Ferreira, M.C., Quaggio, G.B., Fernandes, M.S., Oliveira, R.C., Ximenes, V.F., et al., 2014. Effects of chronic fluoride intake on the antioxidant systems of the liver and kidney in rats. *J. Fluor. Chem.* 168, 212–217.
- Janinacht, R., 2010. Multi-valenced DEAD-box proteins and potential tumor promoters: p68 RNA helicase (DDX5) and its paralog, p72 RNA helicase (DDX17). *Am. J. Transl. Res.* 2, 223–234.
- Jimenez-Cordova, M.L., Gonzalez-Horta, C., Ayllon-Vergara, J.C., Arreola-Mendoza, L., Aguilera-Madrid, G., Villareal-Vega, E.E., et al., 2019. Evaluation of vascular and kidney injury biomarkers in Mexican children exposed to inorganic fluoride. *Environ. Res.* 169, 220–228.
- Kristo, I., Bajusz, L., Bajusz, C., Borlatti, P., Vilmos, P., 2016. Actin, actin-binding proteins, and actin-related proteins in the nucleus. *Histochem. Cell Biol.* 145, 373–388.
- Lima Leite, A., Gualume Vaz Madureira Lobo, J., Barbosa da Silva Peres, H.A., Silva Fernandes, M., Marini, T., Zuclic, F., et al., 2014. Proteomic analysis of gastrocnemius muscle in rats with streptozotocin-induced diabetes and chronically exposed to fluoride. *PLoS One* 9, e106646.
- Lobo, J.G., Leite, A.L., Pereira, H.A., Fernandes, M.S., Peres-Buzalaf, C., Sumida, D.H., et al., 2015. Low-level fluoride exposure increases insulin sensitivity in experimental diabetes. *J. Dent. Res.* 94, 990–997.
- Mali, V.R., Deshpande, M., Pan, G., Thandavarayan, R.A., Palanjandi, S.S., 2016. Impaired ADH2 activity decreases the mitochondrial respiration in H9C2 cardio myocytes. *Cell Signal.* 28, 1–6.
- McDonagh, M.S., Whiting, P.F., Wilson, P.M., Sutton, A.J., Chestnutt, I., Cooper, J., et al., 2000. Systematic review of water fluoridation. *BMJ* 321, 855–859.
- Melo, C.G.S., Perles, J., Zanoni, J.N., Souza, S.R.G., Santos, E.K., Leite, A.L., et al., 2017. Enteric innervation combined with proteomics for the evaluation of the effects of chronic fluoride exposure on the duodenum of rats. *Sci. Rep.* 7, 1070.
- Meng, T., Liu, L., Han, K., Chen, S., Dong, Y., 2017. Transgelin-2: a potential oncogenic factor. *Tumour Biol.* 39, 1070428317702650.
- Millan, P.P., 2013. Visualization and analysis of biological networks. *Methods Mol. Biol.* 1021, 63–88.
- Mitsui, G., Dote, T., Adachi, K., Dote, E., Fujimoto, K., Shimbo, Y., et al., 2007. Harmful effects and acute lethal toxicity of intravenous administration of low concentrations of hydrofluoric acid in rats. *Toxicol. Ind. Health* 23, 5–12.
- Mitsui, G., Dote, T., Yamadori, E., Imanishi, M., Nakayama, S., Ohnishi, K., et al., 2010. Toxicokinetics and metabolism deteriorated by acute nephrotoxicity after a single intravenous injection of hydrofluoric acid in rats. *J. Occup. Health* 52, 395–399.
- Mullenix, P.J., Denbesten, P.K., Schumir, A., Kernan, W.J., 1995. Neurotoxicity of sodium fluoride in rats. *Neurotoxicol. Teratol.* 17, 169–177.
- Nopajun, J., Messer, H.H., Voller, V., 1983. Fluoride absorption from the gastrointestinal tract of rats. *J. Nutr.* 119, 1411–1417.
- Orchard, S., 2012. Molecular interaction databases. *Proteomics* 12, 1636–1662.
- Panesarsham, L., Raghunath, A., Sundarraj, K., Perumal, E., 2019. Acute fluoride exposure alters myocardial redox and inflammatory markers in rats. *Mol. Biol. Rep.* 46, 6155–6164.
- Pereira, H., Dionizio, A.S., Araujo, T.T., Fernandes, M.S., Iano, F.G., Buzalaf, M.A.R., 2018. Proposed mechanism for understanding the dose- and time-dependency of the effects of fluoride in the liver. *Toxicol. Appl. Pharmacol.* 358, 68–75.
- Pereira, H.A., Leite, A.L., Charone, S., Lobo, J.G., Cestari, T.M., Peres-Buzalaf, C., et al., 2013. Proteomic analysis of liver in rats chronically exposed to fluoride. *PLoS One* 8, e75343.
- Pereira, H.A., Dionizio, A.S., Fernandes, M.S., Araujo, T.T., Cestari, T.M., Buzalaf, C.P., et al., 2016. Fluoride intensifies hypercalcaemic diet-induced ER oxidative stress and alters lipid metabolism. *PLoS One* 11, e0158121.
- Ramesh, N., Vuayyaguhavan, A.S., Desai, B.S., Natarajan, M., Murthy, P.B., Pillai, K.S., 2001. Low levels of p53 mutations in Indian patients with osteosarcoma and the correlation with fluoride levels in bone. *J. Environ. Pathol. Toxicol. Oncol.* 20 (23), 7–43.
- Ribeiro, D.A., Cardoso, C.M., Vujra, V.O., M. DE.B.V., Aguiar Jr., O., Pisani, L.P., et al., 2017. Fluoride induces apoptosis in mammalian cells: in vitro and in vivo studies. *Anticancer Res.* 37, 4767–4777.
- Santoyo-Sanchez, M.P., del Carmen Silva-lucero, M., Arreola-Mendoza, L., Barbier, O.C., 2013. Effects of acute sodium fluoride exposure on kidney function, water homeostasis, and renal handling of calcium and inorganic phosphate. *Biol. Trace Elem. Res.* 152, 367–372.
- Saporta, A.J., Chang, H.C., Winkler, C.J., Apicelli, A.J., Klaidney, R.D., Wang, J., et al., 2011. RNA helicase DDX5 is a p53-independent target of ARF that participates in ribosome biogenesis. *Cancer Res.* 71, 6708–6717.
- Shankarum, D., Srinivasulu, S., Subramanian, S., 2004. Effect of fluoride intoxication on lipid peroxidation and antioxidant status in experimental rats. *Toxicology* 204, 219–228.
- Siaréz, P., Quintana, M.C., Hernandez, L., 2008. Determination of bioavailable fluoride from sepiolite by "in vivo" digestibility assays. *Food Chem. Toxicol.* 46, 490–493.
- Taniguchi, T., Inami, Y., Watanabe, M., Masuda, M., Morita, M., Aono, Y., et al., 2016. Resveratrol directly targets DDX5 resulting in suppression of the mTORC1 pathway in prostate cancer. *Cell Death Dis.* 7, e2211.
- UniProt, 2019. UniProt: a worldwide hub of protein knowledge. *Nucleic Acids Res.* 47, D506–D515.
- Vetri, F.F., Schneider, R.E., 1974. Gastrointestinal Alterations in Protein Calorie Malnutrition. *Med. Clin. North Am.* 58 (6), 1487–1505. [https://doi.org/10.1016/s0025-7125\(16\)32085-5](https://doi.org/10.1016/s0025-7125(16)32085-5).
- Wang, C., Chen, Z., Li, S., Zhang, Y., Jia, S., Li, J., et al., 2014. Hepatic overexpression of ATP synthase beta subunit activates PI3K/Akt pathway to ameliorate hyperglycemia of diabetic mice. *Diabetes* 63, 947–959.
- Whitford, G.M., 1992. Acute and chronic fluoride toxicity. *J. Dent. Res.* 71, 1249–1254.
- Whitford, G.M., 1996. The metabolism and toxicity of fluoride. *Monogr. Oral Sci.* 16 (Rev 2), 1–153.
- Whitford, G.M., 2011. Acute toxicity of ingested fluoride. *Monogr. Oral Sci.* 22, 66–80.
- Whitford, G.M., Pashley, D.H., 1984. Fluoride absorption: the influence of gastric acidity. *Calcif. Tissue Int.* 36, 302–307.
- Wong, M.C., Clarkson, J., Glenn, A.M., Lo, E.C., Marinho, V.C., Tsang, B.W., et al., 2011. Cochrane reviews on the benefits/risks of fluoride toothpastes. *J. Dent. Res.* 90, 573–579.
- Yakabe, K., Marukami, A., Kajimura, T., Nishimoto, Y., Saezoka, K., Sato, S., et al., 2016. Functional significance of transgelin-2 in uterine cervical squamous cell carcinoma. *J. Obstet. Gynaecol. Res.* 42, 566–572.
- Yan, X., Yan, X., Morrison, A., Han, T., Chen, Q., Li, J., et al., 2011. Fluoride induces apoptosis and alters collagen I expression in rat osteoblasts. *Toxicol. Lett.* 200, 123–138.
- Yang, L., Lin, C., Liu, Z.R., 2006. p68 RNA helicase mediates PDGF-induced epithelial mesenchymal transition by displacing Axin from beta-catenin. *Cell* 127, 139–155.
- Zhou, H., Zhang, Y., Wu, L., Xie, W., Li, L., Yuan, Y., et al., 2018. Elevated transgelin/INS1 expression is a potential biomarker in human colorectal cancer. *Oncotarget* 9, 1107–1113.